Final Report

Long-Life Slab Replacement Concrete

FDOT Contract Number: BDV25-977-01

Date: March 2015

Submitted to
Research Center (Research.center@dot.state.fl.us)
The Florida Department of Transportation
Research Center
605 Suwannee Street, MS 30
Tallahassee, FL 32399

c/o Dr. Harvey DeFord
Structural Materials Research Specialist
State Materials Office
5007 NE 39th Avenue
Gainesville, FL 32609
Phone: (352)955-6671
Email: Harvey.deford@dot.state.fl.us

Submitted by
Principal Investigator: Dr. Abla Zayed
Department of Civil and Environmental Engineering
University of South Florida
4202 E Fowler Avenue; ENB 118
Tampa, FL 33620-5350
Email: zayed@usf.edu

DISCLAIMER

Approximate Conversions to SI Units (from FHWA)

Symbol	When You Know	Multiply By	To Find	Symbol
Length				
in	inches	25.4	millimeters	mm
ft	feet	0.305	meters	m
yd	yards	0.914	meters	m
mi	miles	1.61	kilometers	km
Area				
in^2	square inches	645.2	square millimeters	mm^2
ft^2	square feet	0.093	square meters	m^2
yd^2	square yard	0.836	square meters	m^2
mi^2	square miles	2.59	square kilometers	km^2
Volume				
fl oz	fluid ounces	29.57	milliliters	mL
gal	gallons	3.785	liters	L
ft^3	cubic feet	0.028	cubic meters	m^3
yd^3	cubic yards	0.765	cubic meters	m^3
NOTE: volumes greater than 1000 L shall be shown in m^3				
Mass				
oz	ounces	28.35	grams	g
lb	pounds	0.454	kilograms	kg
Temperature (exact degrees)				
°F	Fahrenheit	5 (F-32)/9 or (F-32)/1.8	Celsius	°C
Illumination				
fc	foot-candles	10.76	lux	lx
fl	foot-Lamberts	3.426	candela/m^2	cd/m^2
Force and Pressure or Stress				
lbf	pound-force	4.45	newtons	N
lbf/in^2	pound-force per square inch	6.89	kilopascals	kPa

Technical Report Documentation Page

1. Report No.	2. Government Accession No.		3. Recipient's Catalog No.
4. Title and Subtitle Long-Life Slab Replacement Concrete			5. Report Date March 2015
			6. Performing Organization Code
7. Author(s) Abla Zayed, Kyle Riding, Christopher C. Ferraro, Andre Bien-Aime, Natallia Shanahan, Daniel Buidens, Thomas Meagher, Victor Tran, Justin D. Henika, Jerry M. Paris, Caitlin M. Tibbetts and Benjamin E. Watts			8. Performing Organization Report No.
9. Performing Organization Name and Address Department of Civil and Environmental Engineering University of South Florida 4202 E Fowler Avenue; ENB 118 Tampa, FL 33620-5350			10. Work Unit No.
			11. Contract or Grant No. BDV25-977-01
12. Sponsoring Agency Name and Address			13. Type of Report and Period Covered Final Report 3/4/13 to-3/31/15
			14. Sponsoring Agency Code
15. Supplementary Notes None			

16. Abstract

This research was initiated following reports of high incidence of cracking on FDOT concrete pavement replacement slab projects. Field slabs were instrumented for data acquisition from high-early-strength concrete pavement replacement slabs placed on projects funded by the Florida Department of Transportation (FDOT). Data were collected for three slabs located in Jacksonville, Florida, and Gainesville, Florida. A battery of laboratory tests was simultaneously conducted on the FDOT-approved concrete mixture designs used in the instrumented field slabs in addition to mixtures with variable chloride-based accelerator dosage. Temperature and strain data, as well as physical and thermal data, were acquired from slabs from the construction projects. The physical and thermal data acquired from the field were used for modeling description and verification. Subsequent to the field testing and data acquisition, the slabs were inspected for the presence of cracking. Laboratory testing included as-received materials characterization, heat of hydration measurements using isothermal and semi-adiabatic calorimetry for temperature rise assessment, and strength maturity curves for strength assessment. Using ConcreteWorks and HIPERPAV III, the findings indicated that adherence to the approved mixture design is critical. High placement temperatures and concrete placement during the day increased concrete cracking potential. Field additions of accelerator in excess of the approved mixture design were also found to increase the cracking potential.

17. Keywords. Concrete pavement, slab replacement, chloride-based accelerator, placement time, concrete temperature rise, placement temperature, cracking potential.		18. Distribution Statement No restrictions.	
19. Security Classification (this report) Unclassified	20. Security Classification (this page) Unclassified	21. Pages 306	22. Price

Form DOT F 1700.7 (8-72) Reproduction of completed page authorized

ACKNOWLEDGMENTS

This work has been sponsored by the Florida Department of Transportation (FDOT) and the Federal Highway Administration (FHWA). The Principal Investigator appreciates the valuable discussions with Dr. Harvey DeFord, Project Manager, and Mr. Michael Bergin, PE. The authors would like to thank Mr. Richard DeLorenzo, Mr. Jose Armenteros, and Mr. Patrick Gallagher with the FDOT State Materials Office (SMO) and Dr. Gray Mullins and Dr. Danny Winters with the University of South Florida (USF) for their assistance with this research. The following students are acknowledged for their tremendous contributions to this research: Ahmadreza Sedaghat, PE, Philip Hittepole, Shelby Brothers, Jordan Nelson, Richard McDonald, and Ashlie Kerr.

EXECUTIVE SUMMARY

1.1 Background

Recently, identifying the factors or parameters contributing to the cracking of concrete replacement slabs on Florida Department of Transportation (FDOT) projects has gained attention. Concrete slab replacement projects in Florida frequently exhibit high incidences of cracking. Cracking rates in recent projects have ranged from a desirable rate of less than 1% to a completely unacceptable rate of greater than 40%. Typically, the causes of cracking are not reliably determined. This research project entailed the instrumentation and data acquisition from field slabs, testing, and computer modeling of laboratory slabs to determine their behavior, and to assess parameters contributing to higher cracking potential.

1.2 Research Objectives

The primary objective of this investigation was to identify the factors or parameters contributing to the cracking of concrete replacement slabs on FDOT projects. Based on the findings, recommendations were made to minimize such occurrence. Towards satisfying those objectives, a three-part research plan was designed that involved instrumentation and data acquisition from field slabs, laboratory experiments for assessing temperature rise and maturity relationships, and modeling to predict the cracking potential under variable placement conditions.

1.3 Main Findings

The main findings from this study are summarized as follows:

- The concrete used in concrete replacement slabs sometimes has a dosage of chloride-based accelerating admixture in excess of the approved FDOT mixture design.
- Insulated concrete cylinders cast on site for strength determination had higher strengths than uninsulated cylinders.
- The temperature of the concrete at the start of placement and the ambient temperature have a significant effect on the rate of temperature and strength gain of high-early-strength concrete.
- The pavement repair slab placed at the State Materials Office in Gainesville, Florida, exhibited cracking which was hidden by the curing compound until simulated traffic loads removed the curing compound. Cracking was likely the result of thermal and drying effects.

- The currently used white curing compound does not allow for proper visual inspection of replacement slabs for the presence of cracks.
- Higher concrete temperature, higher dosage of chloride-based accelerator, and higher ambient temperature during placement increase the replacement slab cracking probability.
- Modeling and laboratory work identified high thermal stresses, autogenous shrinkage, and warping and curling as the primary mechanisms leading to pavement cracking.

1.4 Recommendations

Based on the findings from this study, the following recommendations were made:

- Revise Section 353-8 of the Standard Specification of Road and Bridge Construction to require replacement slab inspection for cracking after the curing compound has been removed by traffic.
- Require concrete repair slabs to be placed between the hours of 9 pm and 3 am.
- Revise Section 353 to limit chloride-based accelerating admixture usage above that specified by the manufacturer and in the approved FDOT mixture design.

1.5 Recommendations for Future Study

- Develop guidelines for proportioning low-cracking mixtures that could meet FDOT "open-to-traffic" strength criteria under different weather conditions. Currently, the research team has identified one concrete mixture design parameter that influences cracking probability: chloride-based accelerator dose. A project that can identify many of the additional parameters that affect cracking potential and strength gain could be used in developing guidelines.
- Develop repair material categories that would be preapproved for use in different weather conditions and traffic opening times with a low cracking potential. The mixtures would be rated based on the time to reach a desired strength at the lowest temperature expected during curing for that material category. The relationship between the accelerator dosage, concrete temperature, and strength development with time for each mixture category should be established.
- Perform a more extensive study of cracking in pavement slab replacement concrete that measures the in-place concrete pavement performance to validate concrete pavement cracking simulations under controlled conditions. Concrete pavement cracking simulation

software validation will allow for better prediction and field control of concrete material properties and performance.

TABLE OF CONTENTS

Content page

ACKNOWLEDGMENTS v

EXECUTIVE SUMMARY vi

- 1.1 Background vi
- 1.2 Research Objectives vi
- 1.3 Main Findings vi
- 1.4 Recommendations vii
- 1.5 Recommendations for Future Study vii

TABLE OF CONTENTS ix

LIST OF TABLES xiii

LIST OF FIGURES xvi

CHAPTER 1 Introduction 1

- 1.1 Background 1
- 1.2 Research Objectives 1
- 1.3 Research Approach 2
- 1.4 References 5

CHAPTER 2 Literature Review 6

- 2.1 Pavement Full Depth Repair 6
  - 2.1.1 Construction Methods 6
  - 2.1.2 Construction Requirements 8
    - 2.1.2.1 Concrete Placement for Replacement Slabs 9
    - 2.1.2.2 Curing Practices 10
  - 2.1.3 Other Construction Requirements 11
  - 2.1.4 Material Requirements – General 12
  - 2.1.5 Material Requirements – FDOT Specific 13
- 2.2 Causes of New Pavement Failure 14
  - 2.2.1 Causes of Cracking in Concrete Pavements 14
  - 2.2.2 Concrete Volume Change Mechanisms 14
    - 2.2.2.1 Thermal Volume Change 14
    - 2.2.2.2 Autogenous Volume Change 19
    - 2.2.2.3 Drying Shrinkage 22
    - 2.2.2.4 Plastic Shrinkage 23
  - 2.2.3 Restrained Stress 23
  - 2.2.4 Stress Relaxation 25
- 2.3 Methods to Measure Thermal Volume Changes 26

2.3.1 Temperature Rise 26
2.3.2 Coefficient of Thermal Expansion 46
2.4 Stress Assessment 48
2.4.1 Mechanical Properties Development 49
2.4.1.1 Compressive Strength Development 49
2.4.1.2 Tensile Strength 50
2.4.1.3 Elastic Modulus 51
2.4.1.4 Poisson Ratio 51
2.4.1.5 Maturity Relationship Applied to Mechanical Properties 52
2.4.2 Free Shrinkage Measurements 52
2.4.2.1 ASTM Method for Mortar Autogenous Shrinkage 52
2.4.2.2 ASTM C157 for Drying Shrinkage 53
2.4.2.3 Free Shrinkage Methods Used in Literature 53
2.5 Stress Measurements 54
2.5.1 Field Measurements – German/ Geokon Method 54
2.5.2 Laboratory Methods 54
2.5.2.1 Ring Method 54
2.5.2.2 Rigid Cracking Frame 55
2.5.2.3 Thermal Stress Testing Machine 56
2.6 Prediction 56
2.7 References 59

CHAPTER 3 Field Testing 71

3.1 Introduction 71
3.2 Field Questionnaire 74
3.3 Geotechnical Testing 77
3.3.1 Sieve Analysis 77
3.3.2 Limerock Bearing Ratio 80
3.3.3 Dynamic Cone Penetrometer 81
3.4 Fresh Properties of Concrete Testing 86
3.4.1 Unit Weight 86
3.4.2 Placement Temperature 87
3.4.3 Initial Slump 89
3.4.4 Slump Loss 90
3.4.5 Concrete Specimen Fabrication 93
3.4.6 Concrete Specimen Curing 93
3.4.6.1 Ambient Curing 94
3.4.6.2 Protection Curing 94
3.4.6.3 Curing of Specimens in a Cooler 96
3.4.6.4 Curing of Specimens in a Foam Cooler 98
3.5 Hardened Properties of Concrete Testing 101
3.5.1 Compressive Strength 101
3.5.2 Modulus of Elasticity 106
3.5.3 Splitting Tensile Strength 110
3.5.4 Temperature Rise of Concrete Cylinders 113
3.6 Concrete Slab Instrumentation 115

3.6.1 Temperature........118
3.6.1.1 Temperature – Slab 1........118
3.6.1.2 Temperature – Slab 2........120
3.6.1.3 Temperature – Slab 3........122
3.6.2 Strain........124
3.6.2.1 Strain – Slab 1........124
3.6.2.2 Strain – Slab 2........126
3.6.2.3 Strain – Slab 3........128
3.7 References........131

CHAPTER 4 Performance of Pavement Slabs........133

4.1 Field Performance of Slab 1........133
4.2 Field Performance of Slab 2........134
4.3 Field Performance of Slab 3........137
4.4 Slab 3 – Crack Investigation........141
4.5 Findings from Field........146
4.6 References........148

CHAPTER 5 Laboratory Tests for Cracking Potential Sensitivity-As-received Materials Characterization........149

5.1 Introduction........149
5.2 Elemental Oxide Composition of As – received Portland Cements........149
5.3 Cements' Blaine Fineness, Density, and Particle Size Distribution........152
5.4 Mineralogical Analysis for As – Received Portland Cements........154
5.5 Aggregate Properties........162
5.6 References........165

CHAPTER 6 Laboratory Tests for Cracking Potential Sensitivity-Isothermal Calorimetry....167

6.1 Introduction........167
6.2 Heat of Hydration........169
6.3 References........176

CHAPTER 7 Laboratory Tests for Cracking Potential Sensitivity-Semi-Adiabatic Calorimetry........179

7.1 Introduction........179
7.2 Methodology........180
7.3 Results and Discussion........187
7.4 Summary of Semi-Adiabatic Testing........208
7.5 References........210

CHAPTER 8 Assessment of the Accuracy of Concrete Temperature Rise Prediction........212

8.1 Introduction........212
8.2 Concrete Mixtures........213

8.3 Input Parameters 214
8.4 Results 216
8.5 Conclusions 222
8.6 References 223

CHAPTER 9 Concrete Mechanical Properties and Equivalent Age/Maturity Relationships 224

9.1 Introduction 224
9.2 Results and Discussion 228
9.2.1 Mortar Strength Data and Activation Energy 228
9.3 References 238

CHAPTER 10 Cracking Potential Prediction using HIPERPAV 239

10.1 Introduction 239
10.2 Modeling Stress-Strength Relationship of Concrete Pavement Slabs 239
10.2.1 HIPERPAV Temperature Prediction 241
10.2.2 HIPERPAV Mechanical Properties Prediction 242
10.2.2.1 Tensile Strength 242
10.2.2.2 Age-Dependent Coefficient of Expansion 242
10.2.2.3 Age-Dependent Modulus of Elasticity 243
10.2.2.4 Drying Shrinkage 244
10.2.3 HIPERPAV Strain Prediction 245
10.2.3.1 HIPERPAV Thermal Strain Prediction 245
10.2.3.2 HIPERPAV Shrinkage Strain Prediction 246
10.2.3.3 Creep-Adjusted Modulus of Elasticity Prediction 248
10.2.4 HIPERPAV Critical Stress Prediction 249
10.3 Findings 250
10.4 HIPERPAV Inputs 251
10.5 Analysis 256
10.5.1 Effect of Accelerator Dosage 256
10.5.2 Effect of Construction Time of Day 257
10.5.3 Effect of Initial Concrete Placement Temperature 260
10.6 Discussion and Conclusions 262
10.7 References 264

CHAPTER 11 Conclusions and Recommendations 266

11.1 Conclusions 266
11.2 Recommendations 266
11.3 Suggestions for Future Work 267

Appendix A – Activation Energy Fit Curves 268

Appendix B – Arrhenius Plots 272

Appendix C – Construction Steps for Semi-adiabatic Calorimeter 276

LIST OF TABLES

Table 3-1: Slab 1 –Sieve analysis data 77

Table 3-2: Slab 2 –Sieve analysis data 79

Table 3-3: Slab 1 – LBR and maximum dry density 80

Table 3-4: Slab 2 – LBR and maximum dry density 81

Table 3-5: Slab 1 – DCP data 84

Table 3-6: Slab 3 – DCP data 84

Table 3-7: Slab 1 – DCP correlation to CBR...86

Table 3-8: Slab 3 – DCP correlation to CBR...86

Table 3-9: Unit weight measurements (after accelerator addition) 87

Table 3-10: Initial temperature measurements 88

Table 3-11: Initial slump prior to the addition of accelerating admixture.....................................90

Table 3-12: Slab 1 – Slump loss 90

Table 3-13: Slab 2 – Slump loss 91

Table 3-14: Slab 3 – Slump loss 91

Table 3-15: Slab 1 - Compressive strength...103

Table 3-16: Slab 2 – Compressive strength 104

Table 3-17: Slab 3 – Compressive strength 106

Table 3-18: Slab 1 – Modulus of elasticity..107

Table 3-19: Slab 2 – Modulus of elasticity..108

Table 3-20: Slab 3 – Modulus of elasticity..108

Table 3-21: Slab 1 – Splitting tensile strength...111

Table 3-22: Slab 2 – Splitting tensile strength...111

Table 3-23: Slab 3 – Splitting tensile strength...111

Table 5-1: Oxide chemical analysis for as – received cements 150

Table 5-2: Bogue-calculated potential compound content for as – received cements................151

Table 5-3: Particle size analysis, Blaine fineness, and density for as – received cements 151

Table 5-4: Phase content using QXRD 159

Table 5-5: Properties of coarse and fine aggregate..164

Table 6-1: Concrete mix design 167

Table 6-2: Paste proportions for isothermal calorimeter tests 170

Table 6-3: Cumulative heats of hydration at 6 days 173

Table 6-4: Activation energy and hydration parameters for different mixtures 175

Table 7-1: Mixtures design 188

Table 7-2: Calibration factors 189

Table 7-3: Activation energy from isothermal testing...196

Table 7-4: Semi-adiabatic hydration parameters 196

Table 7-5: Adiabatic temperature rise..207

Table 8-1: FDOT slab mixtures materials 213

Table 8-2: Mixture designs 214

Table 8-3: ConcreteWorks general inputs 215

Table 8-4: ConcreteWorks inputs – hydration parameters 215

Table 8-5: ConcreteWorks environmental inputs 216

Table 8-6: Importance of accuracy of depth location for thermocouples 218

Table 9-1: Mix proportions for concrete (kg/m^3) 225

Table 9-2: Mix proportions for mortar mixes (9-cubes mix)..226

Table 9-3: Activation energy summary 233

Table 10-1: Mixture designs 251

Table 10-2: HIPERPAV mixture inputs 252

Table 10-3: HIPERPAV inputs – PCC properties..253

Table 10-4: Initial time stress exceeds strength 256

LIST OF FIGURES

Figure 2-1: Typical stages of the hydration process 15

Figure 2-2: Typical temperature and stress development in restrained concrete members during hydration (adapted from (Breitenbücher 1990))....................16

Figure 2-3: Sketch of total chemical shrinkage and volumetric autogenous deformation (shrinkage) under isothermal conditions (adapted from (Sellevold and Bjøntegaard 2006a)) 20

Figure 2-4: Conceptual effect of creep/relaxation on concrete stresses (adapted from Ruiz et al. 2005) 26

Figure 2-5: Sample Arrhenius plot used to quantify the E_a (kJ/mol)....................35

Figure 3-1: Typical slab replacement 72

Figure 3-2: Sensor placement locations....................73

Figure 3-3: Instrument tree used for sensor placement....................73

Figure 3-4: Field survey for Slab 1 74

Figure 3-5: Field survey for Slab 2 75

Figure 3-6: Field survey for Slab 3 76

Figure 3-7: Grain size distribution curve for Slab 1 78

Figure 3-8: Grain size distribution curve for Slab 2 79

Figure 3-9: Optimum dry density for Slab 1....................81

Figure 3-10: DCP test in progress for Slab 1....................82

Figure 3-11: Locations for DCP testing for Slab 1 83

Figure 3-12: DCP data for Slab 1 85

Figure 3-13: DCP data for Slab 3 85

Figure 3-14: Unit weight measurement for Slab 3....................87

Figure 3-15: Beginning of concrete placement for Slab 3....................88

Figure 3-16: Slump test for Slab 3....................89

Figure 3-17: Slump loss for Slab 1 91

Figure 3-18: Slump loss for Slab 2 92

Figure 3-19: Slump loss for Slab 3 92

Figure 3-20: Concrete cylinder specimen fabrication....93

Figure 3-21: Protection-cured concrete cylinder specimens....95

Figure 3-22: Covering of protection-cured concrete cylinder specimens for Slab 2....95

Figure 3-23: Cooler-cured concrete cylinder specimens 97

Figure 3-24: Temperature of concrete subsequent to placement – Slab 1....97

Figure 3-25: Heavily insulated foam curing box 99

Figure 3-26: Temperature of concrete subsequent to placement – Slab 2....100

Figure 3-27: Temperature of concrete subsequent to placement – Slab 3....101

Figure 3-28: Compressive strength testing in the field....102

Figure 3-29: Compressive strength vs. time for Slab 1 cooler-cured specimens....103

Figure 3-30: Compressive strength vs. time for Slab 2 105

Figure 3-31: Compressive strength vs. time for Slab 3 106

Figure 3-32: Modulus of elasticity vs. time for Slab 1 109

Figure 3-33: Modulus of elasticity vs. time for Slab 2 109

Figure 3-34: Modulus of elasticity vs. time for Slab 3 110

Figure 3-35: Splitting tensile strength vs. time for Slab 1 112

Figure 3-36: Splitting tensile strength vs. time for Slab 2 112

Figure 3-37: Splitting tensile strength vs. time for Slab 3 113

Figure 3-38: Temperature rise of specimens for Slab 1....114

Figure 3-39: Temperature rise of specimens for Slab 2....114

Figure 3-40: Temperature rise of specimens for Slab 3....115

Figure 3-41: Instrumentation at the corner of Slab 1....116

Figure 3-42: Full instrumentation of Slab 2....117

Figure 3-43: Thermocouple on instrument tree for Slab 2 117

Figure 3-44: Temperature at center of Slab 1 118

Figure 3-45: Temperature at edge of Slab 1 119

Figure 3-46: Temperature at corner of Slab 1...119

Figure 3-47: Temperature at center of Slab 2 120

Figure 3-48: Temperature at edge of Slab 2 121

Figure 3-49: Temperature at corner of Slab 2...121

Figure 3-50: Temperature at center of Slab 3 122

Figure 3-51: Temperature at edge of Slab 3 123

Figure 3-52: Temperature at corner of Slab 3...123

Figure 3-53: Strain at center of Slab 1 125

Figure 3-54: Strain at edge of Slab 1 125

Figure 3-55: Strain at corner of Slab 1..126

Figure 3-56: Strain at center of Slab 2 127

Figure 3-57: Strain at edge of Slab 2 127

Figure 3-58: Strain at corner of Slab 2..128

Figure 3-59: Stain at center of Slab 3 129

Figure 3-60: Strain at edge of Slab 3 129

Figure 3-61: Strain at corner of Slab 3..130

Figure 4-1: Application of curing compound to Slab 1 133

Figure 4-2: Slab 1 six months after placement 134

Figure 4-3: Preparations prior to the placement of concrete for Slab 2.....................................135

Figure 4-4: Completion of concrete finishing operations to Slab 2..135

Figure 4-5: Application of curing compound and covering of Slab 2 136

Figure 4-6: Slab 2 – six months after placement 136

Figure 4-7: Slab 2 – grinding defect 137

Figure 4-8: Preparations prior to the placement of concrete for Slab 2....138

Figure 4-9: Concrete finishing operations to Slab 3 138

Figure 4-10. Application of curing compound to Slab 3 139

Figure 4-11: Slab 3 – after placement and loading with HVS....140

Figure 4-12: Slab 3 cracking within and outside the wheel path....140

Figure 4-13: Slab 3 – easily visible cracking within the wheel path. 141

Figure 4-14: Core location map – Slab 3. 142

Figure 4-15: Typical core specimen removed from Slab 3....142

Figure 4-16: Core specimen removed from Slab 3 – Location 1....143

Figure 4-17: Core specimen removed from Slab 3 – Location 1....144

Figure 4-18: Core specimen removed from Slab 3 – Location 2....145

Figure 4-19: Core specimen removed from Slab 3 – Location 3....146

Figure 5-1: Differential particle size distribution for SW cement....153

Figure 5-2: Cumulative particle size distribution for SW cement....154

Figure 5-3: Diffraction pattern for JAX cement 157

Figure 5-4: SW diffraction pattern....158

Figure 5-5: Internal standard calibration curve for M1 alite polymorph....161

Figure 5-6: Grading curve for polite – 87090 coarse aggregate 163

Figure 5-7: Grading curve for GA-397 fine aggregate. Note that the GA-397 As – Received plot line is obscured by the Lab Mix plot line. 164

Figure 6-1: Heat flow for cement paste mixes at 23ºC....172

Figure 6-2: Heat of hydration for cement paste at different accelerator dosages at 23ºC 172

Figure 7-1: Semi-adiabatic calorimeter detail....181

Figure 7-2: Middle thermocouple placed and plugged in....182

Figure 7-3: Semi-adiabatic calorimeter water calibration for temperature loss 189

Figure 7-4: Measured semi-adiabatic temperature SW-C mix 190

Figure 7-5: Measured semi-adiabatic temperature SW-CNA mix 190

Figure 7-6: Measured semi-adiabatic temperature SW-CHA mix 191

Figure 7-7: Measured semi-adiabatic temperature SW-CA mix 191

Figure 7-8: Measured semi-adiabatic temperature SW-CDA mix 192

Figure 7-9: Measured semi-adiabatic temperature for JAX-CA mix 192

Figure 7-10: Temperature differential of SW-C mix 193

Figure 7-11: Temperature differential of SW-CNA mix 193

Figure 7-12: Temperature differential of SW-CHA mix 194

Figure 7-13: Temperature differential of SW-CA mix 194

Figure 7-14: Temperature differential of SW-CDA mix 195

Figure 7-15: Temperature differential of JAX-CA mix..195

Figure 7-16: Influence of α_u on hydration 197

Figure 7-17: Influence of β on hydration...197

Figure 7-18: Influence of τ on hydration 198

Figure 7-19: Effect of dosage of accelerator on α_u and β..199

Figure 7-20: Effect of accelerator dose on the hydration parameter (τ) 199

Figure 7-21: Measured vs. modeled semi-adiabatic temperature for SW-C mix 200

Figure 7-22: Measured vs. modeled semi-adiabatic temperature for SW-CNA mix 200

Figure 7-23: Measured vs. modeled semi-adiabatic temperature for SW-CHA mix 201

Figure 7-24: Measured vs. modeled semi-adiabatic temperature for SW-CA mix 201

Figure 7-25: Measured vs. modeled semi-adiabatic temperature for SW-CDA mix 202

Figure 7-26: Measured vs. modeled semi-adiabatic temperature for JAX-CA mix 202

Figure 7-27: True vs. false adiabatic temperature for SW-C mix..203

Figure 7-28: True vs. false adiabatic temperature for SW-CNA mix..204

Figure 7-29: True vs. false adiabatic temperature for SW-CHA mix..204

Figure 7-30: True vs. false adiabatic temperature for SW-CA mix...205

Figure 7-31: True vs. false adiabatic temperature for SW-CDA mix..205

Figure 7-32: True vs. false adiabatic temperature for JAX-CA mix 206

Figure 7-33: Effect of accelerator dosage on adiabatic temperature rise...................................207

Figure 7-34: Adiabatic temperature rise for each mixture..208

Figure 8-1: SMO – ConcreteWorks predicted temperature vs. measured (top thermocouple) ...217

Figure 8-2: SMO – ConcreteWorks predicted temperature vs. measured (middle thermocouple) 217

Figure 8-3: SMO – ConcreteWorks predicted temperature vs. measured (bottom thermocouple) 218

Figure 8-4: Predicted SW temperature profiles vs. measured SMO..219

Figure 8-5: SW CA mixture at MIA vs. SMO locations 220

Figure 8-6: SW CA temperature at different depths...221

Figure 8-7: Temperature animation at 7 hr...222

Figure 8-8: Temperature animation at 13 hr...222

Figure 9-1: Mix SW-C (w/c = 0.39 and no admixtures) mortar cube compressive strength.......228

Figure 9-2: Mix SW-CNA (air-entrainer and water reducer/retarder) mortar cube compressive strength...229

Figure 9-3: Mix SW-CHA (0.5x accelerator) mortar cube compressive strength......................230

Figure 9-4: Mix SW-CA (accelerator) mortar cube compressive strength................................230

Figure 9-5: Mix SW-CDA (2x accelerator) mortar cube compressive strength.........................231

Figure 9-6: Mix JAX-CA (w/c=0.32) mortar cube compressive strength.................................231

Figure 9-7: Maturity curve for SW-C...234

Figure 9-8: Maturity curve for SW-CNA 234

Figure 9-9: Maturity curve for SW-CHA 235

Figure 9-10: Maturity curve for SW-CA 235

Figure 9-11: Maturity curve for SW-CDA 236

Figure 9-12: Maturity curves for SW Mixes..236

Figure 9-13: Maturity curve for JAX-CA..237

Figure 10-1: Flow chart of HIPEPRAV models used to predict cracking potential....................240

Figure 10-2: HIPERPAV III sample analysis output...250

Figure 10-3: Tensile strength – maturity relationship input in HIPERPAV III..........................254

Figure 10-4: SW ambient temperature profiles 255

Figure 10-5: JAX temperature profile...255

Figure 10-6: SW humidity profiles..255

Figure 10-7: JAX humidity profile 255

Figure 10-8: SW cloud cover profiles..255

Figure 10-9: JAX cloud cover profile..255

Figure 10-10: SW wind speed profiles 256

Figure 10-11: JAX wind speed profile...256

Figure 10-12: Tensile stress and strength of each mixture 257

Figure 10-13: Effect of construction time on SW (SMO) cracking potential.............................258

Figure 10-14: Effect of construction time on SW (Miami) cracking potential...........................259

Figure 10-15: Effect of construction time on JAX cracking potential..259

Figure 10-16: SW effect of initial temperature..260

Figure 10-17: JAX effect of initial temperature 261

Figure 10-18: JAX mixture strength and stress in the pavement bottom and top for 50°F placement temperature 261

Figure 10-19: Temperature profiles 262

Figure A-1: Degree of hydration as a function of age for mix SW-C 269

Figure A-2: Degree of hydration as a function of age for mix SW-CNA...................................269

Figure A-3: Degree of hydration as a function of age for mix SW-CHA....................................270

Figure A-4: Degree of hydration as a function of age for mix SW-CA 270

Figure A-5: Degree of hydration as a function of age for mix SW-CDA....................................271

Figure A-6: Degree of hydration as a function of age for mix JAX-CA 271

Figure B-1: Arrhenius plot for mix SW-C..273

Figure B-2: Arrhenius plot for mix SW-CNA 273

Figure B-3: Arrhenius plot for mix SW-CHA 274

Figure B-4: Arrhenius plot for mix SW-CA..274

Figure B-5: Arrhenius plot for mix SW-CDA 275

Figure B-6: Arrhenius plot for mix JAX...275

Figure C-1: Steel compartment...277

Figure C-2: Perforation along the length of the drum..278

Figure C-3: Male/female connectors attached to the steel compartment.....................................279

Figure C-4: Placement of thermocouples on the outside of the sample chamber........................279

Figure C-5: Foam pouring and placement of compartment...280

Figure C-6: Line-up of insulator foam with compartment...280

Figure C-7: Top surface finishing...281

Figure C-8: Installed smooth acrylic finish 281

Figure C-9: Fabrication of top cover 282

Figure C-10: Marking of best fit position...283

Figure C-11: Finished product..283

CHAPTER 1 Introduction

1.1 Background

Concrete slab replacement projects in Florida encounter high incidences of replacement slab cracking. Cracking rates in recent slab replacement projects have ranged from a desirable rate of less than 1% to an unacceptable rate of greater than 40%. Typically, causes of cracking are not reliably determined. This research was initiated to determine the contributing factors that lead to early-age pavement cracking. In addressing this objective, field, laboratory, and modeling work was conducted. The field activities were led by Dr. Christopher Ferraro, and laboratory- and modeling-based experiments were led by Drs. Kyle Riding and Abla Zayed. Two locations were selected in the State of Florida for the field study: Jacksonville and Gainesville. In the Jacksonville location, two slabs were instrumented, while in Gainesville only one slab was instrumented. For field work, slabs were instrumented for temperature and strain measurements. Companion specimens were obtained from the concrete used in field slabs in order to evaluate the physical and thermal properties of placed concrete in the 3 instrumented slabs. For the laboratory investigation and modeling, as-received materials used in the field mixes were acquired, and concrete mixtures were prepared using the same mixture proportions as field slabs. In order to assess the contribution of material and construction parameters to the cracking probability of concrete repair slabs, a series of experiments was conducted to quantify the effects of different chemical admixture types and dosages on concrete thermal and mechanical properties that contribute to the cracking. The experimental results were then used as inputs in the ConcreteWorks and HIPERPAV software to quantify the tensile stress-to-tensile strength ratio during hardening of each material combination and assess the effect of placement at different times and temperatures. Concrete material properties measured during the experimental program included coefficient of thermal expansion, mechanical properties of hardened concrete, activation energy determined from mortar compressive strength and isothermal calorimetry, and semi-adiabatic temperature rise measurements.

1.2 Research Objectives

The primary objective of this research was to identify the factors or parameters contributing to the cracking of concrete replacement slabs on FDOT projects. Based on the findings of the experimental and modeling work, recommendations are made to aid in minimizing the cracking potential of replacement slabs in FDOT pavement projects.

1.3 Research Approach

The research approach included obtaining background information on slab replacement projects by interviewing personnel experienced in construction and inspection of replacement slabs. Engineers from the FDOT and members of a pavement slab replacement project were interviewed to provide knowledge and experience of typical construction practices as well as potential problems. In addition, a literature review on concrete pavement slabs was conducted. The following physical testing program was developed for the field work on slabs:

1) Physical tests on the base material (granular soil in contact with the pavement) sampled from the project site:
    a) Mechanical Sieve Analysis (ASTM D421 & 422);
    b) Limerock Bearing Ratio (FM 5-515);
    c) Dynamic Cone Penetrometer (ASTM D6951).
2) The following physical tests were performed on fresh and hardened concrete specimens at the construction site:

    a) Unit Weight (ASTM C138);
    b) Temperature (ASTM C1064);
    c) Slump (ASTM C143);
    d) Compressive Strength (ASTM C39);
    e) Compressive Elastic Modulus (ASTM C469);
    f) Splitting Tensile Strength (ASTM C496);
    g) Coefficient of Thermal Expansion (AASHTO T336)

Additionally, field slabs were instrumented to measure temperature and strain development profiles in the three identified slabs during the first day of hardening, starting from the time of placement. The concrete replacement slabs were visually inspected for the presence of cracks at different time intervals.

For laboratory testing, the following tests were conducted in addressing the objectives of this study:

1. Physical, chemical and mineralogical analysis for as-received cements: Blaine fineness, particle size distribution, specific gravity, elemental oxide composition using X-ray florescence, and X-ray diffraction for crystalline phases quantification.

2. Physical analysis for aggregates: particle size distribution, specific gravity, and absorption capacity.

3. Heat of hydration measurements on cement paste: Isothermal calorimetry measurements on pastes with variable accelerator dosage were conducted at three different temperatures to determine the heat-based activation energy for the cementitious system, which is a necessary parameter for concrete adiabatic temperature rise assessment.

4. Strength-based activation energy: activation energy was determined using mortar cubes for 6 different mixtures. This property was experimentally determined to develop the maturity curves for the different concrete mixtures studied.

5. Semi-adiabatic calorimetry of concrete mixtures with variable accelerator dosage: a system was built at the University of South Florida (USF) to assess the hydration parameters and temperature rise for the respective mixtures and study the effects of chemical admixture type, dosage, and combinations on concrete adiabatic temperature rise.

6. Assessment of temperature rise prediction using ConcreteWorks: The software was used together with the experimentally measured data to predict temperature rise in concrete mixtures. The software outputs were subsequently compared with the collected temperature profiles from field slabs.

7. Stress-strength relationship prediction for concrete slabs: HIPERPAV software was used to predict the stress-to-strength ratio and cracking potential for slabs using variable accelerator dosage and placement times.

This report is organized as follows:

A review of the state-of-the-art on concrete repair slab construction, materials, and cracking mechanisms is presented in Chapter 2. The field slab instrumentation, concrete mechanical property testing, and temperature and strain measurements for the three instrumented slabs is described in Chapter 3, while Chapter 4 describes follow-up crack surveys and investigations performed on the instrumented repair slabs. Chapters 5 through 7 describe the laboratory experiments that were performed to quantify concrete material properties required to model the pavement repair slab cracking potential. Chapter 5 describes the testing performed to characterize the as-received concrete constituent materials from the instrumented field sites. Chapter 6 describes the isothermal calorimetry performed to characterize the activation energy calculated from the heat of hydration of the cementitious materials, and to understand the effects of the chemical admixtures on the cement hydration. Chapter 7 describes the effects of concrete mixtures containing accelerating, and water reducing and retarding admixtures on concrete adiabatic heat development as measured through semi-adiabatic calorimetry.

1.4 References

AASHTO T336-11, “Standard Method of Test for Coefficient of Thermal Expansion of Hydraulic Cement Concrete”, American Association of State and Highway Officials, Washington DC, 2011.

ASTM C39 / C39M-12a, Standard Test Method for Compressive Strength of Cylindrical Concrete Specimens, ASTM International, West Conshohocken, PA, 2012.

ASTM C138 / C138M-13, Standard Test Method for Density (Unit Weight), Yield, and Air Content (Gravimetric) of Concrete, ASTM International, West Conshohocken, PA, 2013.

ASTM C143 / C143M-12, Standard Test Method for Slump of Hydraulic-Cement Concrete, ASTM International, West Conshohocken, PA, 2012.

ASTM C469 / C469M-10, Standard Test Method for Static Modulus of Elasticity and Poisson’s Ratio of Concrete in Compression, ASTM International, West Conshohocken, PA, 2010.

ASTM C496 / C496M-11, Standard Test Method for Splitting Tensile Strength of Cylindrical Concrete Specimens, ASTM International, West Conshohocken, PA, 2004.

ASTM C1064 / C1064M-12, Standard Test Method for Temperature of Freshly Mixed Hydraulic-Cement Concrete, ASTM International, West Conshohocken, PA, 2012.

ASTM D421-85(2007), Standard Practice for Dry Preparation of Soil Samples for Particle-Size Analysis and Determination of Soil Constants, ASTM International, West Conshohocken, PA, 2007.

ASTM D422-63(2007)e2, Standard Test Method for Particle-Size Analysis of Soils, ASTM International, West Conshohocken, PA, 2007.

ASTM D6951 / D6951M-09, Standard Test Method for Use of the Dynamic Cone Penetrometer in Shallow Pavement Applications, ASTM International, West Conshohocken, PA, 2009.

FM 5-515, Florida Method of Test for Limerock Bearing Ratio (LBR), Florida Department of Transportation, 2014.

CHAPTER 2 Literature Review

2.1 Pavement Full Depth Repair

2.1.1 Construction Methods

Advancements in concrete admixtures over the last decade led to an increase in the use of high early-strength (HES)-low water-to-cement ratio (w/c) concrete. These concrete mixtures have been widely used in concrete pavement replacement construction as they usually allow the road to be opened to traffic 6 hours after placement. As such, HES (FDOT) concrete is frequently referred to as Rapid Strength Concrete (RSC) (State of California Department of Transportation 2004) or Early-Open-to-Traffic concrete (EOT) (Van Dam et al. 2005). However, since the w/c is low, these mixtures are particularly sensitive to the use of proper construction practices and to environmental conditions such as air temperature, humidity levels, and placement time. Placement time is important because it affects the ambient conditions in which the slab will cure. The California Department of Transportation (State of California Department of Transportation 2004) has had extensive experience with pavement cracking. Over the years, it has been concluded that the causes leading to early cracking are inadequate saw depths, late sawing, restrained stresses from shrinkage or temperature change, stresses from curling or warping, and opening pavement to traffic before adequate strength has been achieved (State of California Department of Transportation 2004).

A literature review was conducted to outline the comparison of construction practices and the differences between state agencies. This literature review is limited to Jointed Plain Concrete Pavement (JPCP). There are nationwide common practices for JPCP pavement construction; however, because of regional weather conditions and available materials, each state has their own practices. Department of Transportation Specifications from Florida (FL) were compared to those in the following states: California (CA), Georgia (GA), Kansas (KS), Kentucky (KY), Texas (TX), Missouri (MO), Minnesota (MN), Michigan (MI), Wisconsin (WI), and Indiana (IN). Additionally, practices described by the Federal Highway Administration (FHWA) were reviewed and compared to the Integrated Materials and Construction Practices for Concrete Pavement (IMCP) manual written by Iowa State University (Taylor et al. 2006).

Different repairs are carried out for different types of cracked pavement slabs. If the damage is from spalling near a joint and the damage does not extend deeper than one-third of the pavement depth (Frentress and Harrington, 2012), a partial depth repair can be made. When transverse or longitudinal cracks extend through a slab, the concrete near the crack needs to be cut to the full depth and removed. In some cases a practice known as stitching or dowel bar retrofitting can be implemented to repair transverse cracks (Lenz, 2011). Corner cracks and shattered slabs also require full-depth replacement. During removal, cracked slabs are saw-cut to the full pavement depth down to the base and removed. These cuts are made up to existing construction joints or repair boundaries, such as transverse and longitudinal joints, which run perpendicular and parallel to the flow of traffic, respectively (Jackson 2007).

Caution needs to be taken to not disturb the base or damage it during the slab removal, and restrictions are in place to prevent the base from being cut more than to a depth of ½ inch (American Concrete Pavement Association 1995). The slabs are first cut into large pieces and then lifted out and trucked off site. Currently, Florida requires that the subgrade be within 2 percent of its optimum moisture content before concrete is placed (Florida Department of Transportation 2013). California often uses rigid treated base such as cement treated base, lean concrete, or asphalt treated base under the pavement slab, which if damaged during excavation, requires repair with RSC and needs time to harden before the top slab is poured. Asphalt concrete has been used in Florida in the past, however, is more commonly used in new pavements. When pavement repairs are placed over an existing asphalt concrete base, asphalt material that is removed should be repaired following slab removal. A bond breaker should be placed between a rigid treated base and the concrete pavement repair material to minimize the degree of restraint provided by the base In California, plastic sheeting is used as a bond breaker (State of California Department of Transportation 2004).

After the base has been prepared, dowel bars are installed into the longitudinally adjacent slabs, typically 12 inches on center at half the slab depth, to provide longitudinal load transfer between slabs. The dowels are epoxied into the existing slab, and bond breaker is applied to the new slab ends of the dowel bars to prevent them from restraining movement of the slab as it reacts to thermal or shrinkage stresses. While thirty other states polled in the ACPA survey allow epoxy coatings on the dowel bars, Florida does not allow epoxy coatings on dowel bars or tie-rods (American Concrete Pavement Association 1995). Drilling the holes for the dowels is typically done using a gang drill (several drills mounted parallel to a rigid frame), if enough space is available. A minimum of 4 holes can be drilled with the gang drill, and a gang drill is preferred for precision over single-mounted drills or hand-held drills (Florida Department of Transportation 2010). Misalignment of dowels is a large contributing factor to premature cracking in replacement and new pavement slabs. Misaligned dowels prevent lateral movement of the slab during thermal volume changes thus generating stresses in the slab (State of California Department of Transportation 2008). Chen and Won (2007) also observed that improperly installed dowels were not able to relieve the environmental restraints, and were a contributing cause to cracking. Bond breaker is also applied to the vertical faces of the adjacent slabs to reduce restraint on the pavement repair slab. Tie-bars are used to provide load transfer between slabs and prevent longitudinal movement between lanes.

A minimum slab replacement length of 6 feet and full lane-width repairs are recommended; half-lane repairs are not permitted by any of the surveyed agencies (State of California Department of Transportation 2004). Most agencies have concluded that if two repairs are close in proximity, it is more cost effective to repair the full width and length of the entire slab than it is to make additional saw-cuts to repair multiple smaller areas (State of California Department of Transportation 2004).

2.1.2 Construction Requirements

The FDOT has the following construction requirements for a concrete pavement slab replacement mix design: minimum target compressive strength of 2,200 psi at 6 hours and 3,000 psi at 24 hours, slump of 1.5 to 4 inches, entrained air content between 1% to 6%, and a maximum concrete temperature of 100°F before placement and prior to the addition of accelerators. The compressive strength is verified by cylinder testing or by the maturity method as specified in ASTM C1074. Additionally, temperature sensors can be installed in-place if designated by the engineer on site for purposes of monitoring temperature and performing a maturity test (Florida Department of Transportation 2013).

California uses 3 different variations for rapid strength concrete (RSC) based on available lane closure times and strength requirements. The first RSC contains specialty or proprietary cement mixtures and can meet strength requirements within 2-4 hours. The second RSC uses Type III cements with non-chloride accelerator, and a high-range water-reducer (HRWR) admixture.

This second mixture can meet opening strength requirements within 4-6 hours. The third mixture uses a lower dosage of non-chloride accelerator and can meet opening requirements within 12 to 24 hours. The use of each of these three RSC mixtures is determined based on the available lane closure times (State of California Department of Transportation 2004). California has the following opening-to-traffic requirements: 2,000 psi compressive strength, 400 psi flexural strength, 300 psi modulus of rupture from center-point loading, or a 250 psi third-point loading (State of California Department of Transportation 2004). NCHRP Report 540 (Van Dam et al. 2005) documented EOT concrete strength requirements for 11 states utilizing 6- to 8-hour EOT mixes and 20- to 24-hour EOT mixes. The required range for compressive strength before opening was between 2,500 and 3,500 psi, which is higher than required in Florida, and between 300 and 600 psi for flexural strength. Currently, there is no requirement for flexural strength in the FDOT pavement specifications; for bridge decks and pre-cast slabs, the requirements are 550 psi minimum flexural strength, or the minimum compressive strength specified in the plans (Florida Department of Transportation 2013). Some states (Maryland, Missouri, and Ohio) have the same criterion for both 6- to 8-hour EOT strengths and 20- to 24-hour strengths, while others (Michigan and Arkansas) required higher strengths for the 20- to 24-hour EOT Concrete. Georgia uses 3 different mixes that allow the roads to be opened to traffic in 4 hours or in 12-24 hours.

2.1.2.1 <u>Concrete Placement for Replacement Slabs</u>

FDOT requirements state that placement of concrete from ready-mix trucks should occur quickly, and be evenly distributed into the replacement areas to limit working with shovels. Vibration should follow placement for good compaction, especially around dowel bars and the slab perimeter. Finishing should be accomplished through the use of vibratory screeds or straightedges, and match the surrounding surface profile with a maximum height tolerance of +/- 1/8-inch from the adjacent slab. Texturing the surface similar to the surrounding pavement and then taking the appropriate steps to cure the fresh slab as soon as possible is key to minimizing stress on the fresh concrete from drying shrinkage (Florida Department of Transportation 2013). In addition to placement specifications, California requires that the concrete truck drivers are trained on how to retard a mix that is setting (State of California Department of Transportation 2004). Florida prohibits the addition of accelerator, which is added at the job site, to pavement replacement concrete that is more than 60 minutes old (Florida Department of Transportation 2013).

Weather during construction is an important factor that affects the potential for cracking. Adverse environmental conditions that can increase cracking potential include high winds, extreme low and high temperatures, and low humidity. IMCP specification states that concrete should not be placed during periods of high evaporation, unless evaporation retarder films, sun shades, wind breaks, or fogging are used to prevent excessive evaporation from the slab surface that can lead to cracking (Jackson 2007). Some agencies do not permit replacement slabs to be constructed during the daytime hours, as casting at night significantly reduces cracking, and afternoon placements are most likely to crack. For example, California and Georgia only permit concrete placement in the evening between 10:00 p.m. and 2:00 a.m. Placement at night provides the benefit of lower air temperatures and higher humidity levels. Meadows (2007) indicates that lowering the placement temperature reduces the cracking tendency. When compared to a placement temperature of 95°F, placement temperatures of 50°F and 73°F produce a reduced stress-to-strength ratio prior to cooling. This indicates that cooling the fresh concrete prior to placement in hot weather conditions will reduce the amount of strength consumed by thermal effects. Florida does not currently specify the timing of concrete slab placement.

2.1.2.2 Curing Practices

Inadequate curing is often blamed as a major cause of cracking. Well-timed curing and good quality curing compounds are essential, since internal temperature and moisture are essential for proper hydration, especially in EOT concretes. Texas DOT points out that high temperatures generated from rapid-setting concrete can encourage rapid evaporation of water from the surface leading to cracking problems, and that curing protection must start as soon as possible (Lenz 2011). Section 925 (Florida Department of Transportation 2013) lists wet burlap, membrane curing compounds, and sheet materials, such as waterproof paper, polyethylene film and white burlap-polyethylene sheet, as acceptable curing methods. Sprayable curing compounds are also frequently used for curing protection by many agencies. The membrane curing compounds should be suitable for spraying at temperatures prevalent at the time of construction and should form a continuous, uniform film. The FDOT method for curing replacement slabs consists of evenly spraying the curing compound, and then covering the surface and exposed area with 2 layers of white burlap-polyethylene curing blanket (section 925 of FDOT 2013) or insulating blankets approved by the Engineer. The goal is to cover the slab with the curing material as soon as the surface is hard enough to resist marring, and to continue curing the slab until the required 6-hour strength is achieved (Florida Department of Transportation 2013). California only uses power-operated curing compound application to ensure even coating of repair slabs (State of California Department of Transportation 2004).

2.1.3 Other Construction Requirements

Transverse cracks can be controlled through the implementation of shorter slab lengths and more saw cuts (State of California Department of Transportation 2004). The joint spacing should be “chosen to limit stress caused by restraint to movements from creep, shrinkage, and temperature effects” (ACI Committee 318 2011). ACI 224.3R-95 (ACI Committee 224 2008) recommends that transverse joint spacing “should not be much more than up to 24 times the slab thickness (typically 21 times for stabilized bases and 24 times for non-stabilized), and not farther than 20 ft apart regardless of thickness.” The depth of initial cut should be at least 0.25 times the slab thickness to ensure crack formation at the joint (1/3 of the slab thickness for stabilized-base pavements). Florida requires the maximum spacing between the joints to be limited to 15 ft (Nazef et al. 2011). FHWA advises that repairs made longer than 10 to 13 feet long should be constructed with an intermediate joint to prevent cracking (State of California Department of Transportation 2004). Longitudinal joints are also of importance in concrete pavement construction and are used to prevent cracking along the pavement centerline, as they help to alleviate the effects of curling (ACI Committee 224 2008). FDOT limits the spacing between longitudinal joints to 14 ft (Nazef et al. 2011).

Saw-cutting operations should begin as soon as the concrete is able to support the weight of the saw-cutting equipment and operator (ACI Committee 224 2008). The FDOT (Florida Department of Transportation 2013) puts a lot of emphasis on timely cutting of joints to prevent uncontrolled cracks. Transverse joints need to be made as soon as the concrete is hard enough to resist raveling from the cut, and before excessive shrinkage cracking occurs. The initial cut should be 1/8-inch wide and to a depth of 1/3 of the slab thickness. The second cut is then to be made to the specifications on the plans. For longitudinal joints, the saw-cutting should be completed as soon as possible after the concrete pavement can support the saw weight and not ravel during saw cutting. In California, timely saw-cutting is also identified as a crucial step in a successful pavement replacement. Cutting joints too early can lead to raveling and cutting too late can lead to random cracking in the repaired area (State of California Department of Transportation 2004).

2.1.4 *Material Requirements – General*

California only uses Type III cements for RSC concrete pavements (State of California Department of Transportation 2004). Georgia uses either Type I or III depending on the construction time frame (Georgia Department of Transportation 2013). All of the 11 states in the NCHRP Report 540 required the use of Type I, II, or III Portland cement for the 20- to 24-hour EOT concrete mixtures, and the specified minimum cement content varied from 564-846 lb/yd^3. Texas specifies a minimum cement content of 658 lb/yd^3 for Type I cement versus 564 lb/yd^3 for Type III cement (Van Dam et al. 2005).

Michigan, Georgia, and Illinois specified that calcium chloride accelerator be used if temperatures drop below 65°F (Florida Department of Transportation 2013). California does not allow the use of chloride-containing accelerators. It has been concluded that the use of chloride-containing accelerators doubles the amount of shrinkage experienced by concrete compared to shrinkage with no accelerator (State of California Department of Transportation 2004). For retarders, if the air temperature is higher than 96°F, their use may not be effective; instead, it is recommended that a slower setting concrete mixture should be used (State of California Department of Transportation 2004).

Supplementary cementitious materials (SCM) are not typically used in rapid concrete pavement repair. However, some states do allow their use for partial cement replacement. Indiana allows 10% fly ash or 15% ground granulated blast furnace slag (GGBFS) addition for 20- to 24-hour EOT concrete (Van Dam et al. 2005). Florida also allows the use of SCMs for concrete pavement (Florida Department of Transportation 2013). See following section for more details on Florida-specific requirements.

Typically a No. 57 or No. 67 stone blend is selected in Florida for replacement slabs (Florida Department of Transportation 2013), and these sizes are used by Texas and Wisconsin as well (American Concrete Pavement Association 1995). The aggregate specification used is an agency-specific requirement, and other states have different requirements. The maximum aggregate size used in pavements in Idaho, Nevada, Michigan, Missouri, and Utah is 2 inches. The smallest coarse aggregates used in pavement are 0.75 inches in Kansas with limestone mixtures, and 1.0 inch in Wyoming, South Carolina, Oklahoma, Indiana and Montana (American Concrete Pavement Association 1995).

2.1.5 Material Requirements – FDOT Specific

Florida allows the use of Type I, IP, IS, II, II (MH) and III cements for pavement slabs. Florida does not require a specific cement content, except that there must be enough cement in the mix design to yield a 6-hour cylinder crushing strength of 2200 psi and a 24-hour strength of 3000 psi (Florida Department of Transportation 2013). The cement content of Florida slab replacement mixes ranges from 800 to 950 lb/yd^3 (Dale DeFord, FDOT, personal communication with the author, February 17, 2015).

The use and acceptance of admixtures is found in Section 924-2 of (Florida Department of Transportation 2013). The Department maintains a list of qualified admixtures which includes the following admixtures: air-entraining, water-reducing (Type A), accelerating (Type C), water-reducing and retarding (Type D), water-reducing and accelerating admixture (Type E), high-range water reducing (Type F) high-range water-reducing and retarding (Type G), high-range water-reducer and plasticizing (Type I), high-range water-reducing, plasticizing, and retarding (Type II), and corrosion inhibitors.

Section 353 of (Florida Department of Transportation 2013) states that “for concrete pavement slab replacement, the use of pozzolans and slag is optional”. The specification, however, does not provide acceptable ranges of replacement percentages for pozzolans and slag. For new pavement, Florida allows fly ash replacement of 18-30% by weight of cement, while for slag, 25-70% replacement by weight of cement is allowed.

Section 901 (Florida Department of Transportation 2013) specifies the requirements for coarse aggregates used by the FDOT for a variety of different applications. Section 901 states that “Coarse aggregate shall consist of naturally occurring materials such as gravel, or resulting from the crushing of parent rock, to include natural rock, slags, expanded clays and shales (lightweight aggregates) and other approved inert materials with similar characteristics, having hard, strong, durable particles, conforming to the specific requirements of this Section.” However, most of the coarse aggregates used in Florida pavement mixes are from limerock. Aggregate selection for pavement replacements should be based on the aggregate reactivity and a low coefficient of thermal expansion. Aggregate selection and mix design are subject to departmental approval. The maximum aggregate size allowed in Florida pavement construction is 1-1/2 inches.

Section 902 (Florida Department of Transportation 2013) states that “Fine aggregate shall consist of natural silica sand, screenings, local materials, or subject to approval, other inert materials with similar characteristics, or combination thereof, having hard, strong, durable particles, conforming to the specific requirements of this Section.” The specification also states that “Silica sand from any one source, having a variation in Fineness Modulus greater than 0.20 either way from the Fineness Modulus of target gradations established by the producer, may be rejected.”

2.2 Causes of New Pavement Failure

2.2.1 Causes of Cracking in Concrete Pavements

ACI report 231R-10 (ACI Committee 231 2010) on early-age cracking identifies thermal- and moisture-related concrete volume changes as the causes of early-age concrete cracking. The report “defines ‘early age’ as the period after final setting, during which properties are changing rapidly.” The early age period is generally approximated to be 7 days. The magnitude of volume changes determines the magnitude of the stresses generated for a given degree of restraint. Both magnitude and timing of these stresses, with respect to concrete mechanical property development, should be considered to be determining factors of the concrete cracking potential.

2.2.2 Concrete Volume Change Mechanisms

2.2.2.1 Thermal Volume Change

When cement is mixed with water, the hydration process begins. Cement hydration is divided into five stages: initial hydrolysis (1), dormant period or period of slow reaction (2), acceleration period (3), post-acceleration period which can be split into deceleration period (4) and steady state period (5) as depicted in Figure 2-1 and Figure 2-2. Figure 2-1 shows the heat flow for a portland cement-water mixture (paste) at 30°C over a period of 7 days and the typical stages of the hydration process. Similarly, Figure 2-2 illustrates the typical temperature profile and stresses associated with the hydration process in a restrained concrete element. The following analysis explains how the temperature and stress profiles develop, and it shows that the specific values/phenomenon depend on the element size and environmental conditions.

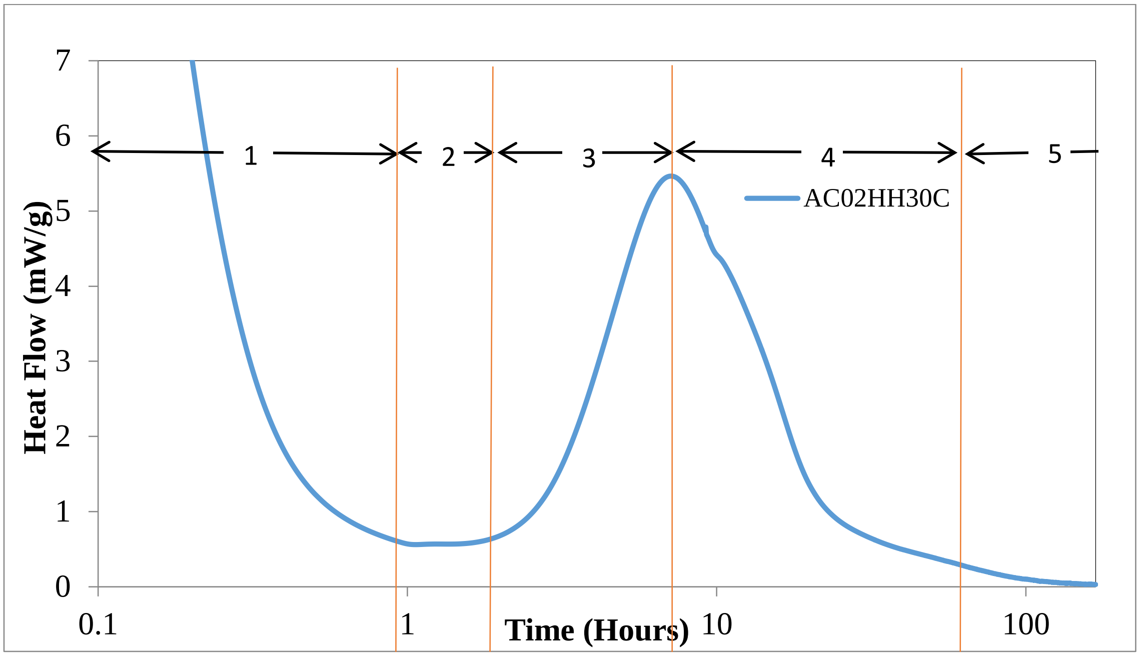

Figure 2-1: Typical stages of the hydration process

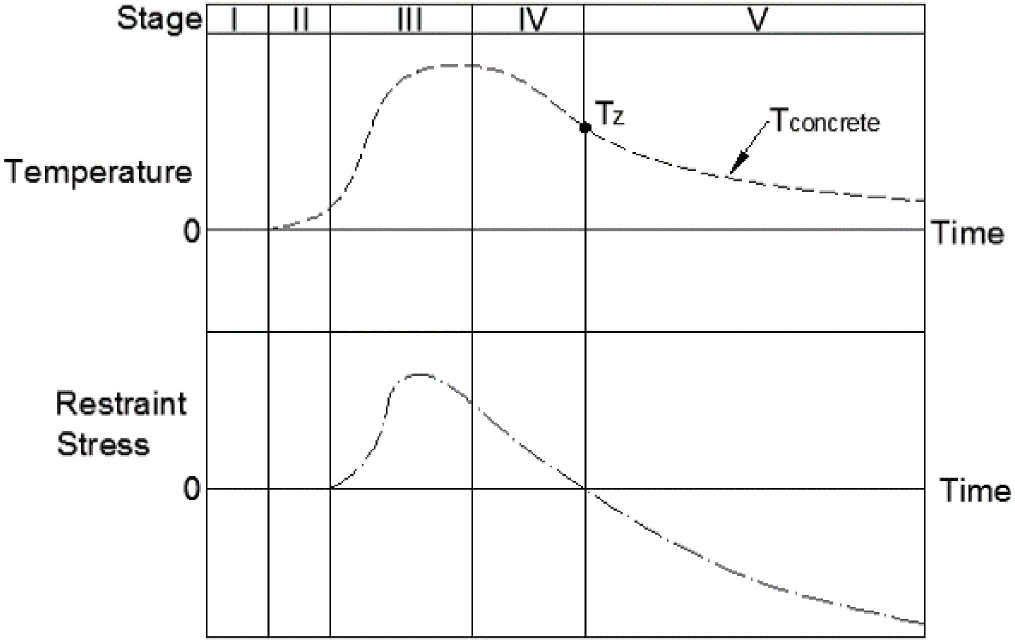

Figure 2-2: Typical temperature and stress development in restrained concrete members during hydration (adapted from (Breitenbücher 1990))

Stage 1, rapid heat evolution, is marked by initial ionic dissolution and nucleation that represents the exothermic wetting and early stage reactions. This stage lasts 15-30 minutes (Hewlett 1998; Mindess et al. 2003). Shortly after these initial reactions, stage 2 begins, and is marked by the slowdown of the initial reactions of C_3A and C_3S. The existence of this dormant period permits the placing and handling of portland cement since the mixture is still in a plastic state. Generally, initial set occurs at the end of this period as the mixture stiffens. During stage 3, the rate of C_3S reaction increases to a maximum, which corresponds to the maximum rate of heat generation. Temperature of the concrete increases to a maximum at the end of stage 3, corresponding to a 20-30% degree of hydration. Final set is reached just before the peak temperature. Stresses generated during stage 3 are relatively small, as concrete is still able to deform plastically during most of this period. In addition, stress relaxation is high in stage 3 (Figure 2-2), which reduces restrained stresses (Breitenbücher 1990; Mehta and Monteiro 2006).

In stage 4, the rate of reaction slows down until it reaches a steady state in stage 5. Concrete usually begins to cool in stage 4 when the heat produced by the hydration reactions becomes progressively less than the heat lost to the surrounding environment. This also corresponds to when the concrete volume ceases to expand and begins to contract. Compressive stresses decrease quickly, and the zero-stress condition is reached at a temperature not far below the maximum observed at the end of stage 3. Since this cooling occurs after final set, concrete volumetric changes experience restraint from the solid framework of the hydration products. It is estimated that the degree of hydration during this stage is about 50-60% (Abdel-Jawad 1988). As the modulus of elasticity of concrete in stage 4 is higher than in stage 3, and stress relaxation is smaller, the tensile stresses generated during stage 4 can be significant. Also, if the tensile stresses exceed the tensile strength of concrete, cracking is likely to occur. The tensile stress generated at this stage can be calculated using Equation 2-1 (Mehta and Monteiro 2006):

$$\sigma_t = K_r \frac{E}{1+\varphi} \alpha \Delta T \qquad \text{Equation 2-1}$$

where

σ_t = tensile stress,
K_r = degree of restraint,
E = elastic modulus,
α = coefficient of thermal expansion,
ΔT = temperature change, and
ϕ = creep coefficient.

The degree of restraint is an important parameter in determining the cracking potential of concrete. Concrete elements are subject to at least some restraint, whether from the subgrade or other structural elements on the macro scale, or to coarse aggregate particles and the solid framework of hydration products on the micro scale. Mihashi and Leite (2004) point out that the amount of restraint is particularly critical for concretes with low w/cm ratios. Restraint can be minimized to some degree by following proper construction practices, such as proper alignment of dowels and application of bond breaker to the vertical faces of adjacent slabs and underneath the slab, and placement of saw-cut joints at the proper time and spacing (ACI Committee 207 2007; ACI Committee 224 2001).

It is evident from Equation 2-1 that the tensile stress is dependent on the mechanical properties of concrete, specifically the elastic modulus and creep. Stresses are low at the early stages of hydration when the elastic modulus of concrete is low and stress relaxation due to creep is high. As hydration proceeds and more solid hydration products are formed, the elastic modulus of concrete increases while creep decreases, thus increasing the cracking potential.

The coefficient of thermal expansion (CTE) of concrete and the concrete temperature change determine the amount of thermal volume change, which is a major contributor to the tensile stresses generated during stage 4 of hydration. A reduction in the CTE will result in the reduction of tensile stresses. As the concrete CTE is essentially the weighted average of the CTE of paste and aggregate, and the aggregates occupy a majority of the volume of concrete, the use of low CTE aggregates is often recommended (Mehta and Monteiro 2006). The temperature change of the placed concrete can be determined using Equation 2-2 (Mehta and Monteiro 2006):

$$\Delta T = \text{placement temperature of fresh concrete} + \text{adiabatic temperature rise} - \text{ambient temperature} - \text{temperature drop due to heat losses} \quad \text{Equation 2-2}$$

The placement temperature is perhaps the easiest parameter to control in terms of preventing or controlling thermal cracking. Many hot-weather concreting specifications recommend addition of ice to mixing water or precooling the aggregates as a means of lowering the maximum temperature during stage 3 of hydration, and reducing the temperature change experienced by concrete (ACI Committee 305 1991). Changing placement time from day to night when the ambient temperature is lower is another effective way of reducing the placement temperature and, consequently, the cracking risk of concrete. Although it may not be possible to control ambient temperature per se, placement times may be optimized to reduce the temperature difference between the concrete and the environment. Riding et al. (2009) observed that night-time placement that allows the concrete to set before the day-time temperature rise, significantly reduces the tensile stresses that develop during cooling in stage 4, and minimizes concrete cracking potential. It is also evident from the above relationship that minimizing the adiabatic temperature rise will minimize the temperature change. Additionally, heat losses in the previous equation refer to the heat transfer to any media that the concrete may be in contact with, such as air, curing water, or formwork.

2.2.2.2 Autogenous Volume Change

As cement begins to hydrate, concrete volume is reduced as the hydration products occupy less volume than initially occupied by water and anhydrous cement. This reduction of the original volume due to hydration is referred to as chemical shrinkage. While concrete is still plastic, chemical shrinkage directly translates to an overall reduction of the concrete volume. However, after the final set, when a solid framework of hydration products has formed, the volume changes due to chemical shrinkage will be restrained by the solid framework. Some of this internal volume change is translated to bulk volume change of concrete (autogenous shrinkage), while the remaining volume difference is translated into empty voids inside the concrete that used to be occupied by the anhydrous cement and water (shown in Figure 2-3).

Autogenous shrinkage is the bulk volume change that results from the consumption of capillary pore water during hydration. Autogenous shrinkage is a result of chemical shrinkage. The underlying mechanism for both autogenous and drying shrinkage is essentially the same – removal and redistribution of water in the concrete pore structure. In practice, as ACI 224R-01(ACI Committee 224 2001) points out, there is no need to separate these phenomena. This loss of water, whether internal or external, generates tensile stresses on the pore walls bringing them closer together resulting in the bulk volume reduction. If concrete is restrained and the stresses exceed the tensile strength, cracking is likely to occur. Autogenous shrinkage has received a lot of attention with respect to early-age cracking of high performance concretes (HPC). These mixes have low w/cm ratios and high contents of cementitious materials. Autogenous shrinkage is considered to be negligible in concretes with w/cm ratios above 0.4 (Van Dam et al. 2005).

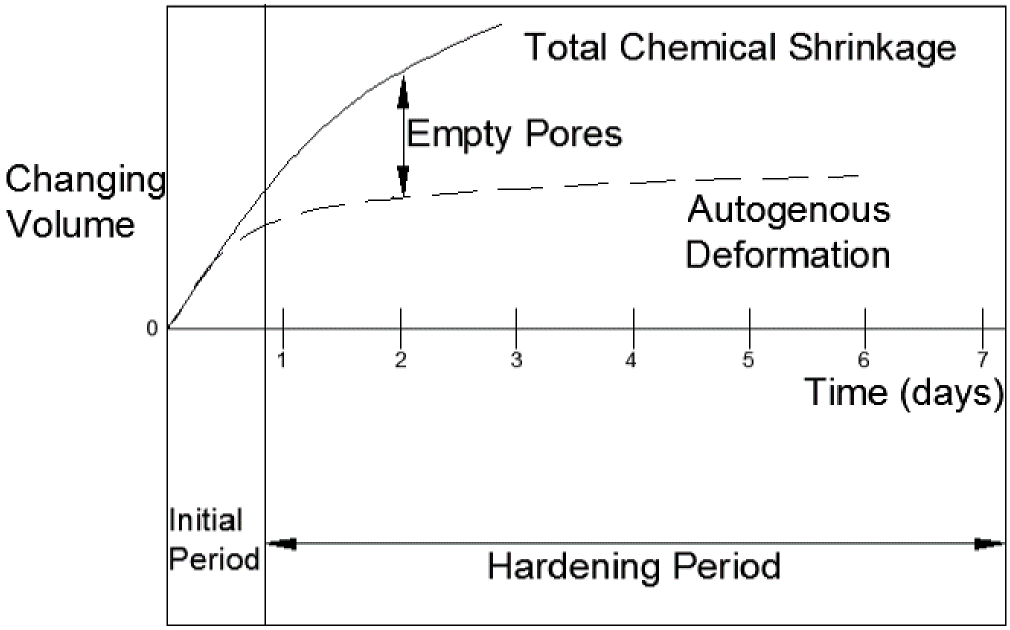

Figure 2-3: Sketch of total chemical shrinkage and volumetric autogenous deformation (shrinkage) under isothermal conditions (adapted from (Sellevold and Bjøntegaard 2006a))

As the degree of hydration (α) increases, so does the empty pore volume. Typical chemical shrinkage values referred to in the literature are 6-7 ml per 100 g of cement (Bentz 2008; Lura et al. 2003). Several mechanisms for autogenous shrinkage have been discussed in the literature: tension of capillary water, disjoining pressure and surface tension of colloidal particles (also referred to as surface free energy) (Hua et al. 1995, 1997; Lura et al. 2003; Mindess et al. 2003). There seems to be general agreement in the literature that stresses due to capillary tension are primarily responsible for autogenous shrinkage (Bentz et al. 2008; Hua et al. 1995, 1997; Mehta and Monteiro 2006).

Immediately after mixing, all the capillary pores in the concrete are saturated. As the water in the existing pores is consumed and new pores are created during the hydration process due to chemical shrinkage, the capillary water is redistributed by the capillary forces, which draw the water out of the larger pores into the smaller ones (Bentz et al. 2001). Now the small pores are saturated, but the large pores are filled with both water and air, which causes a drop in the relative humidity (RH) in the large pores. The RH is generally assumed to be 100% at saturation; however, Lura et al. (2003) reported values of 98% RH at saturation. This is explained by the presence of salts in the pore solution, which lowers the RH.

The water-air menisci that are created in the partially-filled pores are under tension and exert stresses on the pore walls bringing them closer together, which results in autogenous shrinkage. The generated stresses depend on the size of the pore and the RH. It should be noted that capillary stresses only exist at RH above 45%. Below 45% RH, water menisci become unstable and capillary stresses are no longer generated (Mindess et al. 2003). The capillary tension of the menisci can be calculated according to the Kelvin-Laplace equation (Equation 2-3) (Bentz et al. 2008):

$$\sigma_{cap} = \frac{2\gamma \cos\alpha}{r} = \frac{-\ln(RH)\,RT}{V_m} \qquad \text{Equation 2-3}$$

where

σ_{cap} = capillary tension (Pa),

γ = pore solution surface tension (N/m),

α = angle between the pore solution and the pore walls,

r = meniscus radius (m),

V_m = molar volume of the pore solution (m^3/mol),

R = universal gas constant (8.314 J/(mol K)), and

T = temperature (K).

Using this equation, it is possible to calculate the largest pore radius at which the pores are saturated for any given RH (Lura et al. 2003). The relationship between all these parameters is rather complex. As can be seen from the above equation, capillary tension increases as the internal RH is lowered. Capillary tension should also increase as the temperature increases. However, temperature increase also increases RH (Hua et al. 1995), and the effect of RH on σ_{cap} is much more pronounced than that of temperature. It can also be seen from Equation 2-3 that decreasing the pore radius increases the capillary tension. However, one should keep in mind that stresses are generated only in partially filled pores and there are no stresses in saturated pores. As long as all the pores are saturated, the size of the pores does not matter. This explains why internal curing (addition of light-weight aggregate saturated with water) has been found to be very effective in reducing autogenous shrinkage (Bentz et al. 2008). However, high-early-strength (HES) concretes usually have a combination of small pore radii and low RH. A finer pore system is generated by using cements with higher fineness and mixes with lower w/c ratios. Since there is less water available for hydration in the low w/c ratio mixes, the water filling the pores is consumed much faster, generating tensile capillary stresses at an earlier time in the hydration process when the tensile strength of the mix is lower, thus increasing the cracking potential. Even with adequate curing and the use of shrinkage-reducing admixtures (SRAs), it is difficult to completely prevent moisture loss from the field-placed concrete to the environment. As both of these processes occur simultaneously in the field and have the same underlying mechanisms, it may be beneficial to consider them in tandem.

2.2.2.3 Drying Shrinkage

Drying shrinkage refers to concrete volume change due to the loss of moisture to the environment that occurs after final setting. Drying shrinkage results from the loss of water when concrete is exposed to an environment with RH below 100%. During initial drying, moisture is removed uniformly throughout the cross-section of the concrete (Bentz et al. 2001, 2008; Valckenborg et al. 2001). However, a moisture gradient develops with age (ACI Committee 224 2001; Kim and Lee 1999). Drying shrinkage can be minimized by timely application of curing compounds that seal the concrete surface to prevent evaporation, as discussed previously.

Neville (2006) states that the loss of capillary water, “causes little or no shrinkage”, and volume change results from the loss of adsorbed water which is physically bound to the gel particles. Valckenborg et al. (2001) confirmed with NMR measurements on saturated mortar samples that only the capillary water is lost during initial drying. As with autogenous shrinkage, initial drying shrinkage is affected by the size of the capillary pores, with larger pores being emptied first (Bentz et al. 2001). Kim and Lee (1999) observed that the rate of moisture diffusion due to drying increases with increasing w/c ratio. Jankovic and van Mier (2003) also observed that the rate of drying increases with w/c ratio. They also concluded that an increase in pore size will have the same effect on the drying rate. A number of factors can influence the pore structure of concrete. Higher w/c ratio and lower cement fineness will result in a coarse pore structure. Addition of certain admixtures, such as air-entraining agents, will also increase the amount of air voids. Entrained air voids are usually significantly larger than the capillary pores. According to ASTM C125, entrained air voids are 10-1000 µm in diameter, while capillary pores are 10-50 nm (micropores), although they can be as large as 5 µm (macropores) at the beginning of hydration (Mehta and Monteiro 2006). Addition of accelerators leads to smaller capillary pores, which results in higher capillary tension once the pores become unsaturated, leading to higher autogenous shrinkage.

Regardless of the mechanism, hydration or loss of moisture due to external drying, removal of water from the capillary pores results in the increased capillary tension. Since the ITZ has a higher porosity due to higher w/c ratio around the aggregates, the micro-cracking is likely to occur in the ITZ as the larger pores in the ITZ will become partially saturated first. The presence of microcracks may further accelerate the rate of drying (Bazant and Raftshol 1982). To prevent microcracking, Bazant and Raftshol suggest that the maximum stresses should not exceed $0.7f'_t$ for concrete.

2.2.2.4 Plastic Shrinkage

Plastic shrinkage occurs while concrete, still in the plastic stage, is exposed to atmospheric drying, where the drying rate of water from the surface of the concrete exceeds the bleed rate. Plastic shrinkage cracking occurs before final setting, and will not be considered in this study, as it is understood that all the cracking in the repair slabs occur after final set.

2.2.3 Restrained Stress

If concrete is allowed to expand and contract freely, cracking would not occur (ACI Committee 207 2007). In practice, however, all concrete is subject at least to some degree of restraint, whether from the subgrade or other structural elements on the macro scale (external restraint), or coarse aggregate particles and the solid framework of the hydration products as well as differential volume changes on the micro scale (internal restraint). The degree of restraint is defined as the “ratio of actual stress resulting from volume change to the stress that would result if completely restrained” (ACI Committee 207 2007). The degree of restraint is an important parameter in determining the cracking potential of concrete. Nilsson (2003) states that “the degree of restraint is almost proportional to the risk of cracking.” This implies that inadequate construction practices can significantly increase the cracking potential of concrete.

The external sources of restraint in concrete pavements include adjacent concrete pavement slabs, the pavement base, and the length of the pavement slab. Dowels bars connect the slabs, allowing for load transfer between adjacent slabs. The misalignment of dowels will increase the degree of restraint and can lead to cracking. Application of bond breaker is another important measure in minimizing restraint from adjacent slabs. As mentioned previously, bond breaker should be applied to the dowels and the vertical faces of the existing slabs that will be in contact with the new concrete. If the bond breaker is not adequate, restraint stresses will be increased.

The predominant mechanism of restraint in pavements is the interfacial friction between the pavement slab and the subbase. McCullough and Rasmussen (1998) indicated "subbase type has a greater influence on the restraint level in a concrete pavement than any other factor." Zhang and Li (2001) investigated the effect of subbase type on the stresses that develop in pavement due to restraint. They observed that the highest tensile stresses result from the use of stiff bases, like cement-stabilized base, and much lower stresses were associated with loose, unbound bases. They concluded that the tensile stresses from the frictional resistance of stiff bases could be high enough to cause cracking. However, these high tensile stresses can be significantly reduced by the use of a bond breaker between the base and pavement. The two types of bond breaker investigated in this study were a 2 mm layer of sand and a polyethylene sheet. The polyethylene sheeting was found to be most effective in reducing restraint, which is consistent with the experience of California Department of Transportation. McCullough and Rasmussen (1998) recommend the use of asphalt concrete as a bond-breaker.

The weight of the slab itself can also provide a degree of restraint. Wesevich et al. (1987) determined that the slab weight had a direct effect on the frictional resistance to movement for loose, unbound subbases and only a slight effect on stabilized subbases. Additionally, it was noted that the slab length determines the stress magnitude; as the length increases, so does the stress. The rate at which the stress increases with slab length depends on the base type (Zhang and Li 2001). The stresses due to slab length can be eliminated by timely saw-cutting of transverse contraction joints of appropriate spacing as discussed previously.

2.2.4 Stress Relaxation

Creep is defined as “time-dependent deformation under load” (Mindess et al. 2003). When a compressive load is applied, strains will gradually increase over time (compressive creep). Stress relaxation is similar to creep, but it is a time-dependent lowering of stresses while under strain. When concrete experiences tensile stresses, for example due to shrinkage under restrained conditions, concrete will deform and stresses will be reduced over time. Stress relaxation and creep are often used interchangeably with respect to concrete (Mihashi and Leite 2004). Although the mechanism of creep is not well understood, it is believed that concrete creep is caused by the response of CSH gel to the applied stress and redistribution of adsorbed water from CSH to the capillary pores (Mindess et al. 2003).

Creep is influenced by many of the same parameters as drying shrinkage. It is believed that this is because one possible mechanism for creep is water movement through the pore system, similar to a dashpot (Mehta and Monteiro 2006; Mindess et al. 2003). Like all concrete mechanical properties, the magnitudes of creep and stress relaxation depend on the degree of hydration. Creep and Stress relaxation are high at the beginning of hydration and decrease sharply as hydration proceeds.

The effect of stress relaxation on concrete stress is illustrated in Figure 2-4 below (Ruiz et al. 2005). It is evident that stress relaxation has to be taken into account for accurate prediction of cracking potential.

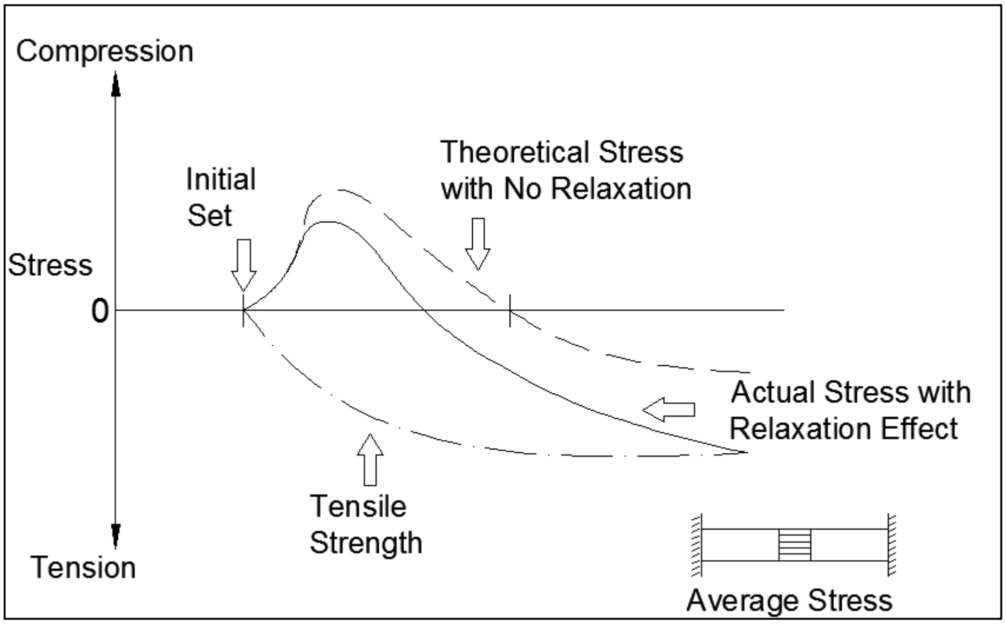

Figure 2-4: Conceptual effect of creep/relaxation on concrete stresses (adapted from Ruiz et al. 2005)

2.3 Methods to Measure Thermal Volume Changes

2.3.1 *Temperature Rise*

As discussed previously, hydration of cement is an exothermic process, which evolves from the chemical and physical reaction between portland cement and water (Bien-Aime 2013; Ferraro 2009; Mindess et al. 2003). De Larrard et al. (1994) indicated that for ordinary portland cement, 150 to 350 joules, per gram of cement, is released during the early stages of hydration. Nevertheless, concrete continues to generate heat well beyond the setting period. According to Gotfredsen and Idorn (1986), at complete hydration, every gram of portland cement has generated 400 to 500 joules, resulting in an adiabatic temperature rise from 60 to 80 °C in the concrete mixture. The temperature rise in a concrete element is controlled by heat balance between heat generated and heat lost to the surroundings. Consequently, the temperature rise associated with the hydration process may lead to excessive temperature differential between the concrete element and its environment, which can result in cracking. The type and amount of cementitious material, initial concrete temperature at placement, ambient temperature, boundary conditions of the structure, and solar radiation intensity affect the temperature development (Schindler and McCullough 2002).

According to ACI 207.2R-07 (ACI Committee 207 2007), the temperature development of the concrete mixture has a significant effect on the cracking observed in a concrete element. At some point in time, because of a deceleration in the amount of heat produced or cooling of the concrete from the environment, the concrete temperature will decrease after an initial rise from the heat of hydration. This decrease in temperature will be accompanied by a shift from compressive stresses to tensile stresses. A continued decrease in concrete temperature could possibly lead to tensile stresses that are greater than the tensile strength of the element. That is, thermal stresses associated with the rate of temperature drop can exceed the tensile strength of concrete, thus leading to cracking.

Concerns over thermal volumetric changes leading to cracking in concrete members were behind a number of studies aimed at understanding the thermal properties of concrete and providing measurement or prediction methods for the temperature rise associated with cement hydration. Ferraro (2009) suggested that for many field applications, an accurate method should be used to predict the temperature distribution and stresses in mass concrete. Poole et al. (2007) also concluded that in-place temperature measurements should be made to characterize the combined effect of time and temperature on concrete properties. It was concluded that adiabatic temperature rise in concrete mixtures is the most representative means of characterizing the temperature rise in the concrete element. The rate of hydration and the hardening process are influenced by concrete temperature. It has been recognized that the size of a concrete member will also have a significant effect on the extent of temperature rise and, therefore, the potential for cracking. In order to predict the thermal volumetric changes in a concrete element, it is necessary to determine the heat generated by cement on hydration. Also, there is a growing interest in the determination of the activation energy through heat of hydration measurements, in order to predict the performance behavior of concrete as it relates to the hydration process (Poole 2007; Riding et al. 2011). The literature indicates that heat of hydration is an important factor that affects setting and behavioral characteristics of portland cements (Ma et al. 1994a).

Several attempts have been made to measure the heat associated with cement hydration, and ultimately its use to understand and predict the behavior of cementitious systems. The science behind the measurement of the heat of reactions is referred to as calorimetry. A number of methods and systems have been developed over the years to capture and measure this heat, namely, adiabatic calorimetry (no heat transfer through system), semi-adiabatic calorimetry (some heat loss by system), and isothermal calorimetry (no temperature change). An isothermal conduction calorimeter is used to measure the heat released by a cementitious system while temperature is maintained constant. The amount of heat generated during the reaction of cement with water is referred to as heat of hydration. Hewlett (1998) and Mindess et al. (2003) concluded that the kinetics of hydration differ for different cements based on their constituents and characteristics. At early ages, the kinetics of hydration is also dominated by the contents of C_3S, C_3A, and gypsum, and by the cement fineness.

For several years, the heat of solution method (ASTM C186) has been the accepted method to measure the heat of hydration of cement, but isothermal conduction calorimetry is now being used as an alternative that gives comparable results. Hewlett (1998) reported that isothermal calorimetry gave a good separation of the hydration reactions for the different cement minerals present. Several researchers have since proposed models aimed at predicting the heat evolved during hydration (Schindler 2002; Sedaghat et al. 2011). Besides, it offers the ability to fix the curing temperature and provides a suitable description of the influence of temperature on the rate of hydration in mass elements (Kada-Benameur et al. 2000; Schindler 2002).

Prior studies (D'Aloia and Chanvillard 2002; Ferraro 2009; Ishee 2011; Kada-Benameur et al. 2000; Ma et al. 1994b; Poole 2007; Schindler and Folliard 2005; Schindler 2002; Xiong and Van Breugel 2001) indicate that isothermal calorimetry can be used to determine activation energy for use in degree of hydration and heat generation calculations. The latter can subsequently be used in conjunction with additional heat measurements on semi-adiabatic and adiabatic systems to predict the temperature rise in concrete elements (Schindler 2002).

As mentioned previously, the thermal stresses due to temperature gradients in concrete elements can contribute to cracking. A major objective in a heat diffusion or conduction analysis is to determine the temperature distribution in a medium based on its essential and natural boundary conditions. The heat diffusion shown in Equation 2-4 provides the basic tool for heat conduction analysis in Cartesian system (Muneer et al. 2003).

$$\frac{\partial}{\partial x}\left(k\frac{\partial T}{\partial x}\right) + \frac{\partial}{\partial y}\left(k\frac{\partial T}{\partial y}\right) + \frac{\partial}{\partial z}\left(k\frac{\partial T}{\partial z}\right) + Q_h = \rho C_p \frac{\partial T}{\partial t} \qquad \text{Equation 2-4}$$

where

T = Temperature (°C),
k = Thermal conductivity (W/m/°C),
Q_h = Rate of heat generation (W/m^3),
ρ = Density (kg/m^3), and
C_p = Specific heat capacity (J/kg/°C)

From the solution of Equation 2-4, the temperature distribution T (x, y, z) can be obtained as a function of time. The equation represents the fundamental law of conservation of energy, where the energy transfer by conduction in a unit volume and the rate of thermal energy generated must be equal to the change of energy stored within the volume. That is, concrete temperature development during the hydration process is determined by: a balance between the heat generated from the concrete mixture and the heat exchanged with its surroundings. According to Khan et al. (1998), the heat generated during hydration is a material property; likewise, the heat dissipated is a function of the type of formwork, exposed surface area, and the ambient conditions of the surroundings. Schindler also noted that on the properties side, cement composition and amount, fineness, water-to-cement ratio, and types and amounts of admixtures are part of a long list of parameters affecting concrete hydration and potential for temperature rise. Furthermore, ambient air temperature, wind speed, relative humidity, solar radiation, and clouds are uncontrolled field parameters that affect the heat dissipation, and should be accounted for in the prediction models of in-place concrete properties (Riding et al. 2011; Schindler 2002).

Strength development of concrete, with a given composition, is a function of its age and temperature. This combined effect of time and temperature on strength can be expressed as maturity, which is a mathematical model or quantitative tool for estimating strength gain in an element based on the temperature history of a particular mix design (Popovics 1998). The maturity concept was proposed in the late 1940s and early 1950s. Carino (1991) provided a historic timeline of the maturity concept and maturity functions. These functions are used to translate the measured temperature history of concrete into a numerical index, which serves as an indicator for strength gain (Carino and Tank 1992). In fact, ASTM C1074 “Standard Practice for Estimating Concrete Strength by Maturity Method” provides two maturity functions. The first, Equation 2-5, was proposed by Saul (Saul 1951).

$$M = \sum (T-T_o)\,\Delta t \qquad \text{Equation 2-5}$$

where

M = Maturity (time-°C),

Δt = Time interval (time),

T = Average temperature of concrete over time interval Δt (°C), and

T_o = Datum temperature (°C)

Equation 2-5, also known as the Nurse-Saul function, defines the value of maturity as the total area under the time-temperature history curves of concrete. Saul is credited for recognizing that during early ages, temperature has a greater effect on strength development, while time has the greater effect at later ages, and that ultimately maturity is an approximation. Saul considered the datum temperature to be -10.5°C and suggested that upon setting, concrete will continue to harden or gain strength at temperatures below 0°C; hence, maturity should be calculated with respect to the lowest temperature at which hardening is observed.

The principle of Nurse-Saul implies that mixtures with the same value of maturity will have the same strength irrespective of temperature history. In other words, only a horizontal shift in strength data should be observed; however, at later ages some mixtures will show higher strengths when cured at lower temperatures. This means that concrete cured at higher temperatures that have higher strength at early ages will ultimately be surpassed by the samples cured at lower temperatures, which results in an intersection of the strength curves where the concrete with the higher strength switches. The phenomenon is known as the “cross-over effect” (Carino and Lew 2001; Schindler 2002). There are a few explanations in the literature on the cross-over effect; Verbeck and Helmuth (1968) and Kjellsen and Detwiler (1992) suggested that the cross-over effect exists due to an increase in initial curing temperature. Basically, for the same mixture, the lower curing temperature leads to higher later-age strength, which crosses the strength curve of the higher temperature (Pinto and Schindler 2010). The implication is that the maturity method is limited due to inherent limitations of the strength prediction models; nevertheless, for several applications, the accuracy of modeling the long-term strength development is not a concern, as the maturity method is only used for monitoring early-age strength development (Carino and Lew 2001).

The second function that has been proposed defines maturity as an equivalent age (Equation 2-6) based on a reference temperature and activation energy.

$$t_e(Tr) = \sum_{t=0}^{t} e^{\frac{-E_a}{R}\left(\frac{1}{273+Tc}-\frac{1}{273+Tr}\right)} \Delta t \qquad \text{Equation 2-6}$$

where

t_e (Tr) = equivalent age at the reference curing temperature (hours),

T_c= temperature of concrete during time interval Δt (hr), (°C),

Tr= reference temperature, °C

E_a= activation energy from isothermal strength development (J/mol), and

R= universal gas constant, 8.3144 J/(mol K)

The equivalent age is defined as the curing age at a constant standard temperature (Tr) that results in the same maturity and the same strength as when cured at a given temperature for a given mixture. The concept was introduced by Freiesleben Hansen and Pedersen (1977) to model the effect of time and temperature on hydration under isothermal curing condition at a specific reference temperature (Tr). The value of 22 ± 1°C is typically used as reference temperature. Carino (1991) concluded that the equivalent age function reflects the behavior of concrete better than the Nurse-Saul Equation. The accuracy of the equivalent age function depends on the accuracy of the activation energy value. ASTM C1074 provides procedures for the quantification of the activation energy based on strength development for mortar mixtures prepared at three different temperatures. Another method was proposed for determining the activation energy based on measurements of the heat generated during hydration using isothermal calorimetry at different temperatures. However, the equivalence of the activation energy based on those two different techniques has been questioned in the literature (Bien-Aime 2013; Ishee 2011; Poole 2007). This is because the strength is dependent on physical and chemical parameters, while the heat of hydration is dependent on chemical parameters.

The term “activation energy” was first introduced in 1889 by the Swedish scientist Swante Arrhenius as the energy that must be supplied to a system for reactions to occur (Laidler 1969). In chemistry, activation energy (E_a) is defined as the minimum energy required for reacting species to form an activated complex. In the cement industry, activation energy is defined as the parameter that best describes the temperature sensitivity of the hydration process (Poole 2007; Schindler 2002). Experimentally, Equation 2-7, known as the Arrhenius equation or the Arrhenius law, has been used to determine the activation energy.

$$k = \mathrm{A}\,\mathrm{e}^{-\left(\frac{\mathrm{E_a}}{\mathrm{RT}}\right)} \text{ or } \ln k = -\frac{\mathrm{E_a}}{\mathrm{RT}} + \ln \mathrm{A} \qquad \text{Equation 2-7}$$

where

k = Specific rate of reaction (typically $s^{-}1$ for 1st order reaction),

A = Pre-exponential term (same unit as k),

E_a = Activation energy (kJ/mol),

R = Universal gas constant, 8.314 J/(mol K), and

T = Temperature (K)

The Arrhenius equation indicates an exponential temperature dependence for the rate of reactions. Recently, the term “apparent” activation energy has been used to reflect the fact that contrary to the idea of a simple chemical reaction implied by the Arrhenius law, the hydration of cement is more complex and the term needs to reflect the interdependence of various reactions and components alike (D’Aloia and Chanvillard 2002; Kada-Benameur et al. 2000; Kjellsen and Detwiler 1993; Wirquin et al. 2002).

The concept of activation energy (E_a) has been used extensively to predict equivalent age, strength, heat evolution, heat dissipation, and thermal cracking. It defines the relationship between reaction rates and curing temperature, and quantifies the amount of energy required for reactions to take place in a given system. Research efforts have shown that chemical and physical properties of cement affect the activation energy and ultimately cement performance. However, there is no consensus in the literature about the proper method of determining activation energy or what value should be used for a particular application. That is, whether there is any equivalence between the activation energy determined from strength development and that assessed through heat of hydration measurements.

Bien-Aime (2013) reported a summary of the E_a values in the literature which are associated with both data sources and using different quantification tools. These values range from 23 kJ/mol to 80 kJ/mol for Type I cement, 31 kJ/mol to 55 kJ/mol for Type I/II cement, and 33 kJ/mol to 50 kJ/mol for Type III cement. Bien-Aime (2013) also examined cements with varying mineralogical composition and fineness, and found that the activation energy is a strong function of cement chemistry and mechanical properties. For instance, for the same cement type, the activation energy is lower at higher fineness; additionally, higher activation energy values have been reported when calculated from strength-based measurements than heat of hydration measurements performed on paste (Bien-Aime 2013; Ferraro 2009; Ishee 2011).

Research efforts also suggested that discrepancies in E_a values can be explained by often neglected factors such as inaccurate material characterization and errors in prediction models or limited variation in mineralogical composition (Ishee 2011; Schindler 2002). Previous research indicated that Bogue estimation of cement compounds is not as accurate as Rietveld analysis, with the latter yielding the actual mineralogical content of cements (Stutzman 2005; Taylor 1997). That is, XRD analysis provides better quantification of the cement mineralogical content resulting in a more accurate prediction of its performance.

There are two main procedures for determining the activation energy; namely, strength-based or heat of hydration-based using isothermal calorimetry. Strength-based measurements are outlined in Annex A1 of ASTM C1074. The procedure is well investigated in the literature. Currently, two functions are being used to determine the necessary parameters to quantify the activation energy based on at least 3 isothermal curing temperatures. The first one is an exponential function (Equation 2-8) proposed by Freiesleben Hansen and Pedersen (1977) and the second one is a hyperbolic function presented in Equation 2-9 (Barnett et al. 2006; Carino and Tank 1992; Carino 1991; Ferraro 2009; Ishee 2011; Pinto and Schindler 2010):

$$S = S_u\, e^{-(\frac{\tau}{t})^{\beta}} \qquad \text{Equation 2-8}$$

where

S = Average compressive strength at age t (MPa),

t = Test age (days),

S_u = Limiting strength (MPa),

τ = Time constant (days) [1/k in the hyperbolic function], and

β = Curve shape parameter (dimensionless)

$$S = S_u \frac{k(t-t_0)}{1+k(t-t_0)} \qquad \text{Equation 2-9}$$

where

S = Average compressive strength at age t (MPa),

t = Test age (days),

S_u = Limiting strength (MPa),

k = Rate constant or rate of reaction (days^{-1}), and

t_o = Age at which strength development is assumed to begin (days)

The parameters (S_u, k, t_o,, β, & τ) for both functions are determined using computer software such as the solver function in Microsoft Excel, as detailed in the works of Bien-Aime (2013), Ishee (2011), Ferraro (2009), and Poole (2007). The software uses least squares to optimize the best-fit parameters through the measured strength versus age data at various curing temperatures. Once these parameters are determined, the activation energy is quantified, using the Arrhenius law (Equation 2-4), using the linear relation between the natural logarithm of rate constants (k or $1/\tau$) and the reciprocal of the isothermal curing temperatures. As displayed in Figure 2-5, Equation 2-4 is the equation of a straight line ($Y = mx + b$). The negative of the slope ($Q = -E_a/R$) is the value of the activation energy (E_a) divided by the universal gas constant (R). The activation energy obtained from strength development is primarily used in determining early-age concrete maturity-strength relationship via the equivalent age concept.

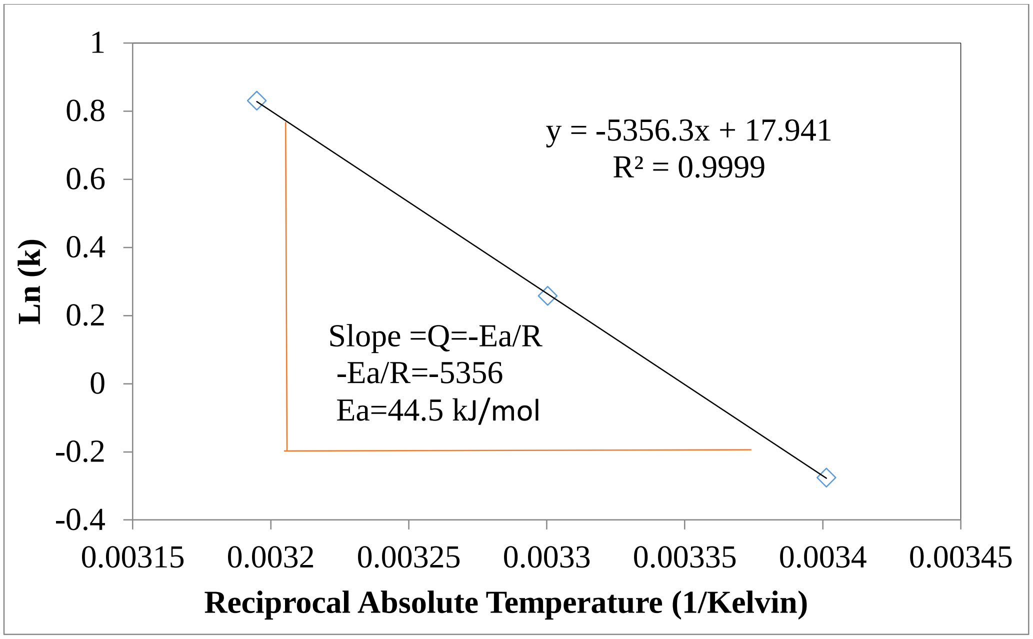

Figure 2-5: Sample Arrhenius plot used to quantify the E_a (kJ/mol)

The activation energy is an important parameter in enabling the prediction of equivalent age, temperature development, and thermal cracking for a concrete structure. In the modified ASTM method C1074, an exponential function (Equation 2-10) is used to characterize cement hydration. This is done by fitting the function through the estimated degree of hydration data to determine the best-fit parameters (α_u, τ, β) at each isothermal curing temperature. Subsequently, the rate of heat development is calculated for each temperature as the inverse of the time constant (τ). The rate constants are then plotted against the reciprocal of the curing temperatures creating a linear relation. The negative slope of that line times the universal gas constant give the activation energy as defined by the Arrhenius relation.

$$\alpha\,(t) = \alpha_u\, e^{-\left(\frac{\tau}{t}\right)^{\beta}} \qquad \text{Equation 2-10}$$

where

$\alpha(t)$ = Degree of hydration at age t,

α_u = Ultimate degree of hydration,

τ = Hydration time parameter (hours),

t = Elapsed time since cement–water interaction (hours), and

β = Shape parameter (dimensionless)

In brief, Equation 2-10 represents the exponential method or Modified ASTM C1074; it was formulated by Poole et al. (2007) based on previous research conducted by Kada-Benameur et al. (2000), Xiong and Breugel (2001), D'Aloia and Chanvillard (2002), Schindler (Schindler 2002), and Schindler and Folliard (2005) on relating calorimeter work to activation energy of cementitious materials. The method follows the same procedures outlined in ASTM C1074 for strength data except the data are based on heat of hydration measurements. Several studies confirm that the method provides reasonable results for a number of prediction models (Ferraro 2009; Ishee 2011; Poole 2007; Riding et al. 2011; Schindler 2002).

For a given system, an adiabatic process is any process in which there is no heat gain or loss (Poole et al. 2007; RILEM Technical Committee 119-TCE 1998). Due to the complexity and cost associated with achieving adiabatic temperature under laboratory setting, several researchers have indicated that the semi-adiabatic system was a simpler and more cost-effective tool in obtaining the adiabatic parameters ($\alpha_{u,}$ τ, β) of a concrete mixture (Poole et al. 2007; Riding et al. 2012). RILEM 119 (RILEM Technical Committee 119-TCE 1998) defines a semi-adiabatic calorimeter as a calorimeter where the maximum heat losses are less than 100 J/(h·K). Poole (2007) provides a detailed and iterative procedure of converting the measured semi-adiabatic temperature rise into adiabatic temperature. A summary of the necessary properties and procedures is provided in the following steps:

1. Determine the following equipment and materials properties
   A. Calibration factor (C_{f1}, C_{f2}) of semi-adiabatic calorimetry
   B. Mineralogical composition of the cement (C_3S, C_2S, C_3A, C_4AF, SO_3, and MgO from XRF or XRD, to enable calculation of total available heat H_u)
   C. Activation energy (E_a) calculated from isothermal testing on paste from at least 3 temperatures or estimated using E_a models (J/mol or kJ/mol)
   D. Specific heat capacities for
      - Cement: (Cp =1140 J/(kg °C)
      - Water: Cp=4186 J/(kg °C) at room Temperature (Need for mix and calibration)
      - Coarse and fine aggregates
   E. Mix Design proportion (ACI 211.1(ACI Committee 211 2009)) (Cement, CA, FA, Water, Admixtures)

2. Prepare concrete specimen
    1. A. Proportion mix per ACI 211.1 (ACI Committee 211 2009) or as provided
    2. B. Mix concrete in accordance with ASTM C192
    3. C. Record room/mixing location temperature, relative humidity
    4. D. Record the initial time and date of mixing (Time of initial contact of water with cement)
    5. E. Measure air content per ASTM C231
3. Run semi-adiabatic test

   This is done to obtain actual temperature rise, heat flux or temperature difference of the mixture.

    1. A. Mold specimen using 6 x 12 in. cylinder
    2. B. Weigh the Sample
    3. C. Insert sample into semi-adiabatic drum
    4. D. Insert thermocouple/temperature probe 6 inches into the top-center of the 6 x12 cylinder to measure the temperature rise, temperature difference or heat flux at specified time interval
    5. E. Record data at the desired time intervals (Record the time and date of initial measurement, typically 5-minute time interval for low curing temperature 23.0±2 ºC)
4. Calculate the adiabatic temperature using cement hydration parameters (α_u, β, τ)

Fitting the cement hydration parameters is done by fitting the measured semi-adiabatic temperature to the concrete semi-adiabatic temperature calculated for the trial hydration parameters and the heat loss (Schindler 2002). The equivalent age concept used in these calculations are similar to Equation 2-6 except that the activation energy (E_a) is obtained from heat of hydration measurements made on paste mixtures using isothermal calorimetry as shown in Equation 2-6.

Next, the process of hydration under adiabatic condition is quantified using the concept of the degree of hydration (α), (Equation 2-11) which is a measure of the fraction of cement that has reacted (Mindess et al. 2003). The value of α varies from 0 to 1, where $\alpha = 0$ means that no reaction occurred and $\alpha = 1$ indicates complete hydration (RILEM Technical Committee 42-CEA 1981). Consequently, for isothermal or adiabatic calorimetry, Poole et al. (2007) indicated that the degree of hydration can be taken as the ratio of the measured cumulative heat released by the mixture at a given time "t" [H(t)] to the total available amount of heat (H_u) calculated from the cementitious chemical properties. It was concluded that while the hydration of cement is based on several simultaneous reactions and that it was not possible for a single parameter to describe this phenomenon completely, the degree of hydration was adequate in describing it (Van Breugel 1991; Schindler 2002).

$$\alpha(t) = \frac{H(t)}{H_u} \qquad \text{Equation 2-11}$$

where

α(t) = Degree of hydration at time (t),

H(t) = Heat evolved from time 0 to time t (J/gram), and

H_u = Total available heat (J/gram)

The total available heat (H_u), Equation 2-12, is quantified as a function of cement composition, the amount of the phase, and type of supplementary cementing materials present in the system (Poole et al. 2007; Schindler and Folliard 2005).

$$H_u = H_{cem}\, P_{cem} + 461\, P_{slag} + 1800\, P_{FA\text{-}CaO\cong} P_{FA} \qquad \text{Equation 2-12}$$

where:

p_{slag} = Ratio of slag mass to total cementitious content,

p_{FA} = Ratio of fly ash mass to total cementitious content,

$p_{FA\text{-}CaO}$ = Ratio of CaO mass in fly ash to total fly ash content,

p_{cem} = Ratio of cement mass to total cementitious content, and

H_{cem} = Heat of hydration of the cement (J/gram).

In addition, the heat of the hydration of the cement (H_{cem}) is function of cement chemistry and is calculated in Equation 2-13:

$$H_{cem} = 500\, PC_3S + 260\, PC_2S + 866\, PC_3A + 420\, PC_4AF + 624\, PSO_3 + 1186\, P_{FreeCaO} + 850\, P_{MgO} \qquad \text{Equation 2-13}$$

where

H_{cem} = Total heat of hydration of portland cement as describe above (J/gram) and

p_i = Ratio of mass of ith component to total cement content obtained from XRF or XRD.

Equation 2-13 is the algebraic sum of the heat of hydration of the individual compounds of a particular cementitious material at complete hydration (Bogue 1947; Lerch and Bogue 1934).

Bogue concluded that the principal source of thermal change, which occurs during the hydration of cement, is the sum of the heat of solution of the several anhydrous compounds and heat from the precipitation of hydrates from the solution. A three-parameter relation (Equation 2-10) is then used to characterize cement hydration from the heats of hydration determined from semi-adiabatic testing.

Finally, the rate of heat evolution (Equation 2-14) for a given concrete mixture can be quantified using a combination of Equations 2-6, 2-10, and 2-11 (Riding et al. 2012;. Schindler and Folliard 2005).

$$Q_h(t) = H_u \; C_c \; \left(\frac{\tau}{te}\right)^{\beta} \left(\frac{\beta}{te}\right) \alpha_u \, e^{-\left(\frac{\tau}{te}\right)^{\beta}} \; e^{\frac{Ea}{R}\left(\frac{1}{Tc+273}+\frac{1}{Tr+273}\right)} \qquad \text{Equation 2-14}$$

where

$Q_h(t)$ = Rate of heat generation (W/m^3),

H_u = Total heat available per mass of cementitious content (J/Kg),

C_c = Cementitious content of concrete mixture (Kg/m^3),

E_a = Activation energy obtained from isothermal calorimetry on paste (J/mol),

α_u = Ultimate degree of hydration (dimensionless),

τ = Hydration time parameter (hours), and

β = Hydration curve slope parameter (dimensionless).

The parameters α_u, β, and τ are changed until the difference between the simulated concrete cylinder temperature that included the temperature loss and measured concrete cylinder temperature in the calorimeter is minimized. The concrete cylinder temperature loss from cooling during the test can be calculated using Equation 2-15.

$$\Delta T = Q_h(t)\, \Delta t \,/\, (\rho \;\, C_p) \; (°C) \qquad \text{Equation 2-15}$$

where

$Q_h(t)$ = Rate of heat generation (W/m^3),

Δt = time interval (hour),

ρ = unit weight of concrete mixture (kg/m^3) in the calorimetry, and

C_p = current specific heat of the concrete mixture [J/(kg≅ºC) as given by Equation 2-16 (Schindler 2002, Poole 2007):

$$C_p(\alpha) = \frac{1}{\rho}\ [W_c\alpha(t_e)\ C_{cef} + W_c\ \ (1 - \alpha\ (t_e))\ C_c + W_aC_a + W_wC_w] \qquad \text{Equation 2-16}$$

where

W_c, W_a, W_w = amount by weight (kg/m^3) of cement, aggregate, and water, respectively,

C_c, C_a, C_w = specific heat [J/(kg·ºC)] of cement, aggregate, and water, respectively, and

C_{cef} = 8.4T_c + 339 [J/(kg·ºC]; fictitious specific heat of the hydrated cement.

While semi-adiabatic calorimetry is used extensively in the research community, there is no established standard or bias on the test results (Ferraro 2009; Poole 2007; Schindler 2002; Weakley 2010). Recently, Riding et al. (2012), using semi-adiabatic testing on 6 x 12 in. concrete cylinders, proposed a model to predict the adiabatic temperature rise in concrete mixtures based on the material properties, mixture proportions, and admixtures types and dosages. Overall, the ability to measure the adiabatic properties of concrete mixes is imperative in monitoring the cracking potential of concrete structures.

In many respects, previous research indicates that many aspects of cement chemistry influence the activation energy, including C_3S, C_2S, C_3A, and C_4AF contents, and Blaine fineness. This understanding comes from the underlying effect of these factors on strength development and heat generated during the hydration process, or simply stated, on the hydration kinetics. The effect of cement composition on the activation energy has not been studied extensively in the literature, especially as related to maturity method. And yet, the concept is well-understood for strength development and rate of heat of hydration, which are primarily used to quantify activation energy. It has been established that all clinker phases contribute to strength development and heat of hydration; but the extent of their individual contributions differs. For example, C_3S, which is the most abundant phase in portland cement clinker, is responsible for early strength gain, whereas C_2S has its primary influence on long-term strength. In general, cements with high C_3S content hydrate more rapidly and have higher early strength (Mindess et al. 2003). However, cements with high C_2S exhibit much slower hydration rate and higher long-term strength.

The contributions of C_3A and C_4AF are relatively complex. Mindess et al. (2003) suggested that while C_3A and C_4AF compete for sulfate ions, C_3A is much more reactive than C_4AF. The behavior of C_3A is controlled by sulfate content (SO_3) and C_3A generates a great amount of heat during its hydration, but its contribution to strength is low (Juenger et al. 2011). (Lerch and Bogue 1934) advanced that cement continues to evolve heat during hardening for at least 6 months, but a great portion develops by the end of 3 days, and that ultimately the rate of heat liberation depends on the chemical composition of the cement. The consensus in the literature is that the order of phases, in terms of their contribution to heat generation in the first few days, is: $C_3A>C_3S>C_4AF>C_2S$.

D'Aloia and Chanvillard (2002) pointed out that mineralogical composition not only plays a major role in the rate of hydration or strength gain, but also influences the activation energy. Riding et al. (2011) concluded that C_3A and C_4AF increase E_a. The implication is that cement with high alumina content will generate a greater amount of heat in the early ages, which affects temperature rise in the concrete and increases the cracking potential.

Review of the literature has illustrated that several aspects of concrete behavior are influenced by the fineness and phase composition of its cementitious constituents. The most prominent trend is that an increase in fineness increases the rate of hydration and rate of strength gain, as more surface area becomes available for the reaction (Maekawa et al. 1999). Consequently, any increase in heat increases the temperature of the mixture and therefore increases the potential for cracking. Also, cements with higher fineness exhibit lower activation energy (Bien-Aime 2013).

There is controversy in the literature about the exact effect of the w/c ratio on activation energy. The values reported by Carino (1991) showed that lowering the w/c resulted in an increase in E_a; yet, Barnett et al. (2006) used two different w/c ratios and observed no significant change in E_a. Poole (2007) concluded that increasing the w/c ratio increases the rate of hydration, thus resulting in lower activation energy. The implication here is that the effect of w/c ratio on E_a is minimal as compared to other factors such as composition or fineness.

Understanding the effect of admixtures on cementitious systems requires a fundamental review of their mechanisms of action and their constituents. An admixture is defined in ASTM

C125 and ACI 116 (ACI Committee 116 2009) as: “a material other than water, aggregates, hydraulic cementitious, and fiber reinforcement that is used as an ingredient in a cementitious mixture to modify its freshly mixed, setting, or hardening properties and that is added to the batch before or during its mixing”. This definition covers both mineral and chemical admixtures. However, this research deals with commonly used chemical admixtures that are added to concrete used in pavement slab replacement in the state of Florida, such as air-entraining admixtures (AEA), water-reducing admixtures (WRA), workability aids, retarding admixtures, and accelerating admixtures (ACI Committee 212 1991). In general, specifications for the different types of chemical admixtures are provided in ASTM C494, and AASHTO M 194. Additionally, air-entraining admixtures are specified in ASTM C260 and AASHTO M 154. A brief review on the effects of chemical admixtures on concrete properties will be presented next.

Air entrainment is added to concrete to primarily control freezing and thawing and improve workability (Mehta and Monteiro 2006; Mindess et al. 2003; Whiting and Nagi 1998). Air entrainment has become an important factor in concrete technology based on the extensive testing and field investigation conducted over the past 50 years. A number of organic salts have been used as AEA in the industry. The most notable are salts of wood resins (vinsol resin), synthetic detergents, salts of petroleum acids, fatty and resinous acids and their salts (Kosmatka et al. 2002; Whiting et al. 1993). While there are a variety of AEA available in the market today, vinsol resin-based AEA are the most used.

The findings indicate that organic additives or air-entraining agents (AEA) are responsible for microscopic air bubbles within the fresh concrete mix (ACI Committee 212 1991; Dolch 1995; Whiting and Nagi 1998). A reduction in bleeding and segregation in fresh concrete is observed due to the use of air-entraining agents (ACI Committee 212 1991; Dolch 1995; Rixom and Mailvaganam 1999). The permeability of concrete to aqueous liquids is also reduced slightly by air entrainment. The concrete is more resistant to sulfate attack and is better protected against corrosion of the embedded steel reinforcement (ACI Committee 212 1991; Rixom and Mailvaganam 1999). However, the major application of AEA is to improve the resistance of concrete to freeze–thaw cycling, especially in the presence of de-icing salts (Rixom and Mailvaganam 1999).

The effect of AEA on volume change due to drying shrinkage has not been studied well. Rixom and Mailvaganam (1999) concluded that AEA does not increase the drying shrinkage of concrete, and Bakharev et al. (2000) also indicated that AEA have no adverse effect on shrinkage. However, air entraining agents are responsible for a marginal increase in creep over time due to higher air content (>6%) (Rixom and Mailvaganam 1999). Because of possible incompatibility (precipitation makes admixtures less effective), air-entraining agents should not be mixed with admixtures containing calcium chloride, but should be added separately (Dolch 1995; Du and Folliard 2005). In addition, ambient temperature has a significant effect on air-entrainment effectiveness, and the variation in entrained air is such that it is inversely proportional to temperature (Kosmatka et al. 2002). That is, more air content is expected at lower temperature for a given dosage of AEA. Additionally, an increase in cement fineness, or an increase in fine fraction of fine aggregates, or dust in coarse aggregates will decrease air content at a specific air-entraining dosage (Du and Folliard 2005).

Water-reducing admixtures (WRA) are classified under ASTM C494 (AASHTO 194) as Type A. They are added to concrete to improve properties (strength, durability) and achieve workability when low w/c is used (ACI Committee 212 1991). The basic role of water reducers is to deflocculate the grouped cement particles and release the water tied up in these agglomerations, which produces a more fluid paste at lower water contents (Collepardi 1995). The mode of action of water reducers involves the absorption onto the early hydration products of C_3A and C_3S. Typically, water reducers contain lignosulfates (lignin), hydroxylized carboxylic acids, and some other carbohydrates (polymers). They have been used primarily in bridge decks, low-slump concrete overlays, and patching concrete.

When water reducers are used for the purpose of lowering water content, a typical increase of about 25 % in compressive strength is anticipated (Mindess et al. 2003). The water content is reduced by 5 to 10 % at a normal dosage of 0.1% per weight of cement (Mindess et al. 2003). The upper limit of the dosage depends on the application and recommendations of the manufacturer. Increased attention needs to be placed on curing and protection due to the potential for cracking and fluctuation of the bleeding rate when water reducers are used. The bleeding rate is a function of the type of chemical used in the water reducing agents. Rixom and Mailvaganam (1999) found that lignosulfonate-based reducers increased air content which decreased bleeding, while hydroxycarboxylic-based reducers increased the rate of bleeding. It was also indicated that in hot and windy surroundings, the rate of evaporation could exceed the bleeding rate, resulting in plastic shrinkage cracking in concrete.

ASTM C494 Type B (retarding) and D (water-reducing and retarding) admixtures are known to delay hydration of cement without compromising the long-term mechanical properties. They are used in concrete to offset the effect of high temperatures, which decrease the setting times, or to avoid complications when unavoidable delays between mixing and placing concrete occur (Mindess et al. 2003). As a result, they have been used in concrete pavement to enable farther hauling, extend the time of plastic grooving and hand finishing, and eliminate cold joints (Kosmatka et al. 2002). When horizontal slabs are placed in sections, retarders are used to provide resistance to cracking resulting from form deflection (Mindess et al. 2003). Type D admixtures are of similar composition to the water reducers, with added retarding materials such as sugars and their derivatives.

Retarders typically lower the rate of hydration of C_3A and C_3S (Cheung et al. 2011; Hewlett 1998; Poole 2007). These admixtures form a film around the cement compounds (by adsorption), thereby preventing or slowing their reaction with water. The thickness of this film will dictate how much the rate of hydration will be retarded; therefore, it is important to guard against overdose to avoid exceeding the critical point where hydration may completely cease (Kosmatka et al. 2002; Mindess et al. 2003). ASTM C494 Type D admixture provides reduction of water content by 8 to 10 % with an addition rate of 3 to 10 fl oz per 100 lbs of cementitious materials. Because of the retarding action, the 1-day strength of the concrete is reduced but the ultimate strength is increased. The rate of drying shrinkage and creep also increases when using retarders, but the ultimate values may not be affected (Mindess et al. 2003). Retarders can accentuate plastic shrinkage by retarding setting unless concrete is protected from loss of moisture. If the concrete has a tendency to crack from plastic shrinkage, these admixtures can aggravate the problem, but if the cracking tendency is due to rapid heat development, they may solve the problem (Collepardi 1995). The same author indicated that WRA affect ultimate drying shrinkage to a small extent. Hydroxylated admixtures increase drying shrinkage at early ages (3-7 days) but this effect decreases over time and even reverses after several months.

ASTM C494 Type C (accelerating) and E (water-reducing and accelerating) admixtures are added to concrete in order to provide a fast set and increase the early strength. Typically, they are liquid-based solutions and contain inorganic compounds such as soluble chlorides, carbonates, silicates, fluorosilicates, and some organic compounds such as triethanolamine (Hewlett 1998). Triethanolamine is often used to counteract the excessive retardation caused by some WRA (Collepardi 1995). Calcium chloride ($CaCl_2$) has been used in concrete since 1885 with its primary application in cold weather concreting (Rixom and Mailvaganam 1999), and it is the most popular choice of accelerator due to its high acceleration rate and low cost. However, in many applications where water-soluble chlorides could potentially reach or exceed the maximum limits specified by ACI 318 (ACI Committee 318 2011), a chloride-free accelerator is used. Furthermore, some state DOTs such as California, prohibit the use of chloride-based accelerators in pavement concrete slabs due to higher shrinkage associated with their use. Non-chloride accelerators (NCA) usually contain calcium nitrate and sodium thiocyanate.

Under normal conditions, calcium chloride is used to speed up the setting and hardening process for earlier finishing or form turnaround. The effects of calcium chloride on concrete properties have been widely studied and quantified. Initial and final setting times of concrete are significantly reduced, but the total effect is a function of dosage, the type of cement, and the mix temperature (ACI Committee 212 1991; Kosmatka et al. 2002). The typical recommended dosage is 8 to 40 fl oz per 100 lbs of cementitious materials (W.R.Grace and Co. 2007). Overall, the compressive and flexural strengths of concrete are substantially improved at early ages, but the long-term strength can sometimes be reduced, especially at high temperatures (Mindess et al. 2003). It has been reported that the drying shrinkage of concrete is increased when using calcium chloride, especially at early ages. The large shrinkage at earlier periods may be attributed mainly to pores size refinement that occurs during hydration. In addition, accelerators increase volume change in concrete under both moist curing and drying conditions due to refined pore structures (ACI Committee 212 1991), thereby increasing the cracking potential of concrete.

In general, temperature rise in concrete containing water reducers and retarders (ASTM Type D) is less at early ages, about the same at 3 days and slightly higher at later ages (Collepardi 1995). The opposite is true for water -reducing and accelerating admixtures (ASTM Type E).

However, the composition and cement content affect the temperature rise more significantly than that due to admixtures.

2.3.2 Coefficient of Thermal Expansion

The coefficient of thermal expansion (CTE) is defined as “the change in unit length per degree of temperature change” (Mehta and Monteiro 2006). In concrete, the CTE is mostly influenced by three factors: the CTE of aggregate, CTE of cement paste, and mix proportions. Neville (2006) states that this parameter is not affected by the air content and suggests only minor effects of cement composition and fineness on CTE, although Mitchell (1953) reported that increasing cement fineness from 1200 to 2700 cm^2/g resulted in a 25% increase in the CTE of paste. The cements used by Mitchell were very coarse by today’s standards, so the effect of fineness remains unclear. Sakyi-Bekoe (2008) reported that the type or fraction of fine aggregate and the w/c ratio only have a minor influence on the CTE of concrete. So, the overall CTE of concrete will be determined mainly by the CTE of coarse aggregate and the CTE of cement paste. Due to its generally high volume in concrete mix, coarse aggregates will have the greatest effect on concrete CTE.

For both coarse and fine aggregates, the CTE is determined by its mineralogy. It has been suggested that thermal expansion of rocks is related to their silica content, with CTE increasing with the silica content (Griffith 1936). The CTE of silica sand is very close to the CTE of paste, which explains why only the effect of coarse aggregate is usually considered. For the typical concrete aggregates, limestone has the lowest CTE, and quartzite has the highest CTE (Emanuel and Hulsey 1977; Mehta and Monteiro 2006). The values reported in the literature for limestone, which is widely used as coarse aggregate in Florida pavements, range from 0.5×10^{-6} microstrain per °F to 6.8×10^{-6} microstrain per °F (Neville 2006). This variability in the reported CTE can be attributed to the differences in the mineralogical composition of the aggregate depending on its source and methods used to measure the CTE. Although it is generally assumed that aggregates expand uniformly in all directions, some studies have shown that carbonate rocks, such as limestone, may exhibit anisotropic thermal expansion that can result in cracking of concrete around the aggregate (Venecanin 1990). When selecting low-CTE aggregate, even though it will result in a lower concrete CTE, one has to keep in mind the expected temperature changes and the thermal compatibility of the concrete components. CTE of aggregate is generally unaffected by the aggregate's moisture content (Emanuel and Hulsey 1977).

There can be a significant difference between the CTE of coarse aggregate and paste. A large difference between the coefficients of thermal expansion of the paste and aggregates can lead to differential thermal volume changes resulting in microcracking at the interfacial transition zone (ITZ) (Hewlett 1998; Neville 2006; Venecanin 1990). The ITZ is the zone of increased porosity, 10-50 nm think, surrounding coarse and fine aggregate as well as any other inclusions, such as fibers or reinforcing steel (Mehta and Monteiro 2006; Mindess et al. 2003). The existence of ITZ is attributed to the "wall effect": the efficiency of cement particle packing is decreased around any inclusion, resulting in a higher local w/cm ratio and a higher degree of hydration (Bernard et al. 2003; Mindess et al. 2003). Accumulation of bleed water around the aggregate also contributes to the higher w/cm ratio and the higher porosity (Mehta and Monteiro 2006).

While these microcracks on their own do not constitute failure, as the concrete is placed under loading conditions or as additional internal stresses are generated, the stresses at the locations of the cracks are going to be significantly higher than the overall stress experienced by the concrete member as a whole. As stresses increase, microcracks will begin to grow in length and become interconnected to form a visible crack. While there is no consensus on the mechanism of rupture, there is general agreement in the literature that failure of normal strength concrete originates in the ITZ and consequently the compressive and the tensile strength of concrete are determined by the quality of the ITZ.

While it may appear that minimizing the ITZ by using low aggregate content and high-cement mixes will improve concrete strength, it has actually been observed that increasing the aggregate content increases both the tensile and compressive strength (Bernard et al. 2003; Van Dam et al. 2005; Stock et al. 1979). Neville suggests that coarse aggregate particles may serve as "microcrack arrestors" by preventing the propagation of microcracks (Neville 2006). Van Dam et al. (2005) point out that increasing cement content leads to increased paste volume and increased paste porosity, which may explain the reduction in strength. Higher paste volume also translates to higher shrinkage potential.

The coefficient of thermal expansion of the paste is generally in the range of 6 x 10^{-6} microstrain per °F to 11 x 10^{-6} microstrain per °F and depends on the moisture content and age of the paste (Neville 2006). CTE increases with the increasing moisture content to a maximum at approximately 60-80% relative humidity inside the paste's pores and then decreases as the relative humidity continues to increase and the pores become completely saturated. It is lowest for a completely saturated paste (100 % moisture content), and is slightly higher for a completely dry paste (0 % moisture content) (Emanuel and Hulsey 1977). The CTE decreases with age due to the increased formation of hydration products with age and the consumption of internal moisture (self-desiccation). Regardless of age, the lowest value for CTE, which is particularly important during initial curing, can be obtained by keeping the concrete saturated (Sellevold and Bjøntegaard 2002). Sellevold and Bjøntegaard (2006b) found that saturated concrete age had no effect on CTE. The CTE of partially-saturated concrete returned to the same value as during final setting after concrete was immersed in water at the age of 11 weeks (Sellevold and Bjøntegaard 2006b).

There are several test methods for measuring the coefficient of thermal expansion of concrete and aggregate. ASTM D5335 utilizes wire and foil strain gages to measure the coefficient of thermal expansion of rocks. Venecanin (1990) suggests measuring CTE on 6" cube specimens cut from coarse aggregate by attaching 4 strain gages on each face of the specimen to account for nonhomogeneous thermal expansion of carbonate aggregates. ASTM C531 provides a specification for measuring the CTE of chemical-resistant mortars, grouts and polymer concrete. This test is limited to a maximum aggregate size of 0.25 in. AASHTO T336 specifies a procedure for determining the coefficient of thermal expansion of hydraulic cement concrete by placing a concrete cylinder into a water bath and measuring the thermal length change of the cylinder with an LVDT.

2.4 Stress Assessment

Stress assessment is an important tool in predicting behavior of field concrete in terms of cracking. ACI report 231R-10 (ACI Committee 231 2010) provides an equation for calculating incremental stress development due to thermal and moisture-related shrinkage as shown in Equation 2-17:

$$\Delta\sigma = (\Delta T \times \alpha_T + \Delta\varepsilon) \times E \times \psi \times R$$ Equation 2-17

where

$\Delta\sigma$ = stress increment (psi),

ΔT = measured temperature change (°F),

α_T = coefficient of thermal expansion (strain/°F),

$\Delta\mathcal{E}$ = strain increment,

E = elastic modulus (psi),

ψ = relaxation coefficient, and

R = degree of restraint.

It is evident from this equation that stresses are not only a function of volume change, but also of concrete mechanical properties: elastic modulus and stress relaxation. Elastic modulus and stress relaxation are, like most mechanical properties of concrete, time-dependent and are largely determined by the degree of hydration. Elastic modulus and development of other mechanical properties is discussed next. Even though Equation 2-17 accounts for two major causes of early-age cracking, a more accurate stress development prediction is sometimes required. For evaluating cracking potential of concrete pavements, all stresses have to be considered, including thermal, plastic, autogenous, and drying shrinkage, as well curling and warping stresses.

2.4.1 Mechanical Properties Development

In order to model and predict concrete pavement failure, the development of age-related properties has to be assessed in addition to temperature development in the concrete element.

2.4.1.1 Compressive Strength Development

Compressive strength is the most widely used concrete property. Historically, required compressive strength has been specified at 28 days. However, with the emergence of set-accelerating admixtures and finer cement grinds, the accelerated construction schedules may require specifying compressive strength at an earlier age. This is especially critical in pavements where on one hand, the specified compressive strength must be achieved prior to opening to traffic in order to avoid damage to the newly placed concrete pavement, while on the other hand it is important to minimize delays and lane closures.

The major factors determining the compressive strength of concrete are water/cementitious materials (w/cm) ratio, cement composition and aggregate type used, and temperature development of the placed concrete. It is well established that for the same type of materials (cement and aggregate type) w/cm ratio will have the greatest effect on compressive strength: decreasing the w/cm ratio increases compressive strength (Mindess et al. 2003; Neville 2006). For early-opening-to-traffic (EOT) pavements, Van Dam et al. (2005) recommend using a w/cm ratio below 0.4 to achieve the required high-early strengths, although they do point out that w/cm below 0.36 can result in increased autogenous shrinkage.

Development of compressive strength in concrete is attributed mainly to the formation of calcium silicate hydrate (CSH) from the hydration of C_3S and C_2S. C-S-H comprises approximately 60% of the hydrated cement paste volume (Mehta and Monteiro 2006). C_3S is responsible for early-age strength gain as it reacts more rapidly, and C_2S determines the strength gain at later ages. Although cement fineness does not affect the ultimate strength of concrete, it does have a major effect on the rate of strength gain – the higher the fineness the higher the rate of strength gain. It has been well established that increased temperature also results in a higher rate of strength gain; however, the ultimate strength in this case is lowered. The use of set-accelerating admixtures increases the rate of hydration and increases concrete temperature, which consequently results in a lower ultimate strength.

2.4.1.2 Tensile Strength

Although compressive strength is often stipulated in the project specifications, it is useful to know the tensile strength of concrete as well. When internal tensile stresses exceed the tensile strength, cracking will occur. As mentioned previously, tensile stresses develop in early-age concrete due to thermal volume change, autogenous shrinkage, and drying shrinkage. Similar to compressive strength, tensile strength increases with time, but at a lower rate (Neville 2006). In addition to age, tensile strength is affected by the fraction of coarse aggregates in the mix, the type of aggregate used, and aggregate grading. As mentioned previously, increasing aggregate content results in improved compressive and tensile strength (Stock et al. 1979). Tensile strength is also affected by curing, even more so than the compressive strength, with inadequate curing resulting in lower tensile strengths (Neville 2006).

There are several different test methods for measuring concrete tensile strength: direct tension, flexure, and splitting (ASTM C496). In addition, flexural strength can be measured with a center-point test (ASTM C293/AASHTO T177) or a three-point test (ASTM C78/AASHTO T97). Several researchers have suggested different mathematical expressions relating compressive strength to the tensile strength (Bortolotti 1990; Oluokun 1991; Raphael 1984). Mehta and Monteiro (2006) state that tensile strength is generally equal to 10-15 % of compressive strength.

In addition to tensile strength, tensile strain capacity may be of interest. It has been suggested that tensile strain capacity can be a better predictor of thermal cracking risk. Mehta and Monteiro (2006) define tensile strain capacity as “the failure strain under tension”. Houghton (1976) suggested that the tensile strain capacity could be estimated by dividing the modulus of rupture by the modulus of elasticity. Swaddiwudhipong et al. (2003) proposed that tensile strain capacity is proportional to the direct tensile strength divided by the modulus of elasticity in tension. It was also proposed that tensile strain capacity does not appear to be affected by compressive strength, age, size or fraction of aggregates, or presence of mineral admixtures.

2.4.1.3 Elastic Modulus

The translation of stresses into strains and vice versa is determined by the elastic modulus of the material. A number of different equations for prediction of elastic modulus development have been presented in the literature relating the elastic modulus to compressive strength or the degree of hydration, generally computed based on the amount of heat evolved during hydration (De Schutter and Taerwe 1996). According to Mindess et al. (2003), the type and amount of aggregate has a significant effect on the elastic modulus. That is, the elastic modulus of concrete is strongly affected by the elastic modulus of the aggregate, which is affected by aggregate porosity (Mehta and Monteiro 2006). At the early stages of concrete modulus development, the effect of the elastic modulus of the aggregate dominates over the effect of the aggregate volume fraction; however, aggregate volume becomes more important at later ages (Bernard et al. 2003).

2.4.1.4 Poisson Ratio

Poisson’s ratio is defined as “the ratio of the lateral strain to the axial strain within the elastic range” (Mehta and Monteiro 2006). Poisson’s ratio decreases during the early stages of hydration as water is being consumed by the hydration reactions. After setting, when water is no longer a continuous phase, Poisson's ratio increases as the concrete begins to stiffen (Bernard et al. 2003). Typical values for concrete are around 0.15-0.20 (Mehta and Monteiro 2006).

2.4.1.5 Maturity Relationship Applied to Mechanical Properties

It is possible to estimate the in-place concrete compressive strength by applying the maturity method if a maturity-strength relationship has been previously developed for the concrete mixture. Since the curing conditions in the field are different from the lab-cured cylinders, the cylinder compressive strength may differ from that of the in-place concrete. The maturity method has gained popularity in recent years, as it is fast, inexpensive and non-destructive. Maturity testing is frequently used to determine the appropriate time for formwork removal, joint saw-cutting, and allowing traffic on concrete pavements. Maturity curves have to be established for each concrete mix, either in the laboratory in advance of concrete placement or at the beginning of concrete placement. Maturity curves are not universal; any variation in the materials or in the mixing procedures and equipment will result in different maturity curves. It should be noted that the maturity method cannot account for the effects on concrete strength of variations in the field placement techniques or curing procedures.

Prior to concrete placement, temperature sensors are embedded in the structure for monitoring the actual in-place concrete temperature profile. The sensors are monitored by the maturity meters, which calculate the in-place concrete maturity. This maturity value is then used to estimate the in-place compressive strength based on the maturity curves established at the beginning of the project (Smith 2005). Olek et al. (2002) reported a good correlation between maturity and flexural strength of concrete. They used the maturity data to estimate the modulus of rupture for deciding the appropriate time for opening the pavement to traffic.

2.4.2 Free Shrinkage Measurements

2.4.2.1 ASTM Method for Mortar Autogenous Shrinkage

ASTM C1698 provides a test method for measuring the autogenous strain in order to evaluate the early-age cracking potential for mixtures with w/cm below 0.4. This test method allows for testing cement pastes or mortars, including chemical or mineral admixtures, or both. The paste or mortar is placed into a corrugated plastic mold that is sealed on all sides. The mold provides negligible restraint allowing the specimen to expand or contract freely. The length change of the specimen is measured using a dilatometer starting at setting time and up to a specified age. The specimens are kept at a constant temperature and are free from external forces. At the end of the test, the autogenous strain is calculated based on the initial length of specimen at the time of setting and the final length at the specified time t. Although this standard mentions that the autogenous strain of concrete is expected to be lower than that observed in the mortar, and the strain in the mortar is going to be lower than in the paste, it does not provide a method for correlating the strain observed in mortar or paste to that expected in concrete. It also does not provide guidelines on maximum strain above which cracking is likely to occur at a particular age. A model for predicting the ultimate shrinkage of concrete based on test results for paste has been proposed by Hansen and Almudaiheem (1987).

2.4.2.2 ASTM C157 for Drying Shrinkage

The procedure for evaluating drying shrinkage potential is outlined in ASTM C157. This procedure is applicable to both mortars and concretes. Specimens are demolded after 24 hours and are cured in lime water for 28 days. The initial length readings are taken with a comparator both after demolding and at the end of the curing period, after which the specimens are stored at a constant temperature and relative humidity. Length change of specimens is measured up to 64 weeks.

2.4.2.3 Free Shrinkage Methods Used in Literature

Other methods besides ASTM C157 and ASTM C1698 of measuring concrete cracking potential have been discussed in the literature. The free-deformation frame (Slatnick et al. 2011) allows for measurement of autogenous shrinkage stresses for unrestrained concrete specimens. In this method concrete specimens are sealed to prevent drying and the temperature of the surroundings is matched to the temperature of the concrete to prevent thermal volume changes. After the specimen sets, steel plates that are used as forms are removed from the specimen and the specimen is allowed to expand or contract freely. The autogenous deformation is measured by linear potentiometers threaded to invar bars that are attached to small plates embedded in the concrete at opposite ends. Measurements of free shrinkage can then be used together with the mechanical properties to calculate the elastic stress in concrete. The free deformation frame enables a comparison of different concrete mixtures in terms of their autogenous shrinkage potential, and provides insight to the mix design parameters negatively affecting autogenous shrinkage.

2.5 Stress Measurements

Several instrumentation and test methods have been developed to assess the stress for both field and laboratory settings. Those methods however, show a combined effect of shrinkage (thermal, autogenous, and drying shrinkage) and stress relaxation, and these two are not easily separated (ACI Committee 231 2010).

2.5.1 Field Measurements – German/ Geokon Method

Geokon Inc. developed a concrete stress meter (Model 4370) capable of measuring concrete stresses in the field. According to the manufacturer, the stress meter contains a short vibrating wire load cell in series with an 18-inch long cylinder framed by a smooth-walled porous plastic. The instrument is embedded in the field and filled up with the concrete that is being placed. Stress is then calculated based on the cross-sectional area of the cylinder and the load measured by the vibrating load cell as a result of the stress applied by the surrounding concrete.

2.5.2 Laboratory Methods

The instruments for laboratory measurement of concrete stress development are detailed in ACI 231R-10 (ACI Committee 231 2010). These methods include: ring test, rigid cracking frame, and thermal stress testing machine.

2.5.2.1 Ring Method

The procedure for the ring method is outlined in AASHTO T334 and ASTM C1581. This test measures the age of cracking and cracking sensitivity of cementitious materials from mortar or concrete specimens under restrained shrinkage. A concentric steel ring containing four strain gauges on its inner surface is used. The gauges measure the strain development, which is a measure of the induced stress resulting from autogenous and drying shrinkage. Several advances have been made in this area which include development of cracking potential envelopes based on stress rate versus time–to-cracking relationship (See et al. 2004). The maximum drying shrinkage at 7 days can be estimated based on the elastic modulus of the concrete mixture at 7 days using the envelope curves (ACI Committee 231 2010). Subsequently, the level (low to high) of cracking potential can be estimated for rapid assessment. The disadvantage of the method is that it does not separate autogenous shrinkage from drying shrinkage. Similarly, Hossain and Weiss (2004), found that while this test method can assess residual stress and stress relaxation in a concrete specimen, it does not provide quantitative information about the time of failure. In addition, Schlitter et al. (2010) indicated that the ring method is limited to isothermal curing conditions, and in response, developed a dual concentric rings test to quantify residual stress resulting from chemical reactions, hydration shrinkage, or thermal movement in concrete subjected to large variation in temperatures.

2.5.2.2 Rigid Cracking Frame

A rigid cracking frame can be used to assess early-age uniaxial stress under restrained conditions. The device allows for a sealed specimen to undergo volume changes due to heat of hydration and autogenous shrinkage. This test method was originally developed in Munich, Germany (Springenschmid et al. 1994). The cracking frame consists of 2 mild steel cross heads that feature dovetail-shaped formwork connected to each other through solid INVAR alloy bars, with torqued bolted connections to provide a high degree of restraint. The entire frame features insulated temperature-controlled formwork to maintain a target temperature profile approximately equal to that of a 50-mm thick concrete element. Full bridge strain gages mounted on the invar are used to measure small deformations as the concrete hydrates and experiences deformations. These deformations along with other mechanical properties can be used to quantify the early-age concrete stress relaxation and predict the cracking tendency of different concrete mixtures. In order to produce results in a reasonable time, the concrete specimen is cooled at a cooling rate of 1°C/ hour if the concrete has not cracked by four days after mixing. The temperature at which cracking occurs is referred to as the cracking temperature (Whigham 2005). The cracking frame can either be used isothermally or the concrete temperature can be varied to match that of the field concrete. Unlike the free-deformation frame, the rigid cracking frame provides a degree of restraint to the concrete specimen, which allows stress measurement under conditions that are more akin to those experienced by concrete in the field. In addition to the stresses generated by restrained autogenous shrinkage, the rigid cracking frame allows for measurement of concrete stress relaxation. As illustrated in Figure 2-4, it is necessary to determine stress relaxation in order to be able to accurately predict concrete stress development leading to cracking.

2.5.2.3 <u>Thermal Stress Testing Machine</u>

Similar to the rigid cracking frame, Schöppel et al. (1994) developed a temperature-stress testing machine (TSTM) capable of measuring the restraint stresses in the concrete element at 100% degree of restraint at early ages. The TSTM includes: approximately 60 in. x 6 in. x 6 in. formwork, a load cell, fixed/adjusted cross-heads, and a heating and cooling system. These components permit the simulation of temperature development under fully restrained conditions. The stress measurements are initiated when the fresh concrete stiffens, which typically occurs in the first few hours after pouring, and runs continuously thereafter. Similarly, the level of restraint and the temperature conditions (isothermal, semi-adiabatic) dictate the properties the machine can estimate. These material properties include thermal / non-thermal stress, Young's modulus, tensile strength and failure strain, which are necessary for determining the stress generated and cracking tendency of the concrete structure.

2.6 Prediction

There are several software packages available today for evaluating concrete performance and failure criteria. Typically, the software provides a valuable tool for assessing the effect of different mix parameters, environmental conditions, and construction practices on the cracking potential. The one most commonly used for pavement is HIPERPAV (The Transtec Group 2009), sponsored by the Federal Highway Administration. HIPERPAV has been designed specifically for jointed plain concrete pavement (JPCP) and continually reinforced concrete pavement assessment. It allows the user to evaluate stress development and risk of cracking during the first 72 hours, as well as evaluate the long-term pavement performance. This report is limited to the early-age cracking in JPCP, and long-term performance evaluation is not included in this discussion.

In predicting the magnitude of stresses in early-age concrete pavement, four major categories of variables are considered by HIPERPAV: mixture design parameters, pavement design, construction parameters and environmental factors (Lee et al. 2003). Mix design parameters include cement and aggregates types and amounts, presence of mineral and chemical admixtures, and w/cm ratio. As for pavement design, pavement slab thickness has to be considered as well as subbase type and friction, which determine the degree of restraint, joint spacing, and the required flexural strength and modulus of elasticity. Time of placement, the initial concrete temperature, curing, time of saw-cutting, and time of opening to traffic are all of significance.

Finally, environmental parameters include air temperature, relative humidity, wind speed, and solar radiation (Lee et al. 2003). McCullough and Rasmussen (1998) provide the general equation parameters used for stress modeling as shown in Equation 2-18:

$$\sigma(t,x) = f[\alpha_c(t), \Delta T(t,x), Z_c(t,x), E_c(t,x), \nabla T(t,x), \nabla M(t,x), \ldots] \qquad \text{Equation 2-18}$$

where

σ = stress in concrete due to restrained movements,

t = time variable,

x = space variable,

α_c = coefficient of thermal expansion of concrete,

Z_c = shrinkage due to moisture loss,

E_c = modulus of elasticity,

ΔT = temperature change from the concrete set temperature,

∇T = temperature gradient in the pavement, and

∇M = moisture gradient in the pavement.

An algorithm based on the temperature development model, temperature-dependent volumetric changes, as well as mechanical property development is used by HIPERPAV to predict early-age cracking. The equations used by HIPERPAV for temperature modeling have been described in detail in Chapter 3. It should be noted that the predicted concrete temperature development is not provided as an output in the free version of HIPERPAV III (The Transtec Group 2009). HIPERPAV allows the user to input the actual maturity data collected in order to improve the accuracy of the mechanical development modeling.

In addition to thermal and shrinkage stresses, HIPERPAV also accounts for the curling stresses generated by the temperature gradient between the top and the bottom of the slab. During the day, the top of the slab, which is in contact with the ambient air, will be warmer than the bottom of the slab, which is in contact with the cool subgrade. The top of the slab will expand more, and the edges of the slab will tend to curl down. However, the weight of the concrete slab (gravity) will resist this movement, thus creating tensile stresses in the bottom of the slab. At night, the subgrade is warmer than the air, so the bottom of the slab will expand more and edges will tend to curl up, generating tensile stresses at the top of the slab (ACI Committee 224 2008; Lee et al. 2003). Curling stresses at the mid-slab edge can be calculated using Equation 2-19:

$$\sigma_t = \frac{C \times E_c \times \alpha_T \times \Delta T}{(1-\nu^2)} \quad \text{Equation 2-19}$$

where

σ_t = tensile stress,

C = factor that accounts for slab length, thickness, and subgrade stiffness,

E_c = elastic modulus,

α_T = coefficient of thermal expansion,

ΔT = temperature difference between the top and the bottom of the slab, and

υ = Poisson's ratio.

HIPERPAV evaluates tensile stresses developing in the concrete and evaluates them against the tensile strength development at each step. HIPERPAV provides the user with a stress and strength development vs. time plot. When the predicted stress exceeds the predicted tensile strength, the probability of failure is indicated. HIPERPAV III also provides an option to perform sensitivity analysis to determine the impact of varying a particular parameter of cracking potential.

ConcreteWorks (Concrete Durability Center 2007) was also developed for evaluation of the effect materials and construction practices on concrete structure durability (Folliard et al. 2008). ConcreteWorks can be used for four different types of concrete members: mass concrete, precast beams, bridge decks, or concrete pavements. ConcreteWorks evaluates environmental inputs, member geometry, mix design parameters, mechanical properties, and construction methods. Like HIPERPAV, ConcreteWorks allows the user to input maturity data for modeling the development of concrete mechanical properties. The outputs provided by ConcreteWorks depend on the selected member type. For concrete pavements, ConcreteWorks provides the temperature prediction, which will be compared with the experimentally-determined results.

2.7 References

AASHTO M154-06 “Standard Specification for Air- Entraining Admixtures for Concrete” American Association of State Highways and Transportation Officials. Washington, D.C, 2011.

AASHTO M194M/M 194-06 “Standard Specification for Chemical Admixtures for Concrete” American Association of State Highways and Transportation Officials. Washington, D.C, 2006.

AASHTO T97-10 “Standard Method of Test for Flexural Strength of Concrete (Using Simple Beam with Third-Point Loading)” American Association of State Highways and Transportation Officials. Washington, D.C, 2010.

AASHTO T177-10 “Standard Method of Test for Flexural Strength of Concrete (Using Simple Beam with Center-Point Loading)” American Association of State Highways and Transportation Officials. Washington, D.C, 2010.

AASHTO T334-08 “Standard Method of Test for Estimating the Cracking Tendency of Concrete” American Association of State Highways and Transportation Officials. Washington, D.C, 2012.

AASHTO T336-11 “Coefficient of Thermal Expansion of Hydraulic Cement Concrete” American Association of State Highways and Transportation Officials. Washington, D.C, 2011.

ASTM C78 / C78M-10e1, Standard Test Method for Flexural Strength of Concrete (Using Simple Beam with Third-Point Loading), ASTM International, West Conshohocken, PA, 2010.

ASTM C125-13, Standard Terminology Relating to Concrete and Concrete Aggregates, ASTM International, West Conshohocken, PA, 2013.

ASTM C157 / C157M-08e1, Standard Test Method for Length Change of Hardened Hydraulic-Cement Mortar and Concrete, ASTM International, West Conshohocken, PA, 2008.

ASTM C186-13, Standard Test Method for Heat of Hydration of Hydraulic Cement, ASTM International, West Conshohocken, PA, 2013.

ASTM C192 / C192M-13, Standard Practice for Making and Curing Concrete Test Specimens in the Laboratory, ASTM International, West Conshohocken, PA, 2013.

ASTM C231-09a, Standard Test Method for Air Content of Freshly Mixed Concrete by the Pressure Method, ASTM International, West Conshohocken, PA, 2009.

ASTM C260 / C260M-10a, Standard Specification for Air-Entraining Admixtures for Concrete, ASTM International, West Conshohocken, PA, 2010.

ASTM C293 / C293M-10, Standard Test Method for Flexural Strength of Concrete (Using Simple Beam With Center-Point Loading), ASTM International, West Conshohocken, PA, 2010.

ASTM C494 / C494M-13, Standard Specification for Chemical Admixtures for Concrete, ASTM International, West Conshohocken, PA, 2013.

ASTM C496 / C496M-11, Standard Test Method for Splitting Tensile Strength of Cylindrical Concrete Specimens, ASTM International, West Conshohocken, PA, 2004.

ASTM C531-00(2012), Standard Test Method for Linear Shrinkage and Coefficient of Thermal Expansion of Chemical-Resistant Mortars, Grouts, Monolithic Surfacings, and Polymer Concretes, ASTM International, West Conshohocken, PA, 2012.

ASTM C1074-04, Standard Practice for Estimating Concrete Strength by the Maturity Method, ASTM International, West Conshohocken, PA, 2004.

ASTM C1581 / C1581M-09a, Standard Test Method for Determining Age at Cracking and Induced Tensile Stress Characteristics of Mortar and Concrete under Restrained Shrinkage, ASTM International, West Conshohocken, PA, 2009.

ASTM C1698-09, Standard Test Method for Autogenous Strain of Cement Paste and Mortar, ASTM International, West Conshohocken, PA, 2009.

ASTM D5335-08, Standard Test Method for Linear Coefficient of Thermal Expansion of Rock Using Bonded Electric Resistance Strain Gauges, ASTM International, West Conshohocken, PA, 2008.

Abdel-Jawad, Y. (1988). “The relationships of cement hydration and concrete compressive strength to maturity.” University of Michigan.

ACI Committee 116. (2009). *Cement and Concrete Terminology*. American Concrete Institute, Farmington Hills, MI.

ACI Committee 207. (2007). *ACI 207.2R-07 Report on Thermal and Volume Change Effects on Cracking of Mass Concrete*. American Concrete Institute, Farmington Hills, MI.

ACI Committee 211. (2009). *ACI 221.1-91: Standard Practice for Selecting Proportions for Normal, Heavyweight and Mass Concrete (Reapproved 2009)*. American Concrete Institute, Farmington Hills, MI.

ACI Committee 212. (1991). *ACI 212.3R-91: Chemical Admixtures for Concrete*. American Concrete Institute, Detroit, MI.

ACI Committee 224. (2001). *ACI 224R-01: Control of Cracking in Concrete Structures Reported by ACI Committee 224*. American Concrete Institute, Farmington Hills, MI.

ACI Committee 224. (2008). *ACI 224.3R-95: Joints in concrete construction*. American Concrete Institute, Farmington Hills, MI.

ACI Committee 231. (2010). *ACI 231R-10: Early-Age Cracking: Causes, Measurement, and Mitigation*. American Concrete Institute, Farmington Hills, MI.

ACI Committee 305. (1991). *ACI 305.1-91: Hot Weather Concreting*. American Concrete Institute, Farmington Hills, MI.

ACI Committee 318. (2011). *Building Code Requirements for Structural Concrete (ACI 318-11) and Commentary*. American Concrete Institute, Farmington Hills, MI.

American Concrete Pavement Association. (1995). *Guidelines for Full-Depth Repair*. Skokie, IL.

Bakharev, T., Sanjayan, J. ., and Cheng, Y.-B. (2000). “Effect of admixtures on properties of alkali-activated slag concrete.” *Cement and Concrete Research*, 30(9), 1367–1374.

Barnett, S. J., Soutsos, M. N., Millard, S. G., and Bungey, J. H. (2006). “Strength development of mortars containing ground granulated blast-furnace slag: Effect of curing temperature and determination of apparent activation energies.” *Cement and Concrete Research*, 36, 434–440.

Bazant, Z., and Raftshol, W. (1982). “Effect of cracking in drying and shrinkage specimens.” *Cement and Concrete Research*, 12(2), 209–226.

Bentz, D., Hansen, K., Madsen, H., Vallée, F., and Griesel, E. (2001). “Drying/Hydration in Cement Pastes during Curing.” *Materials and Structures*, 34, 557–565.

Bentz, D. P. (2008). “A review of early-age properties of cement-based materials.” *Cement and Concrete Research*, 38(2), 196–204.

Bentz, D. P., Sant, G., and Weiss, J. (2008). “Early-Age Properties of Cement-Based Materials. I: Influence of Cement Fineness.” *Journal of Materials in Civil Engineering*, 20(July), 502–508.

Bernard, O., Ulm, F.-J., and Lemarchand, E. (2003). “A multiscale micromechanics-hydration model for the early-age elastic properties of cement-based materials.” *Cement and Concrete Research*, 33(9), 1293–1309.

Bien-Aime, A. J. (2013). “Effect of Cement Chemistry and Properties on Activation

Energy.” Master's Thesis: University of South Florida.

Bogue, R. H. (1947). *The Chemistry of Portland Cement*. Reinolds Publishing Corp., New York, NY.

Bortolotti, L. (1990). “Interdependence of concrete strength parameters.” *ACI Materials Journal*, 87(1), 25–26.

Breitenbücher, R. (1990). “Investigation of thermal cracking with the cracking-frame.” *Materials and Structures*, 23(3), 172–177.

Carino, N. J. (1991). “The Maturity Method.” *Handbook on Nondestructive Testing of Concrete*, CRC Press, Boca Raton, FL, 101–146.

Carino, N. J., and Lew, H. S. (2001). “The Maturity Method : From Theory to Application.” *Proceedings of the 2001 Structures Congress & Exposition*, American Society of Civil Engineers, Washington, DC, 1–19.

Carino, N. J., and Tank, R. C. (1992). “Maturity Functions for Concretes Made with Various Cements and Admixtures.” *ACI Materials Journal*, 89(2), 188–196.

Chen, D. H., and Won, M. (2007). “Field Investigations of Cracking on Concrete Pavements.” *Journal of Performance of Constructed Facilities*, 21(6), 450–458.

Cheung, J., Jeknavorian, A., Roberts, L., and Silva, D. (2011). “Impact of admixtures on the hydration kinetics of Portland cement.” *Cement and Concrete Research*, 41(12), 1289–1309.

Collepardi, M. M. (1995). “Water Reducers/Retarders.” *Concrete Admixtures Handbook: Properties, Science and Technology*, V. Ramachandran, ed., Noyes Publications, Park Ridge, NJ.

Concrete Durability Center. (2007). “ConcreteWorks (Version 3.1.0) [Software].” <Available from www.texasconcreteworks.com>.

D’Aloia, L., and Chanvillard, G. (2002). “Determining the ‘apparent’ activation energy of concrete: Ea—numerical simulations of the heat of hydration of cement.” *Cement and Concrete Research*, 32(8), 1277–1289.

De Larrard, F., Acker, P., and Le Roy, R. (1994). “Shrinkage Creep and Thermal Properties.” *High Performance Concrete: Properties and Applications,* S. Shah and S. Ahmad, eds., McGraw Hill, New York, NY, 65–114.

De Schutter, G., and Taerwe, L. (1996). “Degree of hydration-based description of mechanical properties of early age concrete.” *Materials and Structures*, 29(6), 335–344.

Dolch, W. L. (1995). “Air-Entraining Admixtures.” *Concrete Admixtures Handbook: Properties, Science and Technology*, V. S. Ramachandran, ed., Noyes Publications, Park Ridge, NJ, 518–557.

Du, L., and Folliard, K. J. (2005). “Mechanisms of Air Entrainment in Concrete.” *Cement and Concrete Research*, 35(8), 1463–1471.

Emanuel, J. H., and Hulsey, J. L. (1977). “Prediction of the thermal coefficient of expansion of concrete.” *ACI Journal Proceedings*, 74(4), 149–155.

Ferraro, C. (2009). “Determination of Test Methods for the Prediction of the Behavior of Mass Concrete.” PhD Dissertation: University of Florida.

Florida Department of Transportation. (2010). *Standard Specifications for Road and Bridge Construction*. Tallahassee, FL, 966.

Florida Department of Transportation. (2013). *Standard Specifications for Road and Bridge Construction*. Tallahassee, FL.

Folliard, K. J., Juenger, M., Schindler, A., Riding, K. A., Poole, J. L., Kallivokas, L., Slatnick, S., Whigham, J., and Meadows, J. L. (2008). *Prediction Model for Concrete Behavior - Final Report*. Austin, TX, 77.

Freiesleben Hansen, P., and Pedersen, J. (1977). “Maturity computer for controlled curing and hardening of concrete.” *Nordisk Betong*, 1, 19–34.

Frentress, D., and Harrington, D. (2012). *Guide for partial-depth repair of concrete pavements*. National Concrete Pavement Technology Center, Iowa State University, Ames, IA, 46.

Georgia Department of Transportation. (2013). *Standard Specifications Construction of Transportation Systems*. Atlanta, GA.

Gotfredsen, H., and Idorn, G. (1986). “Curing technology at the Faroe Bridge, Denmark.” *Properties of Concrete at Early Ages*, J. F. Young, ed., American Concrete Institute, Detroit, MI, 17–32.

Griffith, J. H. (1936). *Thermal expansion of typical American rocks*. Iowa State College of Agriculture and Mechanic Arts.

Hansen, W., and Almudaiheem, J. (1987). “Ultimate drying shrinkage of concrete-influence of major parameters.” *ACI Materials Journal*, 84(3), 217–223.

Hewlett, P. C. (Ed.). (1998). *Lea’s Chemistry of Cement and Concrete*. Arnold, New York, NY.

Hossain, A. B., and Weiss, J. (2004). “Assessing residual stress development and stress relaxation in restrained concrete ring specimens.” *Cement and Concrete Composites*, 26(5), 531–540.

Houghton, B. D. L. (1976). “Determining Tensile Strain Capacity of Mass Concrete.” *ACI Journal Proceedings*, 73(12), 691–700.

Hua, C., Acker, P., and Ehrlacher, A. (1995). “Analyses and models of the autogenous shrinkage of hardening cement paste I. Modelling at macroscopic scale.” *Cement and Concrete Research*, 25(7), 1457–1468.

Hua, C., Ehrlacher, A., and Acker, P. (1997). “Analyses and models of the autogenous shrinkage of hardening cement paste II. Modelling at scale of hydrating grains.” *Cement and concrete research*, 27(2), 245–258.

Ishee, C. A. (2011). “Evaluating the Performance of Portland Cement under Differing Hydration Conditions.” PhD Dissertation: McGill University, Montreal, Canada.

Jackson, S. (2007). “The IMCP Manual: An Overview.” *Surface Transportation*, 3(3), 16–18.

Jankovic, D., and van Mier, J. (2003). “Drying of Porous Media : Numerical and Experimental Approach.” *EURO-C 2003, Computational Modeling of Concrete Structures*, AA Balkema Publishers, St. Johann im Pongau, Austria.

Juenger, M. C. G., Winnefeld, F., Provis, J. L., and Ideker, J. H. (2011). “Advances in alternative cementitious binders.” *Cement and Concrete Research*, 41(12), 1232–1243.

Kada-Benameur, H., Wirquin, E., and Duthoit, B. (2000). “Determination of apparent activation energy of concrete by isothermal calorimetry.” *Cement and Concrete Research*, 30(2), 301–305.

Khan, A. A., Cook, W. D., and Mitchell, D. (1998). “Thermal Properties and Transient Thermal Analysis of Structural Members during Hydration.” *ACI Materials Journal*, 95(3), 293–302.

Kim, J. K., and Lee, C. S. (1999). “Moisture diffusion of concrete considering self-desiccation at early ages.” *Cement and Concrete Research*, 29(1999), 1921–1927.

Kjellsen, K. O., and Detwiler, R. J. (1992). “Reaction kinetics of PC Mortars Hydrated at Different Temperatures.” *Cement and Concrete Research*, 22(1), 1063–1082.

Kjellsen, K. O., and Detwiler, R. J. (1993). “Later Ages Strength Prediction by a Modified Maturity Method.” *ACI Materials Journal*, 90(3), 220–227.

Kosmatka, S. H., Kerkhoff, B., and Panarase, W. (2002). *Design and Control of Concrete*. Portland Cement Association, Skokie, IL.

Laidler, K. (1969). *Theories of Chemical Reaction Rates*. McGraw Hill, New York, NY.

Lee, E. B., Lamour, V., Pae, J. H., and Harvey, J. (2003). *Analysis of Sensitivity of Plain Jointed Concrete Pavement in California to Early-age Cracking using HIPERPAV*. University of California.

Lenz, R. W. (2011). *Pavement Design Guide*. Texas Department of Transportation.

Lerch, W., and Bogue, R. H. (1934). “Heat of hydration of portland cement pastes.” *Bureau of Standards Journal of Research*, 12(5), 645–664.

Lura, P., Jensen, O. M., and van Breugel, K. (2003). “Autogenous shrinkage in high-performance cement paste: An evaluation of basic mechanisms.” *Cement and Concrete Research*, 33(2), 223–232.

Ma, W., Sample, D., Martin, R., and Brown, P. W. (1994a). “Calorimetric Study of Cement Blends Containing Fly Ash, Silica Fume, and Slag at Elevated Temperatures.” *Cement, Concrete, and Aggregates*, 16(2), 93–99.

Ma, W., Sample, D., Martin, R., and Brown, P. W. (1994b). “Calorimetric Study of Cement Blends Containing Fly Ash, Silica Fume and Slag at Elevated Temperatures.” *Cement, Concrete, and Aggregates*, 16(2), 93–99.

Maekawa, K., Chaube, R., and Kishi, T. (1999). *Modeling of Concrete Performance: Hydration, Microstructure Formation, and Mass Transport*. E & FN Spon, London, UK.

McCullough, B. F., and Rasmussen, R. O. (1998). *Fast Track Paving: Concrete Temperature Control and Traffic Opening Criteria for Bonded Concrete Overlays Volume I -Final Report*. Transtec, Inc., Austin, TX.

Meadows, J. L. (2007). “Early-age cracking of concrete structures.” Master's Thesis: Auburn University.

Mehta, P. K., and Monteiro, P. J. M. (2006). *Concrete: Microstructure, Properties and Materials*. McGraw-Hill, New York, NY.

Mihashi, H., and Leite, J. P. D. B. (2004). “State-of-the-Art Report on Control of Cracking in Early Age Concrete.” *Journal of Advanced Concrete Technology*, 2(2), 141–154.

Mindess, S., Young, J. F., and Darwin, D. (2003). *Concrete*. Prentice Hall, Upper Saddle River, NJ, 644.

Mitchell, L. (1953). “Thermal expansion tests on aggregates, neat cements, and concretes.” *Proceedings - American Society for Testing and Materials*, 53, 963–977.

Muneer, T., Kubie, J., and Grassie, T. (2003). *Heat Transfer: A problem solving approach*. Taylor & Francis, New York, NY.

Nazef, A., Greene, J., Lee, H., Byron, T., and Choubane, B. (2011). *Portland Cement Concrete Pavement Specifications : State of the Practice*. 33.

Neville, A. M. (2006). *Properties of Concrete*. Pearson Education Limited, Harlow, England.

Nilsson, M. (2003). *Restraint Factors and Partial Coefficients for Crack Risk Analyses of Early Age Concrete Structures*. 1402–1544.

Olek, J., Cohen, M., Scholer, C., and Mandrekar, D. R. (2002). *Use of Modulus of Rupture, Fatigue Resistance and Maturity in Determining Opening to Traffic Time for Concrete Pavements*. West Lafayette, IN, 99.

Oluokun, F. (1991). “Prediction of concrete tensile strength from its compressive strength: an evaluation of existing relations for normal weight concrete.” *ACI Materials Journal*, 88(3), 302–309.

Pinto, R. C., and Schindler, A. K. (2010). “Unified modeling of setting and strength development.” *Cement and Concrete Research*, 40, 58–65.

Poole, J. L. (2007). “Modeling Temperature Sensitivity and Heat Evolution of Concrete.” PhD Dissertation: University of Texas at Austin.

Poole, J. L., Riding, K. A., Folliard, K. J., Juenger, M. C. G., and Schindler, A. K. (2007). “Methods for Calculating Activation Energy for Portland Cement.” *ACI Materials Journal*, 104(1), 303–311.

Popovics, S. (1998). *Strength and Related Properties of Concrete: A Quantitative Approach*. John Wiley & Sons, Inc., New York, NY.

Raphael, J. (1984). “Tensile strength of concrete.” *ACI Journal Proceedings*, 81(2), 158–165.

Riding, K. A., Poole, J. L., Folliard, K. J., Juenger, M. C. G., and Schindler, A. K. (2011). “New model for estimating apparent activation energy of cementitious systems.” *ACI Materials Journal*, 108(5), 550–557.

Riding, K., Poole, J., Folliard, K. J., Juenger, M. C. G., and Schindler, A. K. (2012). “Modeling Hydration of Cementitious Systems.” *ACI Materials Journal*, 109(2), 225–234.

Riding, K., Poole, J., Schindler, A. K., Juenger, M. C. G., and Folliard, K. J. (2009). “Effects of Construction Time and Coarse Aggregate on Bridge Deck Cracking.” *ACI Materials Journal*, 106(5), 448–454.

RILEM Technical Committee 119-TCE. (1998). “Adiabatic and semi-adiabatic calorimetry to determine the temperature increase in concrete due to hydration heat of the cement.” *RILEM Report 15, Prevention of Thermal Cracking in Concrete at Early Ages*, R. Springenschmid, ed., E & FN Spon, London, UK, 315–330.

RILEM Technical Committee 42-CEA. (1981). “Properties of Set Concrete at Early Ages State of the Art Report, Materials and Structures.” *Materials and Structures*, 14(84), 399–450.

Rixom, R., and Mailvaganam, N. (1999). *Chemical Admixtures for Concrete*. Routledge, New York, NY.

Ruiz, J. M., Rasmussen, R. O., Chang, G. K., Dick, J. C., and Nelson, P. K. (2005). *Computer-Based Guidelines For Concrete Pavements Volume III-Technical Appendices*. Transtec, Inc., Austin, TX.

Sakyi-Bekoe, K. (2008). “Assessment of the Coefficient of Thermal Expansion of Alabama Concrete.” Master's Thesis: Auburn University.

Saul, A. (1951). “Principles Underlying the Steam Curing of Concrete at Atmospheric Pressure.” *Magazine of Concrete Research*, 2(6), 25–33.

Schindler, A. A. K., and Folliard, K. K. J. (2005). “Heat of hydration models for cementitious materials.” *ACI Materials Journal*, 102(1), 24–33.

Schindler, A., and Folliard, K. (2005). “Heat of hydration models for cementitious materials.” *ACI Materials Journal*, 102(1), 24–33.

Schindler, A. K. (2002). “Concrete Hydration , Temperature Development, and Setting at Early-Ages.” PhD Dissertation: University of Texas at Austin.

Schindler, A. K., and McCullough, B. F. (2002). "The Importance of Concrete Temperature Control During Concrete Pavement Construction in Hot Weather Conditions." *Transportation Research Record: Journal of the Transportation Research Board*, 1813, 3–10.

Schlitter, J. L., Senter, A. H., Bentz, D. P., Nantung, and J., W. W. (2010). "A Dual Concentric Ring Test for Evaluating Residual Stress Development due to Restrained Volume Change." *Journal of ASTM International*, 7(9), 1–13.

Schöppel, K., Plannerer, M., and Springenschmid, R. (1994). "Determination of Restraint Stresses and of Material Properties During the Hydration of Concrete with Temperature-Stress Testing Machine." *RILEM Proceedings 25, Thermal Cracking in Concrete at Early Ages*, R. Springenschmid, ed., E & FN Spon, London, UK.

Sedaghat, A., Bien-Aime, A. J., Zayed, A., and Sandberg, P. (2011). "Measurement and Prediction of Heat of Hydration of Portland Cement Using Isothermal Conduction Calorimetry." *Proceedings of the International Conference on Structural Engineering, Construction and Management*, Sri Lanka, 1–11.

See, H. T., Attiogbe, E. K., and Miltenberger, M. A. (2004). "Potential for restrained shrinkage cracking of concrete and mortar." *Cement, Concrete, and Aggregates*, 26(2), 123–130.

Sellevold, E. J., and Bjøntegaard, Ø. (2002). "Coefficient of thermal expansion of concrete: effects of moisture." *Proceedings of the Third International Research Seminar on Self-Desiccation and Its Importance in Concrete Technology*, Lund, Sweden, 67–75.

Sellevold, E. J., and Bjøntegaard, Ø. (2006a). "Driving forces to cracking in hardening concrete: thermal and autogenous deformations." *2nd International Symposium on Advances in Concrete through Science and Engineering*, J. Marchand, B. Bissonnette, R. Gagne, M. Jolin, and F. Paradis, eds., Quebec City, Canada, 125–139.

Sellevold, E. J., and Bjøntegaard, Ø. (2006b). "Coefficient of thermal expansion of cement paste and concrete: Mechanisms of moisture interaction." *Materials and Structures*, 39(9), 809–815.

Slatnick, S., Riding, K., Folliard, K. J., Juenger, M. C. G., and Schindler, A. K. (2011). "Evaluation of Autogenous Deformation of Concrete at Early Ages." *ACI Materials Journal*, 108(1), 21–28.

Smith, K. D. (2005). *Maturity Testing for Concrete Pavement Applications*. Federal Highway Administration, Springfield, VA.

Springenschmid, R., Breitenbücher, R., and Mangold, M. (1994). “Development of the Cracking Frame and the Temperature-Stress Testing Machine.” *RILEM Proceedings 25, Thermal Cracking in Concrete at Early Ages*, R. Springenschmid, ed., E & FN Spon, London, UK, 137–144.

State of California Department of Transportation. (2004). *Slab Replacement Guidelines*. Sacramento, CA.

State of California Department of Transportation. (2008). *Maintenance Technical Advisory Guide: Volume II-Rigid Pavement Preservation*. Sacramento, CA.

Stock, A., Hannant, D., and Williams, R. (1979). “The effect of aggregate concentration upon strength and modulus of elasticity of concrete.” *Magazine of Concrete Research*, 31(109), 225–234.

Stutzman, P. E. (2005). “Powder Diffraction Analysis of Hydraulic Cements: ASTM Rietveld Round Robin Results on Precision.” *ICDD Advances in X-Ray Analysis*, 48(1), 33–38.

Swaddiwudhipong, S., Lu, H.-R., and Wee, T.-H. (2003). “Direct tension test and tensile strain capacity of concrete at early age.” *Cement and Concrete Research*, 33(12), 2077–2084.

Taylor, H. F. W. (1997). *Cement Chemistry*. Thomas Telford Publishing, London, UK.

Taylor, P. C., Kosmatka, S. H., and Voigt, G. F. (2006). *Integrated Materials and Construction Practices for Concrete Pavement: A State-of-the-Practice Manual. Center for Transp Res Edu Iowa State Uni*, National Concrete Pavement Technology Center, Iowa State University, Ames, IA, 360.

The Transtec Group. (2009). “HIPERPAV III (Version 3.20.0006) [Software].” <Available from www.hiperpav.com>.

Van Breugel, K. (1991). “Simulation of Hydration and Formation of Structure in Hardening Cements-Based Materials.” PhD Dissertation: Delft University of Technology.

Van Dam, T. J., Peterson, K. R., Sutter, L. L., Panguluri, A., and Sytsma, J. (2005). *Guidelines for Early-Opening to Traffic Portland Cement Concrete for Pavement Rehabilitation, NCHRP Report 540*. Washington, DC, 26.

Valckenborg, R., Pel, L., Hazrati, K., Kopinga, K., and Marchand, J. (2001). “Pore water distribution in mortar during drying as determined by NMR.” *Materials and Structures*, 34(10), 599–604.

Venecanin, S. D. (1990). “Thermal Incompatibility of Concrete Components and Thermal Properties of Carbonate Rocks.” *ACI Materials Journal*, 87(6), 602–607.

Verbeck, G., and Helmuth, R. (1968). “Structures and physical properties of cement paste.” *Proceedings of the Fifth International Symposium on the Chemistry of Cement*, Tokyo, Japan, 1–32.

Weakley, R. W. (2010). “Evaluation of Semi-Adiabatic Calorimetry to Quantify Concrete Setting.” Auburn University.

Wesevich, J. W., Mccullough, B. F., and Burns, N. H. (1987). *Stabilized subbase friction study for concrete pavements*. Center for Transportation Research, University of Texas at Austin, Austin, TX.

Whigham, J. A. (2005). “Evaluation of restraint stresses and cracking in early-age concrete with the rigid cracking frame.” Auburn University.

Whiting, D., and Nagi, M. A. (1998). *Manual on Control of Air Content in Concrete*. Portland Cement Association, Skokie, IL.

Whiting, D., Todres, A., and Nagi, M. A. (1993). *The Synthesis of Current and Projected Concrete Highway Technology (SHRP-C-345)*. Washington, DC.

Wirquin, E., Broda, M., and Duthoit, B. (2002). “Determination of the apparent activation energy of one concrete by calorimetric and mechanical means: influence of a superplasticizer.” *Cement and concrete research*, 32, 1207–1213.

W.R.Grace and Co. (2007), Daraccel water-reducing admixture, ASTM C944 Type E, W.R.Grace and Co.,Cambridge, MA. <http://www.buildsite.com/pdf/wrgrace/Daraccel-Product-Data-320741.pdf>, accessed March 16, 2015

Xiong, X., and Van Breugel, K. (2001). “Isothermal calorimetry study of blended cements and its application in numerical simulations.” *Heron*, 46(3), 151–160.

Zhang, J., and Li, V. C. (2001). “Influence of supporting base characteristics on shrinkage-induced stresses in concrete pavements.” *Journal of Transportation Engineering*, 127(6), 455–462.

CHAPTER 3 Field Testing

3.1 Introduction

A field survey was conducted to provide the input data necessary to realistically model the impact of construction methods commonly used in Florida on cracking probability. This chapter documents field construction information collected, and temperature and strain instrumentation methods and results for three concrete pavement replacement slabs constructed in Florida. The field instrumentation of temperature was performed to validate concrete pavement slab temperature prediction methods currently used. In addition, for each slab replacement location, various geotechnical and material tests were performed to provide data for modelling of the concrete behavior. The material testing was separated into concrete specimen testing and concrete slab testing. The concrete specimen tests as well as the geotechnical laboratory tests were performed at the University of Florida. The concrete slab testing was done with instrumentation placed inside the slab. Figure 3-1 is a photograph of a typical slab replacement conducted in the field.

For each slab replacement, fifty-eight (58) four-inch-by-eight-inch cylindrical specimens were cast using the same concrete that was used for the slab replacement. These specimens were used to obtain physical characteristics of the concrete during curing which included: compressive strength, splitting tensile strength, modulus of elasticity, coefficient of thermal expansion, and heat of hydration. Additionally, temperature and strain sensors were embedded in three locations (center, edge and corner) in each slab for early-age monitoring of the slab replacement. The locations of the temperature and strain sensors within each slab are presented in Figure 3-2. To avoid construction delays, steel frames or “instrument trees” shown in Figure 3-3 were installed prior to concrete placement to properly orient and secure the gages during placement. Strain and temperature sensors were places at elevations 2” from the top surface, 4.5” from the surface (mid-depth) and 2” from the bottom surface.

Two slabs were instrumented during construction on Martin Luther King Jr. Parkway in Jacksonville, FL. An additional slab was constructed at the State Materials Office in Gainesville, FL with similar mixture proportions and the same cement source used in a slab replacement project in Miami, FL two years earlier. The mixture proportions and cement source were chosen to mimic that of the Miami project because that project had a high percentage of cracked slabs.

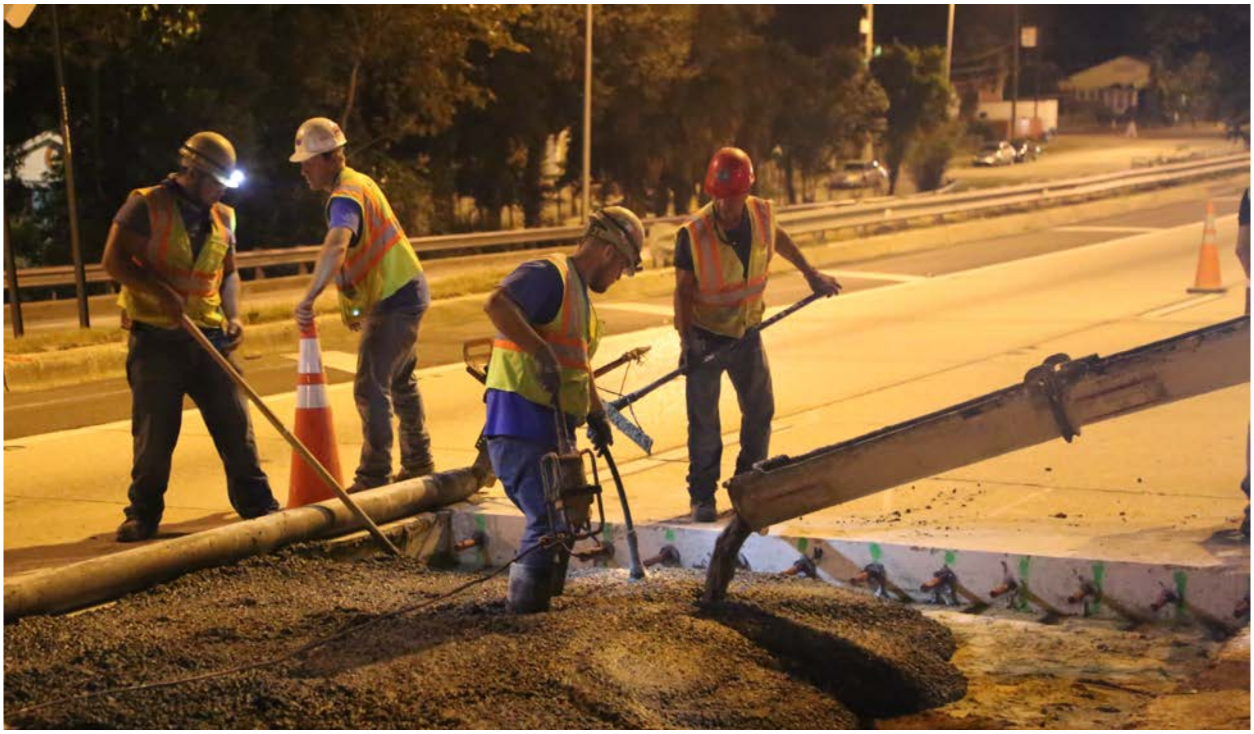

Figure 3-1: Typical slab replacement

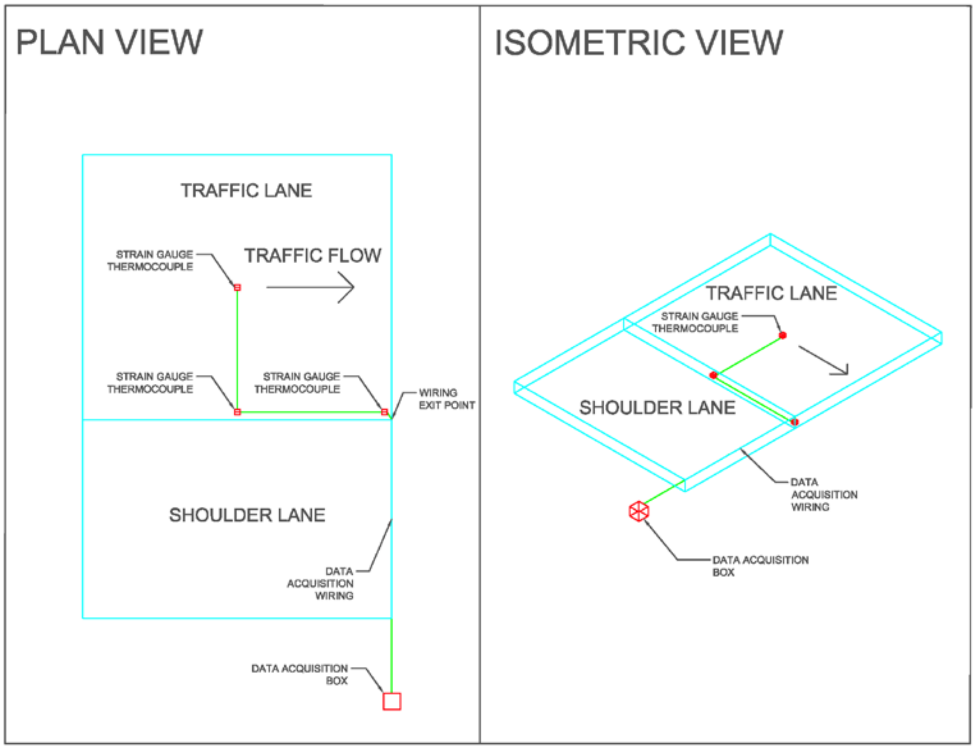

Figure 3-2: Sensor placement locations

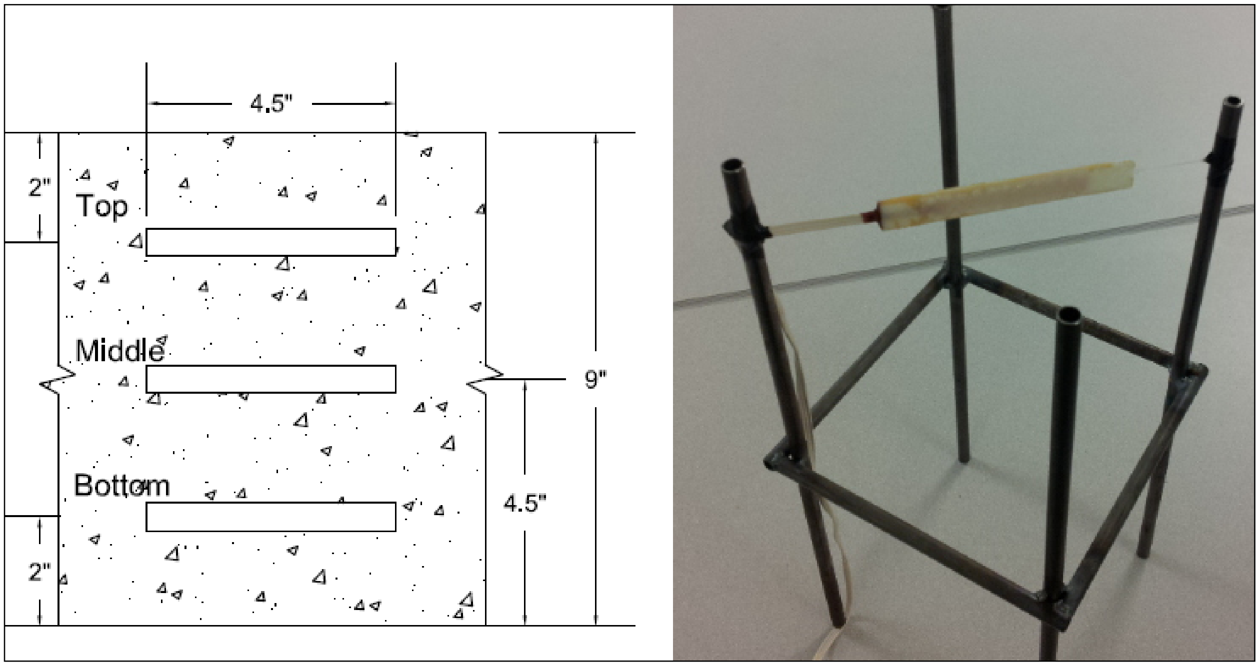

Figure 3-3: Instrument tree used for sensor placement

3.2 Field Questionnaire

The field survey included important information about the slab location and environment at the time of placement as well as a timeline of events during the slab replacement. Figure 3-4 through Figure 3-6 provide the information obtained for each field slab placement.

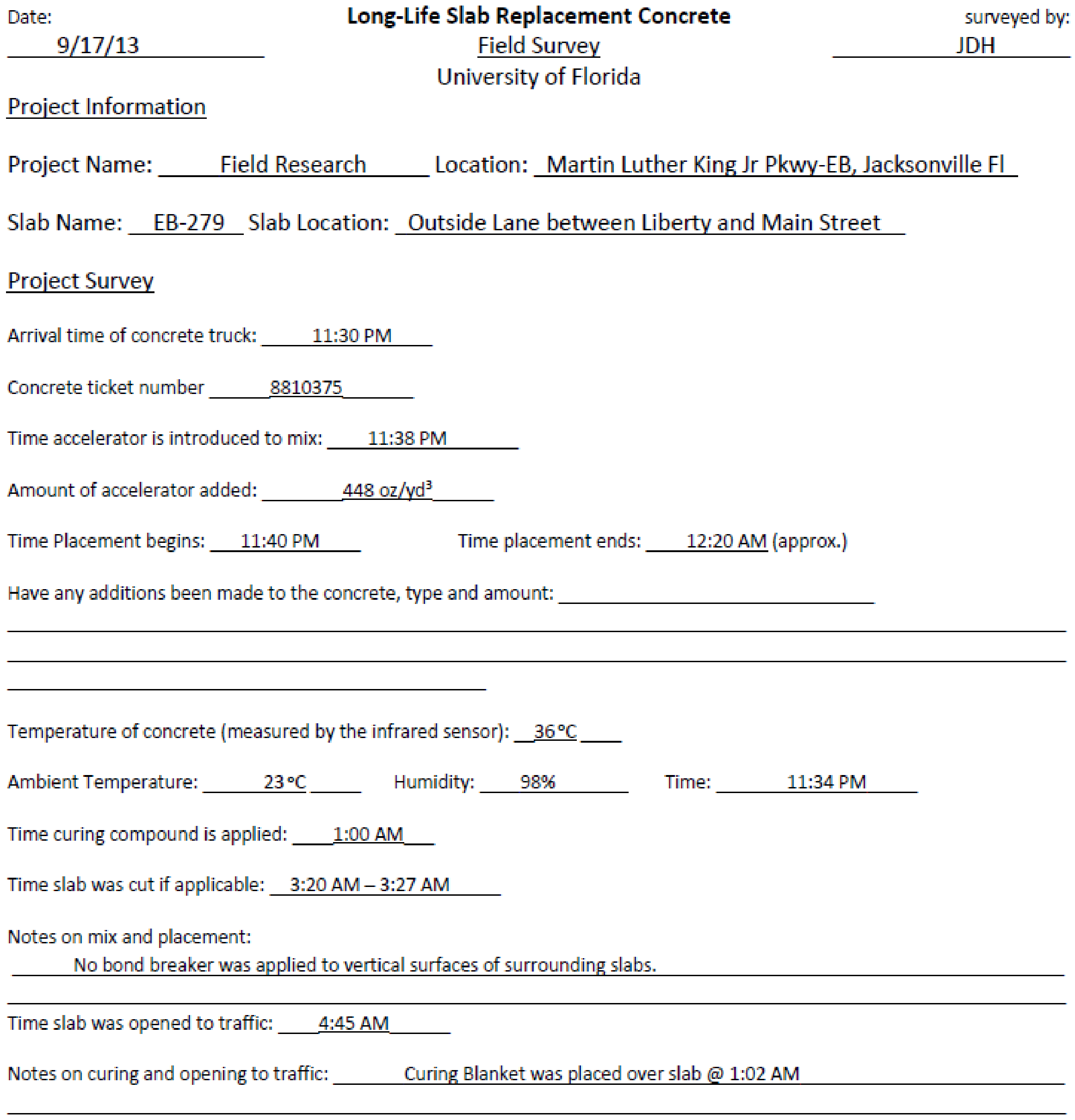

Date: 9/17/13

Long-Life Slab Replacement Concrete
Field Survey
University of Florida

surveyed by: JDH

Project Information

Project Name: Field Research Location: Martin Luther King Jr Pkwy-EB, Jacksonville Fl

Slab Name: EB-279 Slab Location: Outside Lane between Liberty and Main Street

Project Survey

Arrival time of concrete truck: 11:30 PM

Concrete ticket number 8810375

Time accelerator is introduced to mix: 11:38 PM

Amount of accelerator added: 448 oz/yd^3

Time Placement begins: 11:40 PM Time placement ends: 12:20 AM (approx.)

Have any additions been made to the concrete, type and amount:

Temperature of concrete (measured by the infrared sensor): 36 °C

Ambient Temperature: 23 °C Humidity: 98% Time: 11:34 PM

Time curing compound is applied: 1:00 AM

Time slab was cut if applicable: 3:20 AM – 3:27 AM

Notes on mix and placement:
No bond breaker was applied to vertical surfaces of surrounding slabs.

Time slab was opened to traffic: 4:45 AM

Notes on curing and opening to traffic: Curing Blanket was placed over slab @ 1:02 AM

Figure 3-4: Field survey for Slab 1

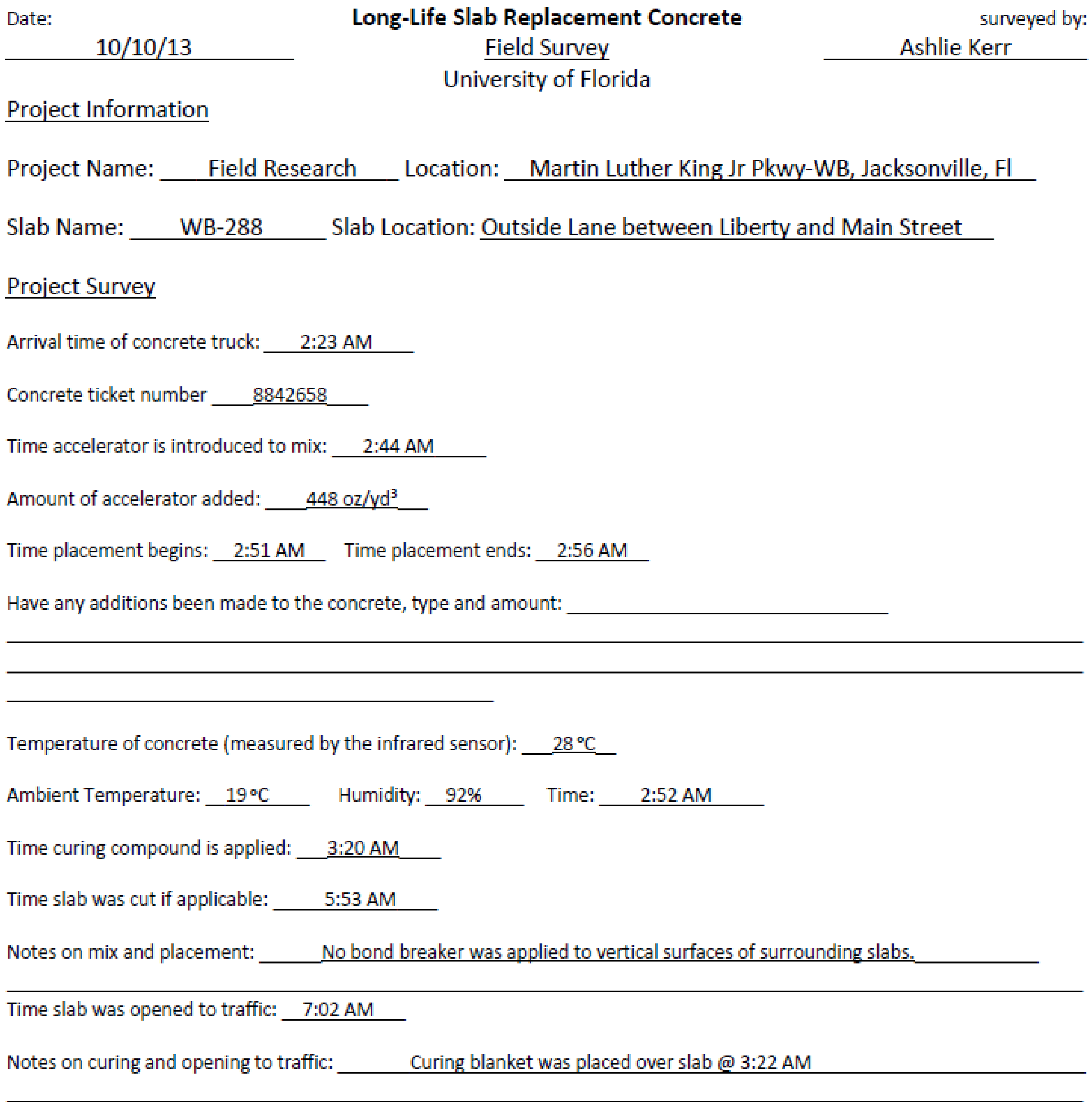

Date: 10/10/13

Long-Life Slab Replacement Concrete
Field Survey
University of Florida

surveyed by: Ashlie Kerr

Project Information

Project Name: Field Research Location: Martin Luther King Jr Pkwy-WB, Jacksonville, Fl

Slab Name: WB-288 Slab Location: Outside Lane between Liberty and Main Street

Project Survey

Arrival time of concrete truck: 2:23 AM

Concrete ticket number 8842658

Time accelerator is introduced to mix: 2:44 AM

Amount of accelerator added: 448 oz/yd^3

Time placement begins: 2:51 AM Time placement ends: 2:56 AM

Have any additions been made to the concrete, type and amount:

Temperature of concrete (measured by the infrared sensor): 28 °C

Ambient Temperature: 19 °C Humidity: 92% Time: 2:52 AM

Time curing compound is applied: 3:20 AM

Time slab was cut if applicable: 5:53 AM

Notes on mix and placement: No bond breaker was applied to vertical surfaces of surrounding slabs.

Time slab was opened to traffic: 7:02 AM

Notes on curing and opening to traffic: Curing blanket was placed over slab @ 3:22 AM

Figure 3-5: Field survey for Slab 2

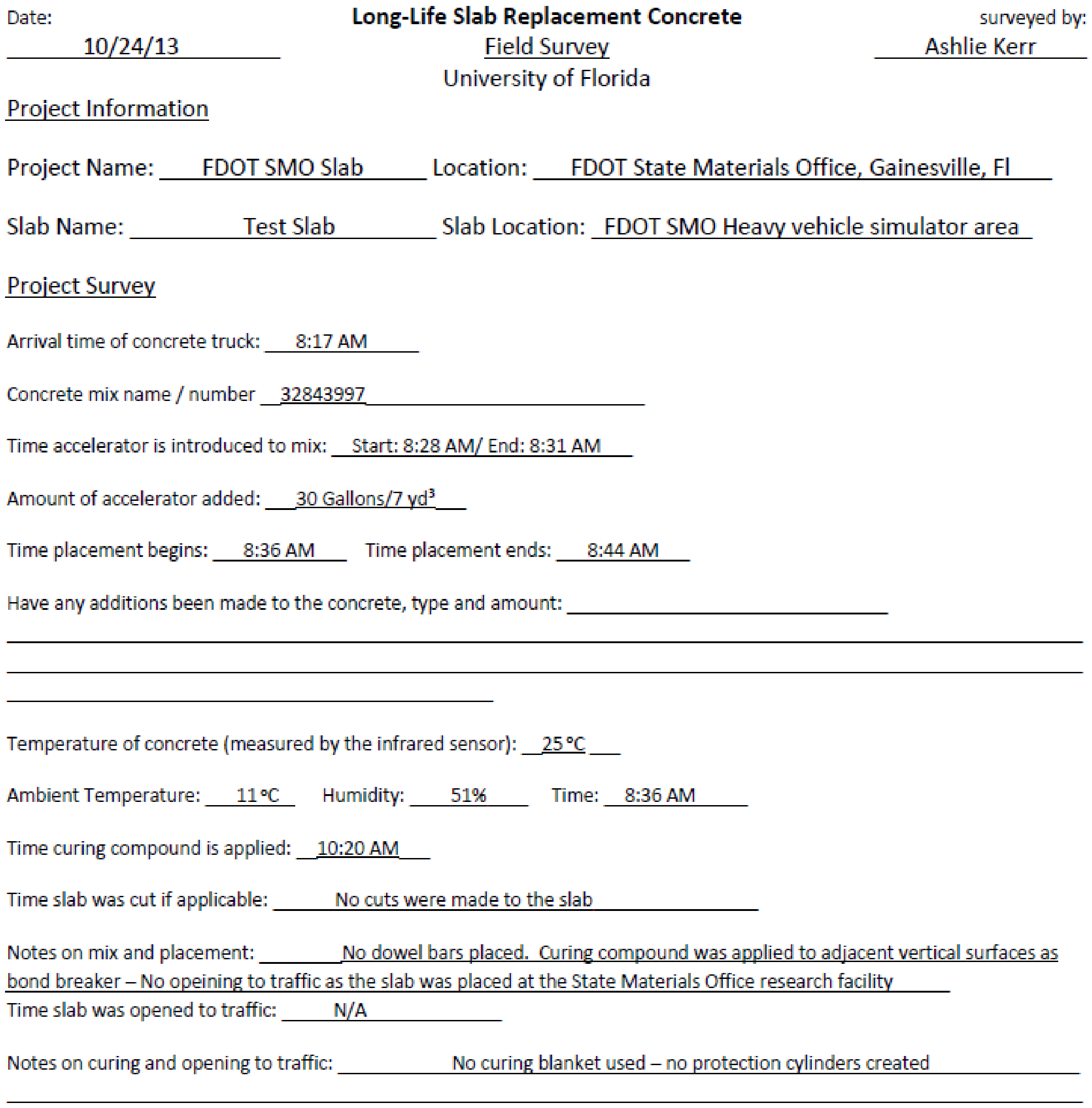

Date: 10/24/13

Long-Life Slab Replacement Concrete
Field Survey
University of Florida

surveyed by: Ashlie Kerr

Project Information

Project Name: FDOT SMO Slab Location: FDOT State Materials Office, Gainesville, Fl

Slab Name: Test Slab Slab Location: FDOT SMO Heavy vehicle simulator area

Project Survey

Arrival time of concrete truck: 8:17 AM

Concrete mix name / number 32843997

Time accelerator is introduced to mix: Start: 8:28 AM/ End: 8:31 AM

Amount of accelerator added: 30 Gallons/7 yd^3

Time placement begins: 8:36 AM Time placement ends: 8:44 AM

Have any additions been made to the concrete, type and amount:

Temperature of concrete (measured by the infrared sensor): 25 °C

Ambient Temperature: 11 °C Humidity: 51% Time: 8:36 AM

Time curing compound is applied: 10:20 AM

Time slab was cut if applicable: No cuts were made to the slab

Notes on mix and placement: No dowel bars placed. Curing compound was applied to adjacent vertical surfaces as bond breaker – No opeining to traffic as the slab was placed at the State Materials Office research facility

Time slab was opened to traffic: N/A

Notes on curing and opening to traffic: No curing blanket used – no protection cylinders created

Figure 3-6: Field survey for Slab 3

3.3 Geotechnical Testing

A subsurface investigation was performed at the three slab replacement sites to determine the properties of the in situ soil. Material characterization is essential for the design and construction of a roadway. Representative soil samples were taken at the two Jacksonville locations for the laboratory tests.

3.3.1 Sieve Analysis

Mechanical sieve analysis tests were performed at the first two slab replacement locations in accordance with ASTM D422. A soil sample was not able to be taken at the third site. The soil samples were prepared according to ASTM D421. To perform this test, the sample of soil was placed into a series of sieves in descending order of mesh opening size. The stack of sieves was then placed on a mechanical sieve shaker for a set amount of time. The amount of soil retained on each sieve was measured and a grain size distribution curve was created. This test determines the gradation of the soil particles and helps classify the soil. From the results, the soil at the first two locations was classified as a "poorly-graded, fine sand" A-3 according to the American Association of State Highway and Transportation Officials (AASHTO) classification system (AASHTO M145). Because there was an asphalt base on slab 3, it was not possible to remove soil or perform a sieve analysis. Table 3-1 shows the sieve analysis data and Figure 3-7 shows a plot of the soil size distribution for slab 1. Table 3-2 shows the sieve analysis data and Figure 3-8 shows a plot of the soil size distribution for slab 2.

Table 3-1: Slab 1 –Sieve analysis data

Sieve No.	**Diameter (mm)**	**Mass of Sieve, M_{sv} (g)**	**Mass of Sieve & Soil, $M_{sv,s}$ (g)**	**Mass of Soil, M_s (g)**	**% Retained on Sieve**	**% Passing Sieve**
10	2.00	481.56	484.92	3.36	0.67	99.33
30	0.600	424.19	431.42	7.23	1.44	97.90
40	0.425	473.98	484.24	10.26	2.04	95.86
60	0.250	368.30	401.87	33.57	6.67	89.19
100	0.150	407.17	675.50	268.33	53.32	35.87
140	0.106	348.38	470.21	121.83	24.21	11.66
200	0.075	322.43	352.62	30.19	6.00	5.66
pan	0.001	379.70	408.18	28.48	5.66	0.00

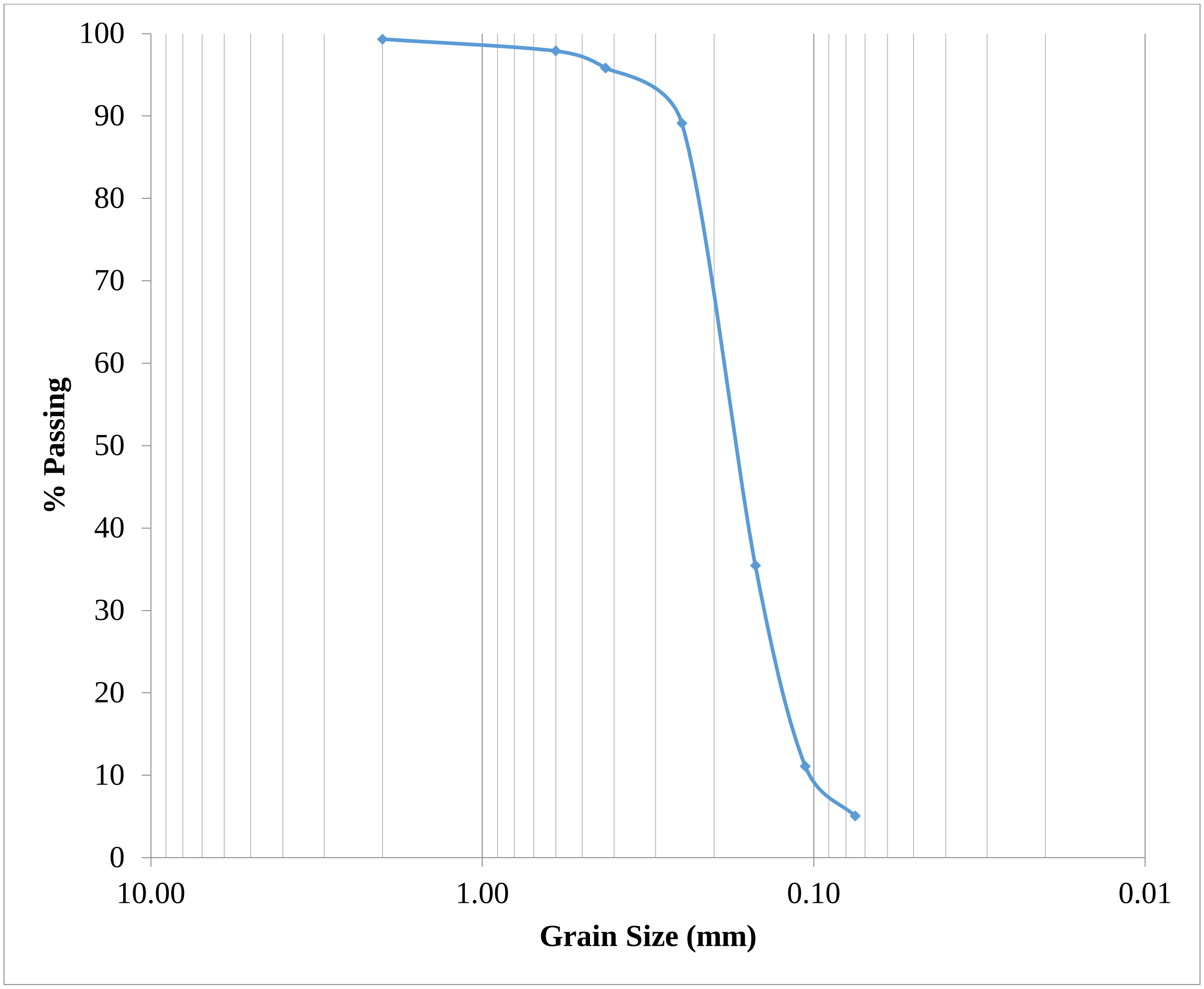

Figure 3-7: Grain size distribution curve for Slab 1

Table 3-2: Slab 2 –Sieve analysis data

Sieve No.	**Diameter (mm)**	**Mass of Sieve, M_{sv} (g)**	**Mass of Sieve & Soil, $M_{sv,s}$ (g)**	**Mass of Soil, M_s (g)**	**% Retained on Sieve**	**% Passing Sieve**
10	2.00	493.36	493.57	0.21	0.04	99.96
30	0.600	417.75	451.41	33.66	6.73	93.23
40	0.425	469.72	499.99	30.27	6.05	87.18
60	0.250	361.06	415.28	54.22	10.84	76.34
100	0.150	351.02	605.43	254.41	50.86	25.47
140	0.106	350.63	446.05	95.42	19.08	6.40
200	0.075	302.99	322.42	19.43	3.88	2.51
pan	0.001	375.00	387.56	12.56	2.51	0.00

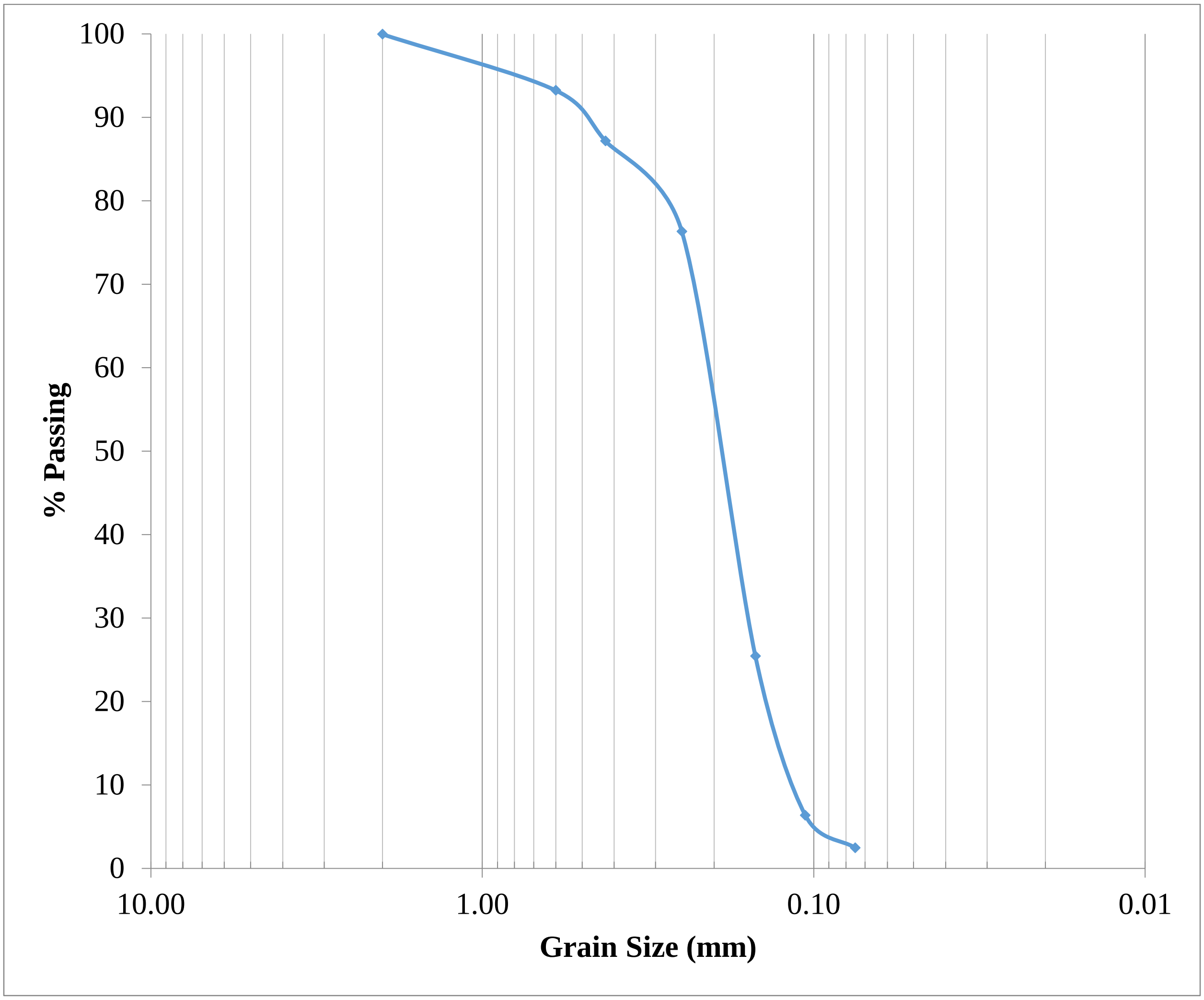

Figure 3-8: Grain size distribution curve for Slab 2

3.3.2 Limerock Bearing Ratio

The Limerock Bearing Ratio (LBR) test is a penetration test used to determine the load bearing capacity of soils. It is used in Florida for evaluating limerock and other soils that are used for base, stabilized subgrade, and subgrade or embankment material. The LBR is found by compacting soils in the laboratory at moistures varying from the dry side of the optimum moisture content to the wet side using a 10-pound rammer dropped from a height of 18 inches. This compaction procedure is a modification of AASHTO T180-10, Method D. This test was performed on soil samples from sites one and two, but soil samples were unavailable for site three. The material tested was to be utilized for the stabilized subgrade layer; therefore, it needed to meet the requirements of Type B Stabilization (LBR-40) according to the FDOT 2009 Rigid Pavement Design Manual. After running the first test, the peak LBR value of 60.3 was found to be at a moisture content of 9.63%. For the next test, the first two samples verified that the LBR value was in accordance with the FDOT specifications, so further testing was not required. Table 3-3 shows the LBR and the maximum dry density, in pounds per cubic foot (pcf), for slab 1 and Figure 3-9 shows the respective optimum soil moisture content. Table 3-4 shows the LBR and maximum dry density for slab 2.

Table 3-3: Slab 1 – LBR and maximum dry density

Sample	Moisture Content (%)	LBR	Maximum Dry Density (pcf)
1	4.89	26.1	111.2
2	7.15	46.3	112.8
3	9.63	60.3	115.6
4	11.18	53.3	112.4
5	14.11	18.2	110.2

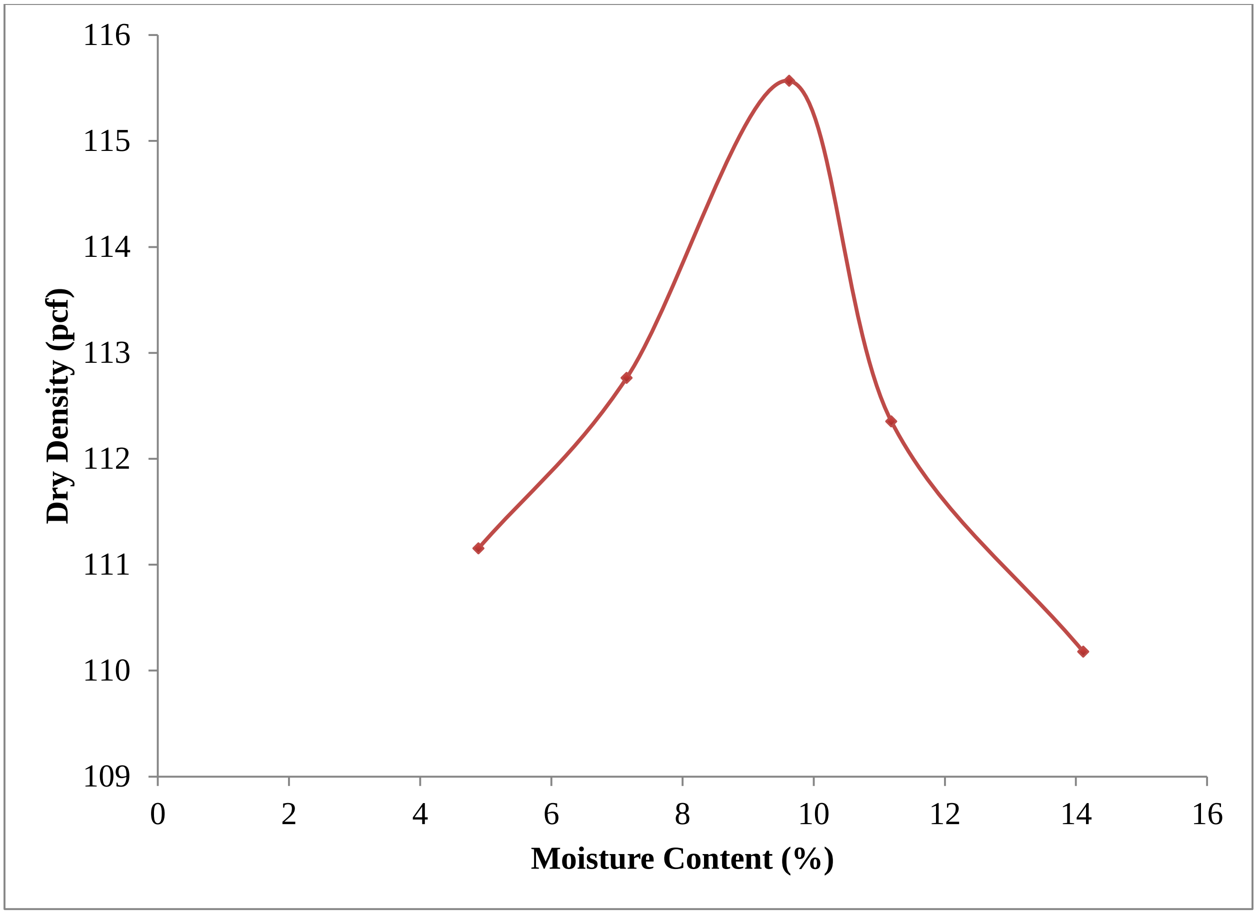

Figure 3-9: Optimum dry density for Slab 1

Table 3-4: Slab 2 – LBR and maximum dry density

Sample	Moisture Content (%)	LBR	Maximum Dry Density (pcf)
1	9.33	70.1	113.6
2	11.05	81.6	113.5

3.3.3 Dynamic Cone Penetrometer

The Dynamic Cone Penetrometer (DCP) test is an in situ penetration test in which a cone is driven into the soil and the number of blows required to advance the cone is recorded as presented in Figure 3-10. The results from the DCP test can be correlated to California Bearing Ratio (CBR) and Limerock Bearing Ratio (LBR) values and can be used to estimate the roadbed modulus (Shoop et al. 2008). The equation for calculating the CBR is provided in Equation 3-1.

This gives an indication of the strength of the in situ soil for the engineer to use in designing the roadway.

$$CBR = \frac{292}{DCP^{1.12}} \quad \text{Equation 3-1}$$

where

CBR: California Bearing Ratio

DCP: Dynamic Cone Penetrometer (mm per blow)

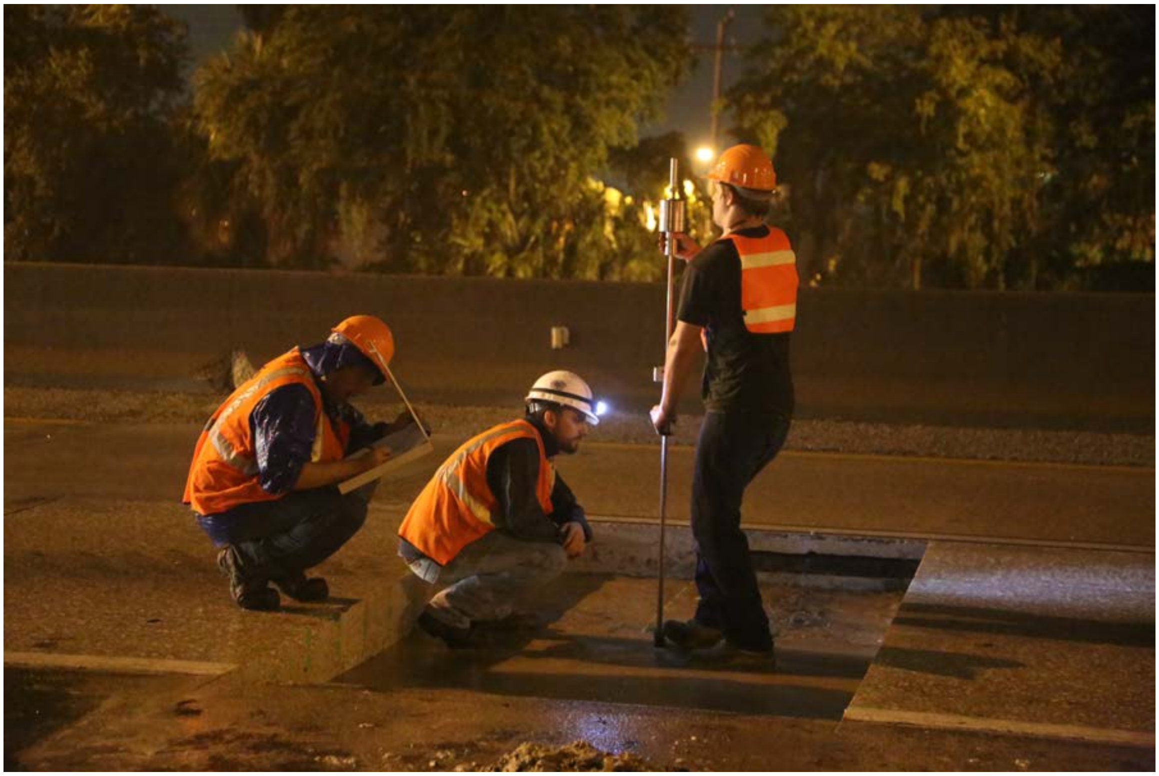

Figure 3-10: DCP test in progress for Slab 1

The test was performed in accordance with ASTM D6951 at the first and third slab replacement locations, as the DCP equipment was not available for the second site visit. The test was performed at three different locations for the first site and at two locations for the third site; the soil collected from each site was of the same composition. Figure 3-11 presents a map of the locations within the slab where the DCP measurements were acquired. For each test, the depth of penetration for a total of 12 blows was recorded and the average penetration rate (inches per blow) was calculated (note that the average value needs to be converted to mm before using in Equation 3-1).

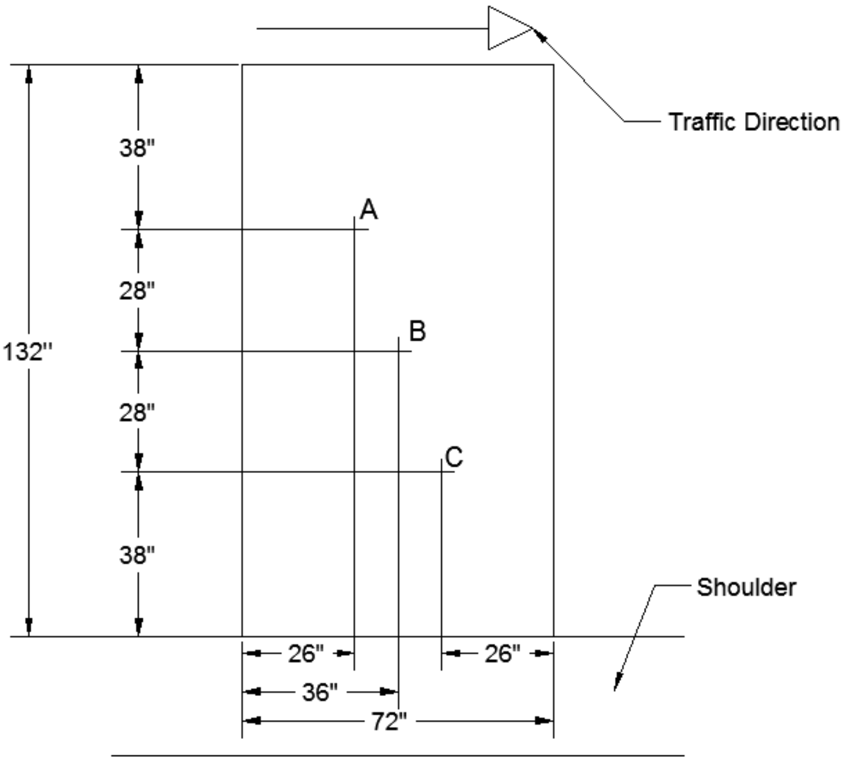

Figure 3-11: Locations for DCP testing for Slab 1

The raw data collected for slabs 1 and 3 are presented in Table 3-5 and Table 3-6, respectively, and the penetration vs. blow count is presented graphically in Figure 3-12 and Figure 3-13. Table 3-7 and Table 3-8 provide the conversion from DCP to CBR as provided by Equation 3-1.

Table 3-5: Slab 1 – DCP data

Blow Count	**Total Penetration (in)**		
	Location A	**Location B**	**Location C**
0	2.3	2.6	2.1
1	3.1	4.2	3.1
2	3.5	5.7	3.7
3	4.6	6.5	4.3
4	5.2	7.2	4.8
5	5.7	7.8	5.3
6	6.2	8.3	5.8
7	6.7	8.7	6.1
8	7.2	9.2	6.6
9	7.8	9.5	7.0
10	8.4	10	7.4
11	9.0	10.4	7.8
12	9.5	10.8	8.2

Table 3-6: Slab 3 – DCP data

Blow Count	**Total Penetration (in)**	
	Location A	**Location B**
0	0.0	0.0
1	0.2	1.8
2	2.0	1.8
3	2.2	4.0
4	3.5	4.0
5	3.7	5.9
6	5.3	5.9
7	5.3	7.3
8	6.8	7.3
9	6.8	8.2
10	8.2	9.7
11	8.2	9.7
12	9.5	11.2

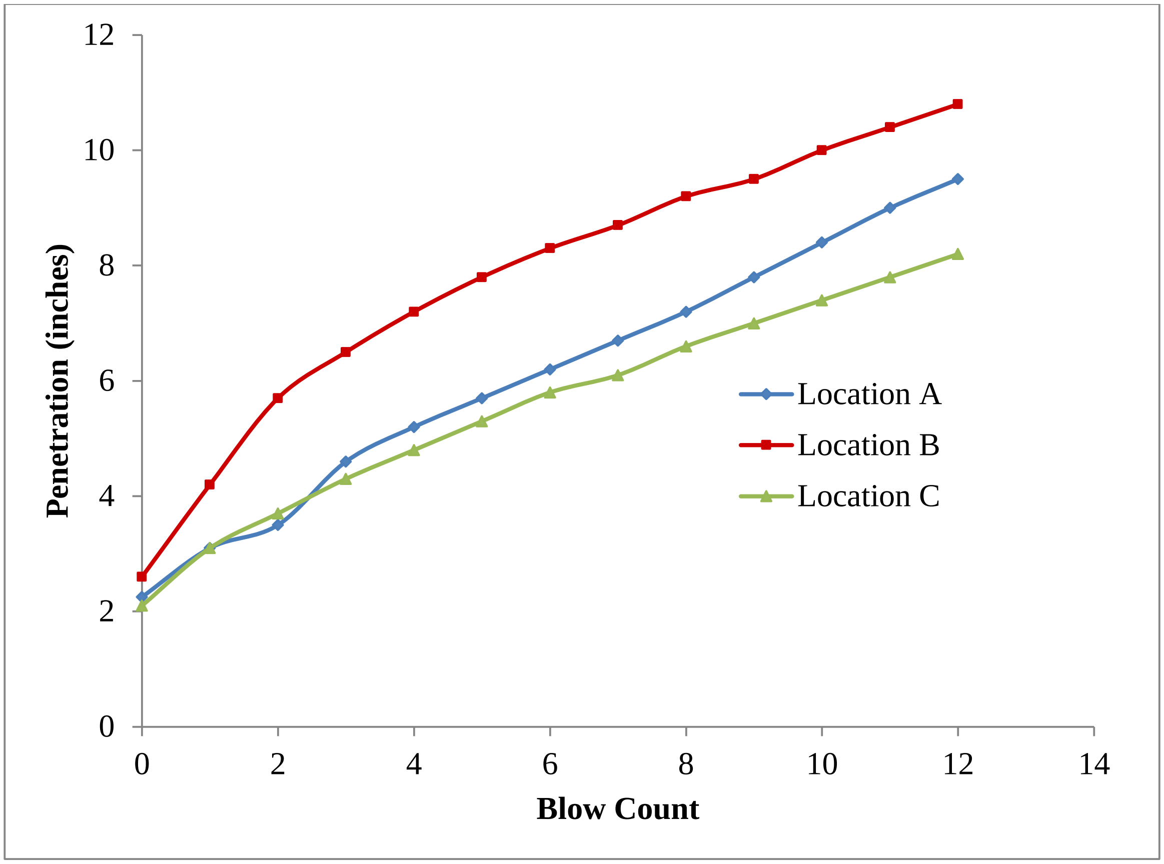

Figure 3-12: DCP data for Slab 1

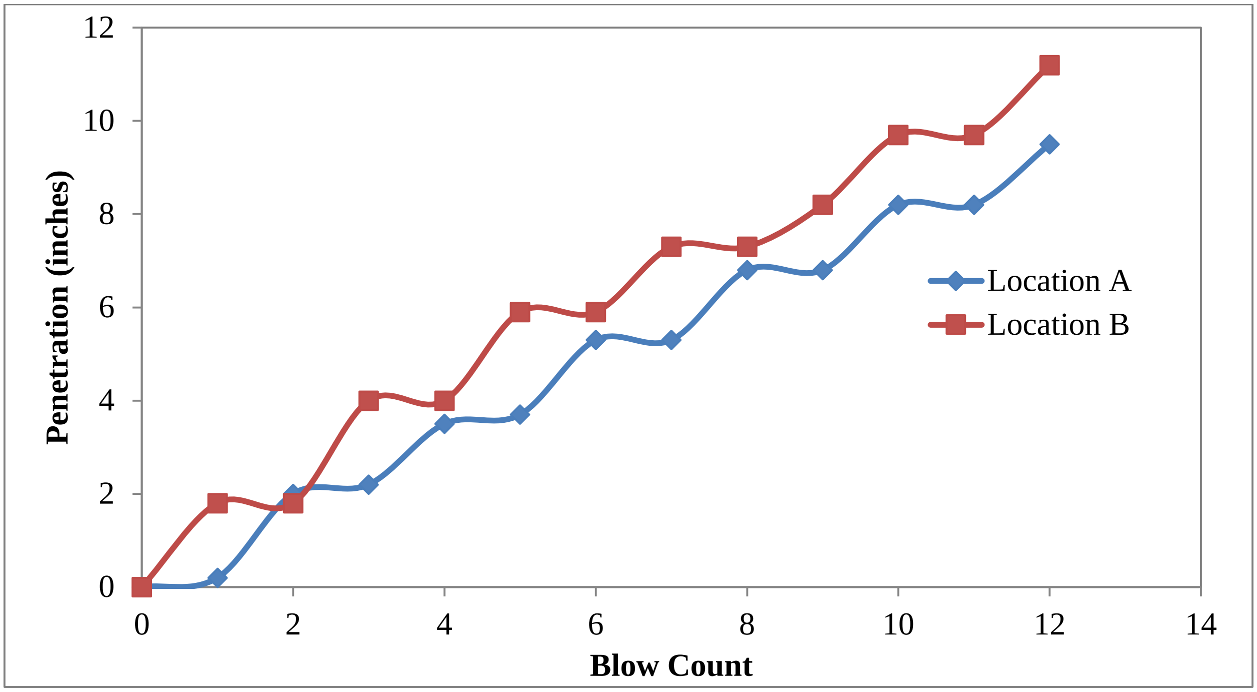

Figure 3-13: DCP data for Slab 3

Table 3-7: Slab 1 – DCP correlation to CBR

Location	DCP (in/blow)	CBR (%)
A	0.604	13.71
B	0.683	11.94
C	0.508	16.64

Table 3-8: Slab 3 – DCP correlation to CBR

Location	DCP (in/blow)	CBR (%)
A	0.792	10.12
B	0.930	8.46

3.4 Fresh Properties of Concrete Testing

3.4.1 Unit Weight

The unit weight of the concrete was measured using a non-standardized method. Due to the unusually rapid-setting nature of the concrete, it was not possible to remove the concrete in the mold prior to set (approximately 15 minutes). Therefore, it was decided to remove the concrete from the mold after it had hardened. A typical six-inch by 12-inch steel cylinder mold was used to measure the unit weight. The measurement of unit weight deviated from ASTM C138, the standard method of acquiring unit weight for concrete, because the measure (or specimen mold) did not meet the specifications prescribed in ASTM C29 (referenced in ASTM C138), which specifically states the height of the measure will not be more than 150% of the diameter. In this case, the steel mold used to acquire density, shown in Figure 3-14, did not meet that specification, as the height was 200% of the diameter. (6”x12”). However, it was deemed reasonable as the typical measures (molds) used to acquire density do not allow the removal of hardened concrete without damage.

Figure 3-14: Unit weight measurement for Slab 3

A summary of the measured concrete unit weight for each of the slabs is presented in Table 3-9. The results indicate that the unit weight is slightly lower than the unit weight of typical normal-weight concrete, which is between 140 and 160 lb/ft^3 (Akroyd 1962) but is typical of concrete which incorporates Florida limerock as the coarse aggregate, and similar values have been obtained in other FDOT research projects (Ferraro 2009).

Table 3-9: Unit weight measurements (after accelerator addition)

Location	Unit Weight (lb/ft^3)
Slab 1	143.01
Slab 2	138.53
Slab 3	141.38

3.4.2 Placement Temperature

The placement temperature of the fresh concrete was obtained for quality assurance for each concrete mixture delivered. On-site temperature measurement is important as the temperature of the concrete can affect the workability, setting time, and rate of strength development. For projects that incorporate accelerating admixtures at high dosage rates, such as this project, the early-age strength is dependent upon temperature (De Belie et al. 2005). The temperature was taken at each location at the point of discharge from the concrete mixing truck as per ASTM C1064 "The standard test method for freshly mixed concrete." Figure 3-15 shows a picture of slab 3 before concrete placement. Table 3-10 shows the initial placement temperatures for the three field slabs.

Figure 3-15: Beginning of concrete placement for Slab 3

Table 3-10: Initial temperature measurements

Location	**Temperature (°C)**
Slab 1	35.5
Slab 2	31.7
Slab 3	25.0

3.4.3 Initial Slump

The slump test measures the consistency of fresh concrete; this measure is related to the workability of the concrete. Good workability results in more uniform properties of the concrete. The concrete must achieve a certain amount of workability for it to fill space evenly. This is especially important near the instrumentation that was in place for concrete testing (the instrument trees). In order to achieve accurate results, the concrete must be in full contact with the instrumentation. Figure 3-16 shows a picture of the slump being read for slab 3.

Figure 3-16: Slump test for Slab 3

The FDOT Standard Specification for Road and Bridge Construction Section 353, Concrete Pavement Slab Replacement, specifies that "When an accelerating admixture is used in solution, the amount of water in the solution is considered to be part of the mixing water." Therefore, it is often the case that a significant increase in slump will take place immediately after the addition of accelerating admixtures to concrete used for slab replacement. Accordingly, the initial slump was measured prior to the addition of the accelerator for slab two and three in accordance with ASTM C143. During the initial site visit (Slab 1) the slump prior to the addition of the accelerating admixture was not obtained as the contractor did not allow slump measurements prior to the addition of the admixture to take place. Table 3-11 shows the initial concrete slump readings for the two slabs.

Table 3-11: Initial slump prior to the addition of accelerating admixture

Location	Initial Slump (in)
Slab 2	2.5
Slab 3	3.5

3.4.4 Slump Loss

Due to the presence of a large quantity of accelerating admixture in the concrete for each of the three slabs, it was decided to measure the slump loss to collect information with regard to the working time available for placing the concrete. The results for slump loss are provided in Tables 3-12 to 3-14 and Figures 3-17 through 3-19. The slump loss (time to reach a slump of zero) was 19 minutes (extrapolated) for slab 1 as compared with 44 minutes for slab 2. The drastic difference in results can be attributed to concrete delivery temperature and ambient temperature for each slab. As reported in Figure 3-4 and Figure 3-5, the delivery temperatures for slabs 1 and 2 were 36˚C and 28˚C, and the ambient temperatures were 23˚C and 19˚C, respectively. The lower ambient and concrete delivery temperatures were intensified for slump loss for slab 3 as the delivery temperature was 25˚C and the ambient temperature was 11˚C. The relatively low temperatures resulted in a relatively long time to attain zero slump, which was approximately 82 minutes, found from extrapolation of the data presented in Figure 3-19.

Table 3-12: Slab 1 – Slump loss

Time from Accelerator Addition (min)	Slump (in)
8	2.75
14	1
18	0.25

Table 3-13: Slab 2 – Slump loss

Time from Accelerator Addition (min)	Slump (in)
10	2.75
13	2.5
17	2.5
26	3.0
32	2.0
38	1.25
44	0

Table 3-14: Slab 3 – Slump loss

Time from Accelerator Addition (min)	Slump (in)
7	7.5
14	7.5
23	4.75
41	3.25
51	2.5
63	1.5

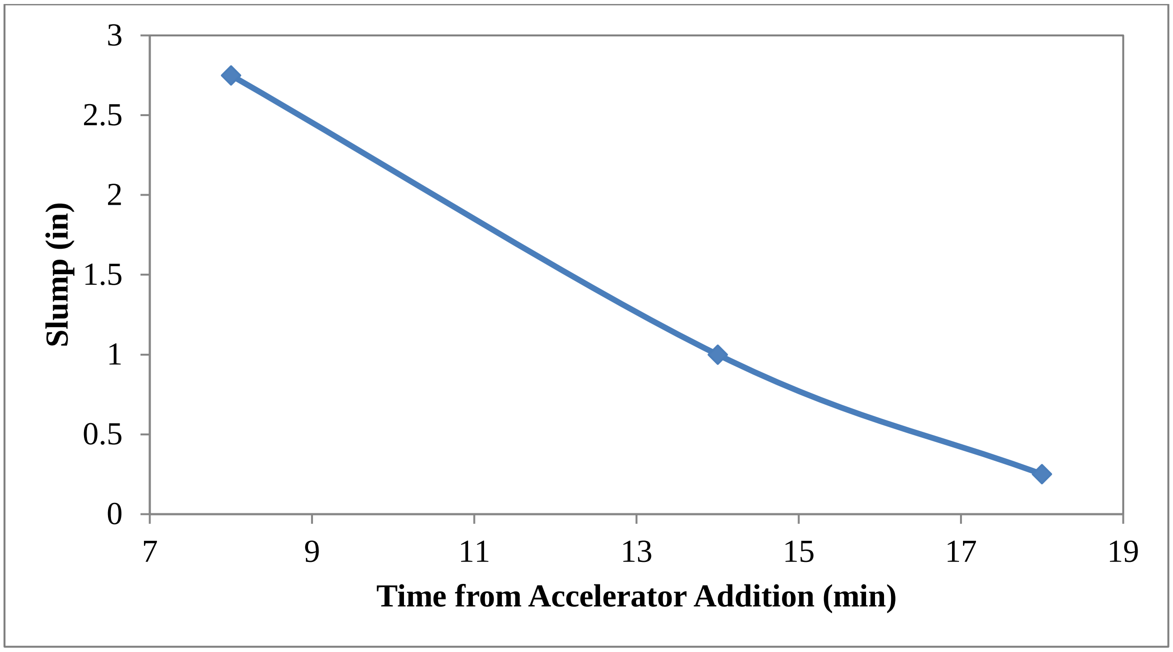

Figure 3-17: Slump loss for Slab 1

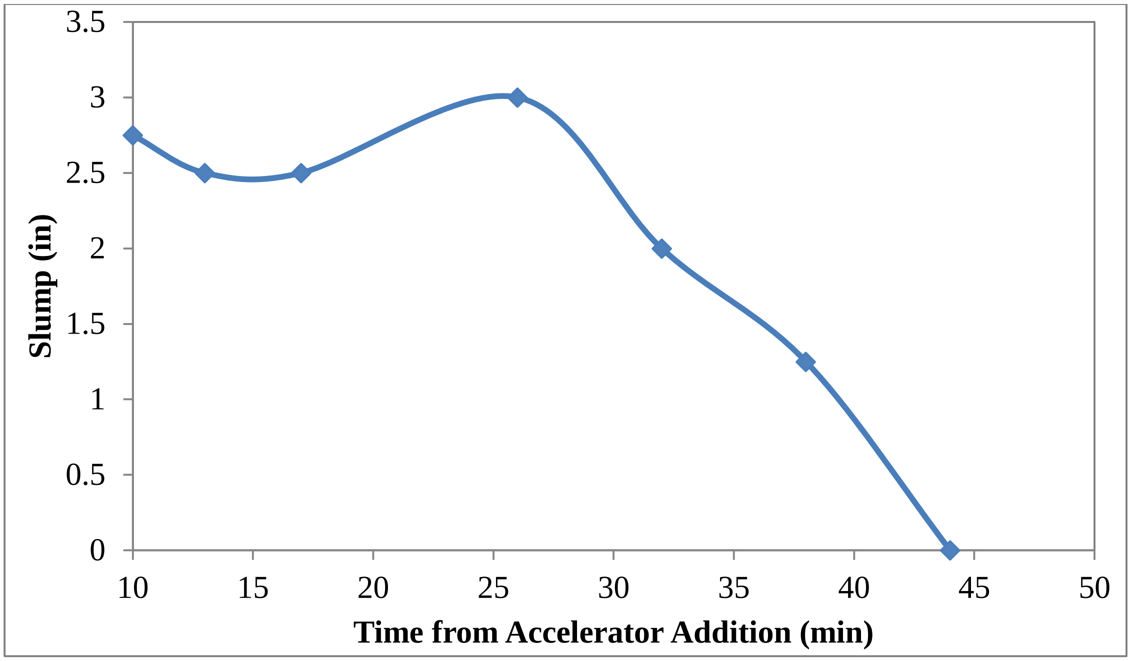

Figure 3-18: Slump loss for Slab 2

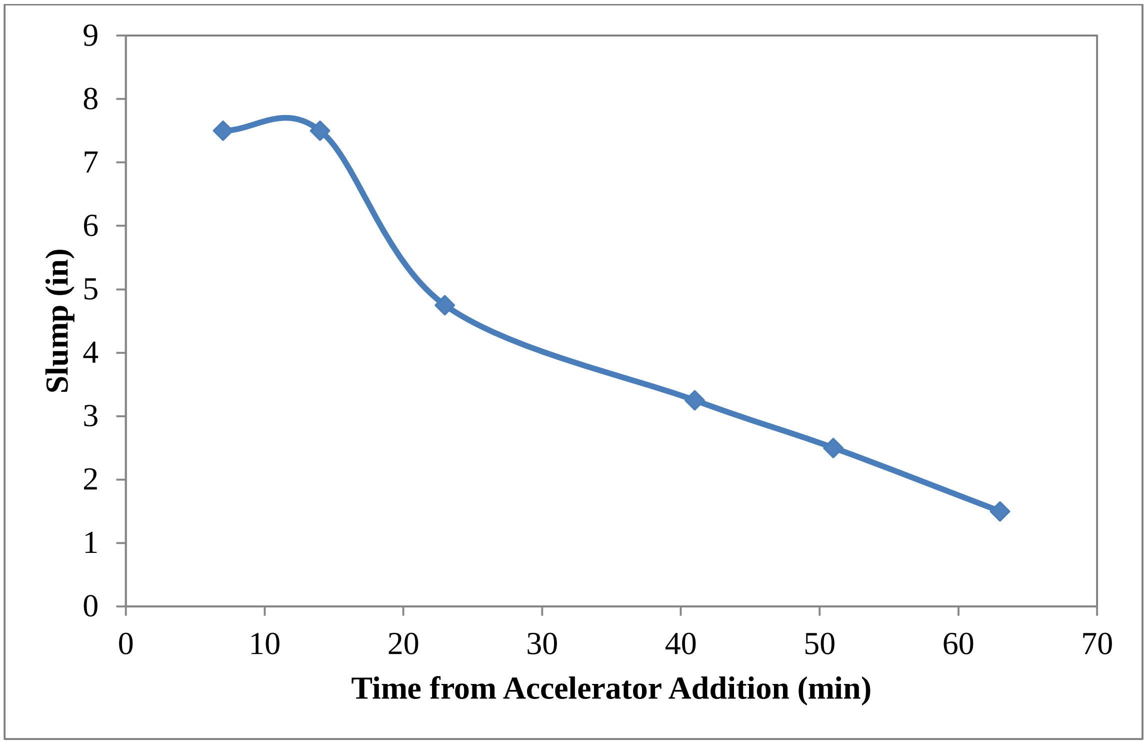

Figure 3-19: Slump loss for Slab 3

3.4.5 Concrete Specimen Fabrication

Concrete cylinder specimens were made on-site from the delivered concrete used for the slab replacement. The cylinder molds used were typical 4”x8” cylinder molds meeting ASTM C31 specifications were used. Due to time limitations imposed by the addition of accelerator to the concrete, a vibrating table, instead of rodding, was used in the field to consolidate the specimens, as shown in Figure 3-20. Specimens for compressive strength, modulus of elasticity, splitting tensile, heat of hydration, and coefficient of thermal expansion testing were created.

Figure 3-20: Concrete cylinder specimen fabrication

3.4.6 Concrete Specimen Curing

It is well documented that concrete will hydrate and gain relative strength and elastic properties at a faster rate when cured at higher temperatures (Malhotra and Carino 1991, Ferraro 2009). Thus, a portion of this research was dedicated to acquiring strength properties at different temperatures in an effort to replicate the relative strength in the concrete slab itself. Generally, the greater the mass of a hydrating concrete member, the greater the internal temperature rise due to the exothermic hydration reactions taking place, and the self-insulation of the surrounding concrete (lower surface-area-to-mass ratio). Therefore, unless insulation is used during the curing of 4' by 8" cylinders, they do not achieve the same temperatures, and resultant strengths, as the concrete replacement slabs. This difference in temperature can produce considerable differences in strength, especially at early ages. Therefore, several different methods of cylinder curing were explored to establish a method that could produce strengths comparable to that of the concrete pavement slabs:

- Ambient curing of specimens
- Protection curing of specimens
- Curing of specimens in a cooler
- Curing of specimens in a foam cooler with a higher degree of insulation

3.4.6.1 Ambient Curing

4" by 8" cylinders were cured under ambient conditions. The cylinders were placed on the ground near the slab without covering.

3.4.6.2 Protection Curing

The acceptance of concrete for slab replacement, per Section 353, Concrete Pavement Slab Replacement, of the FDOT Standard Specifications for Road and Bridge Construction (referred to subsequently as Section 353), is based on plastic properties, the strength of concrete prior to opening of traffic, and 24 hour strength. Typically, the cylinders used for slab acceptance are covered with a blanket adjacent to the last slab placed for the day as shown in Figure 3-21 and 3-22. These cylinder specimens are considered to be "protection-cured" for the purposes of this report.

Figure 3-21: Protection-cured concrete cylinder specimens

Figure 3-22: Covering of protection-cured concrete cylinder specimens for Slab 2

3.4.6.3 Curing of Specimens in a Cooler

In an effort to partially contain the heat generated during curing, cylinders were placed in an insulated cooler for initial curing as presented in Figure 3-23. The grouping together of cylinders also aided in containing the heat generated by reducing the exposed surface area. Section 353 states "Make a minimum of four test cylinders from the last slab for each day of placement to assess strength for protection and opening to traffic (protection set). Cure the protection set of cylinders by methods identical to those used in curing the concrete replacement slabs. Cure the acceptance set of cylinders identical to the protection set of cylinders for the first 6-hours, then by laboratory cured conditions thereafter until the 24-hour strength test." However, there was concern, due to the high accelerator contents, that there could be some self-desiccation during the latter stages of initial curing. Cylinders that are tested in a saturated condition will have a lower compressive strength than those tested in a dry condition (Hilsdorf and Kesler 1966). FDOT specification 353 does not require the protection cylinders to be moist cured for testing prior to the opening of the slab to traffic. However, specification 353 specifically states that the concrete specimens for strength testing must be laboratory-cured subsequent to the opening of the slab to traffic, prior to the 24-hour testing. It has been shown that cylinders cured at high temperatures in the absence of water can achieve artificially high strength as compared to moist cured cylinders when the compressive strength exceeds 1500 psi (Ferraro 2009). Therefore, it was decided to introduce lime-saturated water to the specimens in the cooler after three hours of curing. Unfortunately, as presented in Figure 3-24, the introduction of the water cooled the concrete substantially (from approximately 47˚C to 35˚C).

Figure 3-23: Cooler-cured concrete cylinder specimens

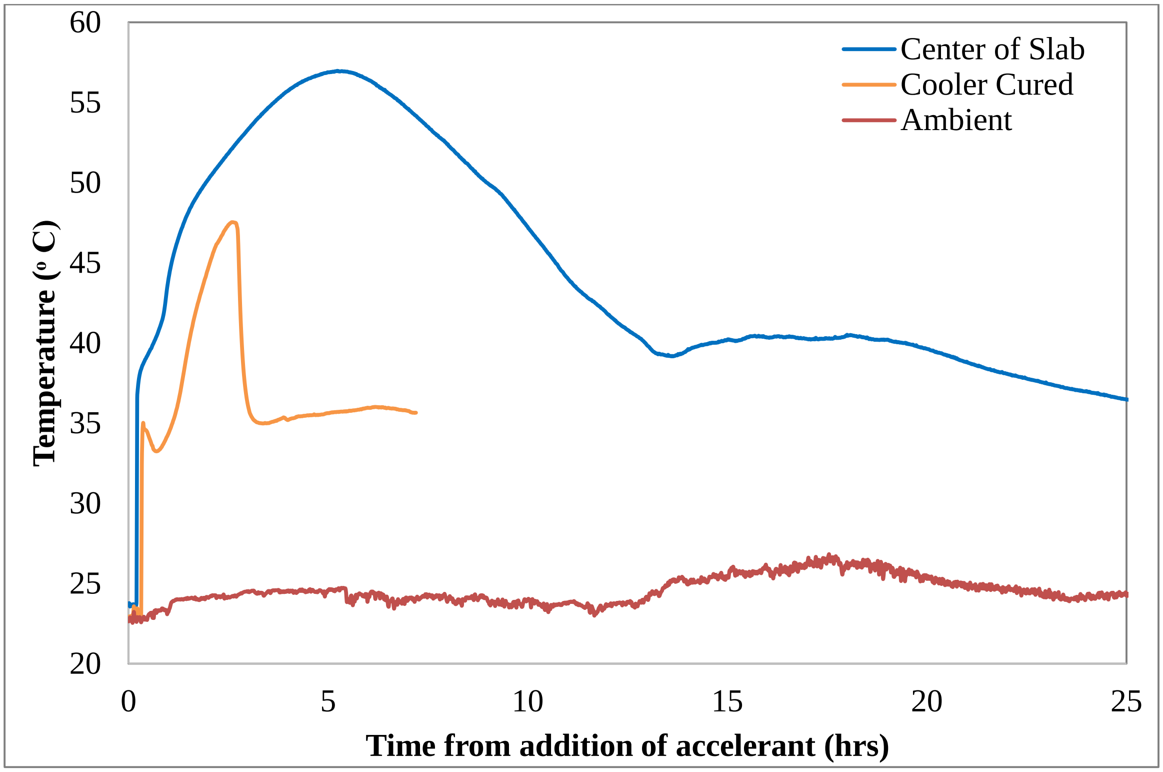

Figure 3-24: Temperature of concrete subsequent to placement – Slab 1

The temperature data for the corner of slab 1 is presented in Figure 3-24 for the protection-cured cylinders and the cylinders placed in the cooler. Since the temperature (and resultant maturity) is lower at the corner locations of the concrete slab, it was considered the best location for comparison of temperature data since this location would represent the minimum maturity attained by the slab.

The cylinders cured using the protection-curing method had very different temperature profiles than that of the concrete slab center. The protection-cured cylinders were left in the ambient conditions until sometime after the concrete was placed and initial set had taken place. Subsequent to initial set they were placed under the tarp with the slab in an attempt to match temperature conditions at the surface of the slab. The lag in temperature rise of protection-cured cylinders, compared to the slab, caused by initial curing under ambient conditions cannot be compensated for by subsequent placement on the curing slab and covering with a blanket. In addition to this, slab 1 protection-cured cylinders were exposed to significant rain, and did not reach their original placement temperature of 35˚C until approximately 2.5 hours after the slab was placed. Furthermore, the temperature dropped relatively rapidly after placement due to the removal of the cover of the slab. After the blanket was removed the cylinders lost heat through the top and sides, whereas the slab only lost heat through the top.

3.4.6.4 Curing of Specimens in a Foam Cooler

Subsequent to the placement of the first slab, it was decided to create a heavily-insulated foam box to better replicate the temperatures experienced in the slab. Since the cylinders initially cured in the cooler from the slab 1 replacement did not reach the temperature attained at the corner of the slab, it was decided to use a well-insulated box to more closely replicate the minimum temperature (maturity) attained in the slab. Figure 3-25 is a photo of the heavily-insulated box used to cure cylinders for Slabs 2 and 3.

Figure 3-25: Heavily insulated foam curing box

Figure 3-26 shows the temperature data obtained from the corner of Slab 2, the protection-cured cylinders, the cylinders placed in the heavily-insulated box, and the cylinders cured in a regular cooler. Similar to the results obtained for Slab 1, the Slab 2 protection-cured cylinders and the cylinders cured in the regular cooler did not attain the temperature reached in the corner of the slab. The cylinders in the heavily insulated foam box did not initially gain temperature at the rate experienced by the corner of the slab; however, the temperature profile obtained by the heavily insulated cooler best replicated the temperature profile in the corner of the concrete slab. Similar to the behavior experienced by the protection cylinders created for Slab 1, the cylinders created for Slab 2 experienced a rapid cooling trend upon the removal of the curing blankets. Upon the introduction of water into the cooler, the cooler cured cylinders experienced a rapid cooling trend, similar to the cylinders created for Slab 1.

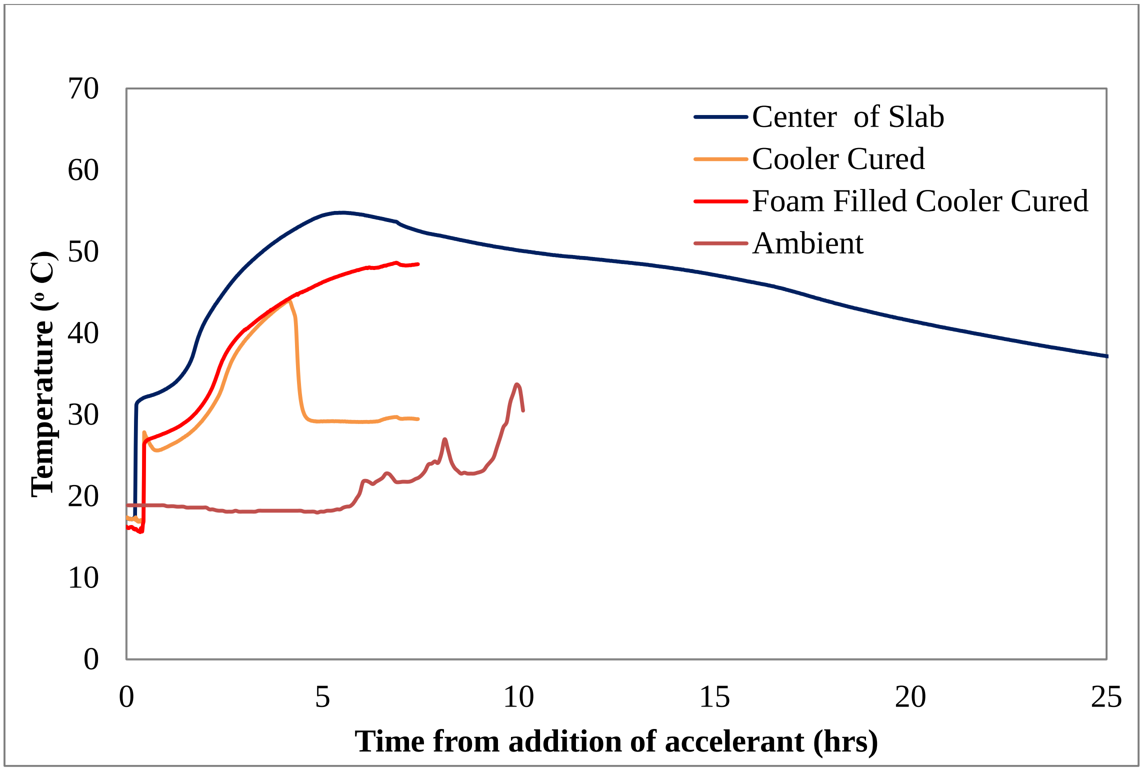

Figure 3-26: Temperature of concrete subsequent to placement – Slab 2

The data presented in Figure 3-27 are the temperature data obtained from the corner of Slab 3, the cylinders placed in the heavily-insulated box, and the regular cooler. The cylinders in the heavily-insulated cooler did not attain the temperature reached in the corner of the slab. The temperature discrepancy between the insulated specimens and the slab was amplified by the fact that the concrete was delivered at a relatively low temperature (25°C). The relatively small mass of the specimens in comparison to the concrete slab and the relatively low ambient temperature were the primary reasons the cylinder specimens created for Slab 3 did not reach temperatures comparable to the slab.

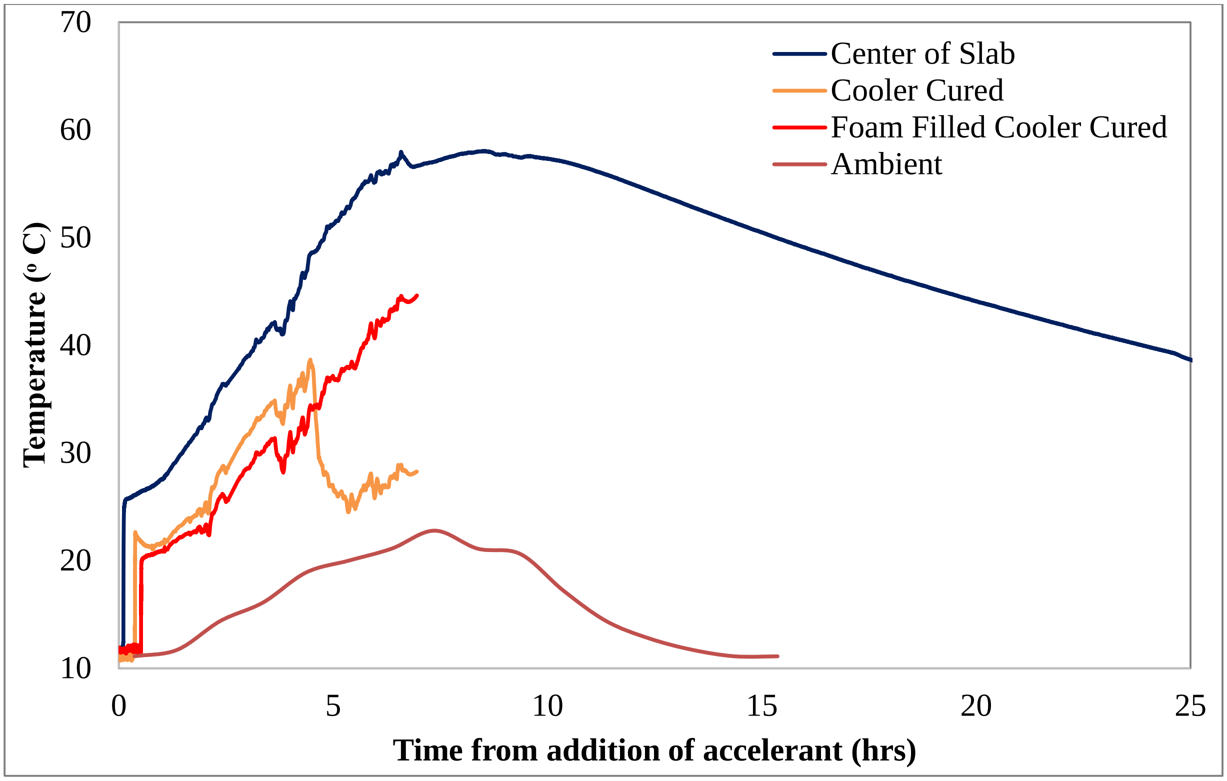

Figure 3-27: Temperature of concrete subsequent to placement – Slab 3

3.5 Hardened Properties of Concrete Testing

3.5.1 Compressive Strength

The compressive strength of concrete slabs is the only strength-related property used to accept the in-place concrete for repair slabs per FDOT specification 353. The acceptance criteria for concrete used for concrete pavement slab replacement requires that the cylindrical specimens achieve 2,200 psi at 6 hours or prior to opening the slab to traffic. Concrete cylinder specimens were made and tested for their compressive strength in accordance with ASTM C39. Figure 3-28 shows the machine used to measure the concrete compressive strength in the field. The cylinder specimens were tested at different times and curing conditions in an effort to identify appropriate curing methods, and to acquire the rate of compressive strength gain with respect to time. Multiple cylinders were tested for each time and the average compressive strength was recorded. As discussed in section 3.4.6, concrete specimens from Slab 1 were cured in a cooler and compared with protection-cured specimens; for the second and third slab locations, concrete specimens were cured via protection-curing, a cooler, and a heavily-insulated foam box before testing.

Figure 3-28: Compressive strength testing in the field

Due to the logistics of the data acquisition, and the large number of early-age test specimens, a mobile field-testing unit was assembled for testing of concrete specimens at the project site. Subsequent to the placement of the slab, the research team performed on-site testing (Jacksonville, Florida, for Slabs 1 and 2) of the compressive and tensile strengths and the modulus of elasticity for the first six hours prior to returning to the University of Florida to complete testing. The results of the compressive testing for slab 1 are presented in Table 3-15. Figure 3-29 presents the compressive strength vs. time for the cylinders cured in the cooler only. Both the protection cylinders and the cooler-cured cylinders were tested at 6 hours, and due to the higher temperatures experienced by the cylinders in the cooler, the compressive strength was approximately 30% higher for those cylinders. The difference in the compressive strength between the protection-cured cylinders and the cooler-cured cylinders is not trivial. Because the cylinders experienced a lower temperature history than the slab, there is potential for the concrete producer to “overdose” the concrete with accelerating admixtures and portland cement in an effort to ensure the companion specimens meet the requirements of Specification 353, (2,200 psi at 6 hours) despite the fact that the companion specimens are not an accurate representation of the concrete within the slab.

Table 3-15: Slab 1 - Compressive strength

Test Time (hr)	**Compressive Strength (psi)**	
	Protection Cured	**Cooler Cured**
1.5	–	250
2	–	690
3	–	1530
4	–	2420
6	2730	3530
12	–	6200
24	–	7560
3 day	–	8800
28 day	–	6340

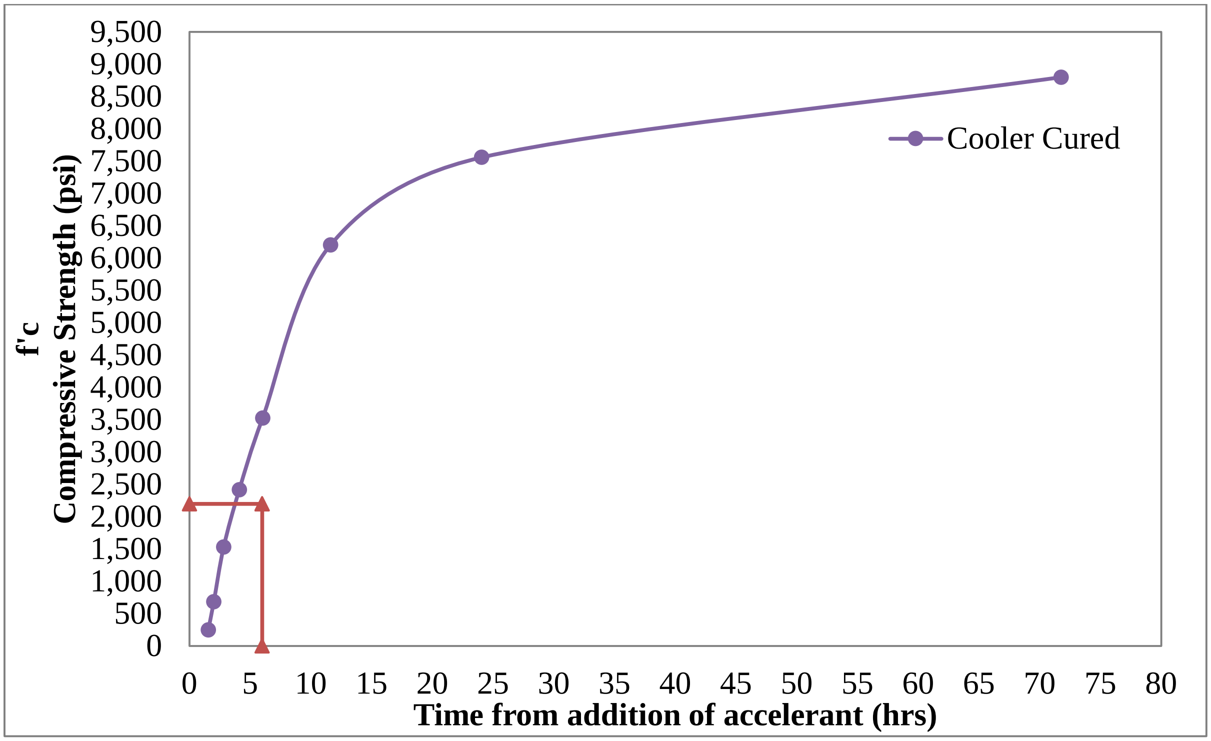

Figure 3-29: Compressive strength vs. time for Slab 1 cooler-cured specimens

The results of the compressive testing for slab 2 are presented in Table 3-16 and Figure 3-30. The results clearly indicate that the insulated environment results in significantly higher strengths when compared with curing in ambient conditions. The use of the highly-insulated foam cooler resulted in a relatively high early strength of the concrete, in excess of 4,000 psi at 6 hours, well in excess of the concrete pavement slab replacement specification.

Table 3-16: Slab 2 – Compressive strength

Test Time (hr)	**Compressive Strength (psi)**		
	Ambient Cured	**Cooler Cured**	**Foam-Insulated Cooler Cured**
2	–	120	–
2.5	–	430	–
3	370	690	950
4	830	1640	2380
6	1460	2950	4100
12	4130	5300	6530
24	6660	6970	–
3 day	–	8910	–
7 day	–	8040	–
28 day	–	7360	–

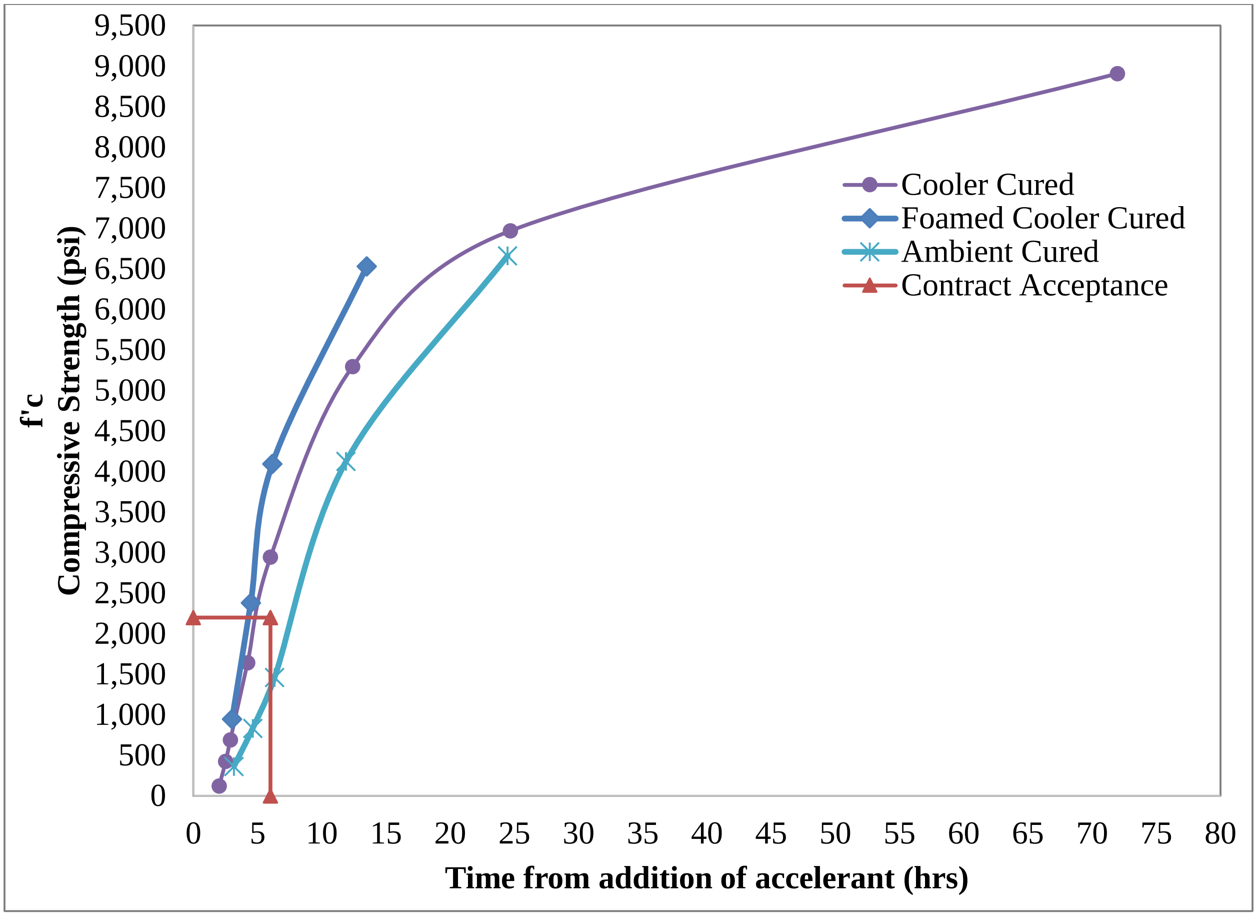

Figure 3-30: Compressive strength vs. time for Slab 2

The results of the compressive strength testing for Slab 3 are presented in Table 3-17 and Figure 3-31. The concrete provided for this project did not meet the requirements of the concrete pavement slab-replacement specification, as it did not achieve 2,200 psi in 6 hours. The primary reason for the low strength can be attributed to low delivery temperature and low ambient temperature. High-early strength concrete mixes are typically hot mixtures, which mean that their properties require a minimum concrete mixture temperature to meet strength-time constraints; otherwise strengths will be too low to meet specifications.

Table 3-17: Slab 3 – Compressive strength

Test Time (hr)	Compressive Strength (psi)		
	Ambient Cured	Cooler Cured	Foam-Insulated Cooler Cured
2	–	100	–
3	170	230	190
4	380	450	410
6	940	900	1140
12	2870	2430	3570
24	–	4180	–
3 day	–	6740	–
7 day	–	6990	–
28 day	–	7810	–

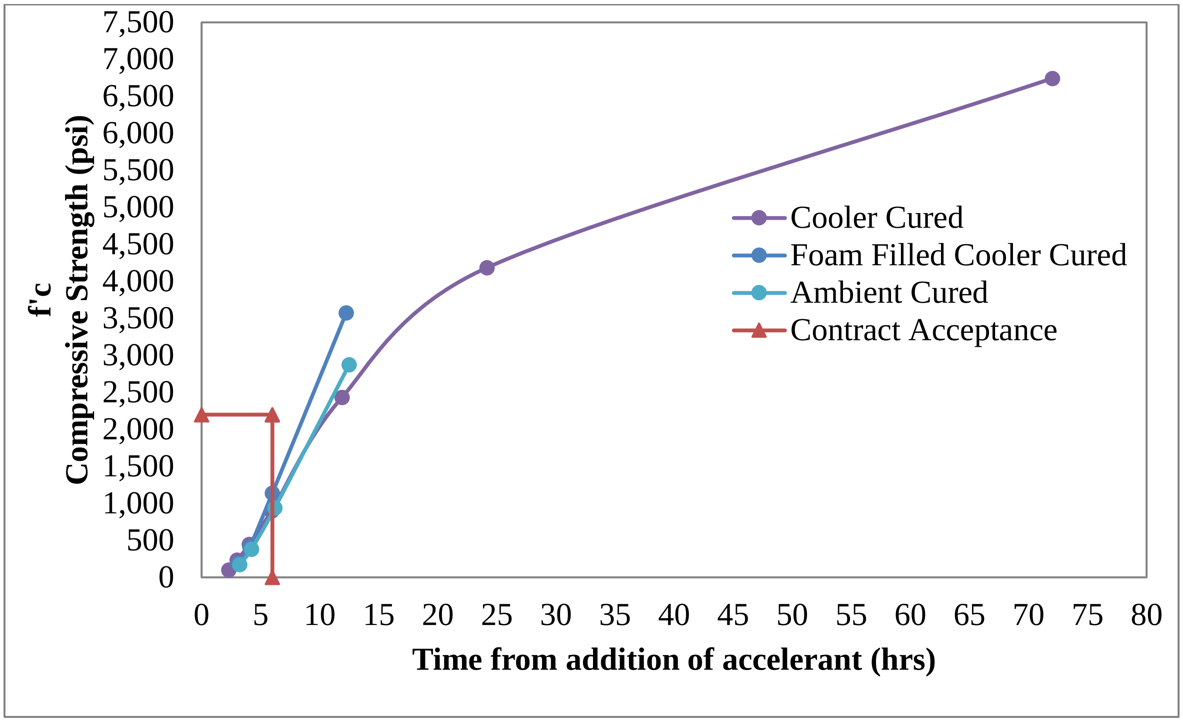

Figure 3-31: Compressive strength vs. time for Slab 3

3.5.2 Modulus of Elasticity

Modulus of Elasticity (MOE) is a mechanical property of concrete that gives an indication of the stiffness of the material. The MOE of concrete used for paving provides the basis for determining the roadway thickness and design. The higher the modulus, the stiffer the material, and as a result, the thinner the required roadway thickness, per AASHTO pavement design methodology. As concrete hydrates, the modulus of elasticity increases, which is analogous to the other strength properties of concrete. However, the increase in modulus of elasticity of hydrating concrete due to elevated temperatures leads to higher stresses that can create a higher probability of cracking. The modulus of elasticity testing of concrete cylinder samples for this research was performed in accordance with ASTM C469. Prior to the modulus of elasticity testing, the ultimate load was obtained via the average compressive strength as per ASTM C39. As per ASTM C469, the specimens were tested up to 40% of ultimate load. The concrete cylinder specimens were cured in a cooler and tested at different times to establish the relationship between the MOE and time. Tables 3-18 through 3-20 and Figures 3-32 through 3-34 present the modulus of elasticity results obtained for each of the slab mixtures. The rate of development of the modulus of elasticity was higher than that of the compressive strength development. Over 50% of the modulus development occurred at approximately 4 hours, and the majority of the development (85%) occurred within 24 hours of placement. As a result, the concrete is relatively brittle at very early ages, which can create the potential for cracking. The range of the MOE at 28 days for each of the mixes was 4,700,000 to 5,225,000 psi. The lowest MOE was experienced by Slab 3. The reason for the relatively low MOE is most likely attributed to the low placement temperature resulting in a delay in the development of hardened properties.

Table 3-18: Slab 1 – Modulus of elasticity

Test Time (hr)	**MOE (psi)**
	Cooler Cured
2	2,000,000
3	2,000,000
4	3,000,000
6	3,600,000
12	4,500,000
24	5,000,000
3 day	5,300,000
28 day	5,250,000

Table 3-19: Slab 2 – Modulus of elasticity

Test Time (hr)	**MOE (psi)**
	Cooler Cured
3	1,250,000
4	3,250,000
6	3,200,000
12	4,250,000
24	4,300,000
3 day	5,050,000
7 day	5,650,000
28 day	5,050,000

Table 3-20: Slab 3 – Modulus of elasticity

Test Time (hr)	**MOE (psi)**
	Cooler Cured
3	400,000
4	1,000,000
6	1,600,000
12	2,650,000
24	3,200,000
3 day	4,350,000
7 day	4,000,000
28 day	4,700,000

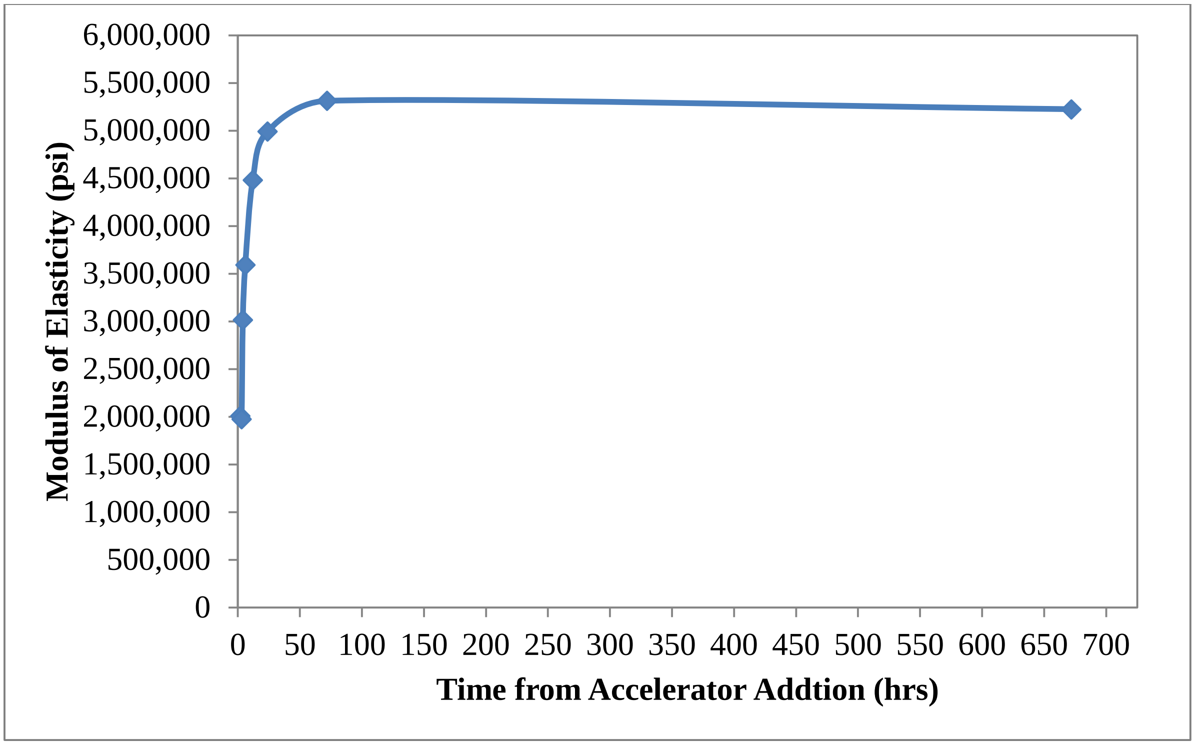

Figure 3-32: Modulus of elasticity vs. time for Slab 1

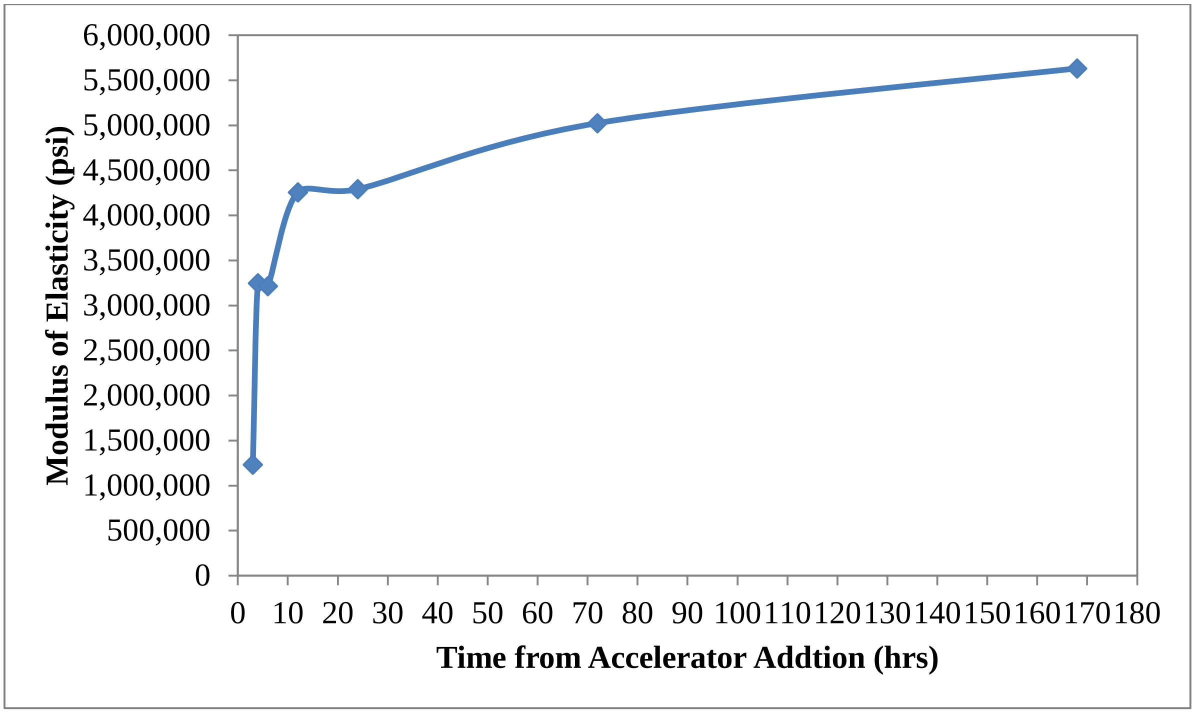

Figure 3-33: Modulus of elasticity vs. time for Slab 2

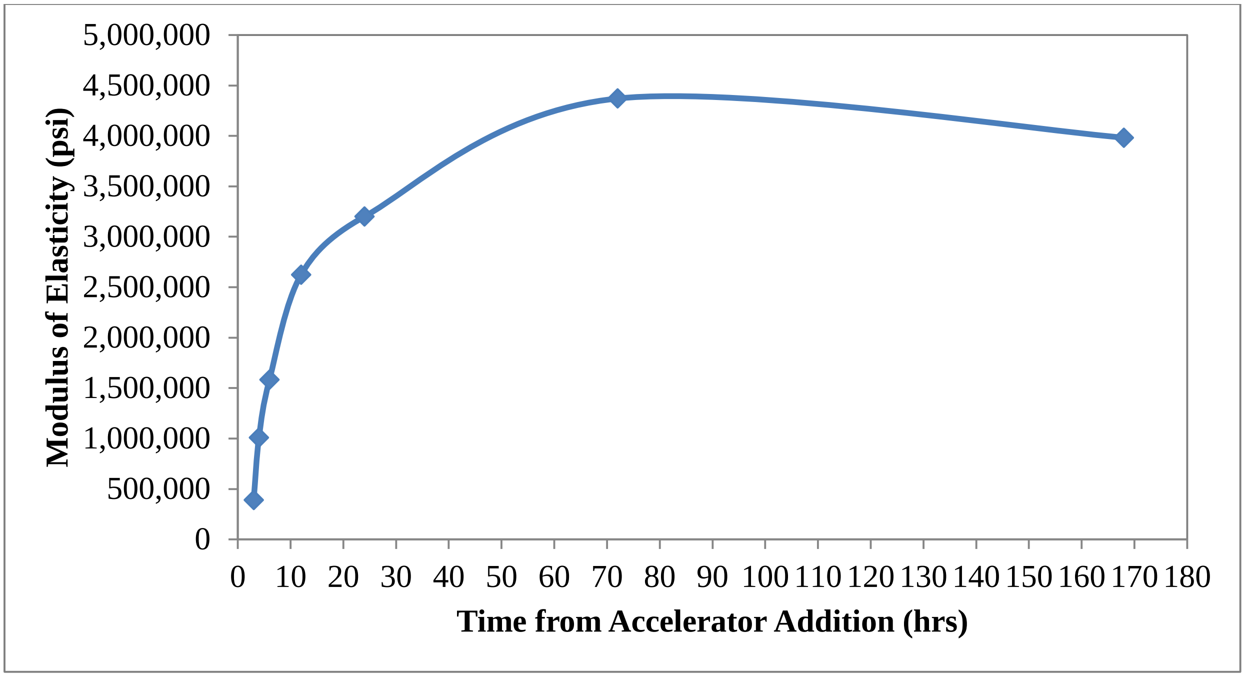

Figure 3-34: Modulus of elasticity vs. time for Slab 3

3.5.3 Splitting Tensile Strength

Splitting tensile strength testing was performed in an effort to obtain the tensile strength of the concrete for modeling purposes. The information obtained from the tensile strength testing is important with respect to modeling for each of the concrete slabs as failure typically takes place in tension. Tables 3-21 through 3-23 and Figures 3-35 through 3-37 present the splitting tensile strength results over time obtained for each of the slab mixtures. The results are consistent with typical findings and compressive strength testing results, where the majority of the strength development occurs within the first six hours, and the reminder of the strength development takes place with the first 3 days with little strength gain afterwards. The tensile strength of the cylinder samples tested within this research was performed in accordance with ASTM C496. Typically, concrete experiences cracking due to tensile forces resulting from internal or external stresses and strains. Therefore, the tensile strength with respect to time was measured to determine the stresses at which the concrete will crack or begin to fail.

Table 3-21: Slab 1 – Splitting tensile strength

Test Time (hr)	**Splitting Tensile Strength (psi)**
	Cooler Cured
3	255
4	405
6	415
72 (3 day)	510

Table 3-22: Slab 2 – Splitting tensile strength

Test Time (hr)	**Splitting Tensile Strength (psi)**
	Cooler Cured
4	280
6	365
12	485
24	550
3 day	640
28 day	630

Table 3-23: Slab 3 – Splitting tensile strength

Test Time (hr)	**Splitting Tensile Strength (psi)**
	Cooler Cured
3	145
4	165
6	365
12	470
3 day	660
7 day	675
28 day	630

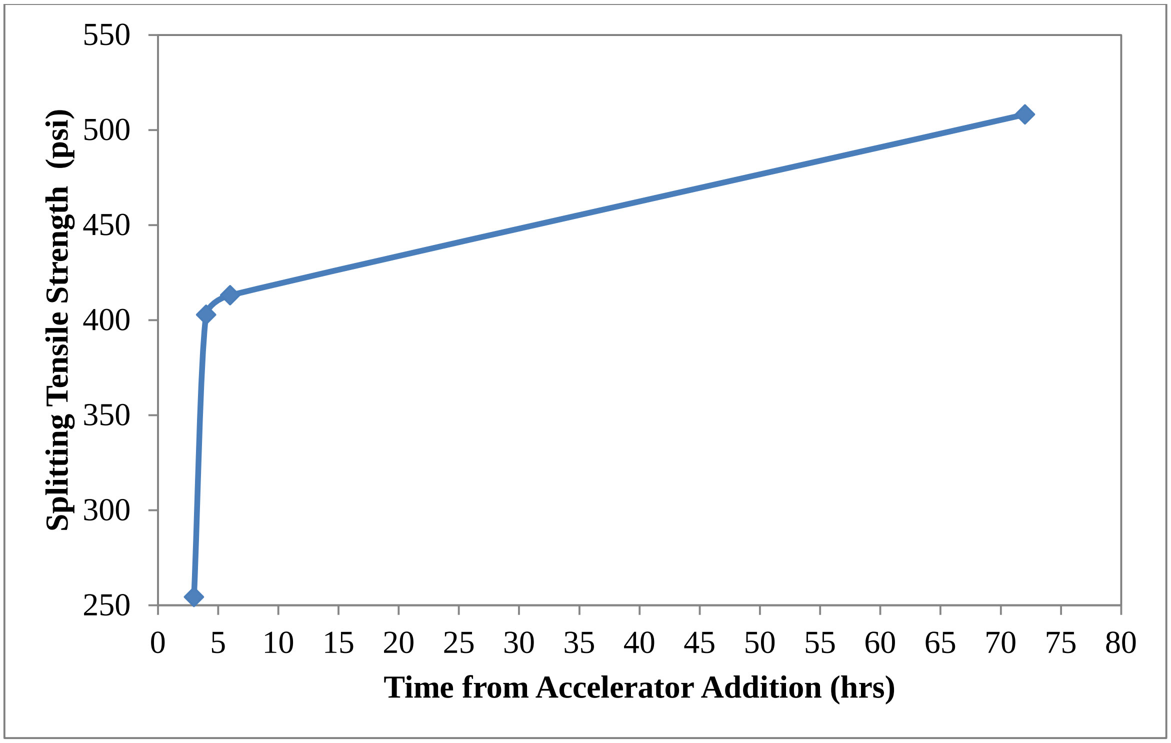

Figure 3-35: Splitting tensile strength vs. time for Slab 1

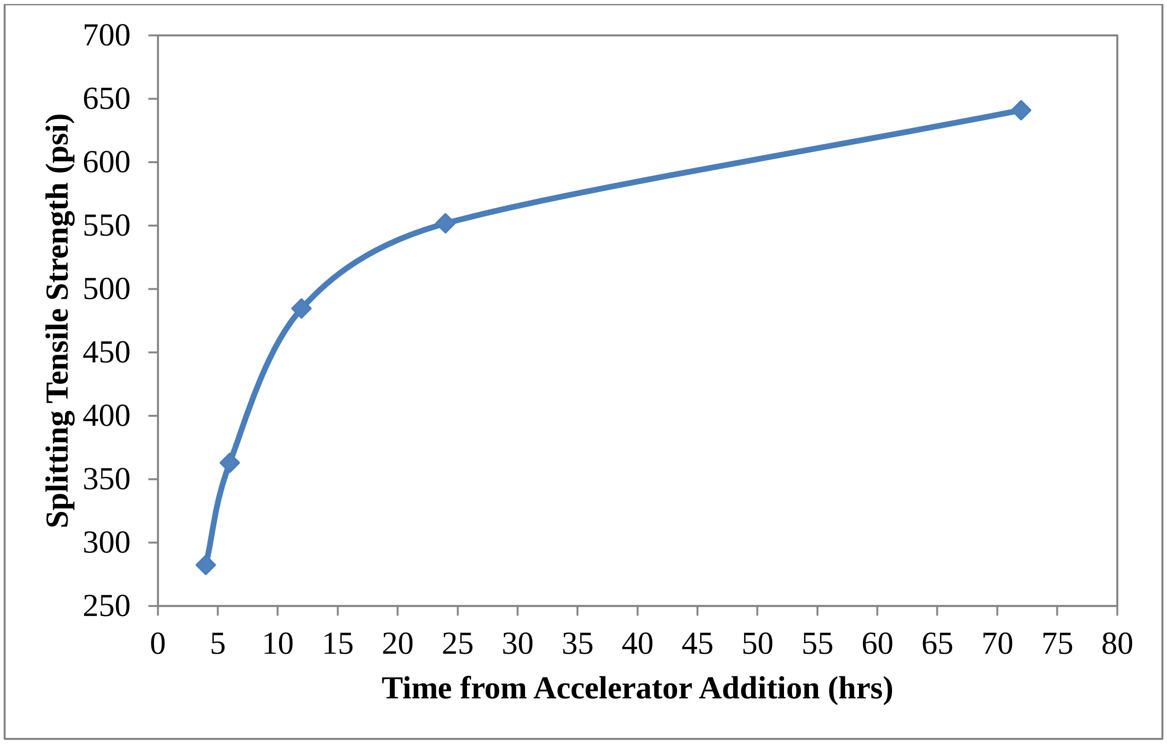

Figure 3-36: Splitting tensile strength vs. time for Slab 2

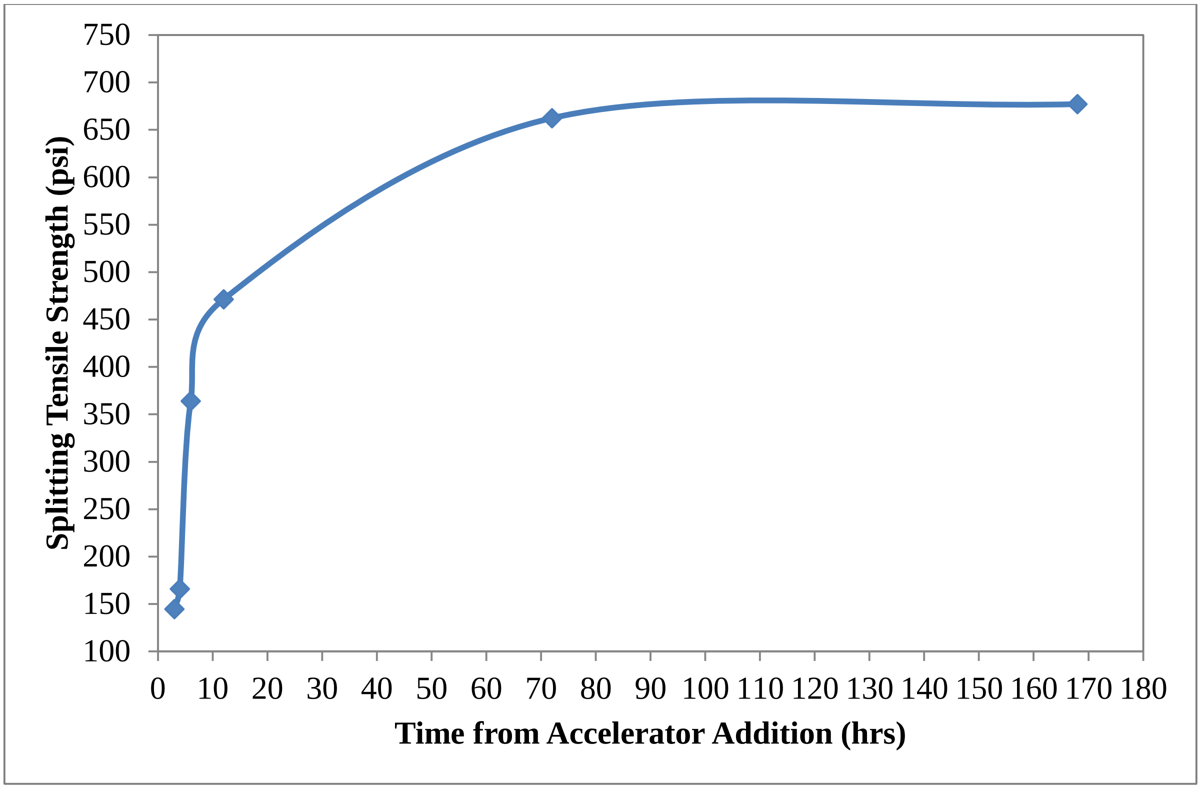

Figure 3-37: Splitting tensile strength vs. time for Slab 3

3.5.4 Temperature Rise of Concrete Cylinders

The temperature rise of the concrete cylinder specimens was measured using a P-Cal 1000 semi-adiabatic calorimeter manufactured by Calmetrix. The P-Cal is used to obtain near adiabatic conditions of the concrete, and because it is relatively small, can be utilized in the field. Since the concrete used for slab replacement contained an abundance of accelerating admixture, there was potential for relatively high temperature rise in the concrete. The peak temperature for all three slabs occurred between five and 15 hours after the accelerator was added as shown in Figures 3-38 through 3-40. The temperature rise as measured by the P-Cal device clearly indicated that the total temperature rise was dependent on the concrete placement temperature. Revisiting Table 3-10, the concrete placement temperatures for slabs 1, 2, and 3 are 35.5°C, 31.7°C and 25.0°C respectively. The resultant maximum temperatures for each slab are 59°C, 55°C and 52°C respectively. Although the P-Cal data was not used to calculate the adiabatic temperature rise in the concrete, it did provide similar peak temperature data to that measured in each of the slabs.

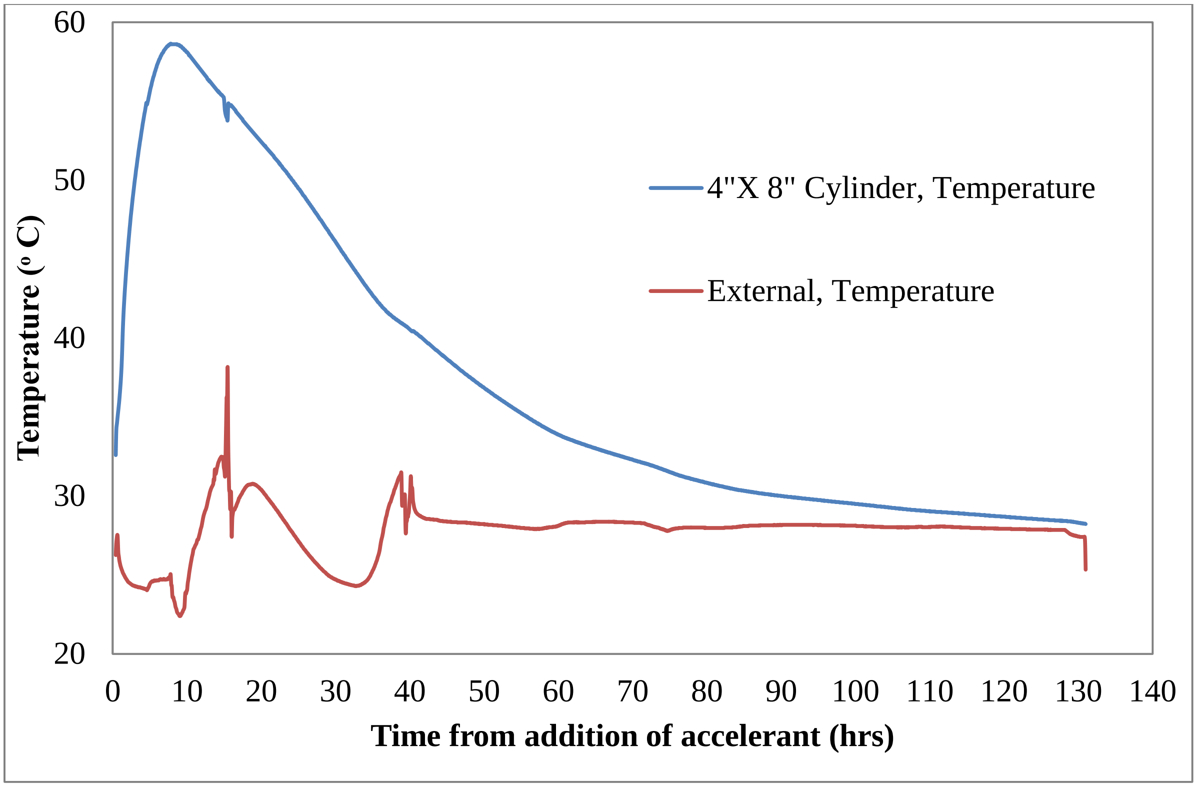

Figure 3-38: Temperature rise of specimens for Slab 1

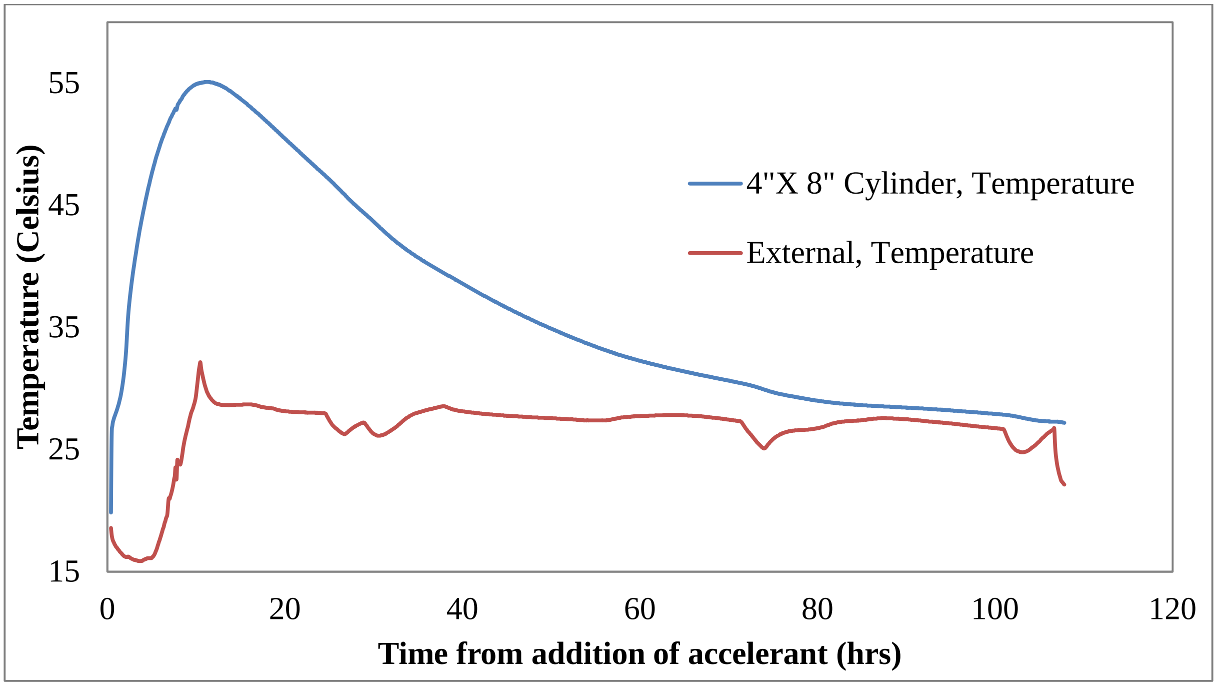

Figure 3-39: Temperature rise of specimens for Slab 2

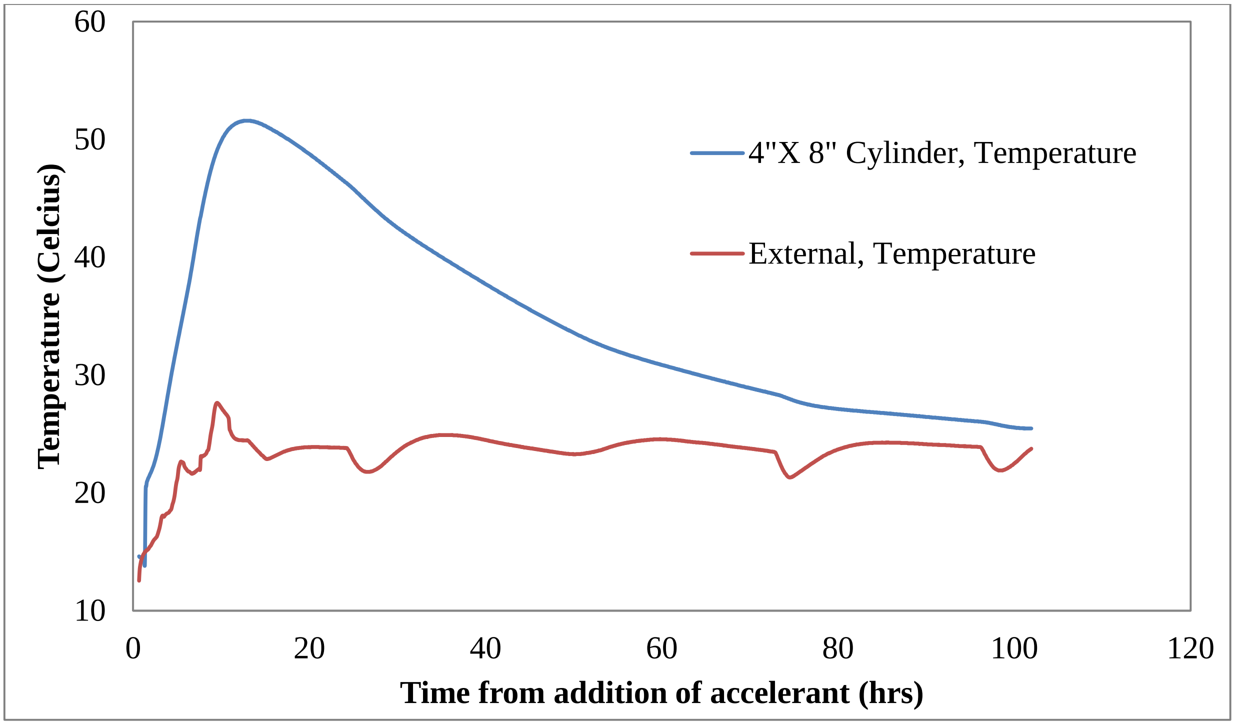

Figure 3-40: Temperature rise of specimens for Slab 3

3.6 Concrete Slab Instrumentation

Measurements of temperature and strain were recorded at the center, edge, and corner of the slab using instrumentation provided by the University of Florida. The instrumentation included three thermocouples and two or three strain gages at each location in the slab. The data were then used to calculate the equivalent age of the roadway. Figure 3-42 through 3-44 present the instrumentation for temperature and strain measurement as typically used for this project.

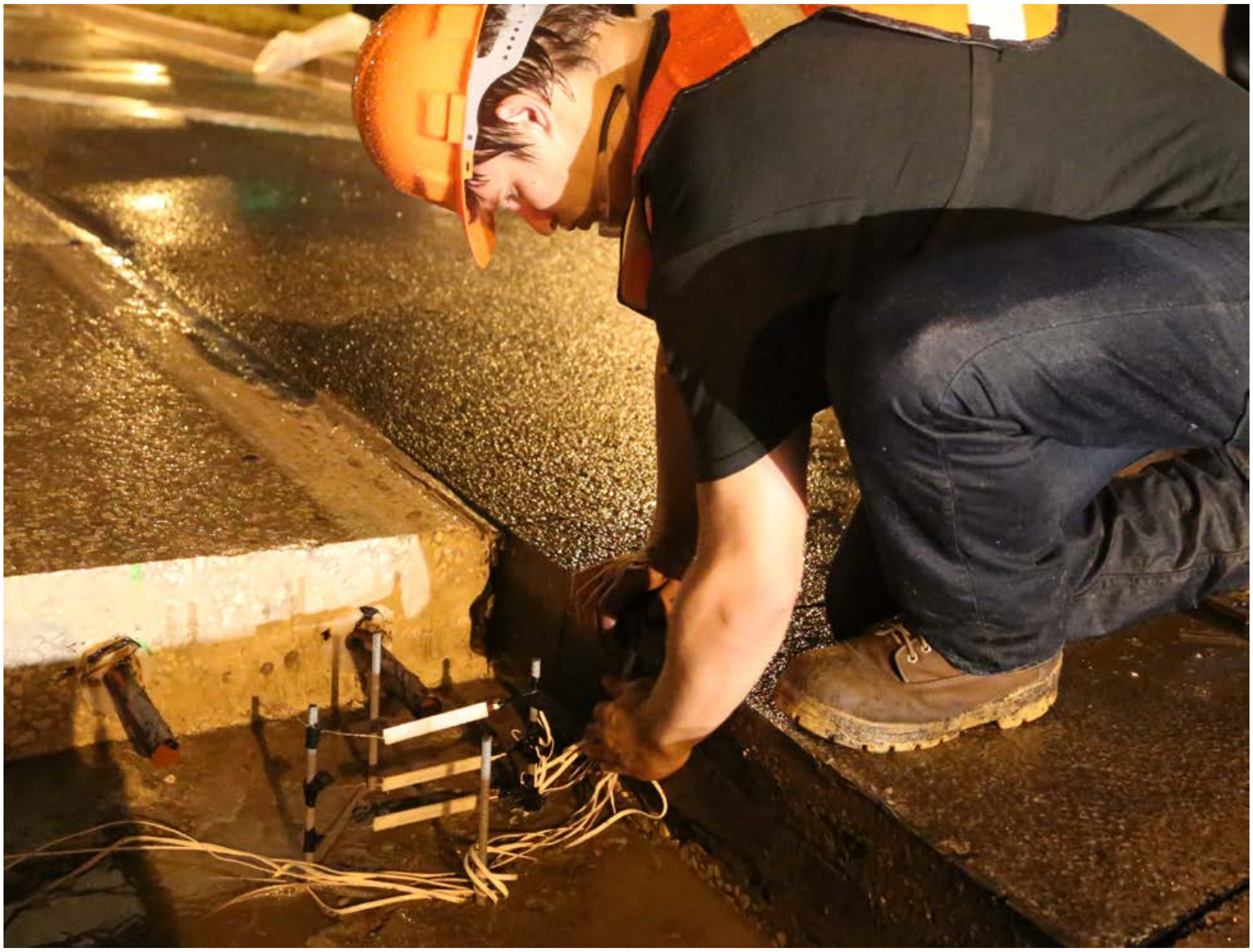

Figure 3-41: Instrumentation at the corner of Slab 1

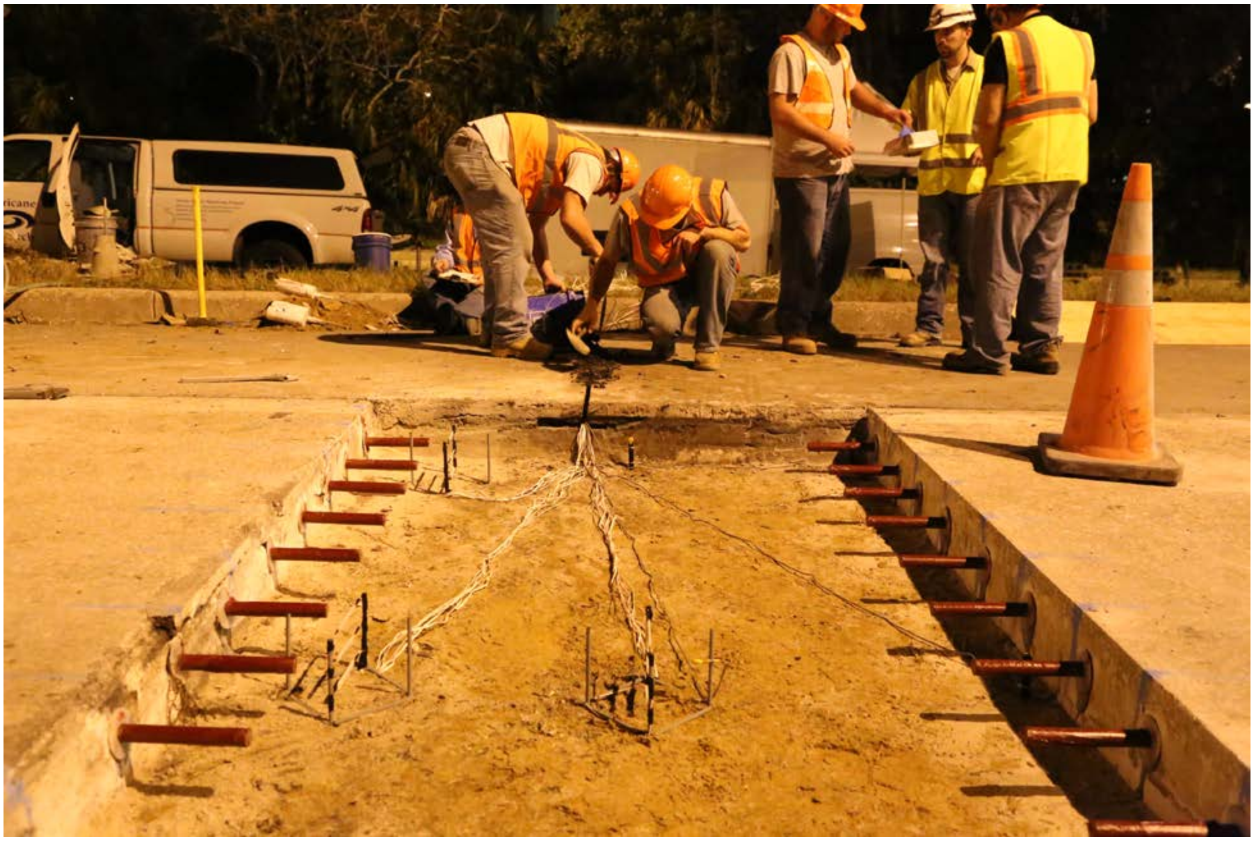

Figure 3-42: Full instrumentation of Slab 2

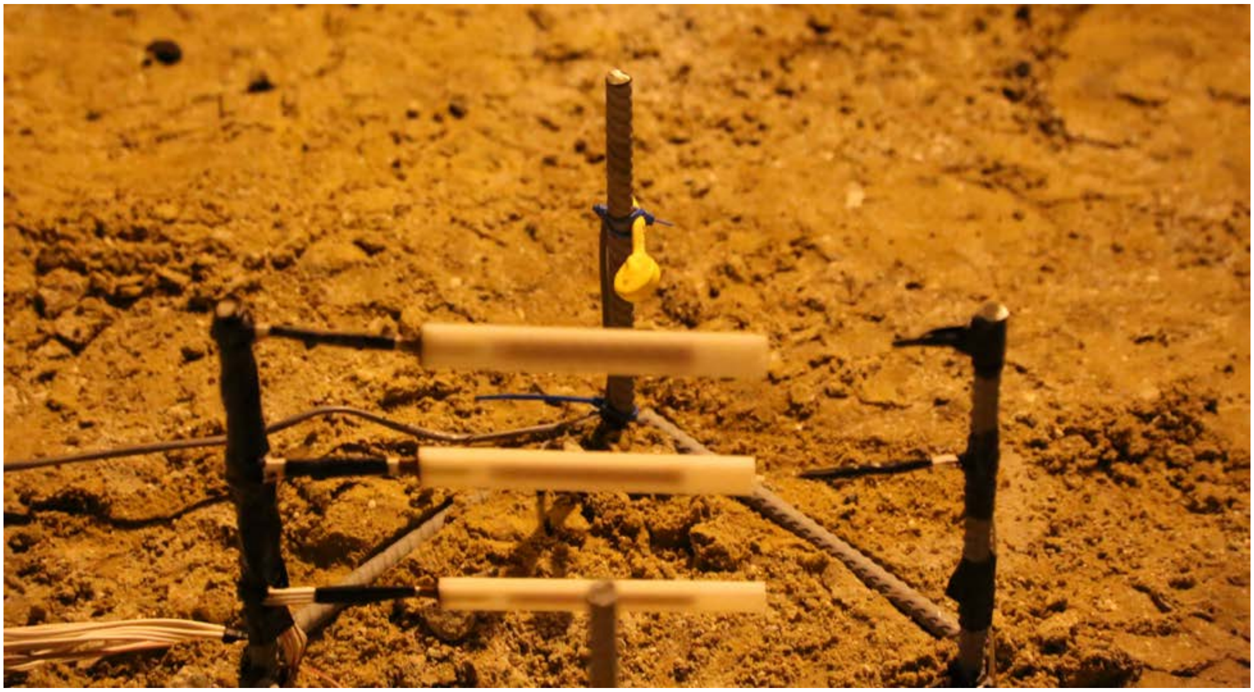

Figure 3-43: Thermocouple on instrument tree for Slab 2

3.6.1 Temperature

The in situ temperature at the edge, middle and corner of each of the slabs was acquired to provide temperature data used for the validation of the computer modeling results obtained by the University of South Florida. The temperature was recorded and used for model input and verification as part of the laboratory portion of this research project.

3.6.1.1 Temperature – Slab 1

Each of the slabs exhibited similar behavior in that the center achieved the highest temperature, the edge experienced a lower temperature and the corner the lowest. The temperature history for Slab 1 locations is presented in Figures 3-45 through 3-47. The ultimate temperature rise, which is attributed to concrete mixture design and placement temperature, was approximately 57°C and occurred approximately six hours after placement. There was a malfunction of the sensor placed in the middle elevation position at the center location of Slab 1. The roadway was opened to traffic while the slab was experiencing the maximum internal temperature recorded, and afterward the slab cooled throughout the day Due to the cloud cover on the morning after placement, the ambient temperature was relatively low and constant.

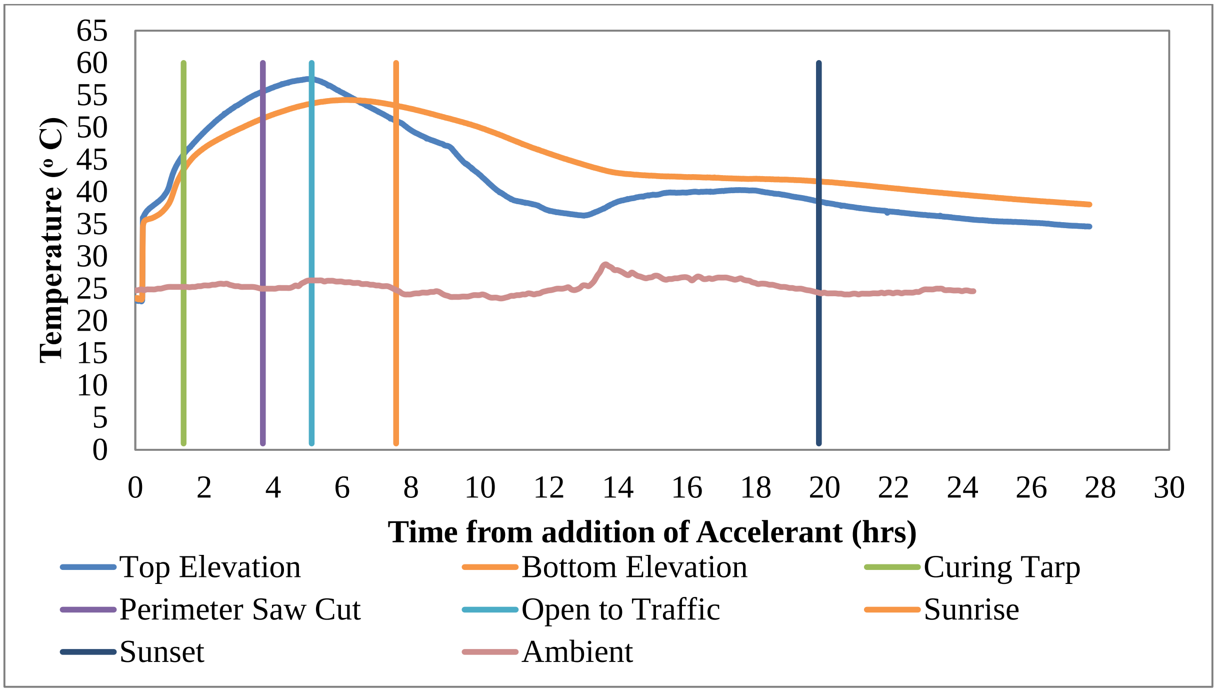

Figure 3-44: Temperature at center of Slab 1

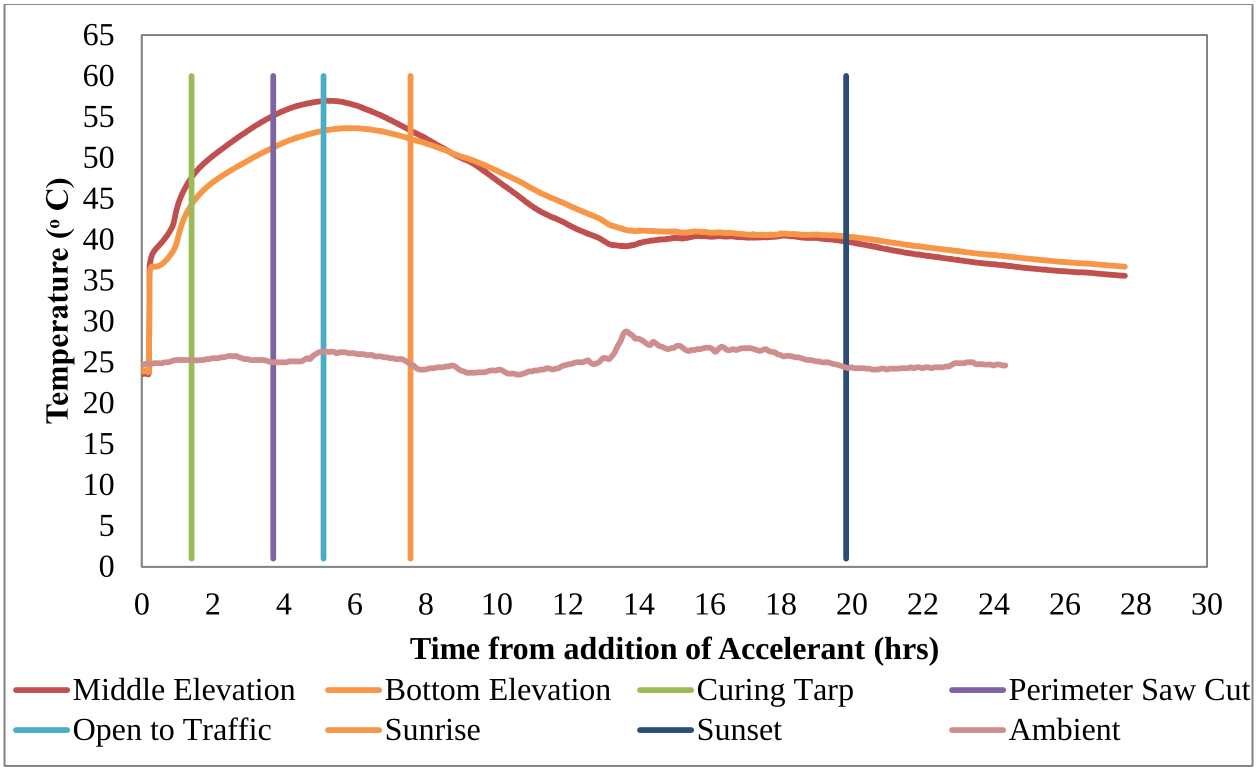

Figure 3-45: Temperature at edge of Slab 1

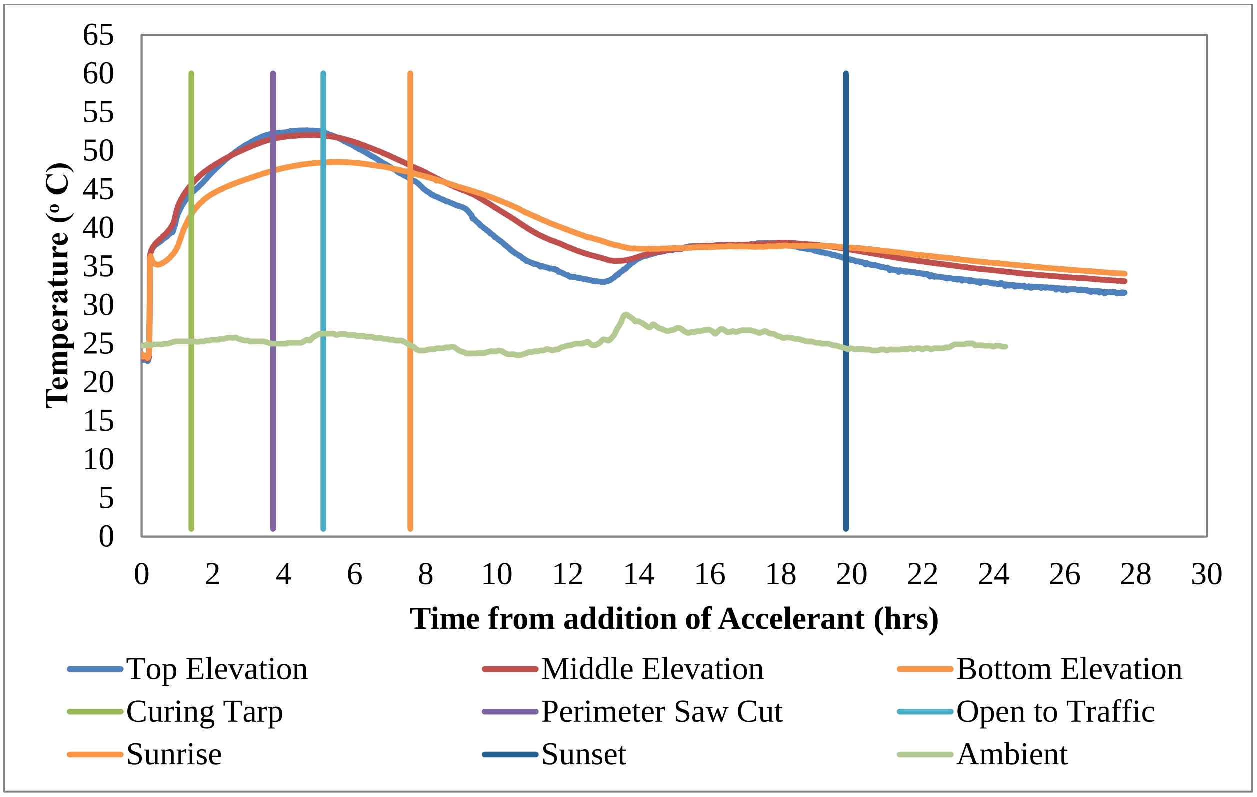

Figure 3-46: Temperature at corner of Slab 1

3.6.1.2 <u>Temperature – Slab 2</u>

The general behavior of Slab 2 with regard to temperature history was similar to Slab 1. The center achieved the highest temperature, the edge experienced a lower temperature, and the corner the lowest. The temperature history for each of the locations is presented in Figures 3-48 through 3-50. The ultimate temperature rise was approximately 55°C and occurred approximately five hours after placement. Similar to the conditions experienced by Slab 1, the roadway was opened to traffic while the slab was experiencing the maximum internal temperature for Slab 2. Subsequent to the opening to traffic, the slab cooled throughout the remainder of the monitoring period. Due to the cloud cover on the morning after placement, the ambient temperature was relatively low and constant. Later in the day, periods of sunshine caused some spikes in temperature, with the highest around 1 PM (11 hours after placement). As a result of the relatively high ambient temperature, the temperature of Slab 2 did not decrease during the daylight hours, similar to that as Slab 1.

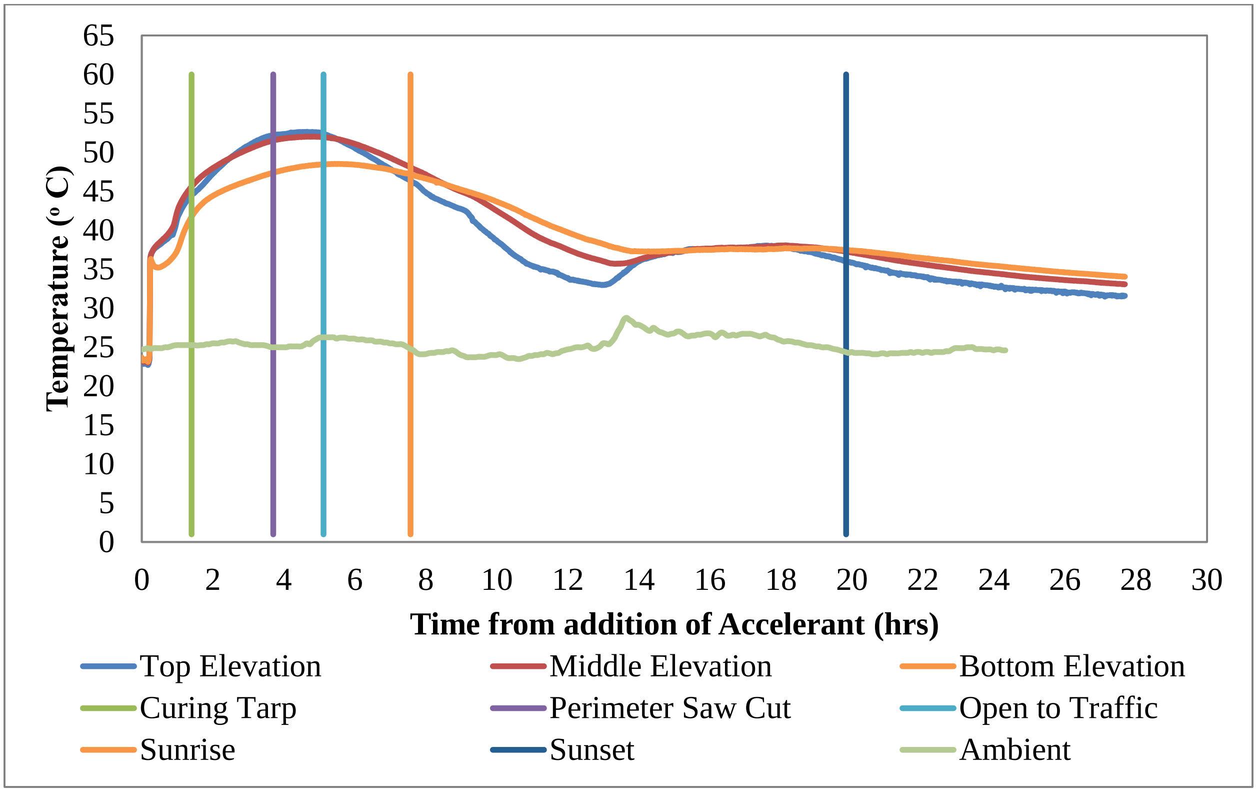

Figure 3-47: Temperature at center of Slab 2

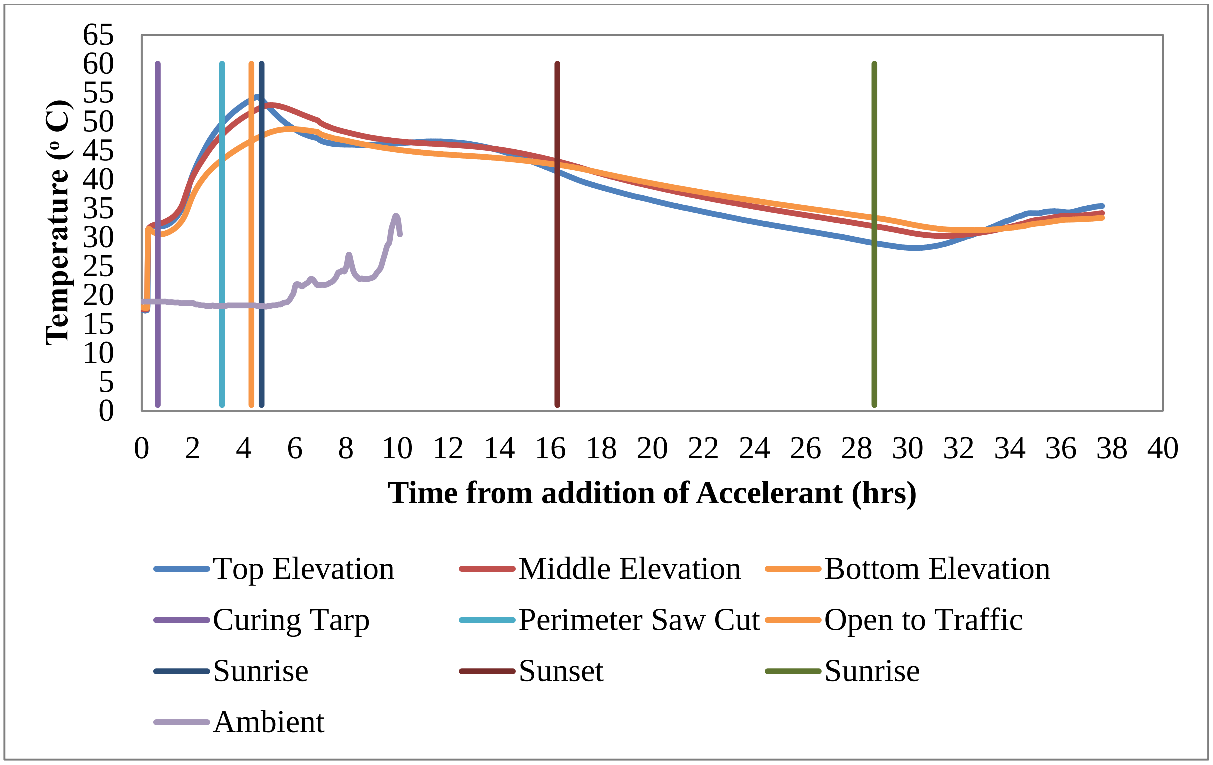

Figure 3-48: Temperature at edge of Slab 2

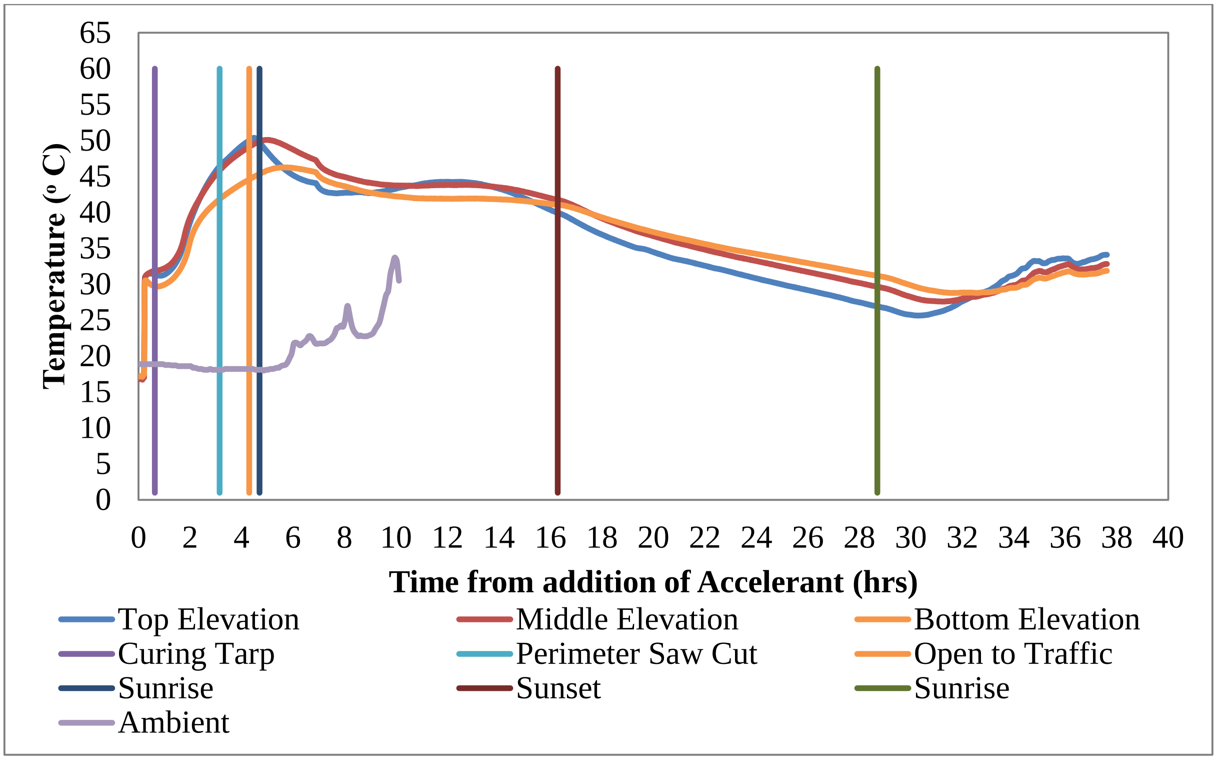

Figure 3-49: Temperature at corner of Slab 2

3.6.1.3 <u>Temperature – Slab 3</u>

The general behavior of Slab 3 was similar to Slabs 1 and 2, with respect to temperature, in that the center achieved the highest temperature, the edge experienced a lower temperature and the corner the lowest. The temperature history for each of the locations is presented in Figures 3-51 through 3-53. One major difference between the behavior of Slab 3 with respect to Slabs 1 and 2 is that it experienced a temperature increase until eight hours after placement, where Slabs 1 and 2 experienced a maximum temperature at approximately five hours after placement. The difference can be attributed to the time of day in which the slab was placed, as Slab 3 was placed after sunrise and the temperature rise of the slab increased throughout the day, trending with ambient temperature and exposure to sunlight. Slabs 1 and 2 were placed at night and the maximum temperature was achieved prior to sunrise. The ultimate temperature rise, which is a function of concrete mixture design and placement temperature, was approximately 57°C for the center of the slab and approximately 55°C for the edge and corner of the slab.

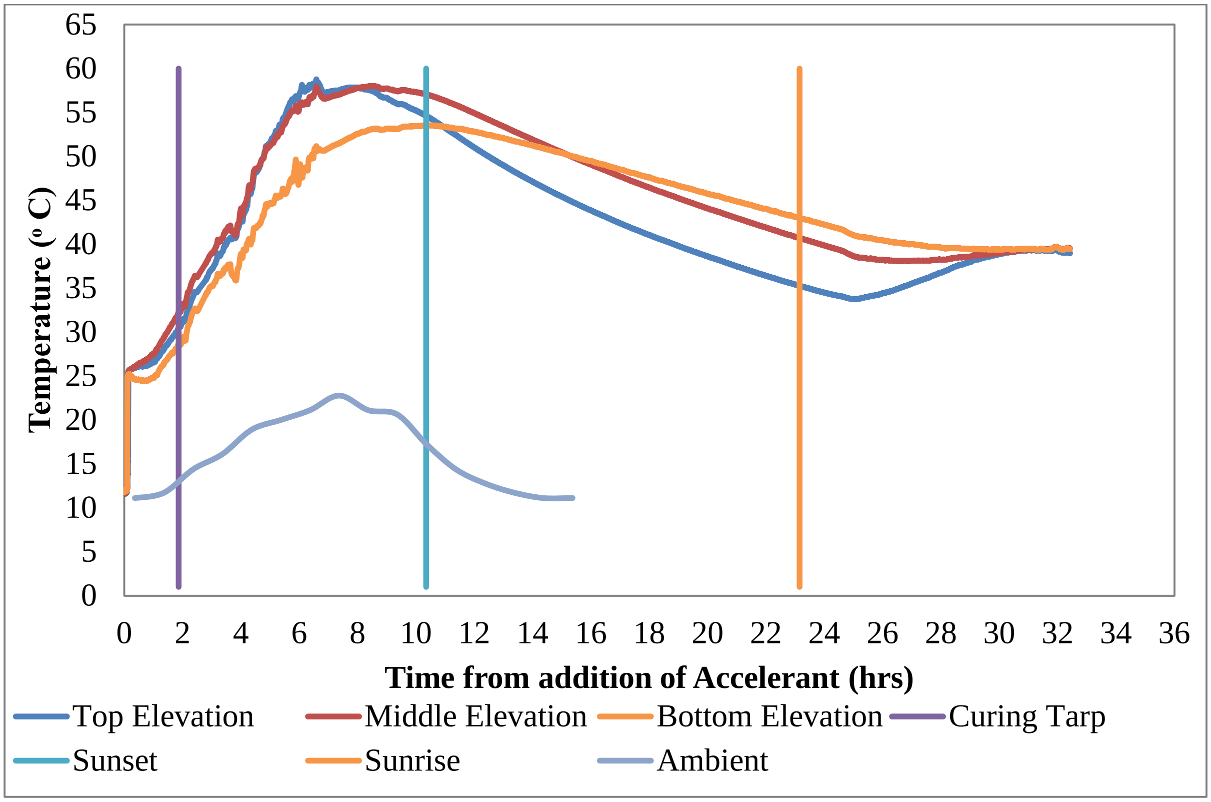

Figure 3-50: Temperature at center of Slab 3

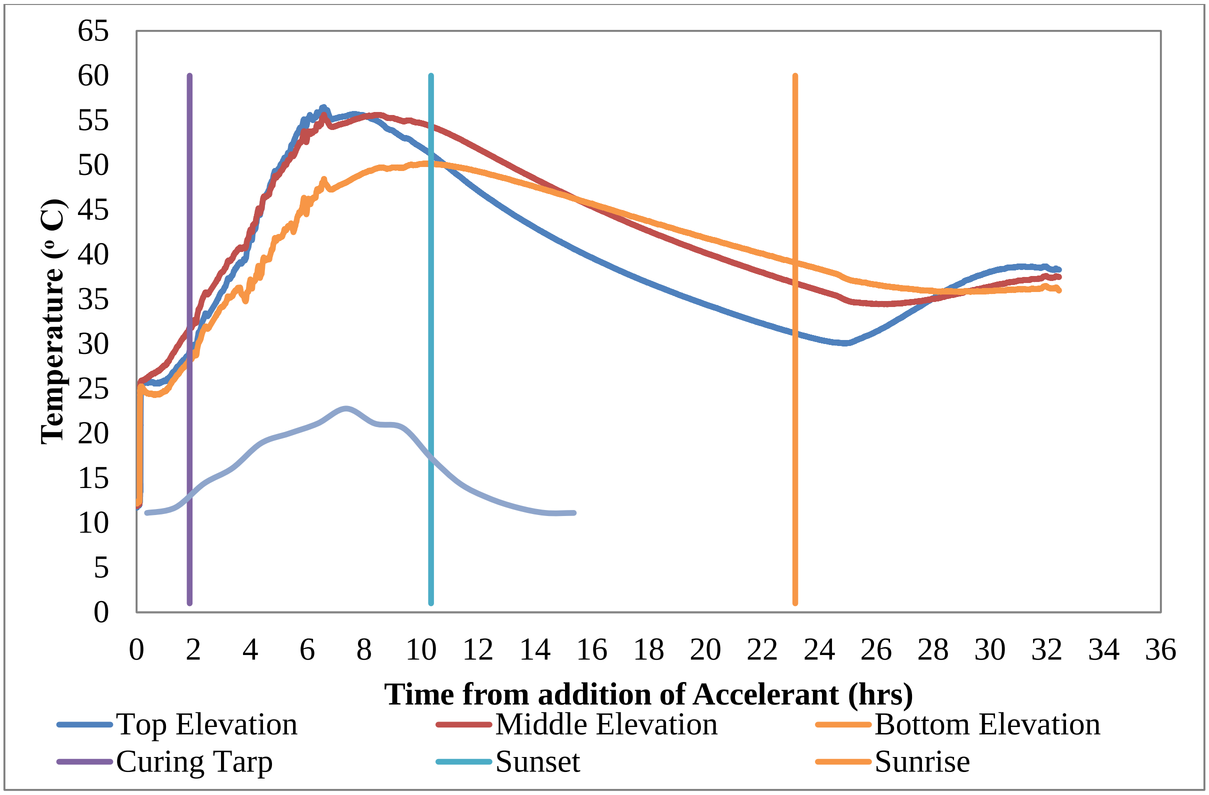

Figure 3-51: Temperature at edge of Slab 3

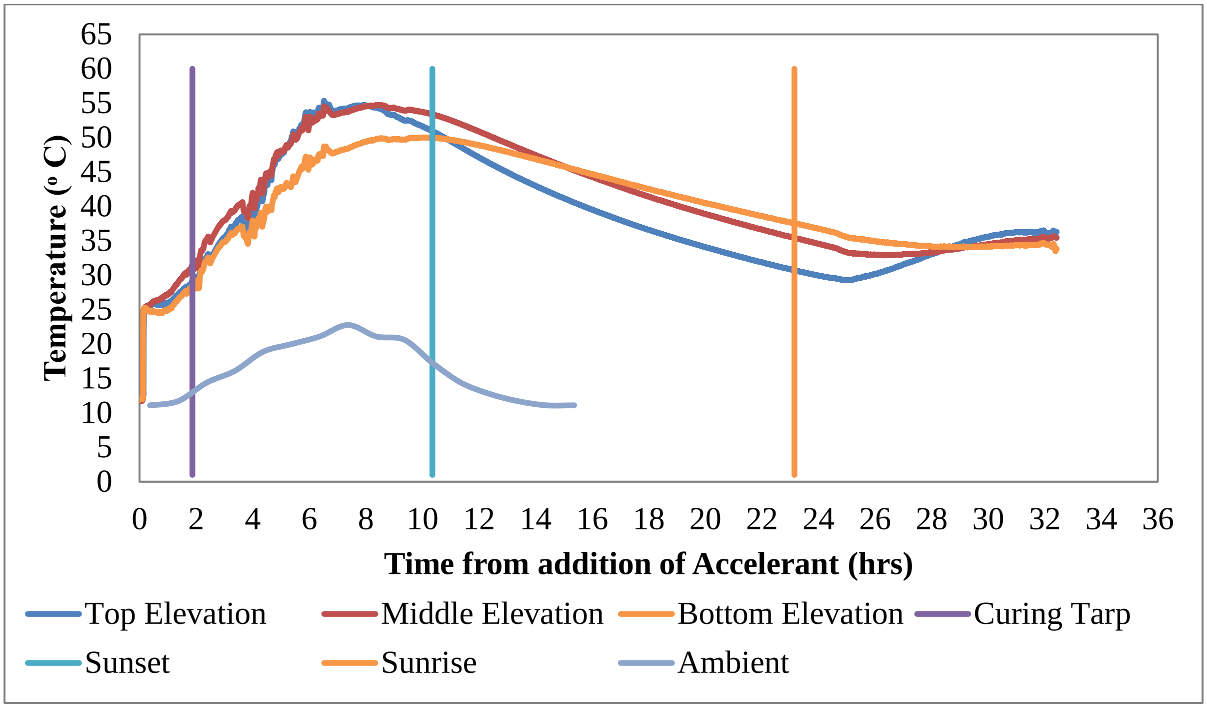

Figure 3-52: Temperature at corner of Slab 3

3.6.2 Strain

The in situ strains were recorded at the edge-middle of slab 1 and center-middle of slabs 2 and 3 in the longitudinal direction of the slab (transverse to the direction of traffic). Typically, the strain experienced in concrete pavement at early ages is primarily due to internal thermal movement. As a result, it is likely that the areas of the slab that experience the largest temperature rise are subject to the largest thermal movement, and therefore, experience the largest levels of strain. Accordingly, the strain at the center, edge, and corner of each slab was recorded and used for model input and verification as part of the laboratory portion of this research project.

3.6.2.1 Strain – Slab 1

In situ strain measurements at the center, edge and corner of Slab 1 were recorded and are presented in Figures 3-54 through 3-56. The strain values for the middle and top of each location within the slab (center, edge and corner) were proportional to the temperature values at very early ages; however, the strain values did not decrease after five hours like the slab temperatures. The potential reason the strain did not exhibit the same relative decrease as the temperature is that the concrete properties change as the concrete progresses from an early-age plastic condition to a stiff body. This stiffening is consistent with a large increase in MOE between 3 and 12 hours.

The values recorded from the strain gauge at the bottom-center of the slab and the bottom-edge of slab do not exhibit large strains. One potential reason for the lack of movement at the bottom of the slab is the restraint provided by the friction between the base material and the slab itself. Accordingly, the corner of the slab did not experience the same degree of restraint (especially at the bottom) and the relative movement is clearly visible in Figure 3-56, where each of the strain gages measured strain/movement to the same degree regardless of vertical position in the slab.

Some of the strain gages measured an abrupt change in strain (increase) after nine hours of data recording. Typically, when abrupt changes occur in strain measurement, they are due to cracking, which provides strain relief (decreased strain). The sudden increase in strain is difficult to explain. This anomaly occurs around the maximum slab temperature, corresponding to the hottest time of the day, so it could have resulted from a combination of high thermal stress and stress due to traffic.

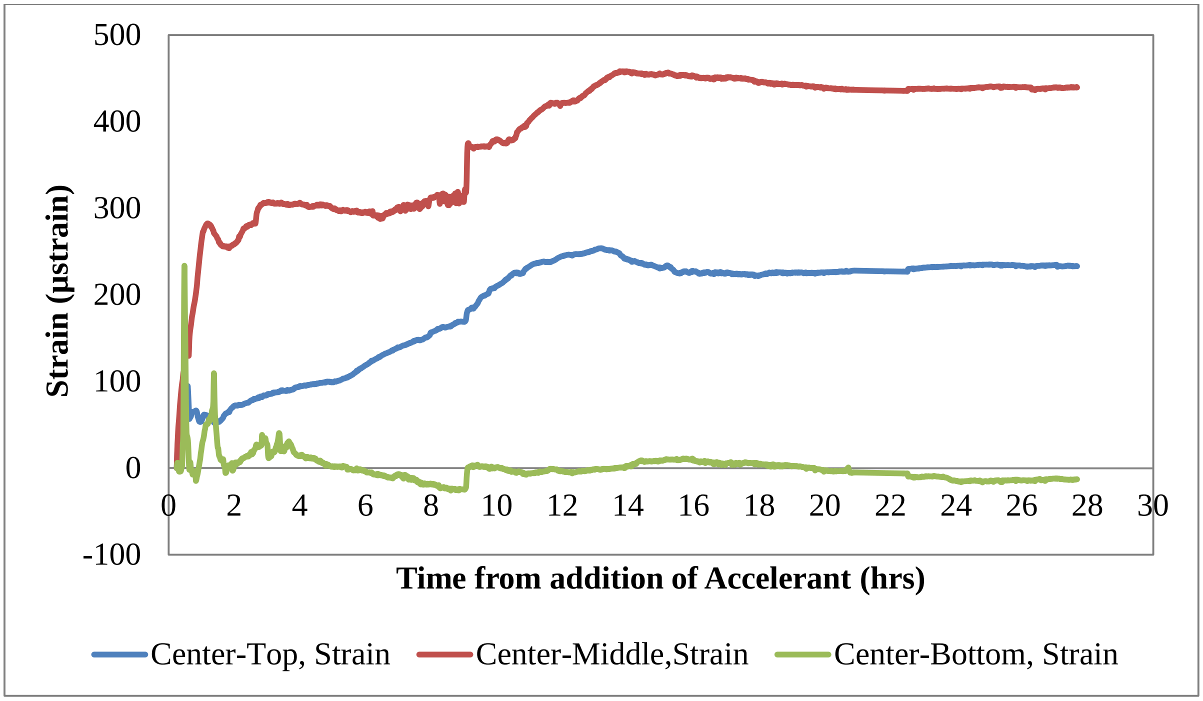

Figure 3-53: Strain at center of Slab 1

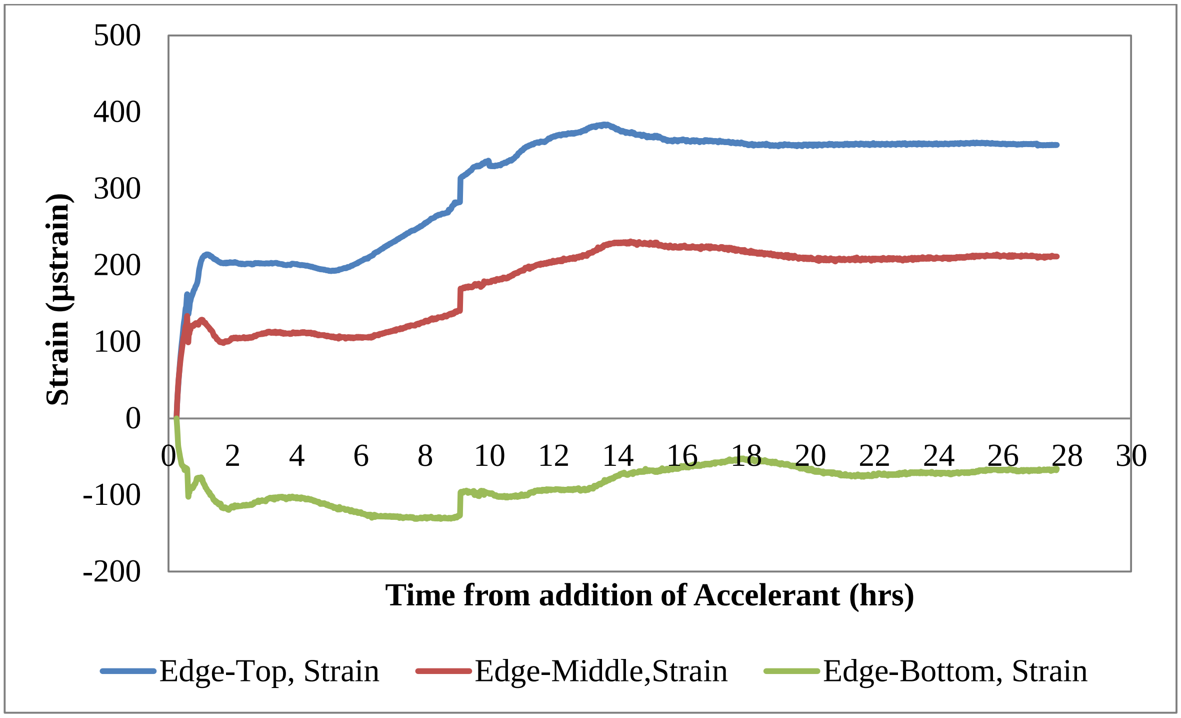

Figure 3-54: Strain at edge of Slab 1

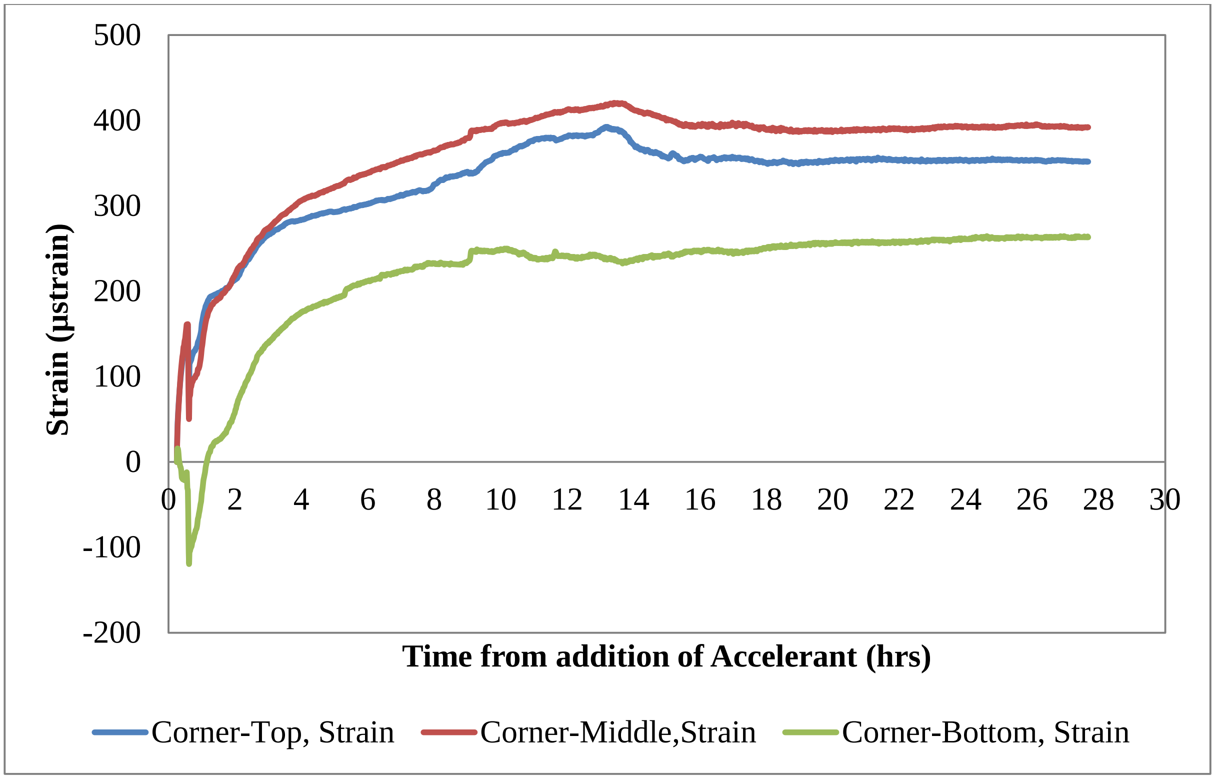

Figure 3-55: Strain at corner of Slab 1

3.6.2.2 Strain – Slab 2

In situ strain measurements at the center, edge and corner of Slab 2 were recorded and are presented in Figure 3-57 through Figure 3-59. The strain values for the top and middle at the center and edge of the slab (center-top, center-middle, edge-top, and edge-middle) do not trend similarly to the temperature at very early ages. Between the time of two hours and five hours after placement, there is a relative decrease in the strain at the center and edge of the slab. Potential reasons for the decrease in the slab strain are early-age shrinkage and microcracking of the slab. After about five hours, the concrete behaved in a similar fashion as Slab 1.

Similar to the behavior in Slab 1, Slab 2 did not exhibit large strains at the bottom-center and bottom-edge positions. The center and corner of slab 2 behaved in relatively the same manner as Slab 1 with the exception of a strain decrease at 24 hours, which could be the result of an internal crack. This strain decrease was not observed at the edge position.

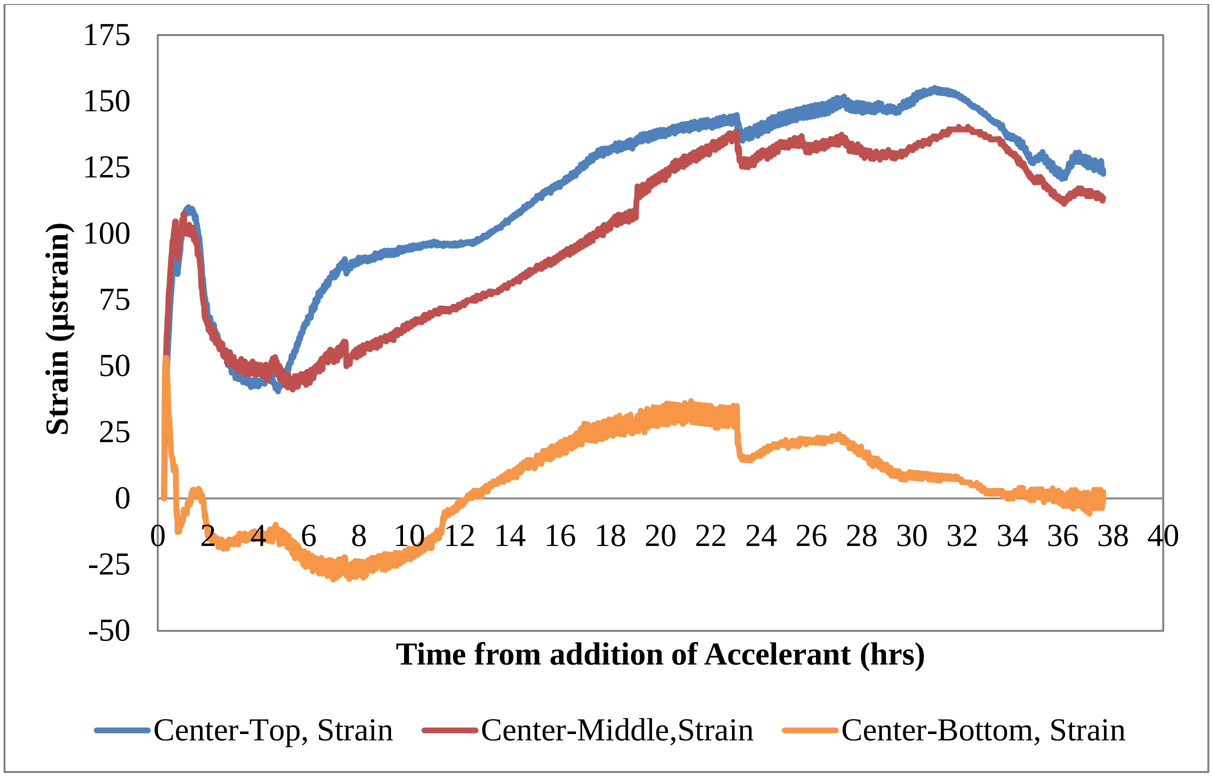

Figure 3-56: Strain at center of Slab 2

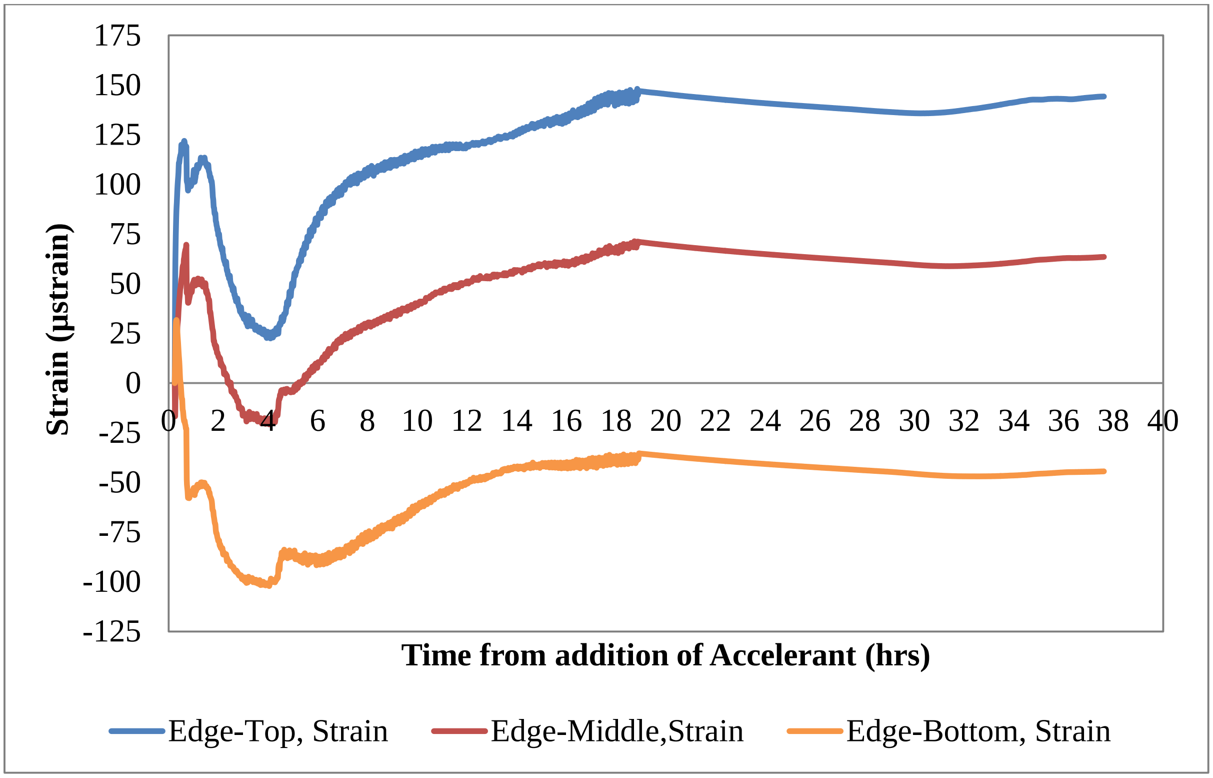

Figure 3-57: Strain at edge of Slab 2

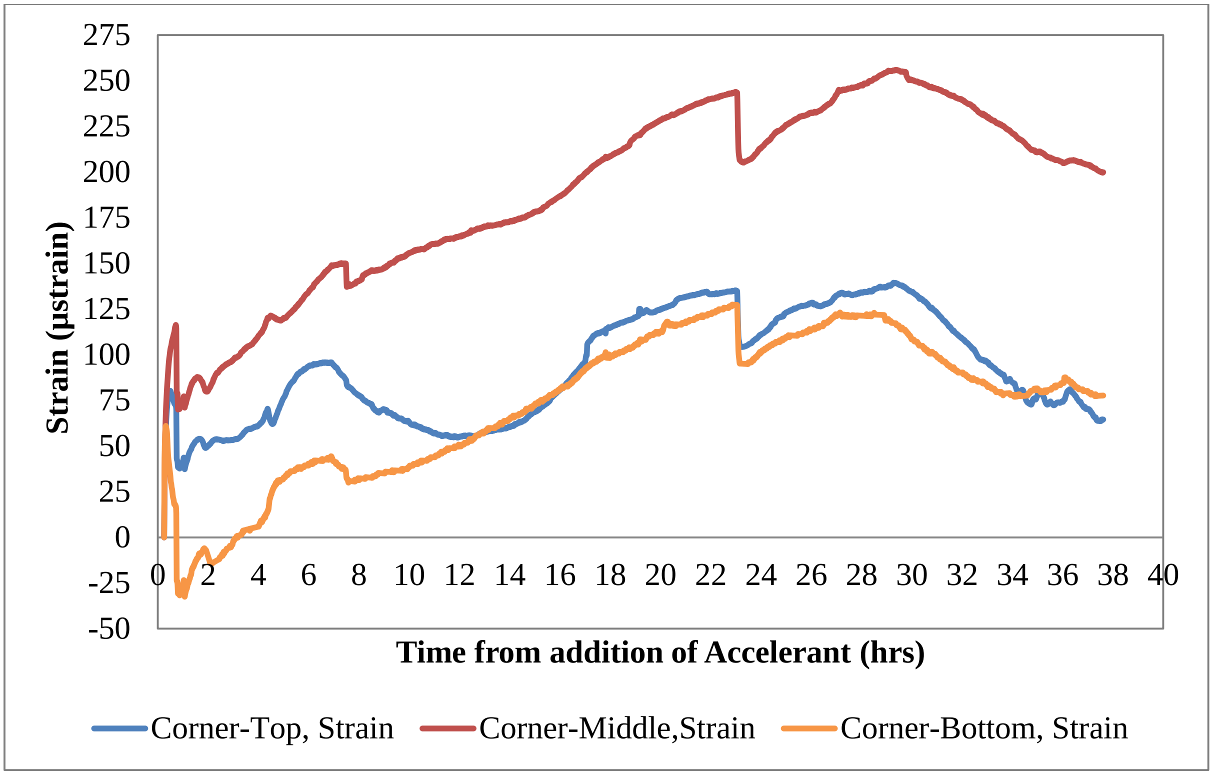

Figure 3-58: Strain at corner of Slab 2

3.6.2.3 *Strain – Slab 3*

In situ strain measurements at the center, edge and corner of Slab 3 were recorded and are presented in Figure 3-60 through 3-62. The strain profiles for the center, edge and corner of the slab are very similar and do not show the early-age drop in strain exhibited by Slab 2. The overall behavior of the strain measurements within Slab 3 is consistent with strain measurements affected only by temperature (and resultant expansion or contraction) within the slab. Also, there were no abrupt changes in the strain readings for Slab 3. The maximum value of strain was reached at approximately nine hours after placement.

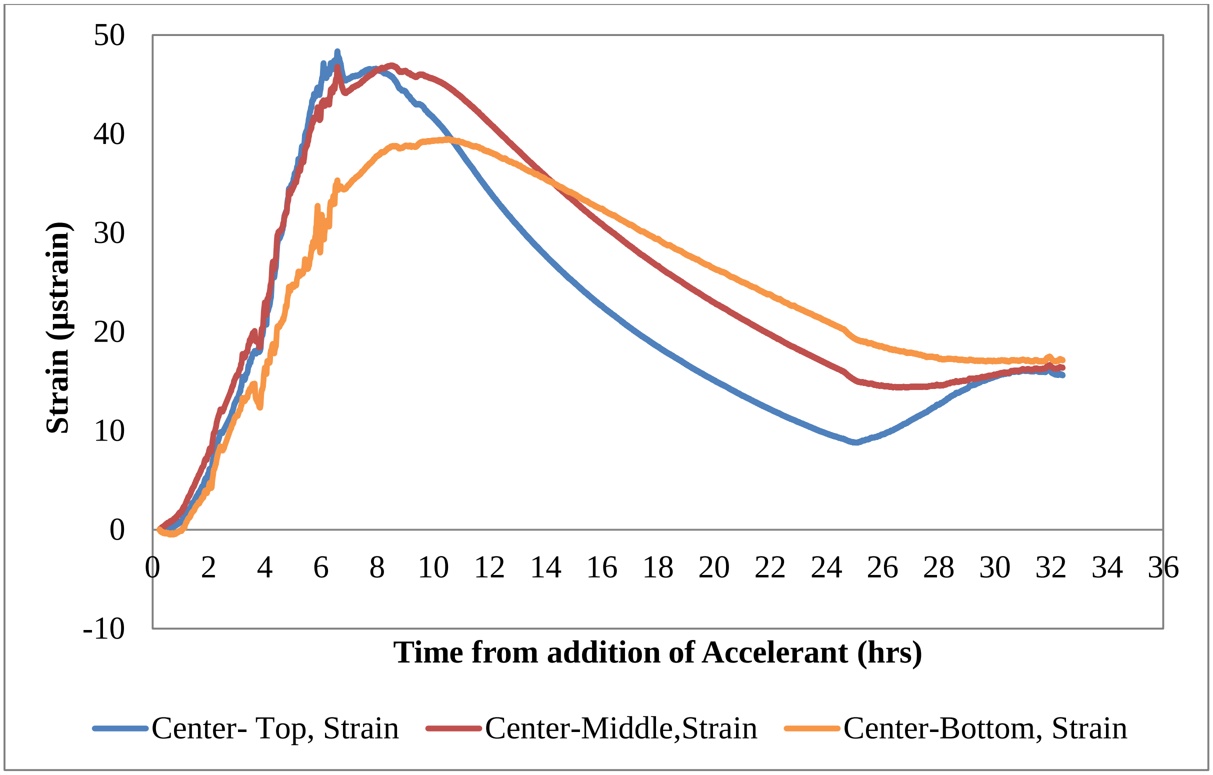

Figure 3-59: Stain at center of Slab 3

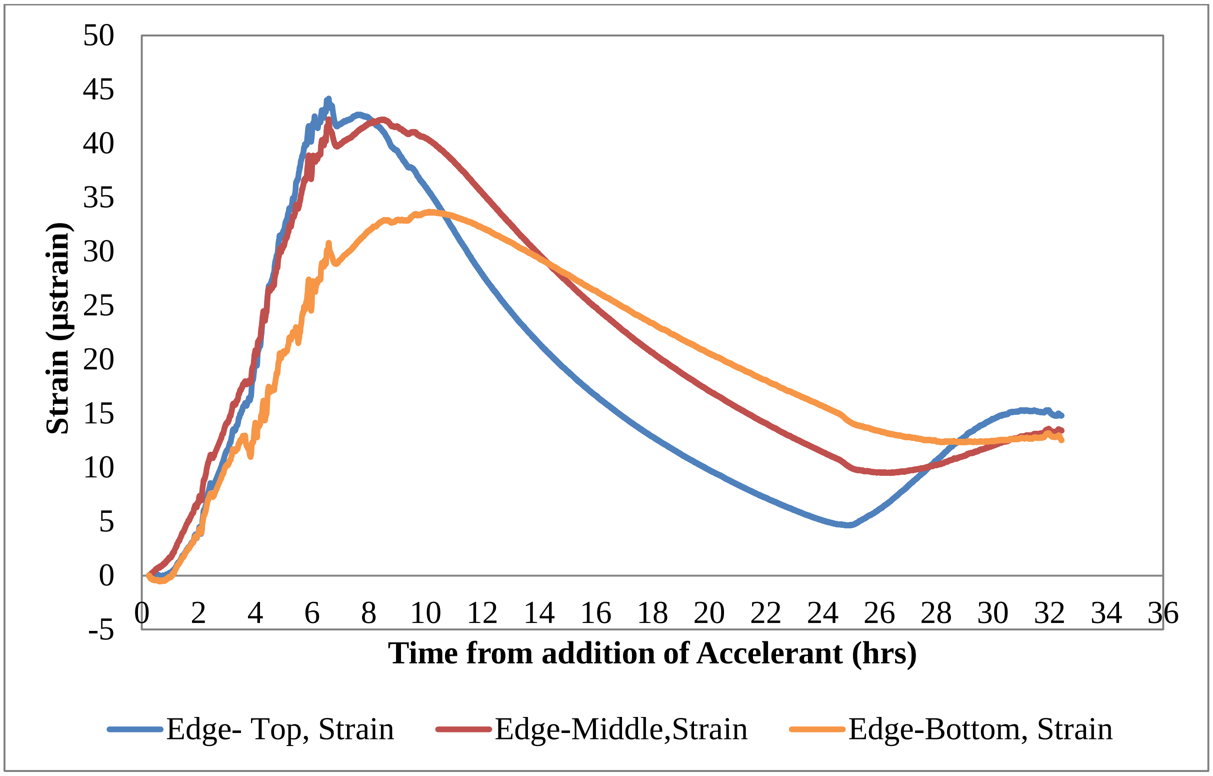

Figure 3-60: Strain at edge of Slab 3

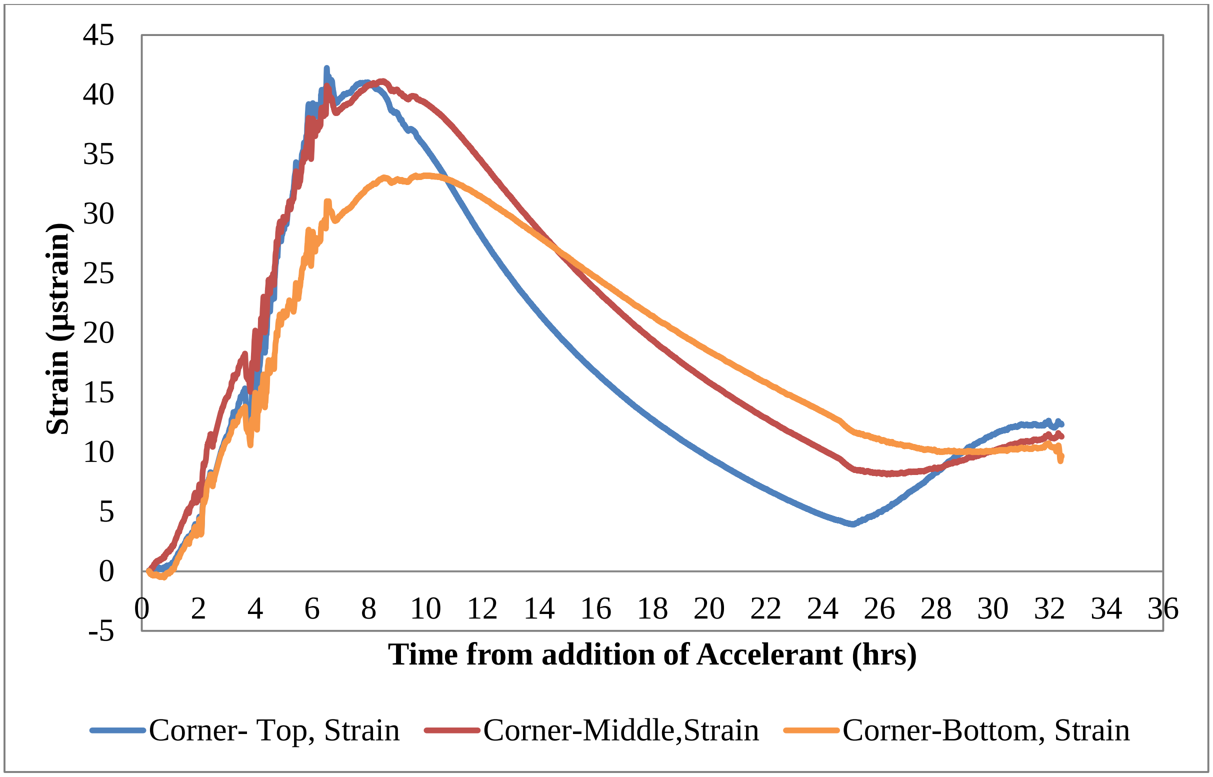

Figure 3-61: Strain at corner of Slab 3

3.7 References

ASTM C29 / C29M-09, Standard Test Method for Bulk Density ("Unit Weight") and Voids in Aggregate, ASTM International, West Conshohocken, PA, 2009.

ASTM C31 / C31M-12, Standard Practice for Making and Curing Concrete Test Specimens in the Field, ASTM International, West Conshohocken, PA, 2012.

ASTM C39 / C39M-12a, Standard Test Method for Compressive Strength of Cylindrical Concrete Specimens, ASTM International, West Conshohocken, PA, 2012.

ASTM C138 / C138M-13, Standard Test Method for Density (Unit Weight), Yield, and Air Content (Gravimetric) of Concrete, ASTM International, West Conshohocken, PA, 2013.

ASTM C143 / C143M-12, Standard Test Method for Slump of Hydraulic-Cement Concrete, ASTM International, West Conshohocken, PA, 2012.

ASTM C469 / C469M-10, Standard Test Method for Static Modulus of Elasticity and Poisson’s Ratio of Concrete in Compression, ASTM International, West Conshohocken, PA, 2010.

ASTM C1064 / C1064M-12, Standard Test Method for Temperature of Freshly Mixed Hydraulic-Cement Concrete, ASTM International, West Conshohocken, PA, 2012.

ASTM D421-85(2007), Standard Practice for Dry Preparation of Soil Samples for Particle-Size Analysis and Determination of Soil Constants, ASTM International, West Conshohocken, PA, 2007.

ASTM D422-63(2007)e2, Standard Test Method for Particle-Size Analysis of Soils, ASTM International, West Conshohocken, PA, 2007.

ASTM D6951 / D6951M-09, Standard Test Method for Use of the Dynamic Cone Penetrometer in Shallow Pavement Applications, ASTM International, West Conshohocken, PA, 2009.

AASHTO T180-10, “Standard Method of Test for Moisture-Density Relations of Soils Using a 4.54-kg (10-lb) Rammer and a 457-mm (18-in.) Drop”, American Association of State and Highway Officials, Washington DC, 2011.

Akroyd, T. (1962). *Concrete: Properties and Manufacture*. Pergamon Press, Oxford, 336.

De Belie, N., Grosse, C. U., Kurz, J., and Reinhardt, H.-W. (2005). “Ultrasound monitoring of the influence of different accelerating admixtures and cement types for shotcrete on setting and hardening behaviour.” *Cement and Concrete Research*, 35(11), 2087–2094.

Ferraro, C. (2009). “Determination of Test Methods for the Prediction of the Behavior of Mass Concrete.” PhD Thesis: University of Florida.

Florida Department of Transportation (2009). *Rigid Pavement Design Manual*. (2009). Tallahassee, FL, 190.

Florida Department of Transportation. (2013). *Standard Specifications for Road and Bridge Construction*. Tallahassee, FL.

Hilsdorf, H.K., Kesler, C.E. (1966). “Fatigue Strength of Concrete Under Varying Flexural Stresses.” ACI Journal, 63(10), 1059-1076.

Malhotra, V. M., and Carino, N. J. (Eds.). (1991). *Handbook on Nondestructive Testing of Concrete*. CRC Press, Boca Raton, FL, 343.

Shoop, S. A., Diemand, D., and Seman, P. M. (2008). *Predicting California Bearing Ratio from Trafficability Cone Index Values*. Hanover, NH, 122

CHAPTER 4 Performance of Pavement Slabs

Slabs 1 and 2 were inspected for defects and cracking prior to the opening of traffic and again after the conclusion of grinding operations. Slab 3, which was placed at the FDOT State Materials Office, was inspected after placement and after being subjected to simulated traffic loading by the heavy vehicle simulator (HVS).

4.1 Field Performance of Slab 1

As discussed in Chapter 3, Slab 1 is located on Eastbound outside (south) lane between Liberty and Main Street on Martin Luther King Boulevard in Jacksonville, Florida. The slab was placed at approximately 11:40 P.M., September 17th. After placement, curing compound was placed on the slab at approximately 12:00 A.M. on September 18th, as shown in Figure 4-1.

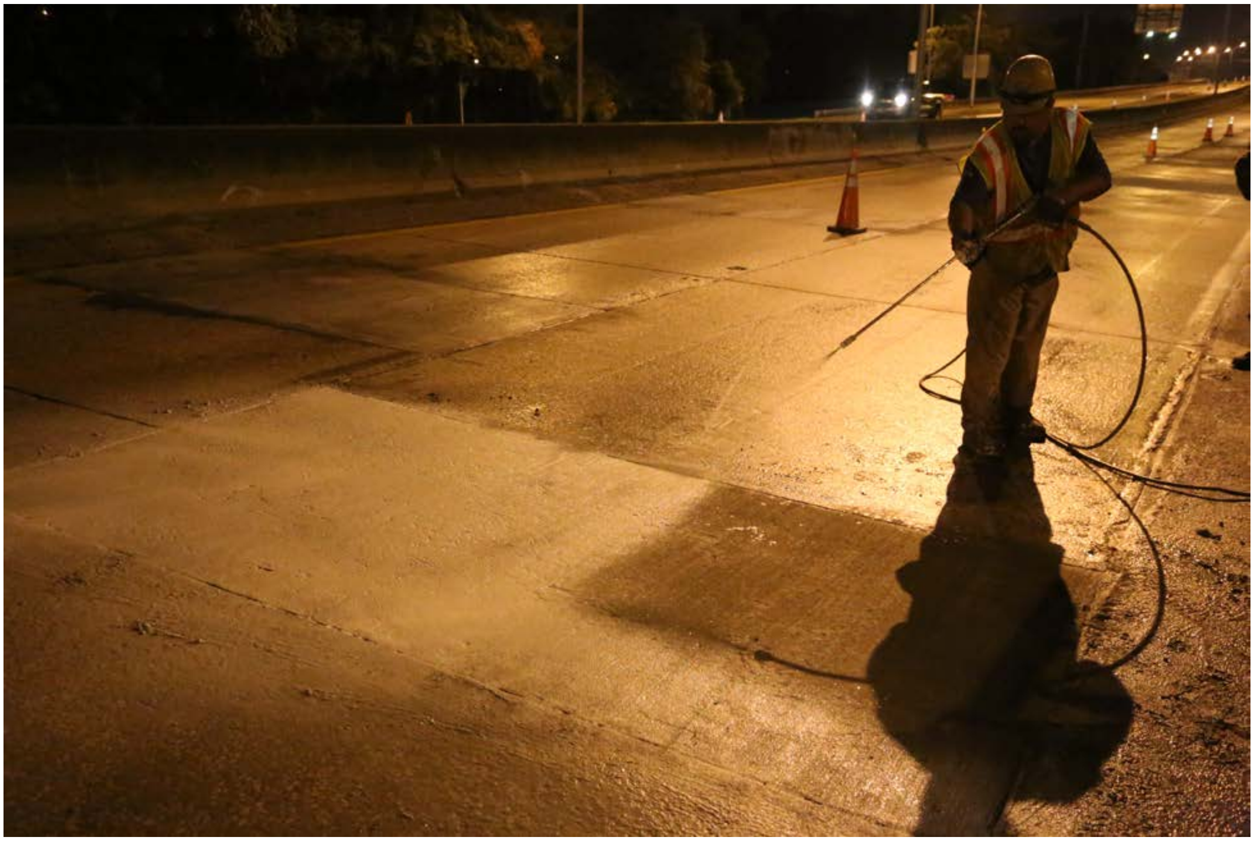

Figure 4-1: Application of curing compound to Slab 1

Section 353-7 (Florida Department of Transportation 2013) requires the surface of the slab to be ground to provide an adequate final surface finish. No cracks in the slab were observed before or after the grinding operations. The final product of Slab 1 is shown in Figure 4-2.

Figure 4-2: Slab 1 six months after placement

4.2 Field Performance of Slab 2

Slab 2 is located on the Westbound outside (north) lane of between Liberty and Main Street on Martin Luther King Boulevard in Jacksonville, Florida. A view of the typical preparation of the roadway prior to the placement of concrete showing the instrumentation for data acquisition is presented in Figure 4-3. Typical finishing and application of curing compound are presented in Figure 4-4 and 4-5, respectively. The slab was placed at approximately 2:51 A.M. October 10th, and curing compound was applied on the slab at approximately 3:20 A.M. Similar to the condition of Slab 1, no cracks were observed in Slab 2 after grinding, as presented in Figure 4-6. However, a small construction defect was visible on the surface of Slab 2. It appears that after grinding, there was a low spot near the wheel path nearest the centerline. A close-up view of this defect is presented in Figure 4-7.

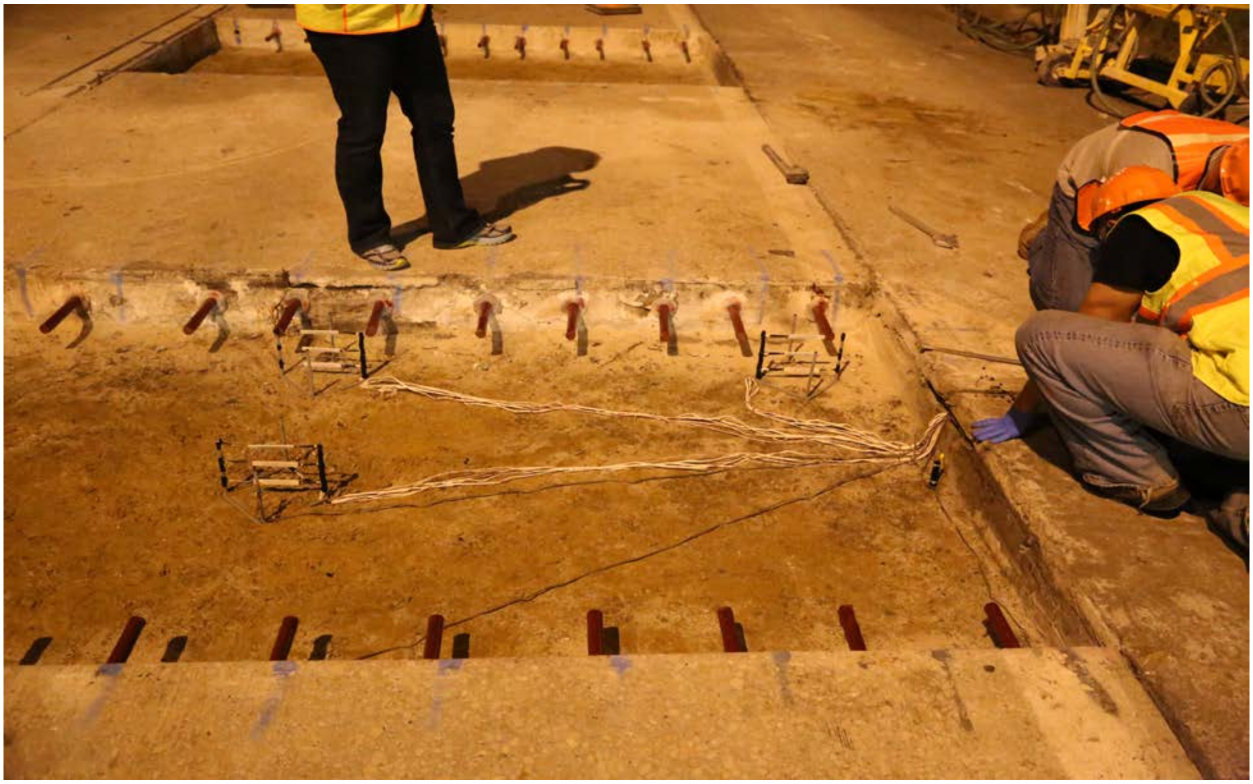

Figure 4-3: Preparations prior to the placement of concrete for Slab 2.

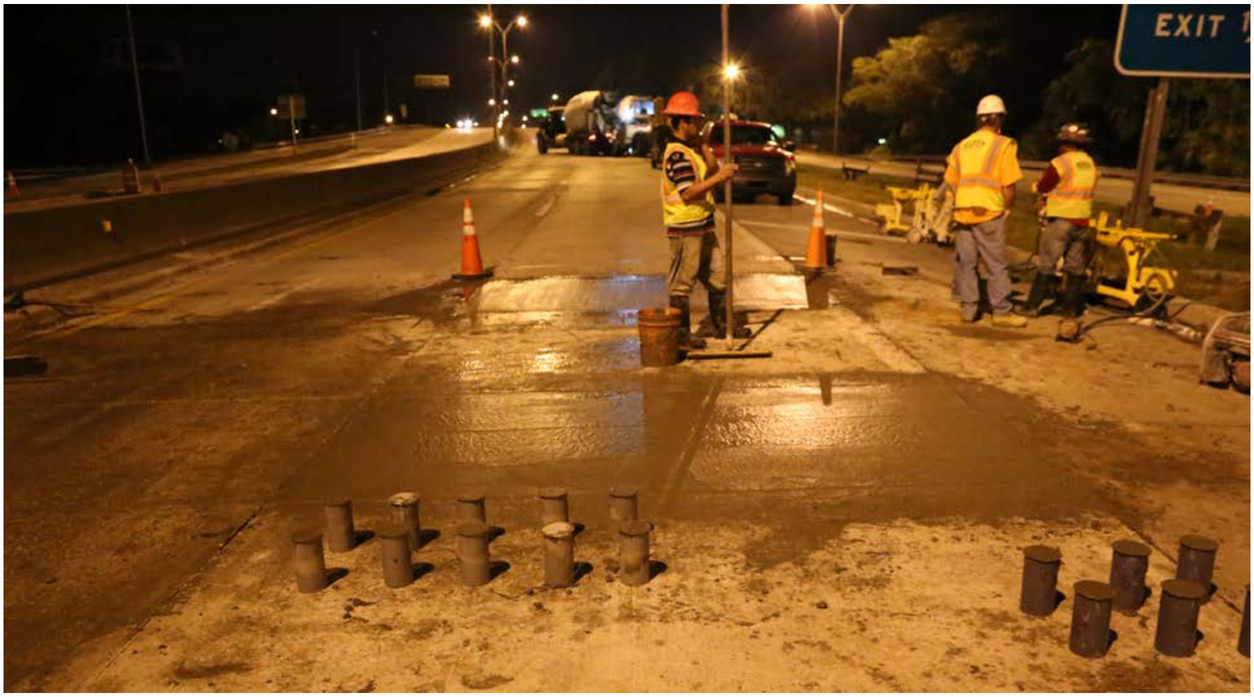

Figure 4-4: Completion of concrete finishing operations to Slab 2

Figure 4-5: Application of curing compound and covering of Slab 2

Figure 4-6: Slab 2 – six months after placement

Figure 4-7: Slab 2 – grinding defect

4.3 Field Performance of Slab 3

Slab 3 was cast in conjunction with a research project conducted by the FDOT pavement research group and was located at the State Materials Office. There were several differences between slabs placed in the field (Slabs 1 and 2) and Slab 3. Slab 3 did not contain any dowel bars, the accelerator content was considerably higher than listed on the mix design (but similar to what occasionally occurs in field repair projects), and the slab surface was not ground. The slab was placed on a relatively cold morning in Gainesville, Florida, and the resultant concrete delivery temperature was low. The effect of the high accelerator content was more than offset by the low concrete placement temperature. A view of the preparation of the slab prior to the placement of concrete with the instrumentation for data acquisition is presented in Figure 4-8. Typical finishing and curing compound application are presented in Figure 4-9 and 4-10 respectively. The slab was placed at approximately 8:36 A.M. October 10th and curing compound was applied on the slab at approximately 10:20 A.M. Similar to the conditions of Slabs 1 and 2, no visible cracks were observed at early ages.

Figure 4-8: Preparations prior to the placement of concrete for Slab 2

Figure 4-9: Concrete finishing operations to Slab 3

Figure 4-10. Application of curing compound to Slab 3

Slab 3 was subjected to approximately 287,000 traverses by the heavy vehicle simulator (HVS) with mostly a 12-kip load; approximately 20% of the loads were 9 or 15 kip. (Rice 2014). One of the difficulties with detecting cracks visually on the surface of the pavement at early ages is due to the presence of a white curing compound layer that conceals the cracks. However, after loading with the HVS, the curing compound was worn away in the wheel path, as shown in Figure 4-11. It was much easier to see cracks in the wheel path where the curing compound was worn away than on the rest of the slab where curing compound obscured the surface, as presented in Figure 4-12. Typical cracks are presented in Figure 4-13. The maximum size of the cracks was about 0.009” in the wheel path and 0.004” outside the wheel path.

Figure 4-11: Slab 3 – after placement and loading with HVS

Figure 4-12: Slab 3 cracking within and outside the wheel path

Figure 4-13: Slab 3 – easily visible cracking within the wheel path.

4.4 Slab 3 – Crack Investigation

The FDOT Standard Specification Section 353-6 states “If any uncontrolled cracks appear during the life of the contract, remove and replace the cracked slab” (Florida Department of Transportation 2013). Therefore, if Slab 3 had been placed on an FDOT roadway project, it may have eventually required replacement. As shown in Figures 4-11 through 4-13, the nature of the cracking appears to be due to shrinkage cracking as identified by the American Concrete Institute (ACI)(ACI Committee 224 2007). Several full-depth core samples were taken from the slab to determine the depth of cracking. A total of three cores were taken from locations shown in Figure 4-14. Cores 1 and 3 were taken from the wheel path and core 2 was taken from an area two feet from the edge of the slab. The core lengths were about 11.5” (Figure 4-15).

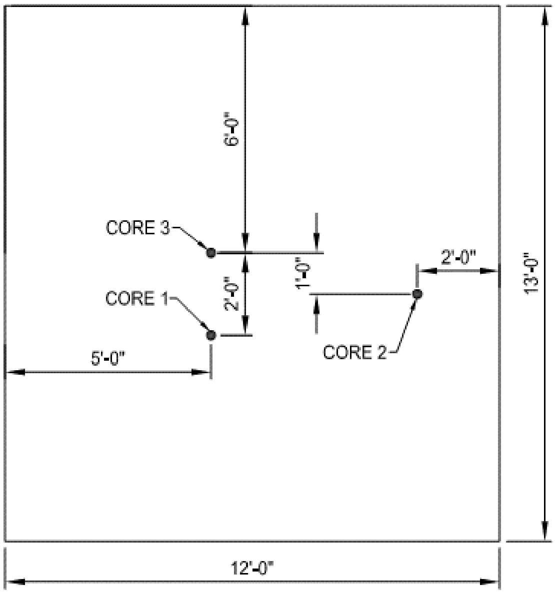

Figure 4-14: Core location map – Slab 3.

Figure 4-15: Typical core specimen removed from Slab 3.

A core taken from Slab 3 at Location 1 is shown in Figure 4-16. As the wet surface dried, the cracks were easily visible, with one crack penetrating to a depth of about 0.5”. The cores were cut longitudinally with a diamond saw perpendicular to the direction of the crack. After cutting, grinding, and polishing, the cores were examined and photographed using a Nikon AZ 1000 Multipurpose Microscope at 6.125X magnification to document the depth of cracking in each core, as presented in Figure 4-17 through 4-19.

Figure 4-16: Core specimen removed from Slab 3 – Location 1.

The use of the microscope for the investigation of the crack depth within each sectioned core provided much greater detail than visual analysis alone. The crack depth observed from the core taken from location 1 is approximately 0.8” (20 mm) as shown in Figure 4-17, which is a composite of two “stacked” microscope images. The crack observed from location 2 is approximately 1.0” (25 mm) as shown in Figure 4-18 which is composite of three stacked microscope images. The crack observed from location 3, shown in Figure 4-19, is approximately 0.2” (5 mm) in depth. The cracks exhibited transgranular fracture through the coarse aggregate, which has been observed in concrete that incorporates Florida limerock as coarse aggregate (Ferraro and Watts 2013). Crack widths of about 0.004” (Figure 4-13) and crack depths of 1” or less are consistent with shrinkage cracking, indicating that the HVS loading did not influence the cracking.

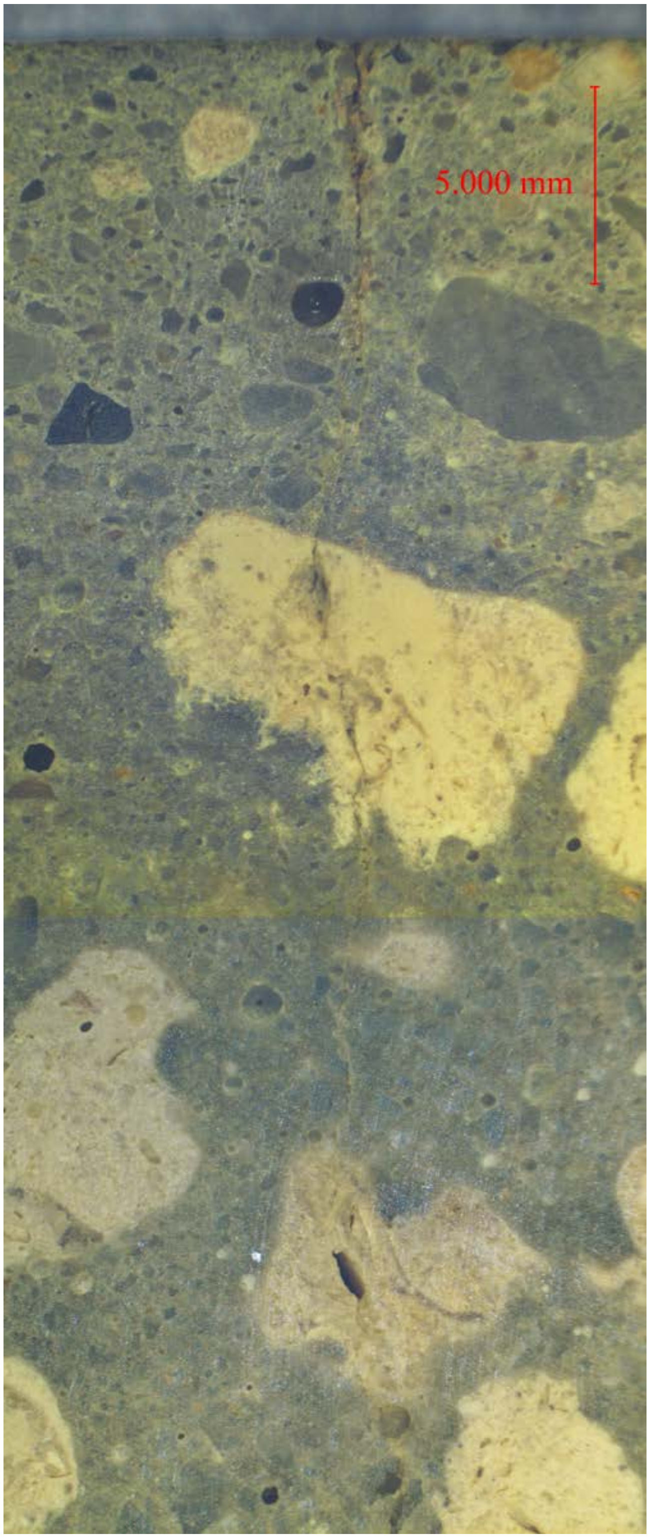

Figure 4-17: Core specimen removed from Slab 3 – Location 1.

Figure 4-18: Core specimen removed from Slab 3 – Location 2.

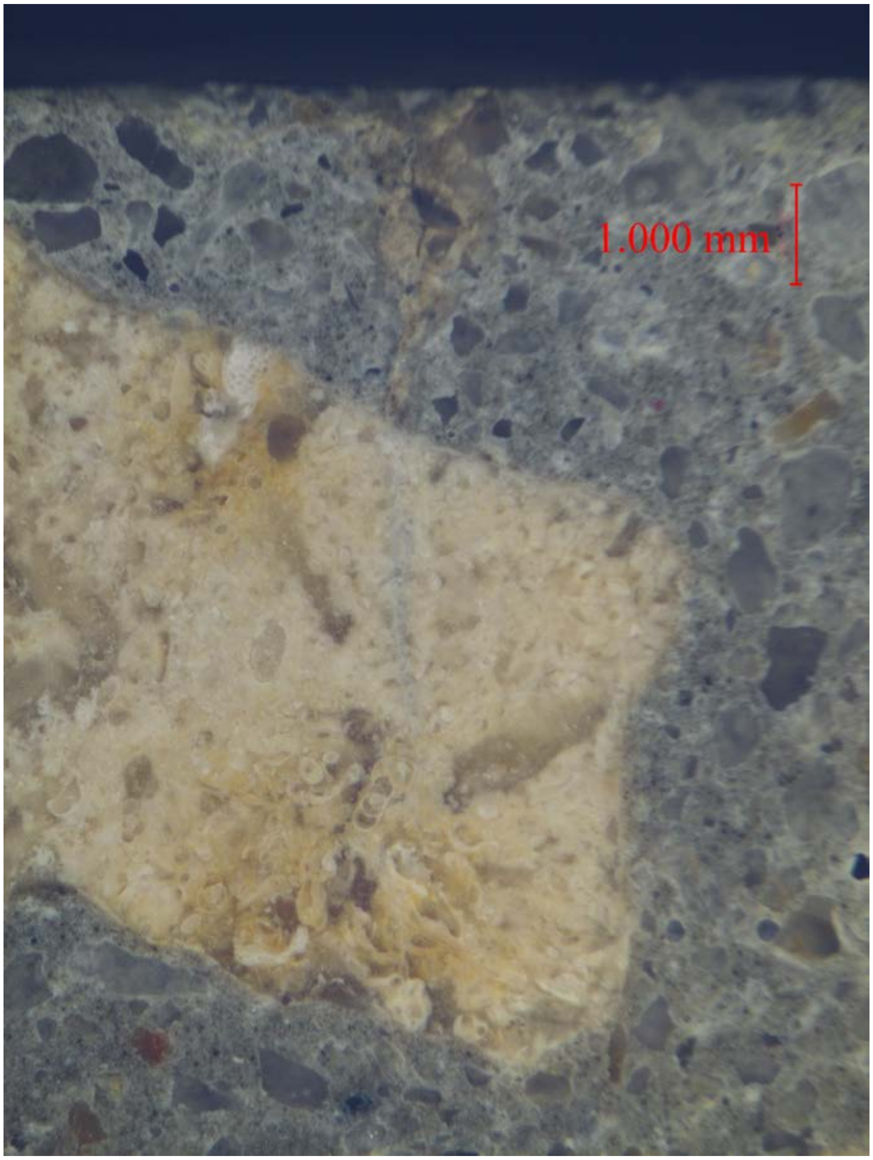

Figure 4-19: Core specimen removed from Slab 3 – Location 3.

4.5 Findings from Field

The main findings from the field work of this study can be summarized as follows:

- The temperature of the concrete at the start of placement and the ambient temperature have a discernible effect on the rate of temperature and strength gain of high-early-strength concrete.

- One of the field slabs exhibited cracking which was hidden by the curing compound until traffic loads removed the curing compound. Cracking was likely the result of thermal and drying effects.

4.6 References

ACI Committee 224. (2007). *ACI 224.1R-07: Causes, Evaluation, and Repair of Cracks in Concrete Structures*. American Concrete Institute, Farmington Hills, MI.

Ferraro, C., and Watts, B. (2013). *Development of Design Parameters for Virtual Cement and Concrete Testing*. Gainesville, FL.

Florida Department of Transportation (2009). *Rigid Pavement Design Manual*. Tallahassee, FL.

Florida Department of Transportation. (2013). *Standard Specifications for Road and Bridge Construction*. Florida Department of Transportation, Tallahassee, FL.

Rice, J., and Lloyd, J. (2014). *Optimization of a pavement Instrumentation Plan for a Full-Scale Test Road: Evaluation*. Gainseville, FL.

CHAPTER 5 Laboratory Tests for Cracking Potential Sensitivity-As-received Materials Characterization

5.1 Introduction

In order to assess the cracking potential of field mixtures and the role of placement time and accelerator dosage, several tests had to be conducted to determine mixture properties necessary for the operation of the modeling software. The software used in this study to assess the cracking risk was the Federal Highway Administration (FHWA) sponsored HIPERPAV (The Transtec Group 2009). Currently, the HIPERPAV temperature module is suppressed; that is, temperature prediction within a slab of a specified mixture design, strength gain, and hydration properties cannot be seen. The only output that is currently available is the stress/strength ratio and cracking potential. This is not ideal for purposes of validating the temperature output prediction via field work. To overcome this problem, ConcreteWorks (Concrete Durability Center 2007) software was used. It uses the same empirical models as HIPERPAV with temperature modules reflecting temperature prediction as a function of time from placement and at different slab depths. This chapter will discuss the laboratory experiments performed to characterize the materials used in the field and laboratory portions of the study.

5.2 Elemental Oxide Composition of As-Received Portland Cements

Two cements (SW and JAX), each from a different supplier, were acquired for the purpose of this study. The cements were selected based on identified FDOT projects by the project manager (PM) Dr. Harvey DeFord. The JAX cement was sampled from the same cement source that was used in field pavement-repair slabs 1 and 2. The SW cement was sampled from the same cement source as used in slab 3. The oxide chemical composition of the as-received cements was conducted using x-ray fluorescence spectroscopy in accordance to ASTM C114. ASTM C150 was used to determine the potential compound composition of cements. The results are depicted in Tables 5-1 and 5-2. The tables include potential phase composition both with and without the adjustment for the limestone addition. Information regarding the percent limestone added to each cement was obtained from the mill certificate if available. The results of cement density measurements are presented in Table 5-3.

Table 5-1: Oxide chemical analysis for as-received cements

Analyze	**SW cement (wt %)**	**JAX cement (wt %)**
SiO_2	20.40	18.78
Al_2O_3	5.20	5.36
Fe_2O_3	3.20	4.44
CaO	63.10	63.36
MgO	0.80	0.96
SO_3	3.60	3.27
Na_2O	0.10	0.13
K_2O	0.38	0.40
TiO_2	0.28	0.27
P_2O_5	0.12	0.65
Mn_2O_3	0.03	0.07
SrO	0.08	0.06
Cr_2O_3	0.01	0.02
ZnO	<0.01	0.08
L.O.I(950°C)	2.80	1.94
Total	100.10	99.81
Na_2O_{eq}	0.35	0.39
Free CaO	2.23	N/A
SO_3/Al_2O_3	0.69	0.61

***** Tests conducted by a certified commercial laboratory

Table 5-2: Bogue-calculated potential compound content for as-received cements

	Without Limestone Correction		**With Limestone Correction**	
Phase	**JAX**	**SW**	**JAX**	**SW**
C_3S	63	52	N/A	50
C_2S	6	19	N/A	19
C_3A	7	8	N/A	8
C_4AF	14	10	N/A	9
C_4AF+2C_3A	25	26	N/A	26
$C_3S+4.75C_3A$	95	92	N/A	89

Table 5-3: Particle size analysis, Blaine fineness, and density for as-received cements

Physical Properties	**SW**	**JAX**
D_{10} (µm)	3.0105	3.7634
D_{50} (µm)	13.0177	12.5429
D_{90} (µm)	29.3028	24.9369
Median size (µm)	13.01767	12.54291
Mean size (MPS) (µm)	15.08836	13.83280
ASTM C204-Blaine Fineness (m^2/kg)	442	427
Density (Mg/m^3)	3.14	3.24

The analyses indicate that JAX cement is higher in its C_3S content but significantly lower in C_2S. Both cements share similar C_3A content but different tetracalcium aluminoferrites with JAX cement having a lower content.

5.3 Cements' Blaine Fineness, Density, and Particle Size Distribution

The last step in manufacturing portland cement involves grinding of portland cement clinker with calcium sulfate or one of its hydrates. The product of this grinding stage is known as portland cement. The fineness to which cement is ground has significant effect on the behavior of cement especially during the early stages of hydration. Blaine fineness was used in this study to measure the cement fineness. It is an indirect measure of the total surface area of each cement sample and can be determined by the air permeability apparatus according to ASTM C204 "Standard Test Method for Fineness of Hydraulic Cement by Air Permeability Apparatus".

Prior to conducting Blaine fineness measurements on the as-received cements, the air-permeability apparatus was calibrated in accordance with ASTM C204 section 4. A sample bed of standard cement SRM 114q obtained from the National Institute of Standards and Technology (NIST) was used. The calibration was run at 21.8°C (71°F) and a relative humidity of 59%. Using the same settings, Blaine fineness was determined for the as-received cements. While the method is widely used in the cement industry for quality control, it offers some drawbacks. For example, a single averaged value may be given to two cements with different proportion of fines; that is, two different cements having the same surface area will give the same Blaine value even though they have very different particle size distribution (PSD) (Mehta and Monteiro 2006). In contrast, particle size distribution measurements provide more accurate insight on the quality and grading of the cement.

PSD measurement describes the frequency and size of particles contained in a sample (Jillavenkatesa et al. 2001). Typical particle sizes in portland cement vary from < 1 μm to 100 μm in diameter (Mehta and Monteiro 2006). Particle size influences the hydration rate and strength; it is also a valuable indicator for predicting cement quality and performance (HORIBA Instruments 2001, 2012). The characterization of the particles of the as-received cements was conducted using the principle of laser diffraction. In Laser diffraction, a particle will scatter light at an angle determined by its particle size. The angle of diffraction increases as the particle size decreases; this method is particularly effective in the particle size range of 0.1 to 3,000 μm (Jillavenkatesa et al. 2001). A LA-950 laser scattering particle size analyzer manufactured by HORIBA Instruments was used to analyze the particle size distribution of the cements. The instrument has the capacity to measure wet and dry samples in the range of 10 nm to 3 mm.

Sample preparation was conducted per manufacturer procedures. An adequate amount of dry cement was homogenized by mechanical agitation through the flow cell of the instrument at the start of measurement (HORIBA Instruments 2001). Figures 5-1 and 5-2 show the laser particle size measurement and cumulative particles size distribution repeatability for the SW cement used in this study. It is worth noting that the results presented are for 3 runs conducted on the same cement. The obvious overlap is indicative of the accuracy and precision of the testing technique. Blaine fineness and particle size distribution characteristics are presented in Table 5-2 for both cements.

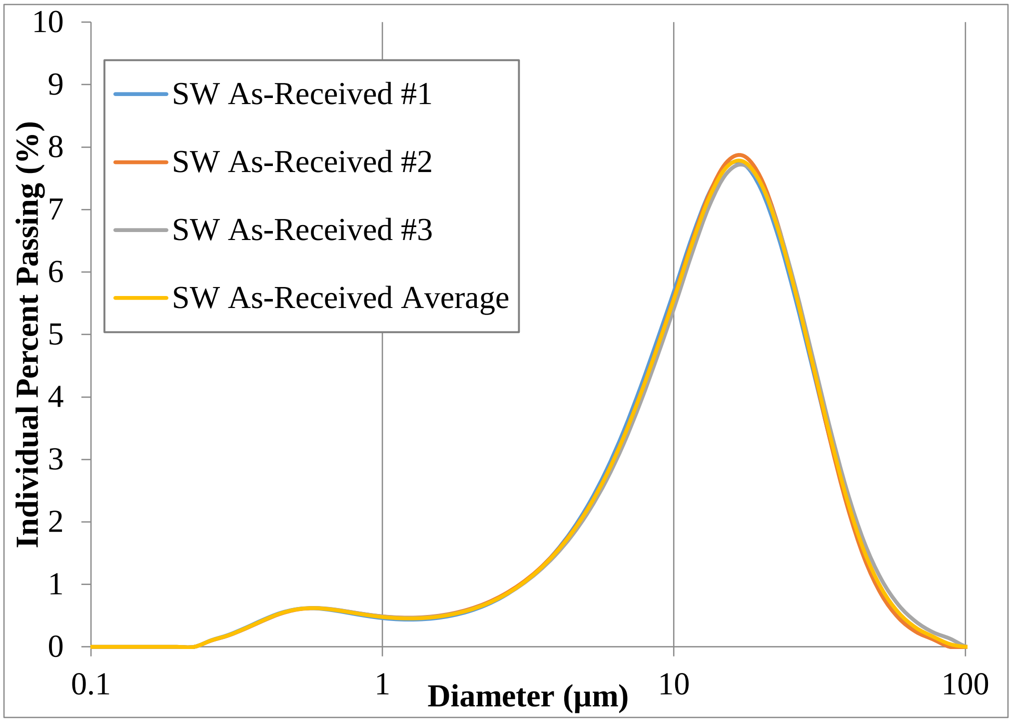

Figure 5-1: Differential particle size distribution for SW cement

.

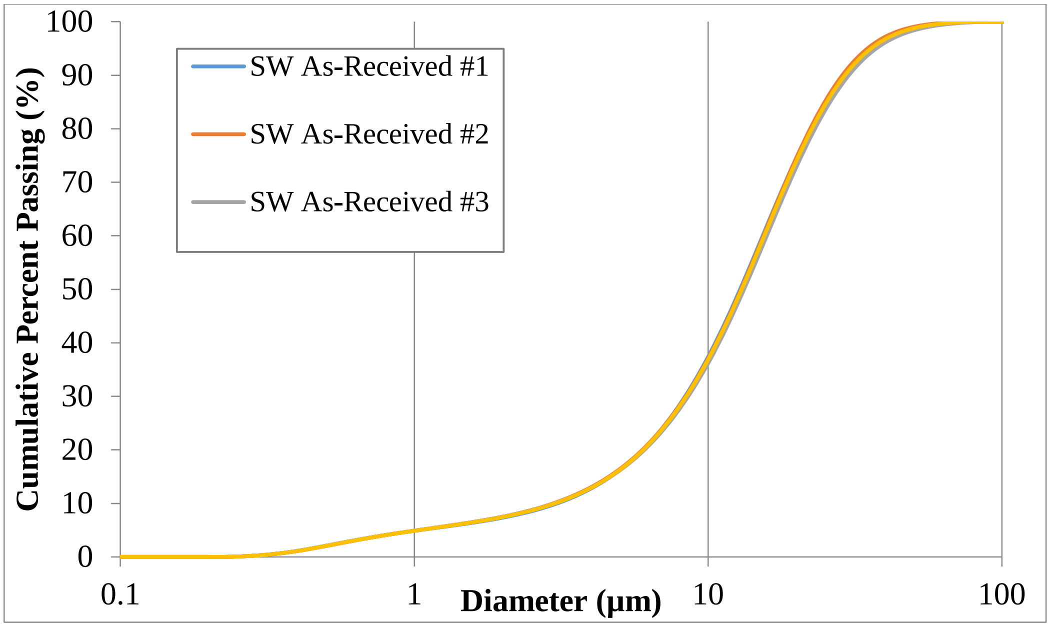

Figure 5-2: Cumulative particle size distribution for SW cement

The expressions of PSD results are based on a volume distribution using measures of D_{10}, D_{50}, and D_{90} (under size %) which identify the 10th, 50th, and 90th percentiles below a given particle diameter (Azari 2010). D_{50} is also defined as the median size; that is, the size that splits the size distribution with half above and half below the specified diameter. Similar to the concept of average, the mean size or mean particle size (MPS) expresses the volume mean as an average of D_{10}, D_{50}, and D_{90} (HORIBA Instruments 2012). In other words, MPS provides an approximation of the central point of the particle size distribution of an entire sample on a volume basis (Azari 2010; HORIBA Instruments 2001, 2012). Triplicate tests were conducted on all as-received cements and averages of the 3 tests were reported.

5.4 Mineralogical Analysis for As – Received Portland Cements

Apart from the bulk elemental oxide analysis, phase content of Portland cement is of great significance. It is understood that different cement phases have different contributions to concrete properties. Stutzman (2005) suggested that the application of accurate measurement techniques for cement phase quantification would improve the knowledge of their influences on cement hydration characteristics, concrete strength development and durability of structures. Additionally, this knowledge renders concrete as a more predictable construction material. X-ray diffraction (XRD) is a direct method of identification and quantification of the crystalline compounds in portland cements (Leng 2008; Maqsood and Iqbal 2010; Stutzman 1996). In this study, quantitative x-ray diffraction was adopted in identifying and quantifying crystalline phases present in both cements used here.

XRD scans of as-received cements (Figure 5-3 and 5-4) were collected in accordance with ASTM C1365 "Standard Test Method for Determination of the Proportion of Phases in Portland Cement and Portland-Cement Clinker Using X-ray Powder Diffraction Analysis". Mixtures of cement and ethanol 200 (99.5% pure) were prepared and wet-ground in a McCrone micronizing mill to a particle size between 1 and 10 micrometers. The wet grinding method was used to avoid the effect of temperature and moisture on gypsum and its possible phase transformation to or from hemihydrate or anhydrite. The samples were then dried in an oven at 43°C. After drying, the samples were placed in a sample holder using a back-loading technique with frosted glass in order to minimize preferred orientation (Bish and Reynolds 1989). X-ray diffraction scans were collected using a Phillips X'Pert PW3040 Pro diffractometer with Cu Kα radiation. The samples were scanned with a step size of 0.02 degrees per step and counting time of 4 seconds per step. The tension and current were set at 45 kV and 40 mA. The divergence slit was fixed at 1°, the receiving slit had a height of 0.2 mm, and the anti-scatter slit was fixed at 1°.

After collecting the x-ray scans of the as-received cements, phase identification was performed using HighScore Plus software. In order to aid the identification of the minor phases as well as the C_3S and C_3A crystal structures, selective dissolutions of the major phases (extractions) were performed for all cements.

Salicylic acid/methanol (SAM) extraction dissolves the silicates and free lime leaving a residue of aluminates, ferrites, and minor phases, such as periclase, carbonates, alkali sulfates and double alkali sulfates (Gutteridge 1979; Stutzman 1996). X-ray diffraction scans of the SAM extraction residues were collected for all the cements used in this study. In addition to minor phase identification, SAM residues were used to determine the presence of the C_3A polymorph. Tricalcium aluminate can be present in cement either in cubic or orthorhombic form or as a combination of both. Although the XRD patterns of cubic and orthorhombic C_3A are very similar, orthorhombic C_3A does not have a peak at 2θ of 21.8˚. In addition, cubic C_3A has only one peak at 2θ of 33.3˚, while orthorhombic C_3A has two peaks in this angular range, one at 2θ of 32.9˚ and another at 2θ of 33.2˚ (Stutzman 1996; Taylor 1997).

Potassium hydroxide/sucrose extraction dissolves aluminates and ferrites, thus leaving a residue of C_3S, C_2S, alkali sulfates and MgO (Stutzman 1996). Potassium hydroxide/sucrose extraction residues were used to identify the alite polymorph present in cements. Although alite has a number of polymorphs (triclinic, monoclinic, and rhombohedral)(Hewlett 1998), only monoclinic polymorphs are generally present in cements. Monoclinic alite has three polymorphs: M1, M2, and M3 (Taylor et al. 2000), although it is generally accepted that only M1 and M3 polymorphs exist in commercial clinkers (Courtial et al. 2003; Taylor 1997). X-ray diffraction scans were collected for the 5 angular windows recommended by Courtial et al. for alite polymorph identification (Courtial et al. 2003).

Cement phase quantification was performed using the Rietveld refinement. Rietveld refinement is a well-established technique used for quantitative x-ray diffraction (QXRD) analysis. It is based on fitting the whole pattern, which allows overlapped peaks to be resolved. A simulated pattern based on theoretical crystal structures input by the user is iteratively compared to the collected x-ray pattern and refined based on a number of parameters, which describe the crystal structure of the phases and their amount in the sample, and equipment characteristics. Two scans were collected and two Rietveld refinements were performed for each cement. The average results of the two scans is reported Table 5-4.

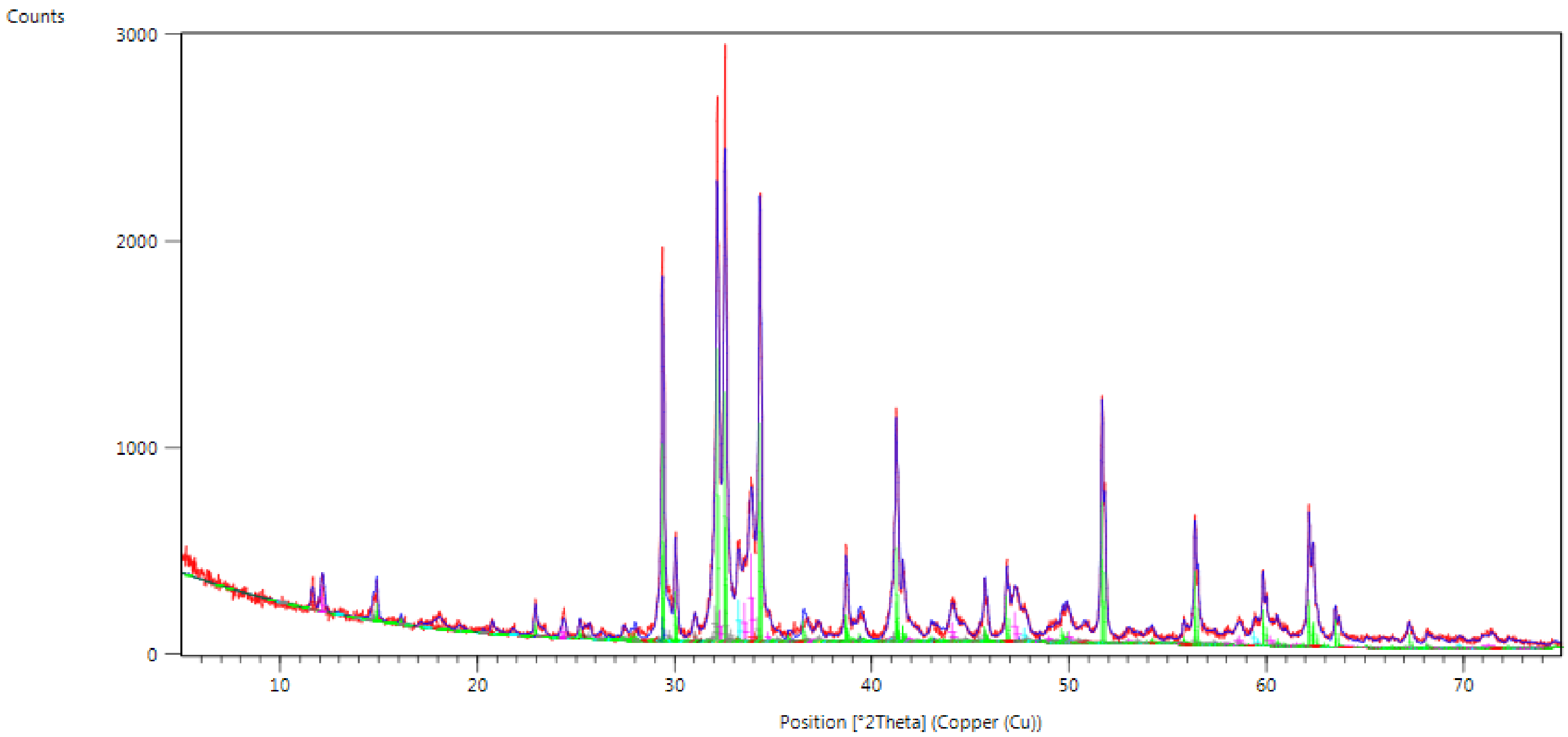

Figure 5-3: Diffraction pattern for JAX cement

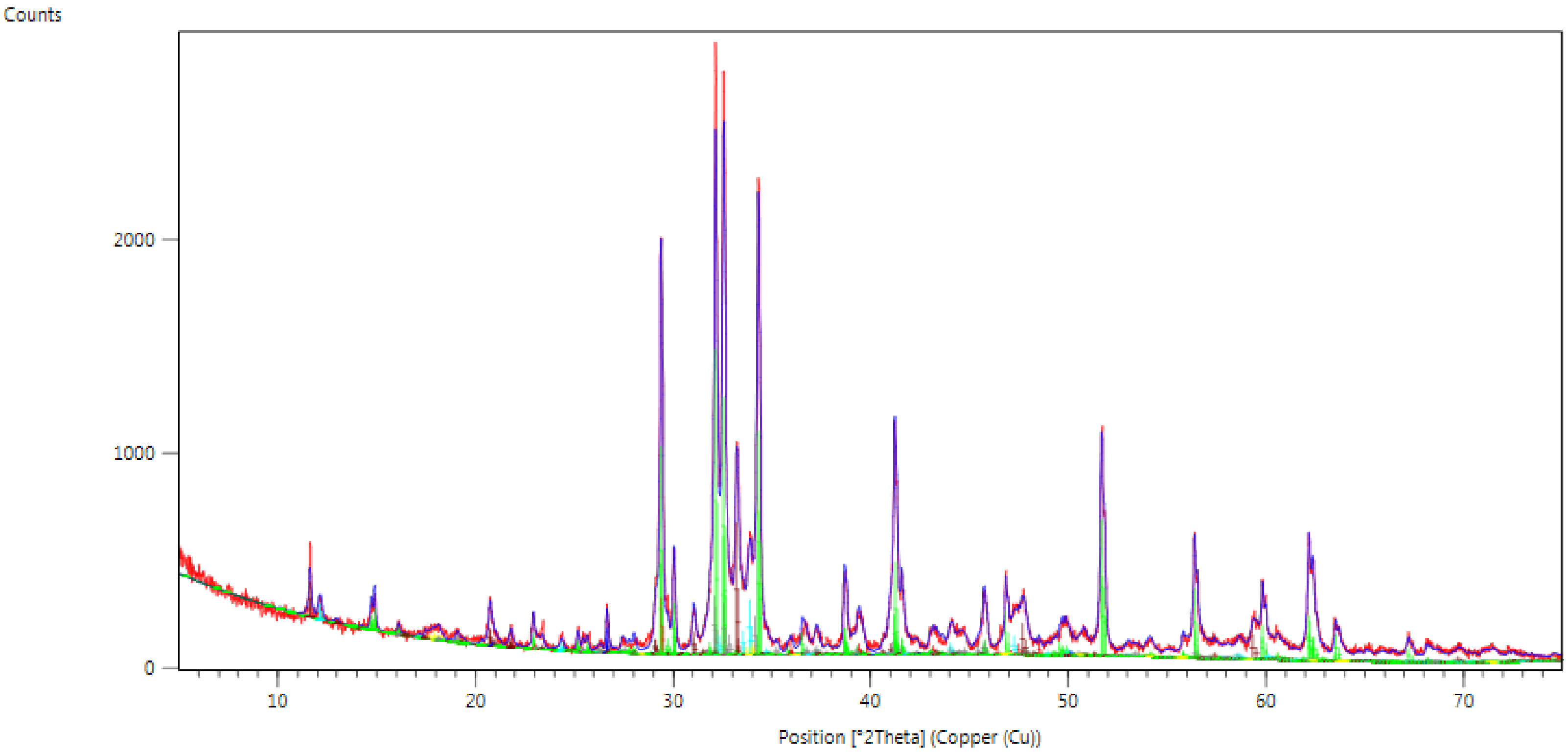

Figure 5-4: SW diffraction pattern

Table 5-4: Phase content using QXRD

Cement Phase	**Analysis method**	**SW**	**JAX**
C_3S (%)	Rietveld	52.0	57.4
C_3S (%)	Calibration curve	49	56
C_2S (%)	Rietveld	20.7	17.6
C_3A (%)	Rietveld	10.2	4.6
C_3A (%)	Calibration curve	7	7
C_4AF (%)	Rietveld	5.7	12.0
Gypsum	Rietveld	4.4	1.6
Hemihydrate	Rietveld	1.6	2.8
Anhydrite	Rietveld	0.2	0.4
Calcite	Rietveld	2.1	0.9
Lime	Rietveld	0.1	0.0
Portlandite	Rietveld	2.0	2.4
Quartz	Rietveld	0.9	0.1
Periclase	Rietveld	0.0	0.0
Arcanite	Rietveld	0.0	0.0
Syngenite	Rietveld	0.0	0.0

In addition to Rietveld refinement, the amount of alite in each cement was verified using the internal standard calibration curve. Internal standard analysis is based on the principle that the peak intensity of a phase, determined either as peak height or peak area, is directly proportional to the amount of this phase in the sample, as described by Equation 5-1 (Klug and Alexander 1974):

$$\frac{I_{ij}}{I_{ks}} = K\frac{x_j}{x_s} \qquad \text{Equation 5-1}$$

where

I_{ij} = intensity of peak i of phase j,

I_{ks} = intensity of peak k of the internal standard,

x_j and x_s = weight fraction of the phase j and the internal standard respectively, and

K = constant.

The advantage of the single-peak internal standard analysis is that quantification of the phase of interest is not affected by any other phases present in the sample, meaning that, unlike Rietveld analysis, it is not affected by unidentified or amorphous content.

The alite calibration curve was prepared by mixing samples of known C_3S content with 10% by total weight of sample of an internal standard following the general procedures described by Klug and Alexander (1974). Titanium dioxide (TiO_2) obtained from the National Institute of Standards and Technology (NIST) as part of the Standard Reference Material (SRM) 674b set was selected as an internal standard. TiO_2 was selected for three reasons: it has a mass absorption coefficient (MAC) close to that of cements, portland cement does not typically contain TiO_2, and most of the TiO_2 diffraction peaks do not interfere with the major peaks of portland cement.

Standard reference clinkers SRM 2686a, SRM 2687 and SRM 2688 were obtained from NIST and were used as a source of C_3S for the standardization mixtures. These clinkers have certified phase compositions and are representative of the modern-day clinkers produced by the cement industry. The clinkers were first ground with a mortar and pestle to reduce the particle size to below 45 microns and then ground in the McCrone micronizing mill for 10 minutes with ethanol prior to collecting x-ray diffraction scans.

After observing 5 angular alite windows for these clinkers as described previously, it was determined that SRM 2688 contained the M1 alite polymorph and was suitable for the preparation of the M1-C_3S calibration curve. SRM 2688 contains 64.95% of alite. Ground SRM 2688 was mixed with 10% TiO_2 to produce the 65% point on the calibration curve. In order to produce the 40 and 50% points for the calibration curve, SRM 2688 was diluted with C_3A in order to achieve the required alite content. Alite content of the sample was calculated for the SRM 2688/C_3A mixture excluding the TiO_2 addition.

The samples were mixed in the McCrone micronizing mill for 10 minutes with 5 mL of ethanol per every gram of sample as recommended by ASTM C1365. This was done to achieve homogeneous dispersion of the internal standard throughout the sample. After mixing, the sample was dried in an oven at 40 °C in order to evaporate the ethanol. Samples were loaded into the sample holder using the back-loading technique and scanned using the settings described previously. Three samples were analyzed for each point on the calibration curve.

The diffraction pattern collected for each sample was analyzed with HighScore Plus software in order to determine the areas of 51.8° 2θ peak of alite and the 54.3° 2θ peak of TiO_2. The area ratios of the alite peak to the TiO_2 peak were plotted against the alite content of the sample fraction excluding TiO_2 as shown in Figure 5-5. Subsequently, ground cements were mixed with 10 % TiO_2 to determine the area ratios in the as-received cements.

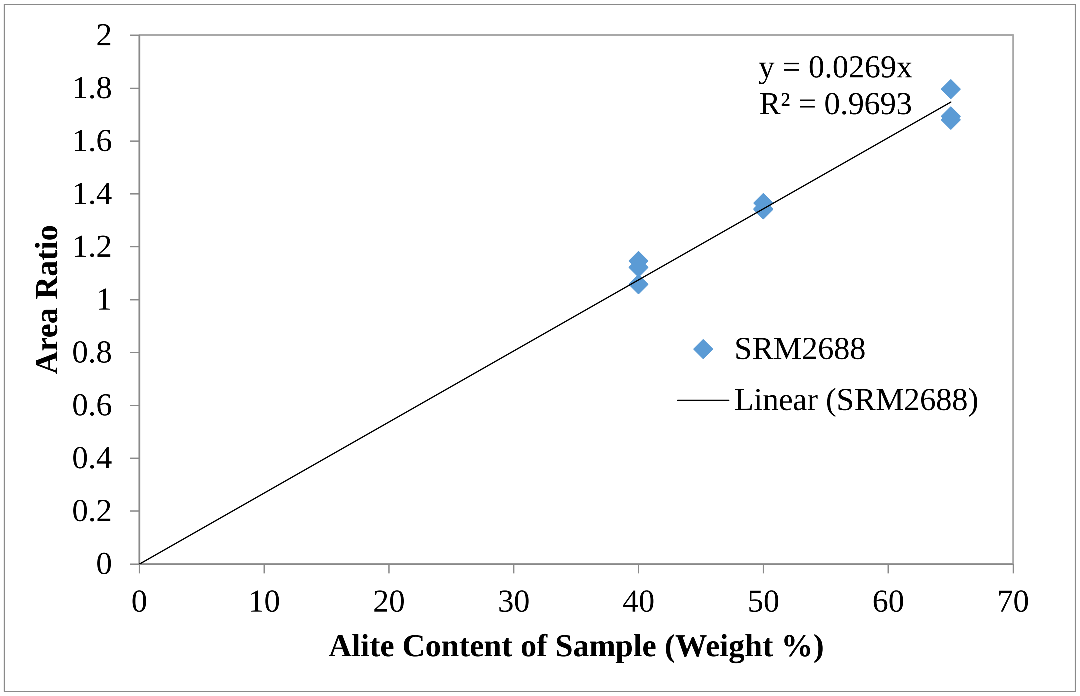

Figure 5-5: Internal standard calibration curve for M1 alite polymorph

As discussed previously, mineralogical phase composition of cements was quantified with Rietveld analysis. Alite amount was also calculated based on the internal standard calibration curve. Based on observing the five angular windows recommended by Courtial et al. (2003), it was determined that alite was present in the as-received cements as the M1 polymorph. Table 5.4

shows that the results obtained for alite based on Rietveld refinement and the calibration curve methods are in general agreement. The disagreement between the phase content determined through XRD and potential phase content determined through ASTM C150-12 is expected as indicated in the published literature (Stutzman 2005; Stutzman 1996; Taylor 1997).

5.5 Aggregate Properties

Coarse and fine aggregates used in the two locations identified by the PM for the current study were acquired. The cement for the Jacksonville location did not exceed 45 pounds, which has limited the ability to conduct additional laboratory tests on concrete mixtures. For this location, experiments were limited to isothermal calorimetry and limited maturity tests. For the Gainesville location, properties determined for the aggregates were: particle size distribution, bulk specific gravity (BSG) and absorption capacity (AC) for the coarse and fine aggregates. The tests were conducted in accordance to ASTM C33, ASTM C127 and C128 for coarse and fine aggregates, respectively. The results are presented in Figure 5-6 and 5-7 and Table 5-5.

During this phase of work, the aggregates were washed prior to grading and separating them into different sieve sizes. Aggregates were then compiled in preparing for different concrete mixes.

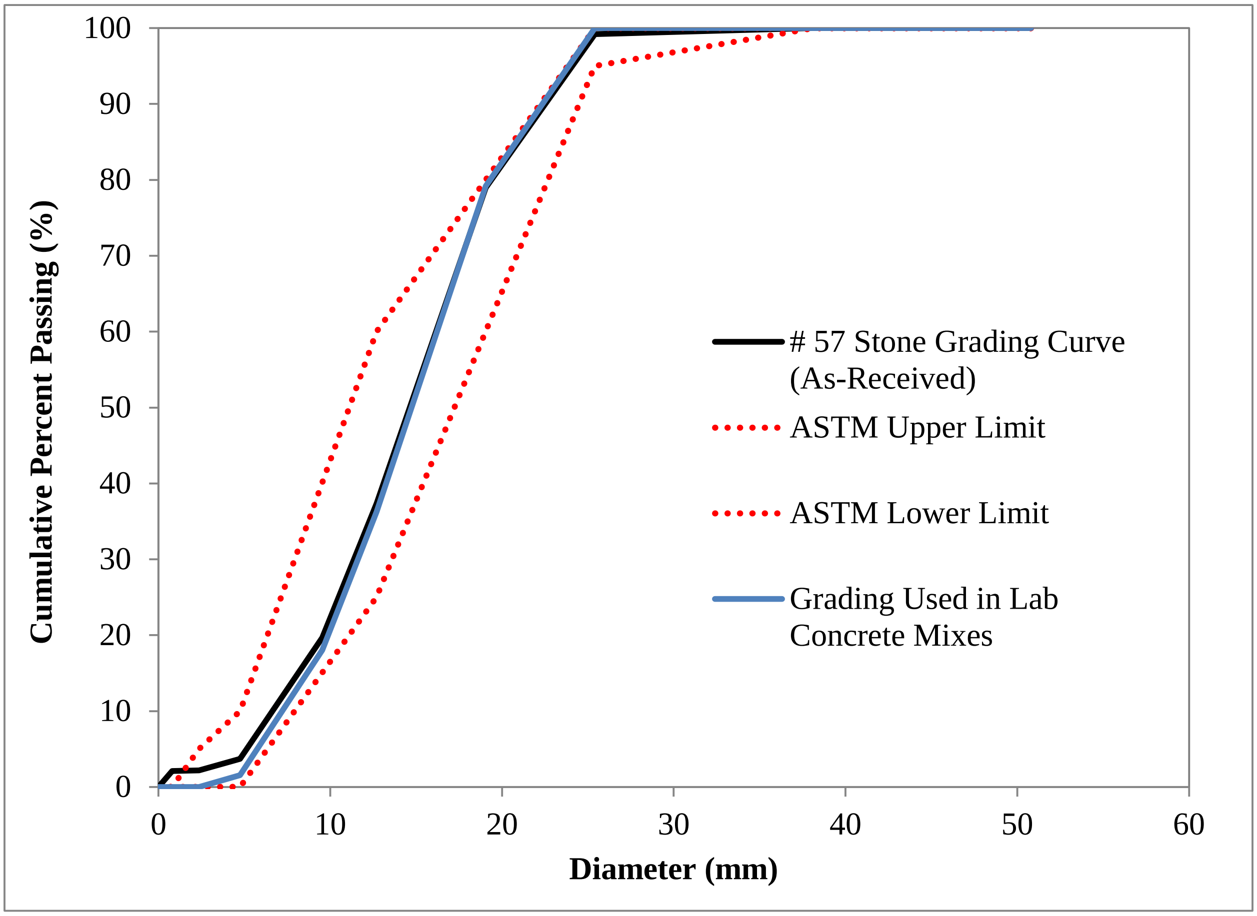

Figure 5-6: Grading curve for oolite – 87090 coarse aggregate

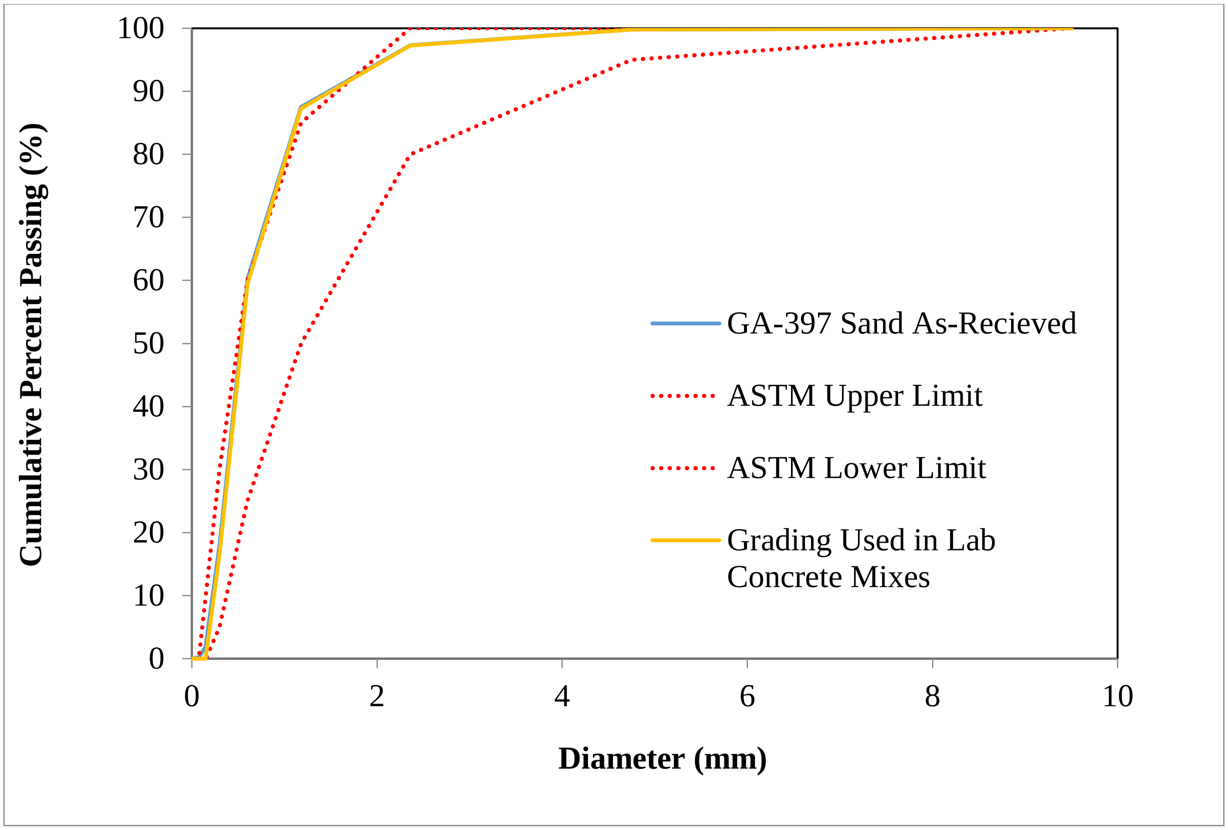

Figure 5-7: Grading curve for GA-397 fine aggregate.
Note that the GA-397 As-Received plot line is obscured by the Lab Mix plot line.

Table 5-5: Properties of coarse and fine aggregate

Property	**Oolite-87090**	**GA-397 Fine Aggregate**	**76349 Fine Aggregate**
BSG(OD)	2.36	2.65	2.77
BSG(SSD)	2.43	2.66	N/A
%AC	3	0.3	0.24

5.6 References

ASTM C33 / C33M-08 (2010), Standard Specification for Concrete Aggregates, ASTM International, West Conshohocken, PA, 2010.

ASTM C114-11b, Standard Test Methods for Chemical Analysis of Hydraulic Cement, ASTM International, West Conshohocken, PA, 2011.

ASTM C127-12, Standard Test Method for Density, Relative Density (Specific Gravity), and Absorption of Coarse Aggregate, ASTM International, West Conshohocken, PA, 2012.

ASTM C128-12, Standard Test Method for Density, Relative Density (Specific Gravity), and Absorption of Fine Aggregate, ASTM International, West Conshohocken, PA, 2012.

ASTM C150 / C150M-12, Standard Specification for Portland Cement, ASTM International, West Conshohocken, PA, 2012.

ASTM C204-11e1, Standard Test Methods for Fineness of Hydraulic Cement by Air-Permeability Apparatus, ASTM International, West Conshohocken, PA, 2011.

ASTM C1365-06 (2011), Standard Test Method for Determination of the Proportion of Phases in Portland Cement and Portland-Cement Clinker Using X-Ray Powder Diffraction Analysis, ASTM International, West Conshohocken, PA, 2011.

Azari, H. (2010). *Statistical Modeling of Cement Heat of Hydration Using Phase and Fineness Variables*. National Cooperative Highway Research Program, Transportation Research Board of the National Academies, NCHRP web-only Document 167.

Bish, D., and Reynolds, R. J. (1989). “Sample Preparation for X-Ray Diffraction.” *Modern Powder Diffraction*, D. Bish and J. Post, eds., The Mineralogical Society of America, Washington, DC, 73–99.

Concrete Durability Center. (2007). “ConcreteWorks (Version 3.1.0) [Software].” <Available from www.texasconcreteworks.com>.

Courtial, M., de Noirfontaine, M.-N., Dunstetter, F., Gasecki, G., and Signes-Frehel, M. (2003). “Polymorphism of tricalcium silicate in Portland cement: a fast visual identification of structure and superstructure.” *Powder Diffraction*, 18(1), 7–15.

Gutteridge, W. A. (1979). “On the Dissolution of the Interstitial Phases in Portland Cement.” *Cement and Concrete Research*, 9(3), 319–324.

Hewlett, P. C. (Ed.). (1998). *Lea’s Chemistry of Cement and Concrete*. Arnold, New York, NY.

HORIBA Instruments. (2001). *LA-950 Instructional Manual*. Irvine, CA.

HORIBA Instruments. (2012). “A Guidebook to Particle Size Analysis.” <http://www.horiba.com/fileadmin/uploads/Scientific/Documents/PSA/PSA_Guidebook.pdf > (Nov. 14, 2012).

Jillavenkatesa, A., Dapkunas, S. J., and Lum, L. (2001). *Particle Size Characterization*. National Institute of Standards and Technology (NIST), Special Publication 960-1.

Klug, H. P., and Alexander, L. . (1974). *X-ray Diffraction Procedures: For Polycrystalline and Amorphous Materials*. J. Wiley & Sons, Hoboken, NJ.

Leng, Y. (2008). *Materials Characterization: Introduction to Microscopic and Spectroscopic Methods*. J. Wiley & Sons, Singapore, 45–79.

Maqsood, A., and Iqbal, K. (2010). “Materials Characterization by Non-Destructive Methods.” *Journal of the Pakistan Materials Society*, 4(1), 31–38.

Mehta, P. K., and Monteiro, P. J. M. (2006). *Concrete: Microstructure, Properties and Materials*. McGraw-Hill, New York, NY.

Stutzman, P. E. (1996). *Guide for X-Ray Powder Diffraction Analysis of Portland Cement and Clinker*. Gaithersburg, MD, 1–38.

Stutzman, P. E. (2005). “Powder Diffraction Analysis of Hydraulic Cements: ASTM Rietveld Round Robin Results on Precision.” *ICDD Advances in X-Ray Analysis*, 48(1), 33–38.

Stutzman, P. E. (1996). *Guide for X-Ray Powder Diffraction Analysis of Portland Cement and Clinker*. Gaithersburg, MD, 1–38.

Taylor, H. F. W. (1997). *Cement Chemistry*. Thomas Telford Publishing, London, UK.

Taylor, J. C., Hinczak, I., and Matulis, C. E. (2000). “Rietveld Full-Profile Quantification of Portland Cement Clinker: The Importance of Including a Full Crystallography of the Major Phase Polymorphs.” *Powder Diffraction*, 15(1), 7–18.

The Transtec Group. (2009). “HIPERPAV III (Version 3.20.0006) [Software].” <Available from www.hiperpav.com>.

CHAPTER 6 Laboratory Tests for Cracking Potential Sensitivity-Isothermal Calorimetry

6.1 Introduction

An objective of this project was to use field data for modeling the cracking potential of high-early-strength (HES) concrete mix designs using HIPERPAV software. The concrete mixture design used in the Miami project and slabs placed at the SMO in Gainesville was designated Slab Mix 1 and the cement was designated SW. The second cement (JAX) was used on a Jacksonville project. The concrete mix designs for the field projects are provided in Table 6-1.

Table 6-1: Concrete mix design

Material	FDOT Gainesville Slab Mixture	FDOT Jacksonville Slab Mixture	Specification
Cement-Type II	900 lb	850 lb	AASHTO M 85
Coarse Aggregate #57	1680 lb	1600 lb	Limerock (Oolite)
Fine Aggregate	831 lb	1101 lb	Silica sand
AEA Admixture - air entrainer	3.0 oz	7.5 oz	AASHTO M 154-AEA
Type D Admixture - water reducer/retarder	45.0 oz	17.0 oz	AASHTO M 194- Type D
Type E Admixture - accelerator	384.0 oz	448.0 oz	AASHTO M 194-Type E
Type F Admixture - high-range water reducer	N/A	29.8 oz	AASHTO M 194- Type F
Water for concrete	324.8 lb	260 lb	
Water-to-Cement Ratio	0.39	0.34	

In addressing the objectives of this research, it was essential to determine the strength and heat generated expressed in terms of equivalent age for the concrete mixes. This subsequently allowed the use of modeling software to predict temperature rise and thermal stresses in concrete pavement slabs. Models predicting thermal stresses and temperature rise in concrete elements rely on temperature sensitivity determination through heat of hydration measurements. As concrete temperature sensitivity is dependent on mixture design and in order to perform accurate modeling, it is imperative to determine this property for each specific mix used. Temperature rise in mass elements is the primary driving mechanism for thermal stresses and accompanying cracking (Schindler 2002).

The activation energy can be determined using isothermal calorimetry (D'Aloia and Chanvillard 2002; Kada-Benameur et al. 2000; Ma et al. 1994; Poole 2007; Poole et al. 2007; Schindler and Folliard 2005; Schindler 2002; Xiong and van Breugel 2001). The exponential method or Modified ASTM C1074 (Poole et al. 2007) for activation energy determination was adopted here. The method follows the same procedures outlined in ASTM C1074 for strength-based activation energy, except that the analysis is based on heat of hydration measurements. The exponential function, which characterizes cement hydration based on degree of hydration, was fit through degree of hydration data to determine best-fit curve parameters (α_u, τ, β). The degree of hydration was calculated from the cumulative isothermal heat of hydration, and the heat of hydration at 100% hydration calculated from the cement composition. The activation energy was subsequently quantified. The published literature indicates that there are several factors that influence activation energy of portland cement or its hydration kinetics; namely, cement mineralogy, fineness, particle size distribution, chemical admixtures and pozzolanic materials (Poole et al. 2011; Schindler 2004). However, the focus of this study was the effect of accelerators on hydration kinetics.

The activation energy or the temperature sensitivity of the hydration process describes the linear relationship between the rate constants and temperature. In this work, the temperature sensitivity of the hydration process in mixes using a water-reducing and set-retarding admixture reducer/set retarder and an accelerating admixture was studied using isothermal calorimetry performed at different temperatures. The temperatures used in the isothermal calorimetry were: 23º, 38º and 48º C. Higher temperatures were attempted but due to pressure build-up during internal mixing, the maximum practical temperature that could be implemented was 48º C. The degree of hydration, expressed as the ratio of the total heat at a specified time to the ultimate total heat of the cement, was then calculated using Equation 2-11 (Poole et al. 2007; Schindler and Folliard 2005; Schindler 2002).

H_u was calculated from the cement composition, as determined from Rietveld analysis, and using the Bogue-determined coefficients for each cement phase as indicated in Equation 2-13.

For each temperature, a degree of hydration curve was calculated as a function of time according to Equations 2-6 and 2-10. Equation 2-10 was then used to characterize cement hydration process through curve fitting to determine the best-fit parameters (α_u, τ, β). Equation 2-10 (Poole 2007; Schindler 2002) was found to provide reasonable results for a number of prediction models. The Solver Function in Microsoft Excel was used to minimize the sum of the squares of the residuals of the calculated values from Equation 2-10 to the measured values in obtaining the best-fit parameters α_u, τ, and β. The activation energy for each mix was then determined from the best-fit straight line of rate constant ($1/\tau$) of the reaction versus [1/T (K)]. The activation energy is equal to the negative product of the slope and the universal gas constant (8.32 J/mol K).

Activation energy or the temperature sensitivity of the hydration process is significant in predicting the temperature rise and cracking potential in massive concrete elements. It is used in prediction models (Poole 2007; Poole et al. 2007; Schindler and Folliard 2005; Schindler 2002) with semi-adiabatic or adiabatic calorimetry measurements to project temperature rise in concrete elements (Schindler and Folliard 2005).

6.2 Heat of Hydration

Heat of hydration (HoH) measurements of the as-received cements as well as mixtures of cement and chemical admixtures were performed in accordance with ASTM C1702 Method A, internal mixing method. Heat flow measurements were performed using TA Instruments' TAM Air isothermal calorimeter. The reference cells contained 12.33 g of Ottawa sand during all the measurements to have similar thermal mass as the paste samples. Two runs were performed for each mixture at each specified temperature, and average values are reported here.

After measuring the required amount of anhydrous cement and water or chemical admixture solutions, the ampoules were placed in the calorimeter and the system was allowed to reach thermal equilibrium. The water or solution containing the admixture was then injected into the vial and the paste was mixed constantly for 60 seconds. For chemical admixtures, solutions of required concentrations were prepared volumetrically in order to minimize errors in measuring small amounts of admixture. Chemical admixtures addition rates are listed in Table 6-2. Since admixtures should not be added at the same time, according to manufacturer recommendations, a slightly different protocol was used for mixing pastes containing admixtures. A solution of water/retarder was injected during the first 10 seconds followed by delayed addition of air-entraining admixture solution (added after 15 seconds of mixing) and accelerating admixture solution (added after 45 seconds of mixing). Heat flow measurements were collected for 7 days. Heat flow and cumulative heat of hydration were normalized per gram of cement in the sample.

Table 6-2: Paste proportions for isothermal calorimeter tests

Material	**SW-C**	**SW-CNA**	**SW-CHA**	**SW-CA**	**SW-CDA**	**JAX-CA**
Cement (g)	3.9800	3.9800	3.9800	3.9800	3.9800	4.5000
AEA admixture (g) / (ml/100 kg of cement)	0.0000 / 0.0	0.0009 / 21.7	0.0009 / 21.7	0.0009 / 21.7	0.0009 / 21.7	0.0027 / 57.8
Type D water reducer/retarder (g) / (ml/100 kg of cement)	0.0000 / 0.0	0.0149 / 325.7	0.0149 / 325.7	0.0149 / 325.7	0.0149 / 325.7	0.0070 / 134.9
Type E (g) / (ml/100 kg of cement)	0.0000 / 0.0	0.0000 / 0.0	0.0744 / 1,389.5	0.1488 / 2,779.0	0.2975 / 5,557.9	0.3135 / 5,179.7
Type F (g) / (ml/100 kg of cement)	N/A	N/A	N/A	N/A	N/A	0.0110 / 227.4
w*/c	0.384	0.384	0.384	0.384	0.384	0.319

* Water present in Type E admixture was included in the calculation of the w/c ratio

Paste samples were prepared with a w/c ratio that matched concrete mixes; namely, 0.384 and 0.319 for the SW and JAX mixes, respectively. To evaluate the SW cement, 5 different paste mixtures were prepared in order to address the objectives of the project on the effect of accelerator dose on concrete pavement cracking potential. Plain mix (C) contained no chemical admixtures, mix (CNA) contained AEA and type D water reducer at the same field dose, mix (CHA) had the same field dose for AEA and water reducer but half accelerator field dose, mix (CA) matched the field mix on all admixtures and mix (CDA) had the same AEA and water reducer dose as the field mix but with double the field mix accelerator dose. Due to limited supply of the JAX cement, only mixes simulating the field mix were prepared. As such, only three mixes (in duplicates) were run for this cement representing the selected 3 isothermal temperatures for activation energy determination.

The results for the isothermal runs are depicted in Figure 6-1 through 6-4. The cumulative heat of hydration values at 6 days are tabulated in Table 6-3. At 23°C, the following effects can be observed. First, comparing C to CNA, the effect of water reducer/retarder on hydration kinetics can be observed. As expected, incorporation of this admixture delayed the main hydration peak, which is related to C_3S hydration. This observed delay in C_3S hydration is well established in the literature (Bishop and Barron 2006; Collepardi 1995; Lagier and Kurtis 2007; Quennoz and Scrivener 2013; Sandberg and Roberts 2003; Taylor 1997). The position of the main peak appears to be delayed by approximately an hour with a slight reduction in the heat flow with admixture addition. The position of the sulfate depletion point appears to be unaffected at the admixture dose implemented here. The CNA mix included AEA as well as water reducer/retarder. The effect of AEA at the used dose is not expected to be of significance on the heat of hydration curve (Dolch 1995; Odler 1998).

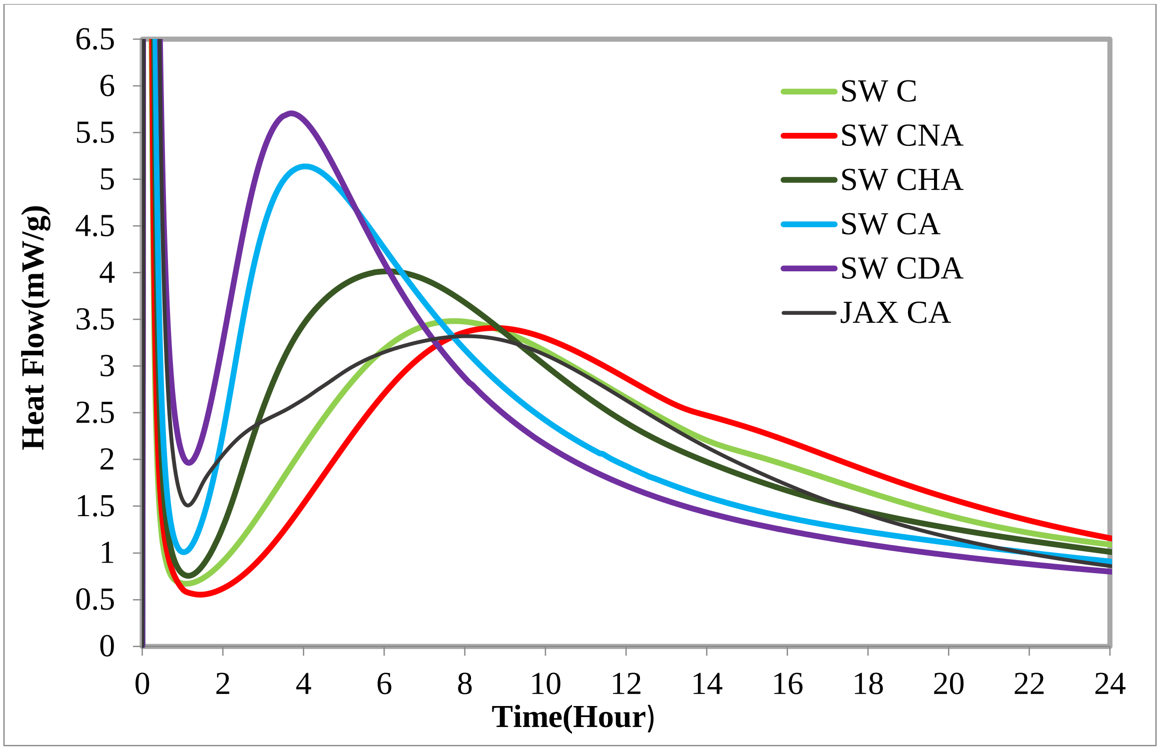

Figure 6-1: Heat flow for cement paste mixes at 23ºC

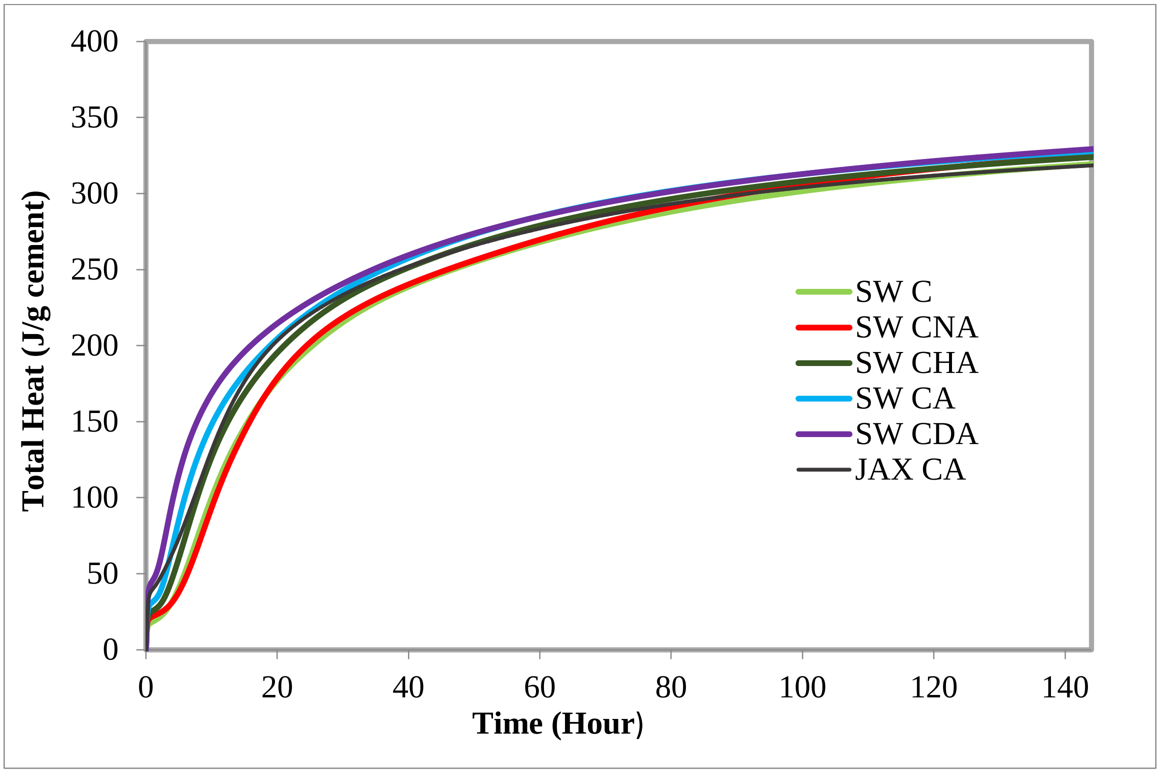

Figure 6-2: Heat of hydration for cement paste at different accelerator dosages at 23ºC

Table 6-3: Cumulative heats of hydration at 6 days

	Cumulative Heat of Hydration (J/g of cement)					
Temperature	**SW-C**	**SW-CNA**	**SW-CHA**	**SW-CA**	**SW-CDA**	**JAX-CA**
23°C	322.5	331.5	327.1	335.9	338.1	322.7
38°C	352.3	361.3	357.0	376.4	381.0	338.2
48°C	336.7	298.2	302.0	323.5	316.9	310.9

As indicated previously, additions of the chloride-based accelerator were done at 3 different levels in mixtures CHA, CA and CDA. Comparing CNA and CHA indicates that the induction period is shorter with an increase in the rate of heat flow in the acceleration period. Additionally, the main peak increased in its intensity and shifted towards shorter hydration time; the effect is clearly accelerator-dose dependent. The effect of chloride-based accelerator on the main peak and C_3S hydration is well documented in the literature (Bentz 2010; Kocaba 2009; Lawrence et al. 2003; Lothenbach et al. 2011; Neville 2006; Ramachandran and Feldman 1978; Ramachandran 1995; Scrivener and Nonat 2011; Tenoutasse 1968); however, information on its effect on C_3A hydration is limited. The peak/shoulder that appears to the left of the main peak in the C and CNA mixes is not clearly resolved in CA or CDA. This would therefore indicate that there is a possible interaction between the accelerator used here and the hydration of the aluminate phases and sulfate availability/solubility. The cement used here (SW) has a high C_3A content (10%).

When comparing JAX-CA paste with SW-CA and SW-CDA paste, JAX-CA had an accelerator dose closer to SW-CDA; however, the total heat generated by JAX-CA was close to SW-C (control, no chemical admixtures) or SW-CNA (air-entrainer and water-reducer, no accelerating admixture). At 3 hours of hydration, the heat generated by JAX-CA paste was slightly lower than CDA but higher than CA pastes; however, on further hydration towards the main peak, the reaction rate appeared to slow down. The observed trend might be due to differences in cement mineralogy and fineness coupled with the introduction of Type F chemical admixture in the JAX-CA mix. Previous mineralogical and physical analyses on JAX and SW cements indicated that the JAX cement had a lower Blaine fineness and higher C_3S content while SW cement had higher C_3A and gypsum content.

Figure 6-2 shows that at 1 day, the order of the heat generated by different mixes, at an isothermal temperature of 23º C was: CDA>CA>CHA>CNA>C. At 6-days, the effect of the chloride-based accelerator dose on the total heat generated by cement paste on hydration was minimal as evident from comparing SW-CNA at 325 J/g to SW-CDA at 329 J/g. Additionally, it appears that the effect of the accelerator dose on the total heat generated by cement paste depends on the cement mineralogy and Blaine fineness. This can be observed when comparing SW-CDA with JAX-CA mixes where it can be seen that the heat generated by the latter continues to be less than the former up to an age of 6 days. In fact, the cumulative heat generated by JAX-CA paste was similar to SW-C at 6 days. Previous mineralogical analyses indicate that JAX cement is higher in its C_3S content but significantly lower in C_2S.

Increasing the isothermal temperature to 38º C increased the total heat generated for all mixes. However, for heat measurements conducted at 48ºC, more pronounced increase occurred only at an earlier age but at an age of six days the total heat was lower than that measured at 38 °C (Berhane 1983).

Results of the isothermal calorimetry data analysis are depicted in Table 6-4 and Appendix A and B. In conducting the analysis, all parameters were allowed to vary (Xu et al. 2010). The results indicate that additions of water reducer and accelerator decreased the activation energy values, making the mixtures less sensitive to temperature. However, the change does not appear to be very sensitive to variation in accelerator dosage. The hydration time parameter (τ), which is related to the timing of maximum heat flow, appears to increase on adding a retarder and decreases with the addition of an accelerator. The duration of the induction period decreases with temperature indicating a higher reaction rate and shorter setting time. The results show that (β), the parameter describing the shape of the hydration curve, increases with temperature for most mixes containing accelerator indicating a higher reaction rate at the linear portion of the hydration curve (Xu et al. 2010). The data presented in Table 6-4 was used in the HIPERPAV to predict temperature rise and cracking potential.

Table 6-4: Activation energy and hydration parameters for different mixtures

Cement	Mix	Temp(°C)	α_u	τ	β	E_a (J/mol)	R^2
SW	C	23	0.799	14.56	0.730	33,004	0.976
		38	0.780	6.69	0.873		
		48	0.709	5.24	1.086		
SW	CNA	23	0.815	15.26	0.738	28,822	0.986
		38	0.794	7.95	0.937		
		48	0.642	6.22	0.841		
SW	CHA	23	0.807	11.73	0.679	24,148	0.918
		38	0.791	6.09	0.841		
		48	0.616	5.64	0.754		
SW	CA	23	0.846	9.99	0.603	25,420	0.945
		38	0.841	5.20	0.733		
		48	0.724	4.59	0.880		
SW	CDA	23	0.949	10.29	0.424	25,574	0.777
		38	0.858	4.41	0.627		
		48	0.687	4.86	0.822		
JAX	CA	23	0.830	9.64	0.602	22,978	0.988
		38	0.809	5.76	0.684		
		48	0.719	4.71	0.764		

6.3 References

ASTM C1702-09a, Standard Test Method for Measurement of Heat of Hydration of Hydraulic Cementitious Materials Using Isothermal Conduction Calorimetry, ASTM International, West Conshohocken, PA, 2009

Bentz, D. P. (2010). “Powder Additions to Mitigate Retardation in High-Volume Fly Ash Mixtures.” *ACI Materials Journal*, 107(5), 508–514.

Berhane, Z. (1983). “Heat of hydration of cement pastes at different temperatures.” *Cement and Concrete Research*, 13(1), 114–118.

Bishop, M., and Barron, A. R. (2006). “Cement Hydration Inhibition with Sucrose, Tartaric Acid, and Lignosulfonate: Analytical and Spectroscopic Study.” *Industrial & Engineering Chemistry Research*, 45(21), 7042–7049.

Collepardi, M. M. (1995). “Water Reducers/Retarders.” *Concrete Admixtures Handbook: Properties, Science and Technology*, V. Ramachandran, ed., Noyes Publications, Park Ridge, NJ.

D’Aloia, L., and Chanvillard, G. (2002). “Determining the ‘apparent’ activation energy of concrete: Ea—numerical simulations of the heat of hydration of cement.” *Cement and Concrete Research*, 32(8), 1277–1289.

Dolch, W. L. (1995). “Air-Entraining Admixtures.” *Concrete Admixtures Handbook: Properties, Science and Technology*, V. S. Ramachandran, ed., Noyes Publications, Park Ridge, NJ, 518–557.

Kada-Benameur, H., Wirquin, E., and Duthoit, B. (2000). “Determination of apparent activation energy of concrete by isothermal calorimetry.” *Cement and Concrete Research*, 30(2), 301–305.

Kocaba, V. (2009). “Development and Evaluation of Methods to Follow Microstructural Development of Cementitious Systems Including Slags.” École Polytechnique Fédérale de Lausanne.

Lagier, F., and Kurtis, K. E. (2007). “Influence of Portland cement composition on early age reactions with metakaolin.” *Cement and Concrete Research*, 37(10), 1411–1417.

Lawrence, P., Cyr, M., and Ringot, E. (2003). “Mineral admixtures in mortars. Effect of inert materials on short-term hydration.” *Cement and Concrete Research*, 33(12), 1939–1947.

Lothenbach, B., Scrivener, K., and Hooton, R. D. (2011). “Supplementary cementitious materials.” *Cement and Concrete Research*, Elsevier Ltd, 41(12), 1244–1256.

Ma, W., Sample, D., Martin, R., and Brown, P. W. (1994). “Calorimetric Study of Cement Blends Containing Fly Ash, Silica Fume and Slag at Elevated Temperatures.” *Cement, Concrete, and Aggregates*, 16(2), 93–99.

Neville, A. M. (2006). *Properties of Concrete*. Pearson Education Limited, Harlow, England.

Odler, I. (1998). “Hydration, Setting and Hardening of Portland Cement.” *Lea’s Chemistry of Cement and Concrete*, P. C. Hewlett, ed., Arnold, New York, NY, 241–297.

Poole, J. J. L., Riding, K. A. K., Juenger, M. C. G., Folliard, K. J., and Schindler, A. K. (2011). “Effect of Chemical Admixtures on Apparent Activation Energy of Cementitious Systems.” *Journal of Materials in Civil Engineering*, 23(12), 1654–1662.

Poole, J. L. (2007). “Modeling Temperature Sensitivity and Heat Evolution of Concrete.” University of Texas at Austin.

Poole, J. L., Riding, K. A., Folliard, K. J., Juenger, M. C. G., and Schindler, A. K. (2007). “Methods for Calculating Activation Energy for Portland Cement.” *ACI Materials Journal*, 104(1), 303–311.

Quennoz, A., and Scrivener, K. L. (2013). “Interactions between alite and C3A-gypsum hydrations in model cements.” *Cement and Concrete Research*, Elsevier Ltd, 44, 46–54.

Ramachandran, V. (1995). “Accelerators.” *Concrete Admixtures Handbook: Properties, Science and Technology*, V. Ramachandran, ed., Noyes Publications, Park Ridge, NJ, 185–285.

Ramachandran, V., and Feldman, R. (1978). “Time-Dependent and Intrinsic Characteristics of Portland Cement Hydrated in the Presence of Calcium Chloride.” *Il Cemento*, 75(3), 311–322.

Sandberg, P., and Roberts, L. (2003). “Studies of cement-admixture interactions related to aluminate hydration control by isothermal calorimetry.” *Seventh CANMET/ACI International Conference on Superplasticizers and Other Chemical Admixtures in Concrete*, V. M. Malhotra, ed., American Concrete Institute, 529–542.

Schindler, A. (2004). “Effect of temperature on hydration of cementitious materials.” *ACI Materials Journal*, 101(1), 72–81.

Schindler, A. K., and Folliard, K. J. (2005). “Heat of hydration models for cementitious materials.” *ACI Materials Journal*, 102(1), 24–33.

Schindler, A. K. (2002). “Concrete Hydration , Temperature Development, and Setting at Early-Ages.” University of Texas at Austin.

Scrivener, K. L., and Nonat, A. (2011). “Hydration of cementitious materials, present and future.” *Cement and Concrete Research*, Elsevier Ltd, 41(7), 651–665.

Taylor, H. F. W. (1997). *Cement Chemistry*. Thomas Telford Publishing, London, UK.

Tenoutasse, N. (1968). "The Hydration Mechanism of C3A and C3S in the Presence of Calcium Chloride and Calcium Sulphate." *V International Symposium of Chemistry of Cement*, Tokyo, 372–378.

Xiong, X., and van Breugel, K. (2001). "Isothermal calorimetry study of blended cements and its application in numerical simulations." *Heron*, 46(3), 151–160.

Xu, Q., Hu, J., Ruiz, J. M., Wang, K., and Ge, Z. (2010). "Isothermal calorimetry tests and modeling of cement hydration parameters." Thermochimica Acta, 499(1-2), 91–99.

CHAPTER 7 Laboratory Tests for Cracking Potential Sensitivity-Semi-Adiabatic Calorimetry

7.1 Introduction

The hydration of cementitious materials is an exothermic process that encompasses chemical and physical reactions between cement and water (Poole 2007; Poole et al. 2007; Riding et al. 2012). These reactions are accelerated by higher temperatures, which cause an increase in the rate at which heat is produced, further increasing the temperature of the concrete (Juenger et al. 2007). The heat generated by the cementitious materials influences several aspects of concrete such as thermal stresses and strength gain, especially during the early ages. Furthermore, the type and amount of cementitious materials and environmental conditions are among the driving forces that control the mixture's behavior and performance. In order to model the early-age concrete repair slab stress development, the heat generation characteristics of the mixture must be quantified, including the rate and amount of heat released during hydration. The HIPERPAV (The Transtec Group 2009) and ConcreteWorks (Concrete Durability Center 2007) software packages quantify the mixture heat generation characteristics through the α_u, β, and τ coefficients described in Equation 2-14.

Adiabatic and semi-adiabatic calorimetry systems have been developed to assess the heat generated in concrete mixtures. The latter is a more economical and practical alternative in determining the adiabatic temperature development of concrete mixtures. Adiabatic calorimetry requires an adiabatic process in which no heat is gained or lost to the system's surroundings. The adiabatic temperature rise provides the basis for simulating temperature development in a concrete member during hardening. RILEM defines an adiabatic calorimeter as a "calorimeter in which the temperature loss of the sample is not greater than 0.02 K/h", while a semi-adiabatic calorimeter is defined as one where "heat losses are less than 100 J/(h·K)"(Springenschmid and Morabito 1998). Because of the difficulty and the expensive equipment needed to eliminate heat gain or loss in an adiabatic calorimetry test, semi-adiabatic testing was developed to estimate the adiabatic heat generated by a mixture. Due to the inherent hydration characteristics of the constituents of the concrete mixture, other physical and chemical properties of the mixture are used to estimate the adiabatic temperature rise from the measured heat rise and heat loss from the semi-adiabatic tests.

The heat loss of semi-adiabatic calorimetry is minimized with the use of insulation, rather than preventing any net heat loss from the concrete specimen such as with adiabatic calorimetry (Poole and Riding 2009). By measuring the heat loss and the concrete measured temperature during semi-adiabatic calorimetry, the adiabatic temperature of the specimen can be calculated. However, in an adiabatic system, the heat lost from the semi-adiabatic test would have contributed to a higher temperature and therefore, a higher rate of hydration. As a result, a model is used to predict the semi-adiabatic temperature curve from an assumed adiabatic temperature rise and the measured heat loss. The true adiabatic temperature is then estimated by changing the assumed adiabatic temperature rise until the calculated semi-adiabatic temperature profile matches the measured semi-adiabatic temperature profile. Currently, there is no standard testing methodology established for semi-adiabatic testing. As a result, this study follows the guidelines outlined in prominent literature (Poole et al. 2007).

7.2 Methodology

Three semi-adiabatic calorimetric runs were conducted for each concrete mixture, to verify the consistency of the testing method and accuracy of the reported values. There was an exception for the mixture containing the JAX cement due to the limited supply of the as-received cement. A total of 6 different concrete mixtures were prepared for this portion of the study with the primary goal of assessing the effects of dosage of a chloride-based accelerator on the cracking potential of concrete pavement slabs.

Semi-adiabatic calorimetry measurements were conducted using equipment constructed at the University of South Florida. A schematic diagram showing the details of the unit is presented in Figure 7-1. The details of the construction steps are provided in Appendix C.

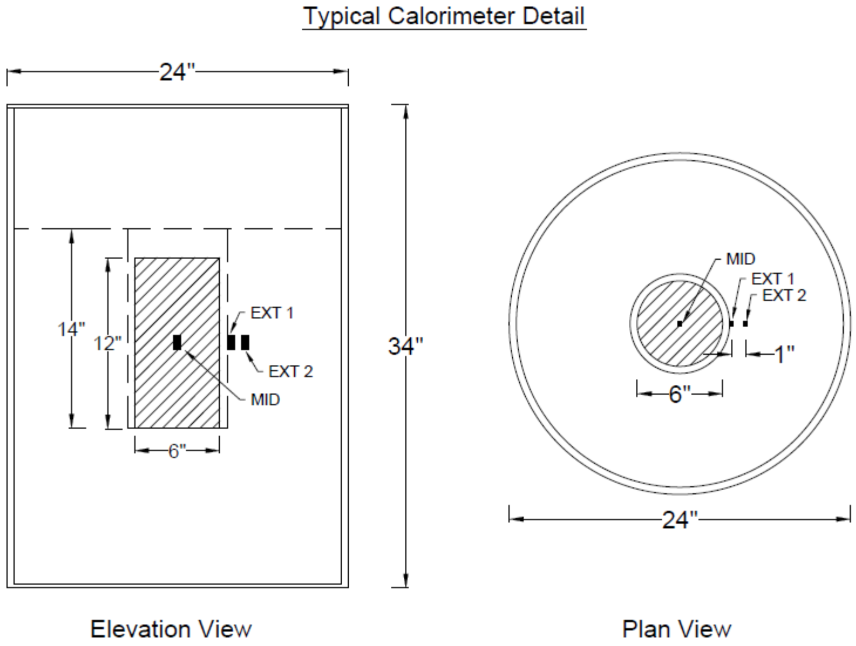

Figure 7-1: Semi-adiabatic calorimeter detail

Type T thermocouples were used to measure the temperature at the center of the concrete specimen and at two specific locations within the insulation. The center thermocouple (MID) was placed 6 inches into the center of the fresh concrete. A plug-in for this thermocouple is available at the edge of the opening as seen in Figure 7-2. A second thermocouple (EXT 1) was attached at the inner edge of the insulation, just outside of the cylindrical void. A third thermocouple (EXT 2) was embedded in the insulation 1 inch away from second thermocouple. Since the thickness of material and temperature of each thermocouple can be measured at specific locations, the insulating properties of the calorimeter can be determined through a calibration process. After initial testing, it was assessed that the heat loss between the second and third thermocouple produced more consistent test results. For this reason, the heat flux between these thermocouples was used for the calculations.

Figure 7-2: Middle thermocouple placed and plugged in

Pico Technology hardware and software was used to record and collect the temperatures. USB TC-08 thermocouple data logger was used to record the temperatures at each calorimeter and the room temperature with an accuracy of ±0.5°C. Temperature measurements from the thermocouples were recorded for a minimum of 160 hours after the concrete was initially placed.

Obtaining the adiabatic temperature rise for a concrete mixture involved calibration of the semi-adiabatic calorimeter, determining mixture temperature sensitivity through isothermal calorimetry, preparing each concrete mixture for testing, and analyzing the data collected during the test. Since no standard of testing is currently available, the steps outlined in the "Hydration Study of Cementitious Materials using Semi-Adiabatic Calorimetry" by Poole et al. were followed closely to determine the adiabatic temperature rise. The following 14 steps were taken to determine the adiabatic temperature rise of each mixture (Poole et al. 2007):

1. A calibration test was performed on the semi-adiabatic calorimeters to determine the specific calibration factors. Calibration of the semi-adiabatic calorimeter was an important step in obtaining the adiabatic temperature rise of the concrete mixture as it provided a means to measure the heat loss by the instrument during testing. The calibration protocol described in (Poole et al. 2007) was used for the calorimeters, and the rate of heat loss, was computed. De-ionized water was used in calibrating the calorimeters since it has a known density of 1,000 kg/m^3 and a known specific heat of 4,186 J/ (kg·°C). It is preferable to heat the water sample to the potential temperature of the concrete structure's environmental surroundings; therefore, the water sample in this study was heated to 80°C and put into a

6”x 12” cylindrical mold. The cylinder was weighed before and after filling it with the heated water, and then placed into the calorimeter. The following steps (A-D) were then used to calculate the calibration factors (C_{f1}, C_{f2}):

A. Record the time (t in hr), water temperature (T_w in °C), and temperature difference between the two external thermocouples (T_d in °C) at 5 minute intervals for 160 hours. The first 5 hours of data were not used since the interior of the calorimeter had to first stabilize with the higher temperature of the test specimen.

B. Calculate the change in temperature of the water (ΔT_w) at each time, t, and record the sum of the changes in temperature ($\Sigma\Delta T_w$).

C. Model the change in temperature of the water using its known density, ρ_w, and specific heat of water, $C_{p,w}$, with the calibration factors (C_{f1} and C_{f2}) using Equations 7-1 and 7-2:

$$\Delta q_h = T_d \cdot (-C_{f1} \cdot \ln(t) + C_{f2}) \qquad \text{Equation 7-1}$$

where

Δq_h = heat transfer (J/h·m^3),

T_d = temperature difference between thermocouples Ext 1 and Ext 2,

C_{f1} = Calibration factor (W/°C),

C_{f2} = Calibration factor (W/°C), and

t = time elapsed from start of test (hr)

$$\sum \Delta T_w{}^* = \sum \frac{\Delta q_h \cdot \Delta t}{\rho_w \cdot C_{p,w} \cdot V_w} \qquad \text{Equation 7-2}$$

where

$\Sigma\Delta T_w^*$ = the sum of the modeled changes in water temperature (°C),

ρ_w = density of water (1000 kg/m^3),

$C_{p,w}$ = specific heat of water (4,186 J/ kg·°C),

V_w = volume of water sample (m^3), and

Δt = time step (s).

D. Perform a regression analysis using the R-squared method with the Solver function in MS Excel to match the modeled change in water temperature to the measured change in water temperature. The Solver function generates the best fit calibration factors (C_{f1} and C_{f2}) which are used to model the change in water temperature.

2. Place the concrete mixture in the mold and weigh the mold. Place the concrete in the calorimeter and record the concrete temperature, time, and heat flux every 5 minutes for the first 160 hours.

3. Determine the heat-based activation energy (E_a) through isothermal calorimetry using the internal mixing protocol (Poole et al. 2007).

4. As part of the iterative method to estimate the true adiabatic temperature of the mixtures, the equivalent age (t_e) needs to be calculated. The equivalent age is computed according to Equation 2-6 using the mixture activation energy (E_a) and Equation 2 in ASTM C1074.

5. Calculate the degree of hydration using the equivalent age of the mixture and the hydration parameters – α_u, β, and τ.

   The three-parameter exponential function, Equation 2-10, was first introduced by Freiesleben Hansen and Pedersen in 1985 to represent the heat development of concrete (Freiesleben Hansen and Pedersen 1985). Pane and Hansen later showed in 2002 the relation between degree of hydration and time can be modeled as Equation 2-10 (Pane and Hansen 2002).

6. Calculate the heat evolved at each time step using the hydration parameters according to (Poole et al. 2007) and the ultimate heat of hydration.

   The total heat of hydration from cement (H_{cem}) at a degree of hydration of 1, is calculated by using the phase compositions from Rietveld refinement and Equation 2-13 (Schindler and Folliard 2005).

   The ultimate heat of hydration (H_u) is the sum of the total heat of hydration from cement along with the total heat of hydration from supplementary cementitious materials (SCMs). Since no SCMs were used in this testing, H_u=H_{cem}. For the cements used here, the ultimate heat of hydration for SW and JAX is 481.8 and 464.9 kJ/kg, respectively.

   The heat evolved was quantified using Equation 2-14 (Schindler and Folliard 2005).

7. Determine the specific heat of the mixture:
   The specific heat of concrete, which is used to determine the change in temperature, was then calculated using Equation 2-17 (Poole 2007).

8. The concrete temperature rise from the heat generation calculated in Equation 2-6 and the specific heat of the concrete at that time step was calculated using Equation 2-17.

9. Start from the original concrete temperature and sum up the change in temperature at each time step as shown in Equation 7-2. The resulting temperature is the "false" adiabatic temperature (T_{adia}*). This temperature does not take into account the heating/hydrating process of the concrete and therefore is lower than the "true" adiabatic temperature; however, it is important as it is used to model the temperature in the concrete cylinder in the semi-adiabatic calorimeter.

$$T_{adia}{}^{*} = T_c + \Delta T \qquad \text{Equation 7-3}$$

10. Account for the losses measured during testing.

Use Equation 7-1 to account for the heat transfer (Δq_h) from the concrete using the temperature differential between the external thermocouples and the calibration factors determined in Step 1. Similar to Equation 7-2, the ΔT_L for the concrete specimen can be calculated using Equation 7-4.

$$\Delta T_L = \frac{\Delta q_h \cdot \Delta t}{\rho_c \cdot C_{p,c} \cdot V_c} \qquad \text{Equation 7-4}$$

where

ΔT_L = change in concrete temperature from losses (°C),
ρ_c = density of concrete mixture (kg/m^3),
$C_{p,c}$ = specific heat of concrete mixture (J/ kg·°C),
V_c = volume of concrete sample (m^3), and
Δt = time step (s)

11. Sum the change in temperature from losses at each time step. Then subtract the sum of the changes in temperature from losses at each time step from the false adiabatic temperature to determine the modeled semi-adiabatic concrete temperature (T_c*) shown in Equation 7-5.

$$T_c{}^* = T_{adia}{}^* - \sum \Delta T_L \qquad \text{Equation 7-5}$$

12. Repeat steps 4-11 for each time step. This modeled semi-adiabatic concrete temperature (T_c*) can now be compared to the actual concrete temperature (T_c) over the entire test period.

13. Use the coefficient of determination (R^2) calculated by comparing the measured concrete cylinder temperature (T_c) to the modeled concrete cylinder temperature (T_c*) for the assumed α_u, β, and τ values to fit these two temperature developments through fitting.

This is an iterative process and is best performed using an automated solver algorithm.

The Solver function in MS Excel was therefore used to determine the best-fit hydration parameters for this comparison. The measured semi-adiabatic concrete temperature can then be plotted versus the modeled semi-adiabatic concrete temperature for each mixture.

14. The "true" adiabatic temperature (T_{adia}) can now be modeled using the best-fit hydration parameters found in Step 13.

    A time step of 0.1 hr for the first 25 hr, then a step of 2.5 hr afterwards was used. The initial concrete temperature was used for the first step, and then steps 4-9 were repeated for each time step. The concrete adiabatic temperature from the previous time step was used as the concrete temperature in step 4, instead of the measured semi-adiabatic concrete sample temperature (Tc). In step 9, the concrete temperature from the previous time step was used to produce the "true" adiabatic temperature rise as seen in Equation 7-3. It is important to note that the "true" adiabatic temperature should be higher than the "false" adiabatic temperature since the higher hydration rate from the higher adiabatic temperature during curing is accounted for.

7.3 Results and Discussion

Six concrete mixtures were analyzed for semi-adiabatic testing. Five of the mixtures used the same cement, SW, and were modifications of one FDOT concrete mix design, while the sixth mixture used JAX cement and was based on an FDOT mix design used on a Jacksonville slab replacement project. The concrete mixtures used in semi-adiabatic calorimetry were proportioned identically to the mix designs shown in Table 7-1.

The five SW mixtures were tested to observe the effects of variable dosages of a chloride-based accelerator on the adiabatic temperature rise. To compensate for the water content of the accelerator, the amount of water added was adjusted to maintain a constant water-to-cement ratio throughout all of the SW mixtures. Table 7-1 shows the concrete mixture designs per cubic yard for each SW mixture and the JAX mixture.

Table 7-1: Mixtures design

Mix Weight per yd^3						
Mixture Name	**SW-C**	**SW-CNA**	**SW-CHA**	**SW-CA**	**SW-CDA**	**JAX-CA**
Materials	Wt. (lb)	Wt. (lb)	Wt. (lb)	Wt. (lb)	Wt. (lb)	Wt. (lb)
Cement	900	900	900	900	900	845
Coarse Agg (SSD)	1680	1680	1680	1680	1680	1611
Fine Agg (SSD)	828	828	828	828	828	1079
AEA	-	0.195	0.195	0.195	0.195	0.488
Type A and D	-	3.367	3.367	3.367	3.367	2.063
Type E	-	-	16.801	33.602	67.203	58.798
Type A and F	-	-	-	-	-	1.309
Mix Water	348	348	338	328	307	239
w/c	0.384	0.384	0.384	0.384	0.384	0.310

One-cubic-foot batches of the five SW mixes were made for the semi-adiabatic calorimetry. For each mixture, the air content was measured by the pressure method according to ASTM C231, and the unit weight was determined by weighing a sample in a container of known weight and volume following ASTM C138. Three 6”x12” concrete cylinder samples were made for semi-adiabatic calorimetry for each mixture, except for the JAX mix, due to the limited amount of JAX cement available. For that mixture, a 0.41-cubic-foot batch was mixed for one 6”x12” cylinder. The volumetric method ASTM C173 was chosen over the pressure method to determine the air content for the JAX mixture since it used less material.

Following calorimeter construction, each semi-adiabatic calorimeter had to be calibrated first to determine the calibration factors that make it possible to establish the baseline of the instrument’s heat loss potential, and subsequent determination of the adiabatic temperature rise of concrete mixtures. The best-fit calibration factors are presented in Table 7-2. Figure 7-3 shows a typical plot of the measured versus modeled temperature losses as determined from the calibration protocol implemented in this study and discussed previously. For the curing timeframe investigated, the data indicate that the measured and modeled temperature losses are in reasonable agreement.

Table 7-2: Calibration factors

Calibration Factors		
Calorimeter	**C_{f1}**	**C_{f2}**
1	0.1104	1.5188
2	0.0356	1.3261
3	0.0395	0.5808

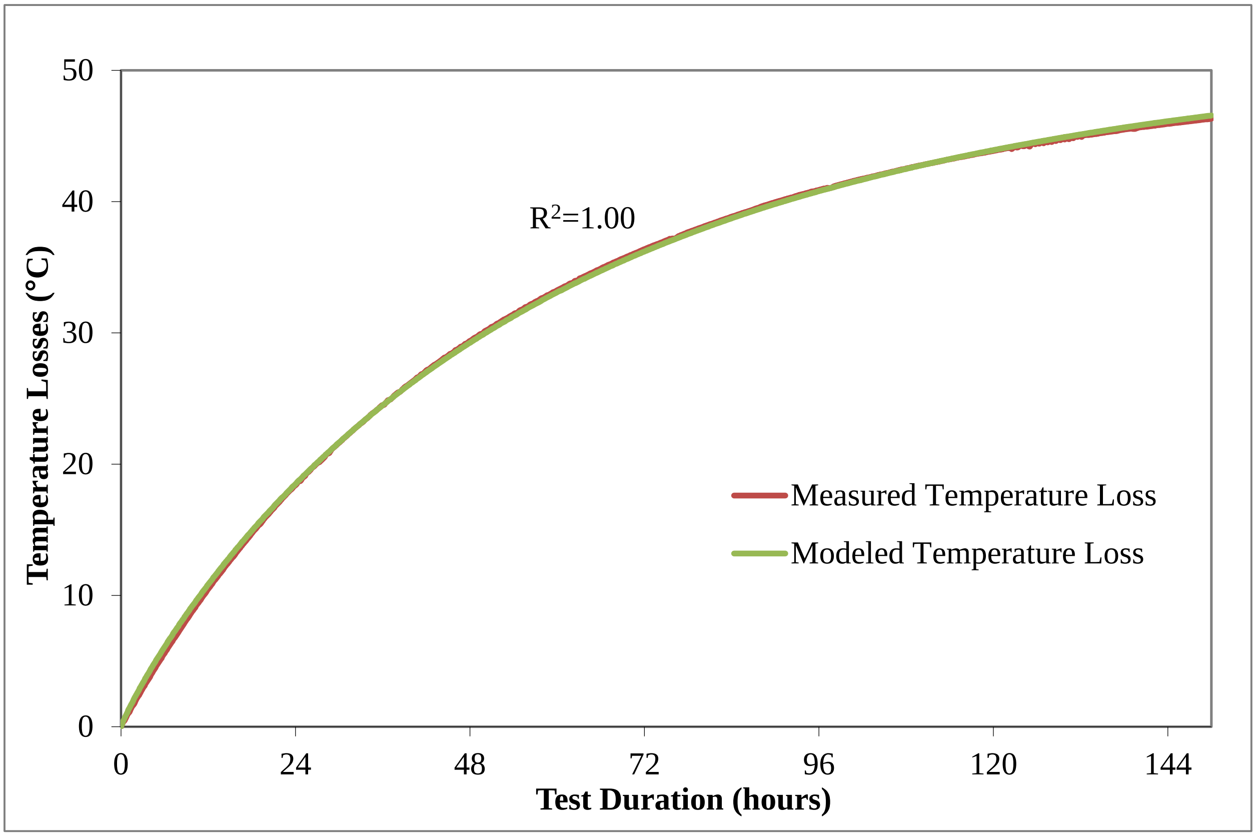

Figure 7-3: Semi-adiabatic calorimeter water calibration for temperature loss

Results for semi-adiabatic measurements for all concrete mixtures are presented in Figures 7-4 through 7-9, where it can be seen that increasing the accelerator dose increased the peak height and shifted the maximum peak to an earlier time, consistent with expected effects of a chloride-based accelerator. Figures 7-10 through 7-15 show the measured temperature differential between the thermocouples EXT 1 and EXT 2 for each mixture. This temperature differential (T_d) is very important as it is ultimately used to calculate the change in temperature due to the loss of heat (Step 10 of procedure for determining the adiabatic temperature profile).

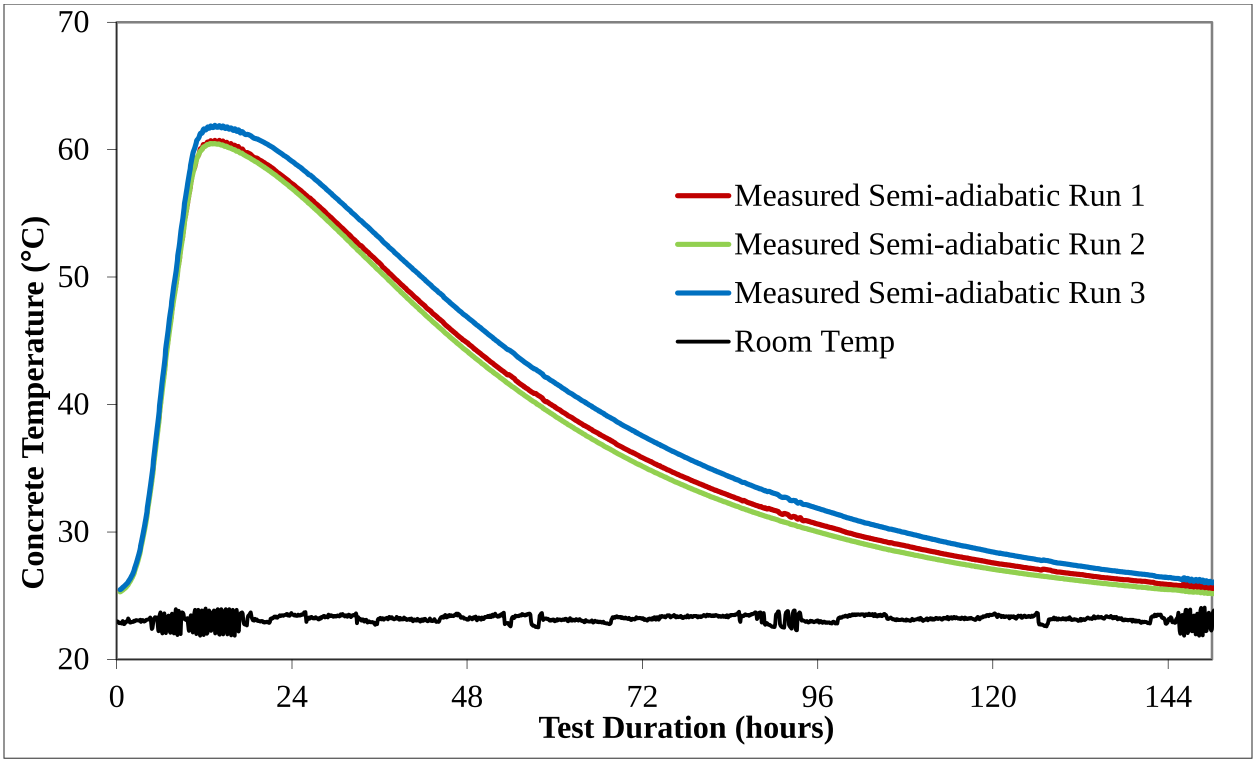

Figure 7-4: Measured semi-adiabatic temperature SW-C mix

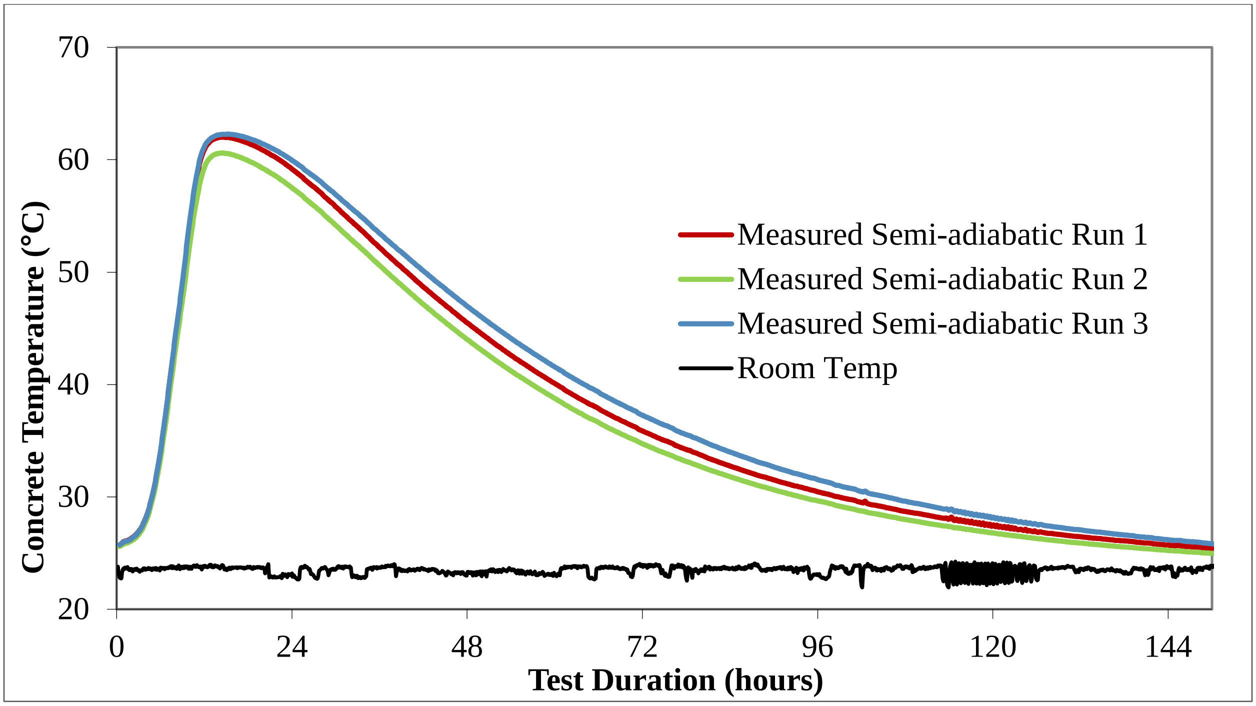

Figure 7-5: Measured semi-adiabatic temperature SW-CNA mix

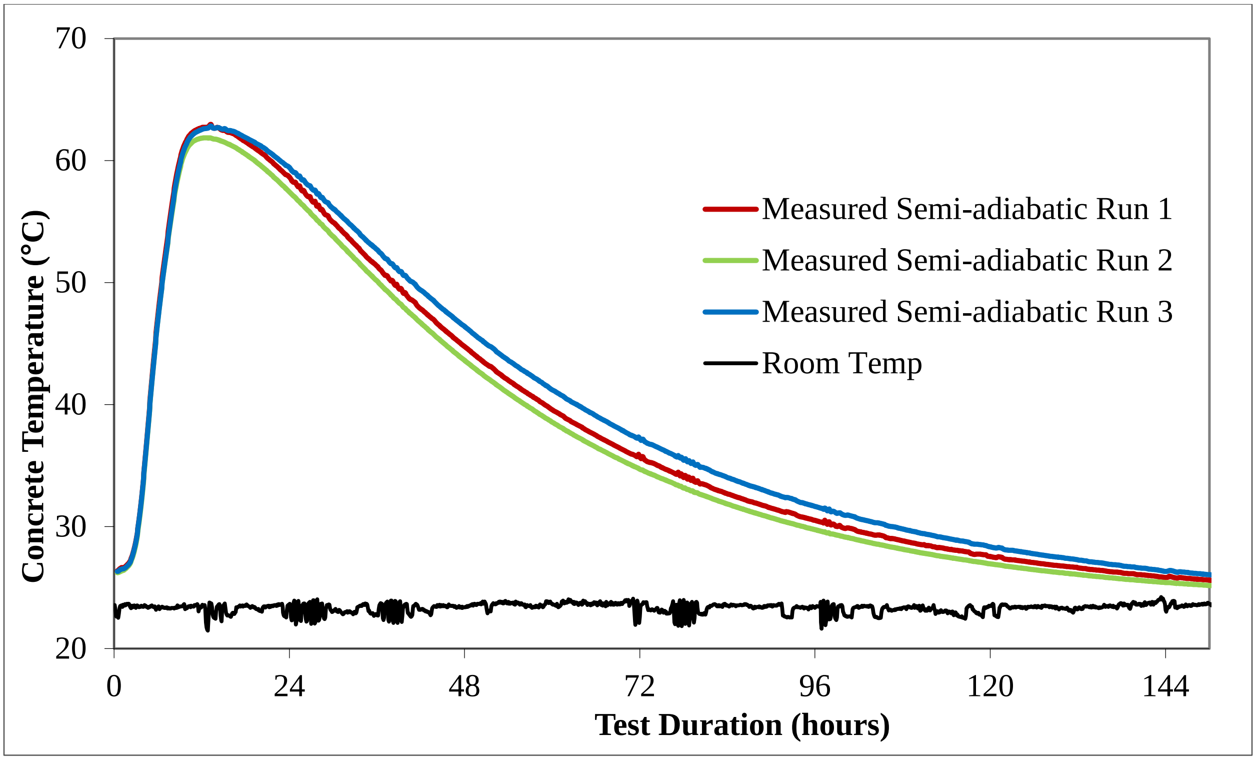

Figure 7-6: Measured semi-adiabatic temperature SW-CHA mix

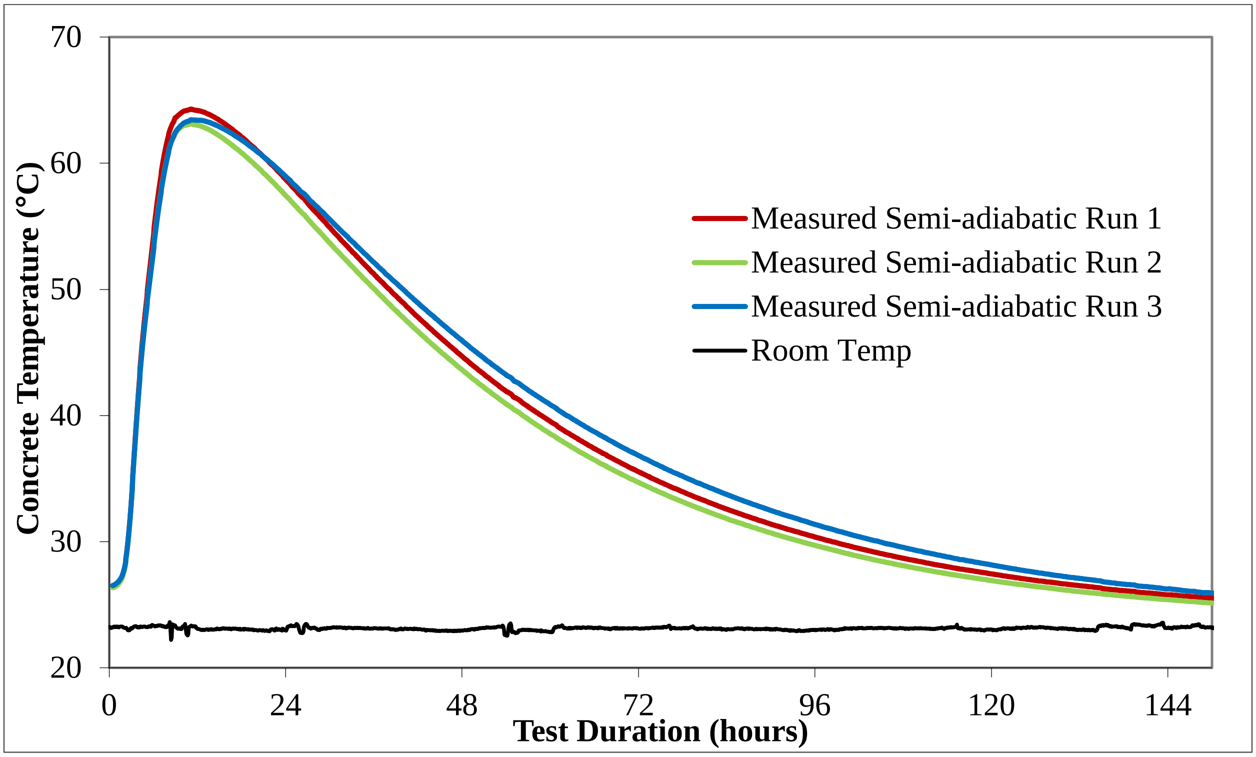

Figure 7-7: Measured semi-adiabatic temperature SW-CA mix

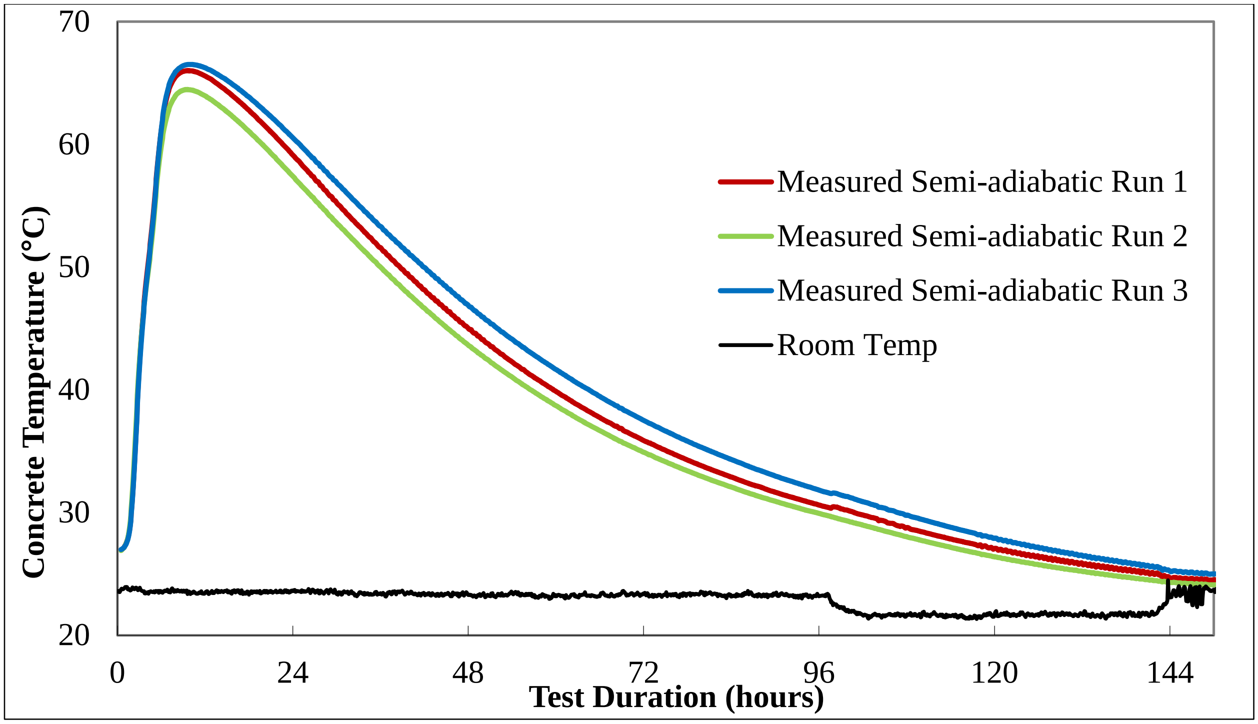

Figure 7-8: Measured semi-adiabatic temperature SW-CDA mix

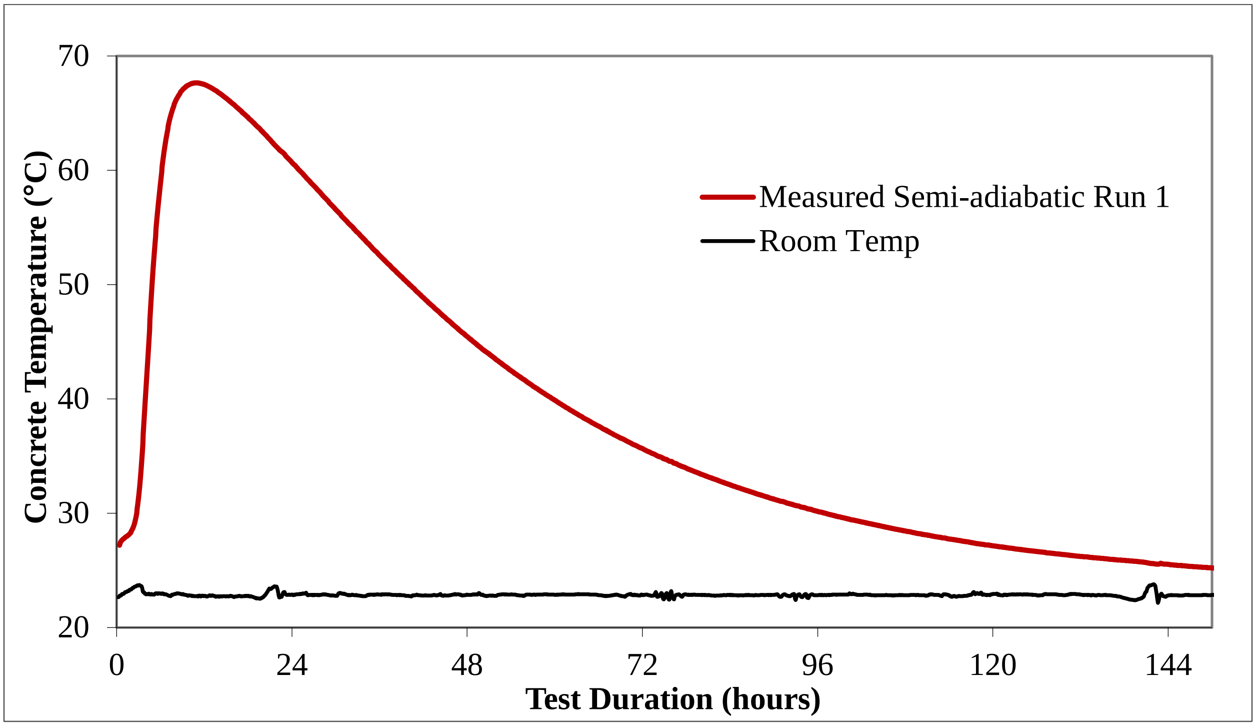

Figure 7-9: Measured semi-adiabatic temperature for JAX-CA mix

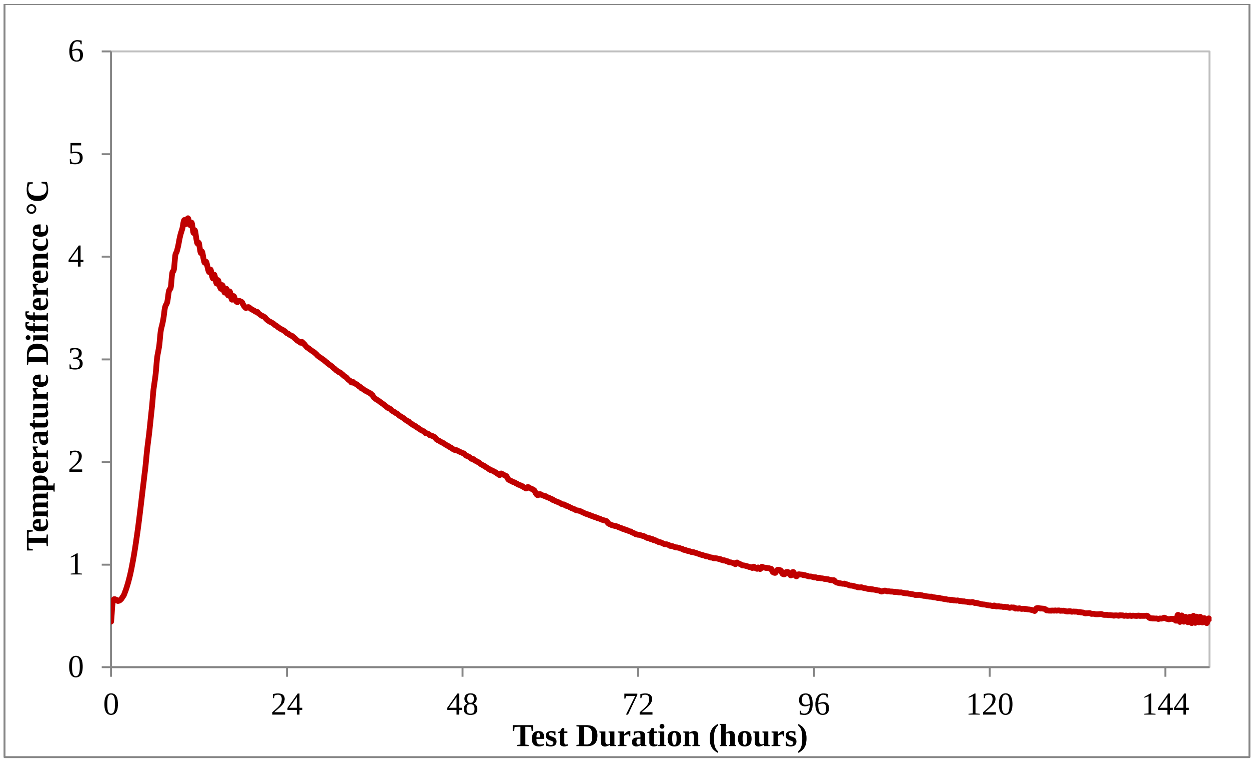

Figure 7-10: Temperature differential of SW-C mix

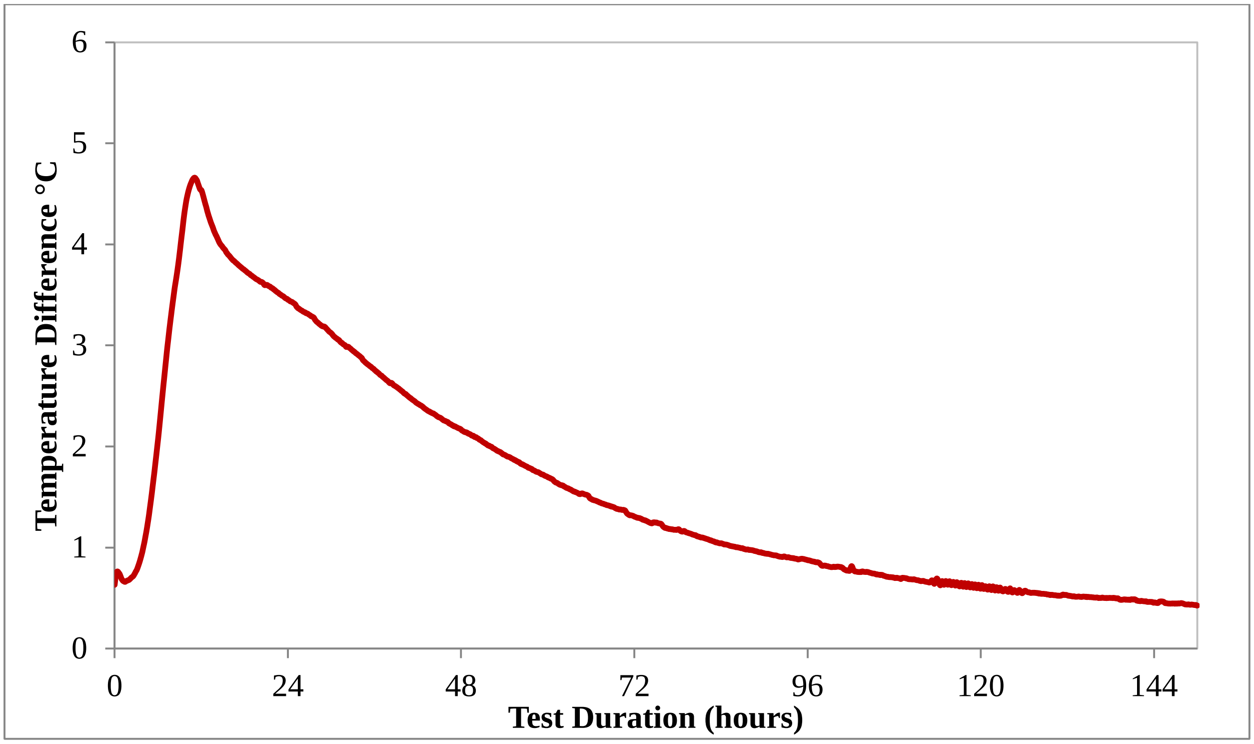

Figure 7-11: Temperature differential of SW-CNA mix

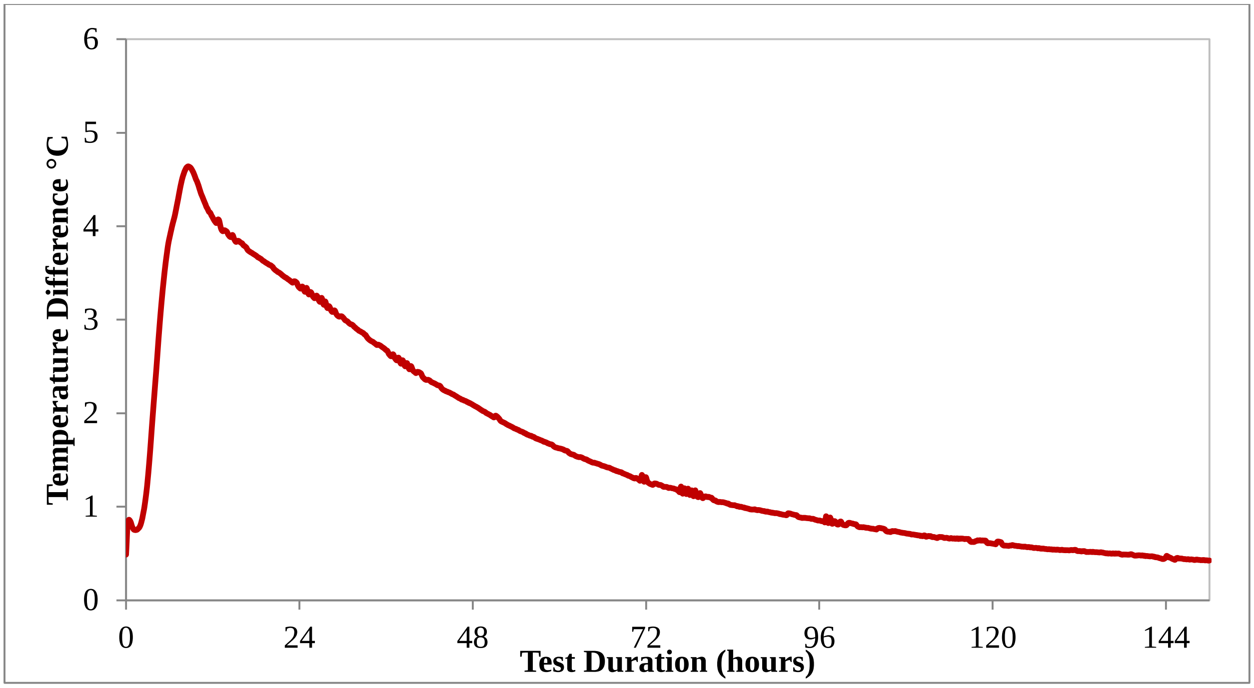

Figure 7-12: Temperature differential of SW-CHA mix

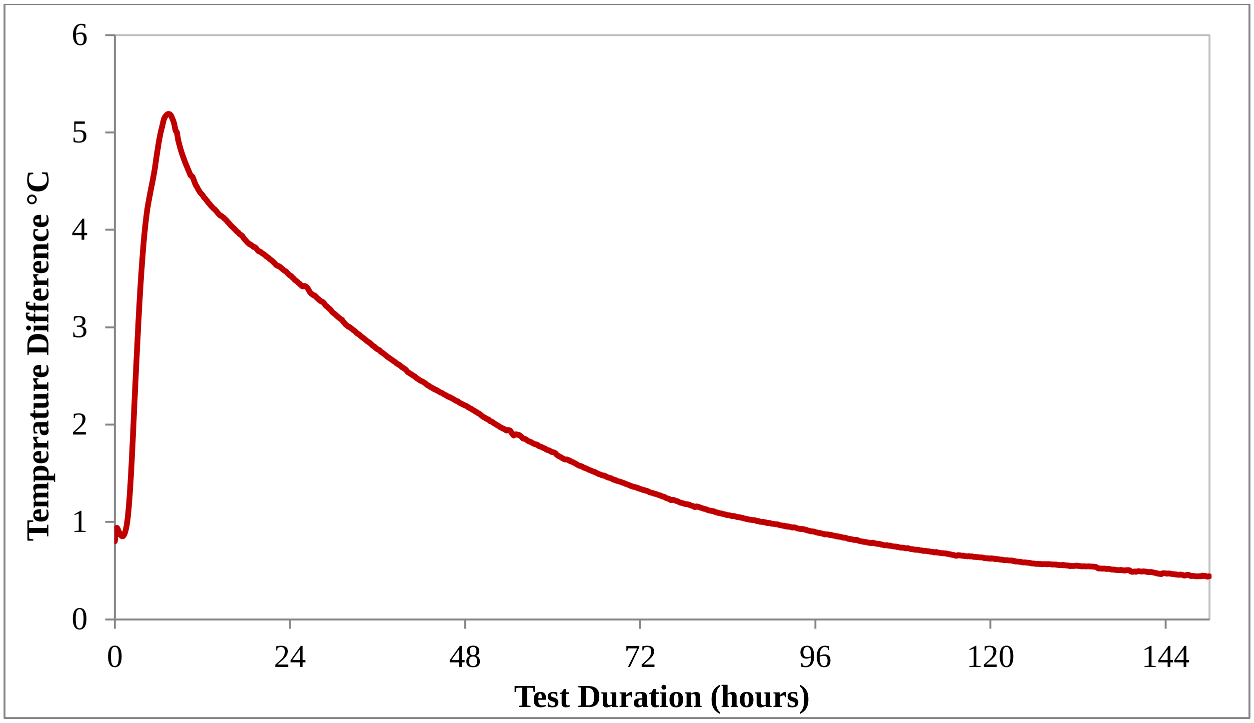

Figure 7-13: Temperature differential of SW-CA mix

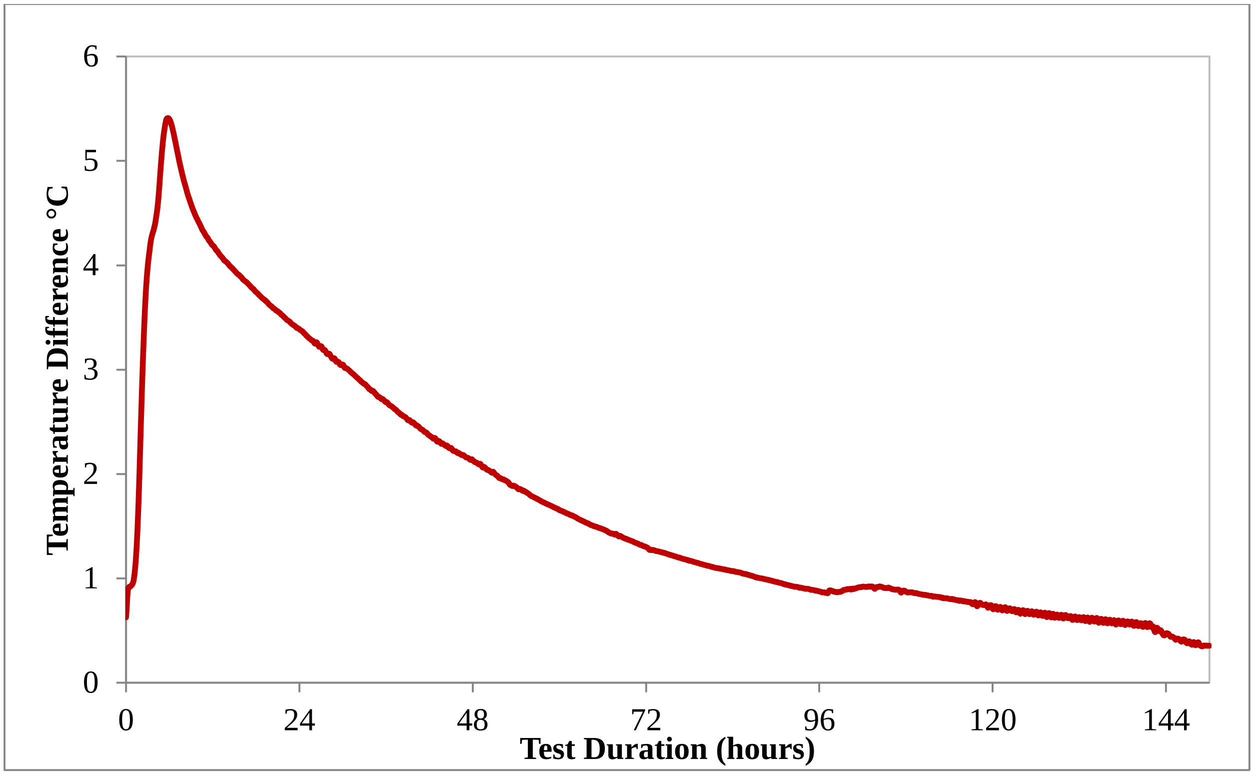

Figure 7-14: Temperature differential of SW-CDA mix

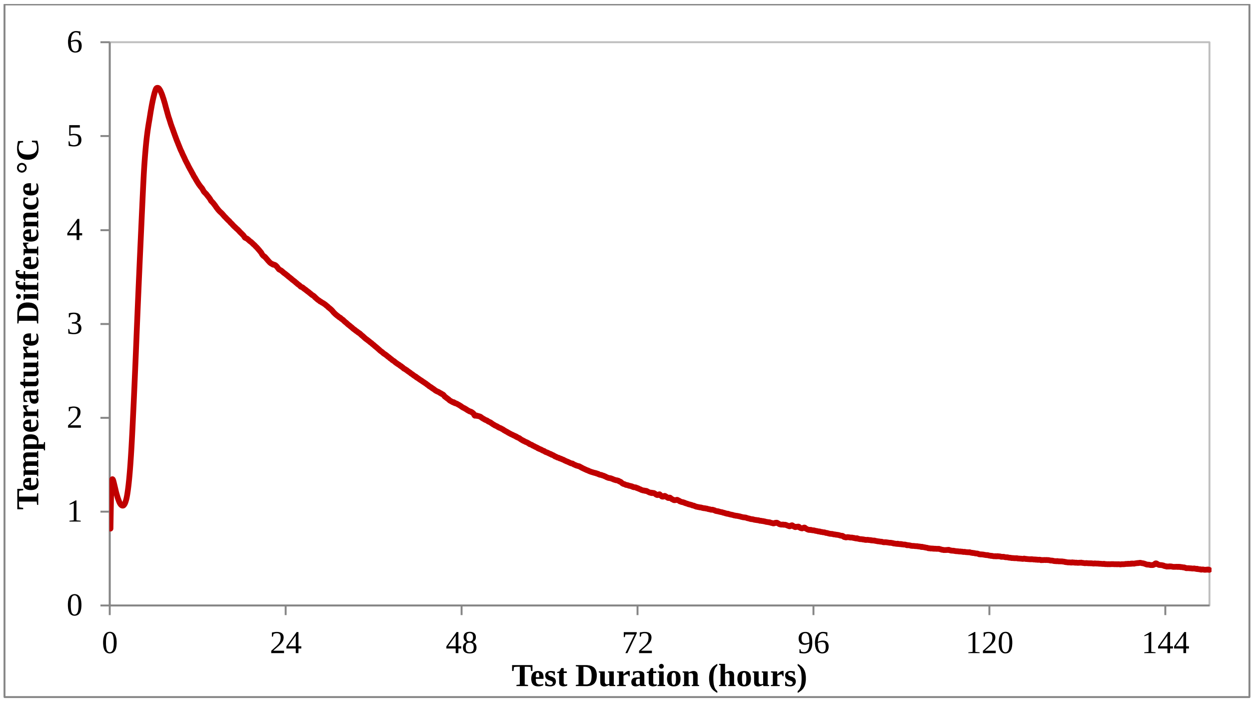

Figure 7-15: Temperature differential of JAX-CA mix

Activation energy values, determined from previous isothermal calorimetry work, Table 7-3, were used to calculate the equivalent age. The hydration parameters α_u, β, and τ, Table 7-4, were determined using the iterative process described in the methodology section. The effects of these hydration parameters on the degree of hydration are presented in Figures 7-16 through 7-18. The lowest and highest parameters from the SW mixtures were used along with the middle parameter value from SW-CA to show these trends. The higher α_u, simply shifts the curve up, while a higher β value indicates a higher slope in the hydration curve and a higher τ value shifts the hydration curve to longer times.

Table 7-3: Activation energy from isothermal testing

Mixture	**SW-C**	**SW-CNA**	**SW-CHA**	**SW-CA**	**SW-CDA**	**JAX-CA**
Activation Energy (J/mol)	33,004	30,784	24,148	25,420	25,574	22,978

Table 7-4: Semi-adiabatic hydration parameters

Average Semi-Adiabatic Parameters	**Mix**					
	SW-C	**SW-CNA**	**SW-CHA**	**SW-CA**	**SW-CDA**	**JAX-CA**
β =	0.836	1.111	0.944	0.825	0.743	1.072
τ (hrs)=	11.596	11.567	8.759	7.938	6.783	7.000
α_u=	0.741	0.685	0.725	0.746	0.772	0.737

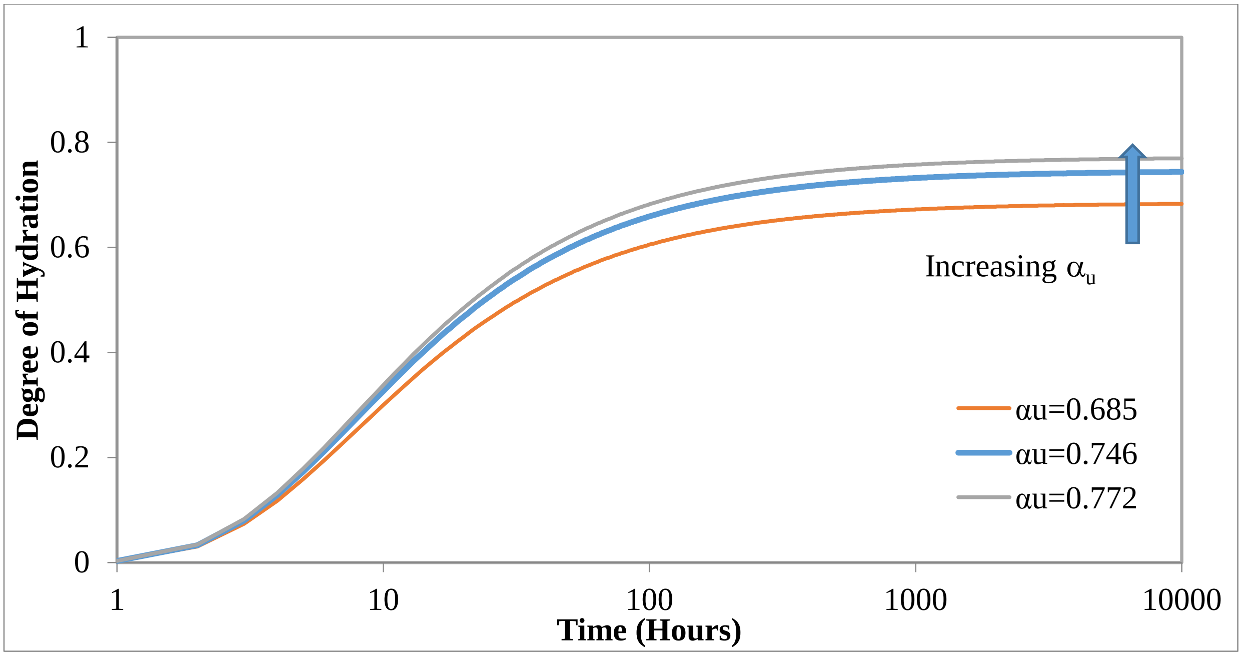

Figure 7-16: Influence of α_u on hydration

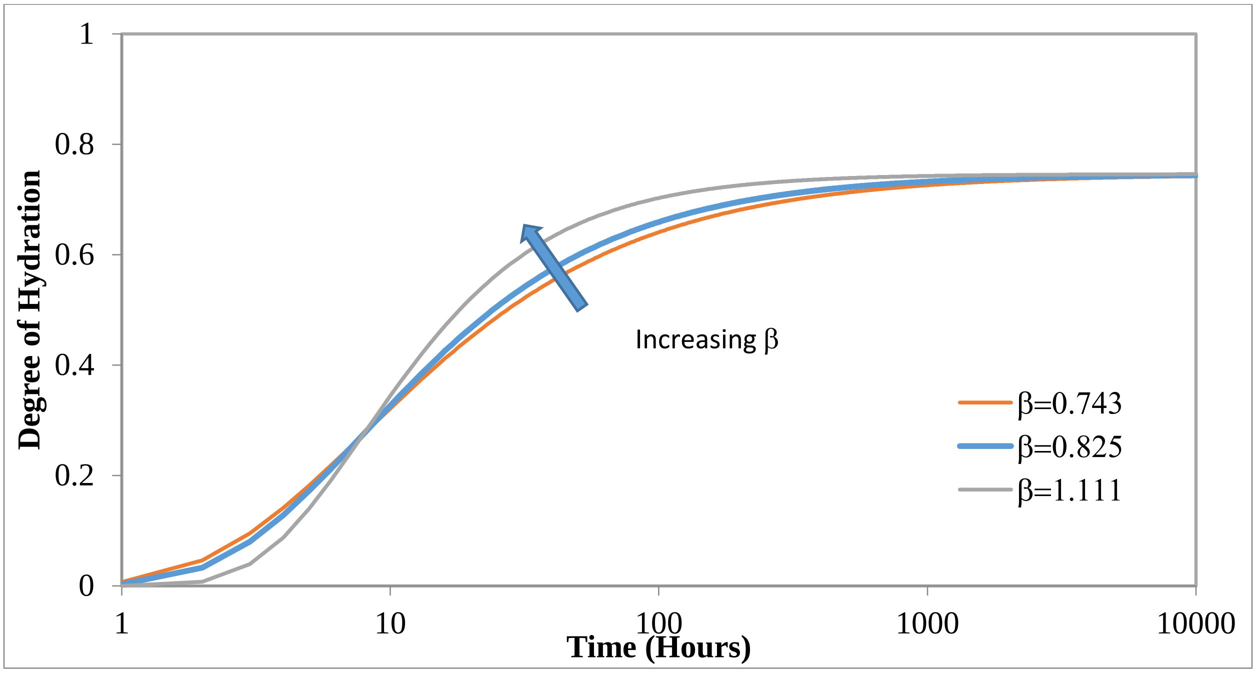

Figure 7-17: Influence of β on hydration

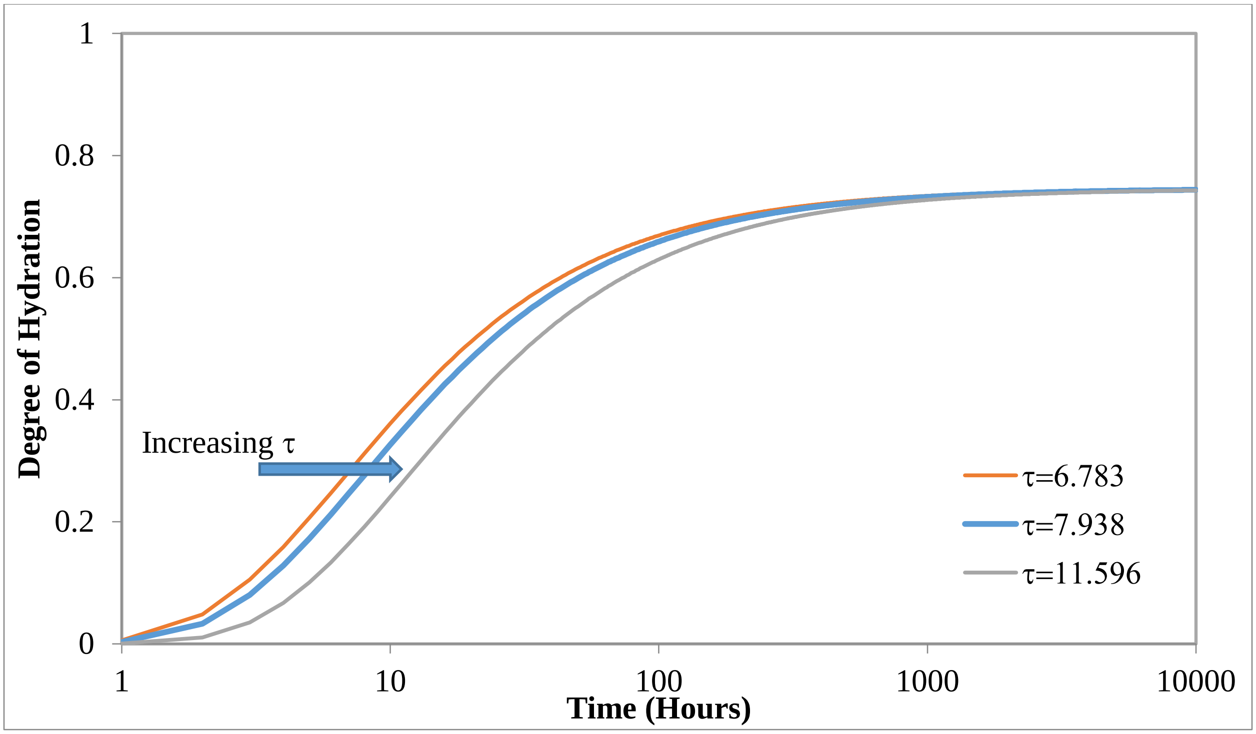

Figure 7-18: Influence of τ on hydration

The results displayed in Figures 7-19 and 7-20 indicate that increasing the accelerator dosage increased α_u. There was a decreasing trend in the shape parameter, β, with an increase in the accelerator dose. It is important, however, to keep in mind that it is the combination of α, τ, and β values that determines the rate of hydration. Thus, the effect of the admixture on one curve fit parameter cannot be viewed in isolation. The time parameter, τ, also has a downward trend with increasing the accelerator dosage as seen in Figure 7-20. A decrease in τ shifts the hydration curve to the left. This indicates that hydration occurs at an earlier time as the accelerator dosage is increased. This trend is expected since accelerators are used to increase early strength and decrease setting time.

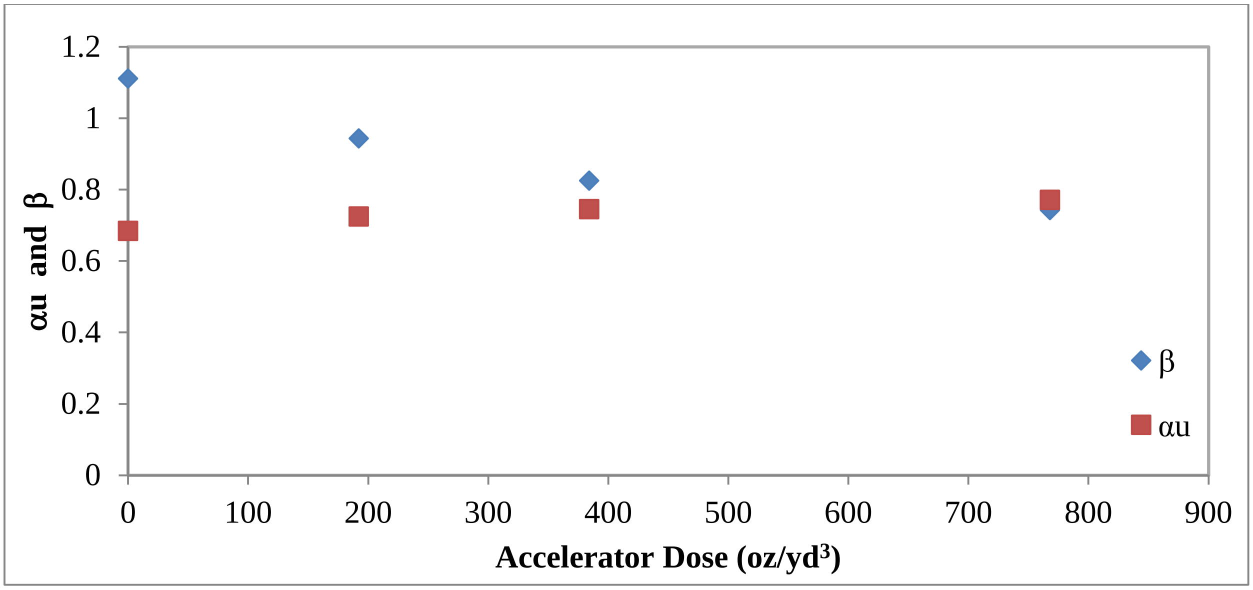

Figure 7-19: Effect of dosage of accelerator on α_u and β

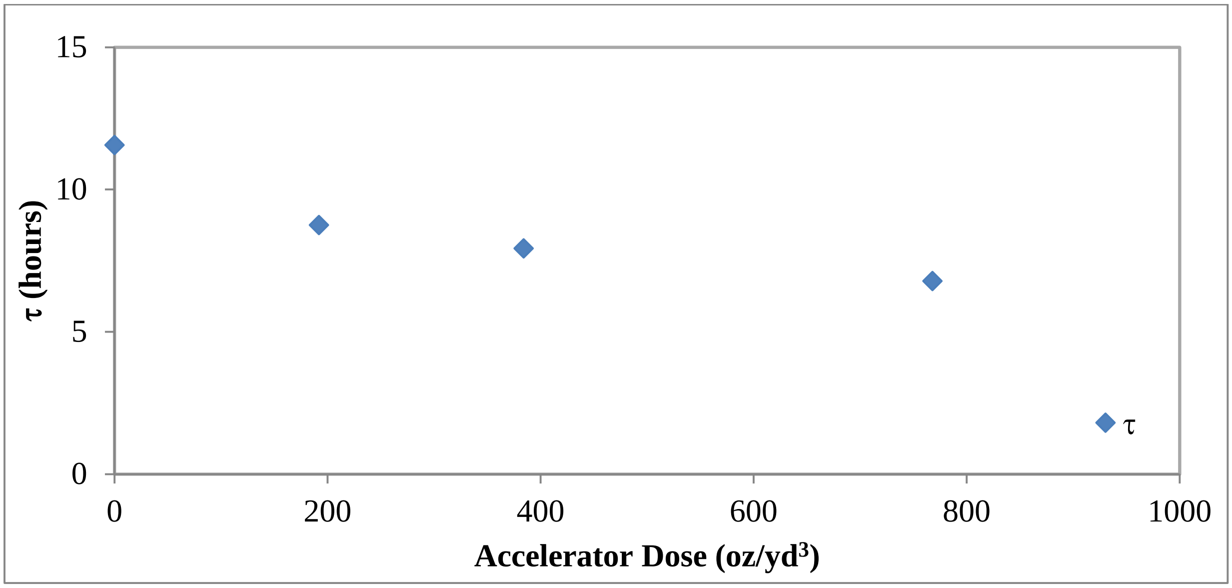

Figure 7-20: Effect of accelerator dose on the hydration parameter (τ)

The hydration parameters were used to determine the best-fit curve to model the experimentally measured semi-adiabatic temperature. The measured semi-adiabatic concrete temperature and the modeled semi-adiabatic temperature for each mixture are depicted in Figures 7-21 through 7-26 where it can be seen that the measured and modeled curves show excellent agreement.

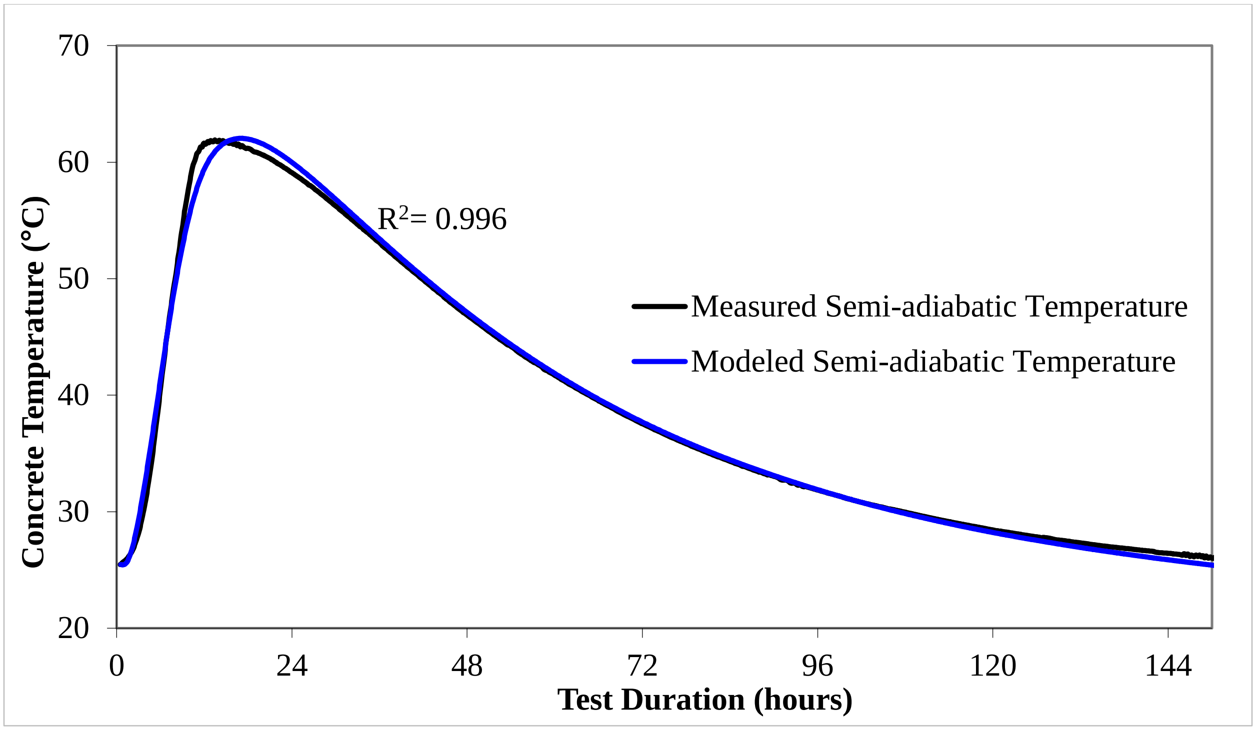

Figure 7-21: Measured vs. modeled semi-adiabatic temperature for SW-C mix

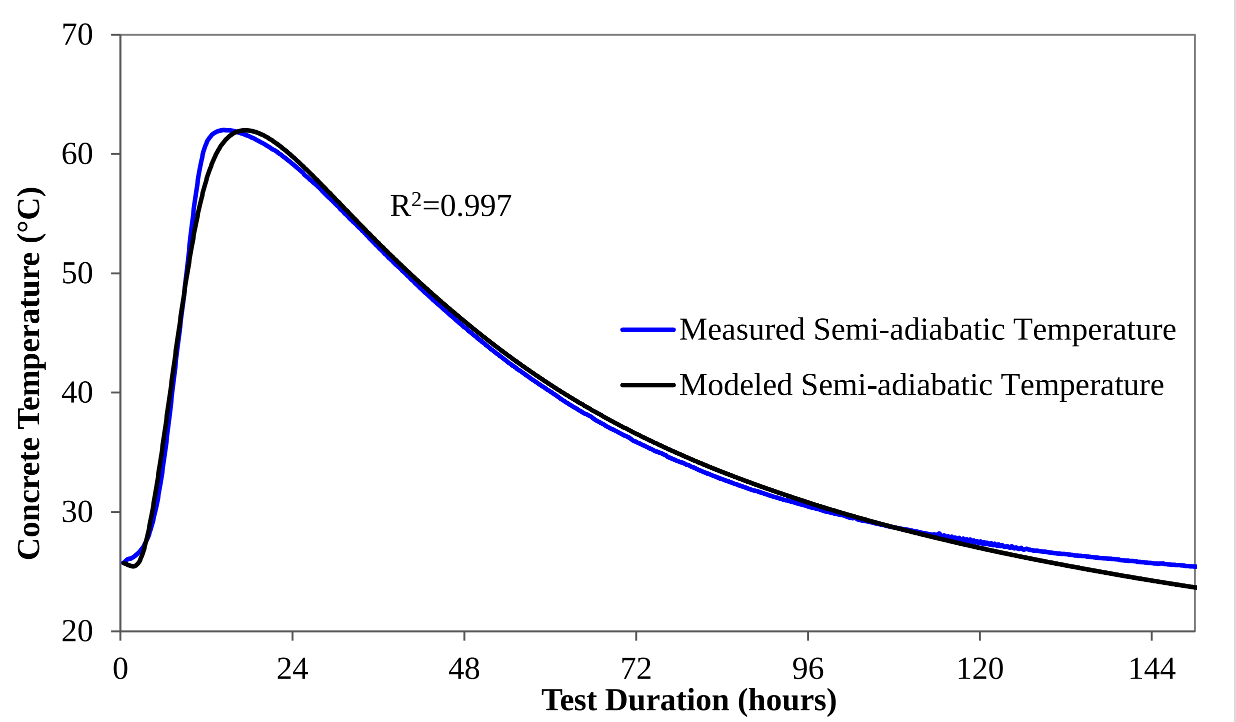

Figure 7-22: Measured vs. modeled semi-adiabatic temperature for SW-CNA mix

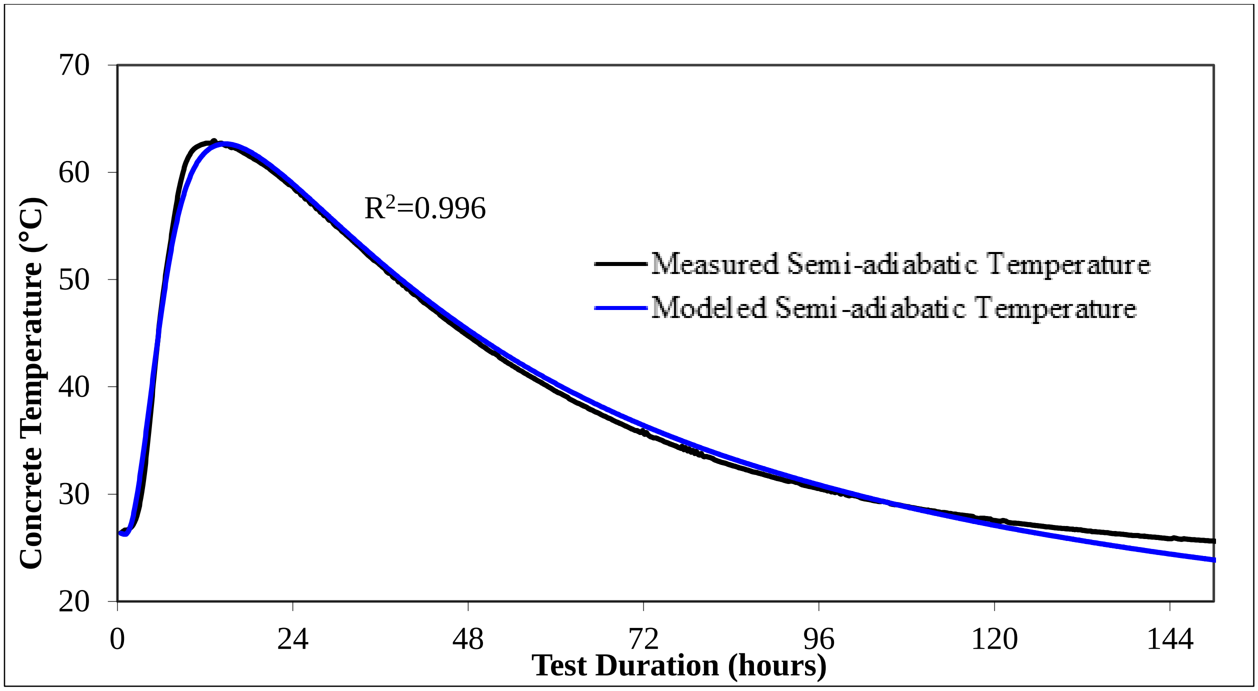

Figure 7-23: Measured vs. modeled semi-adiabatic temperature for SW-CHA mix

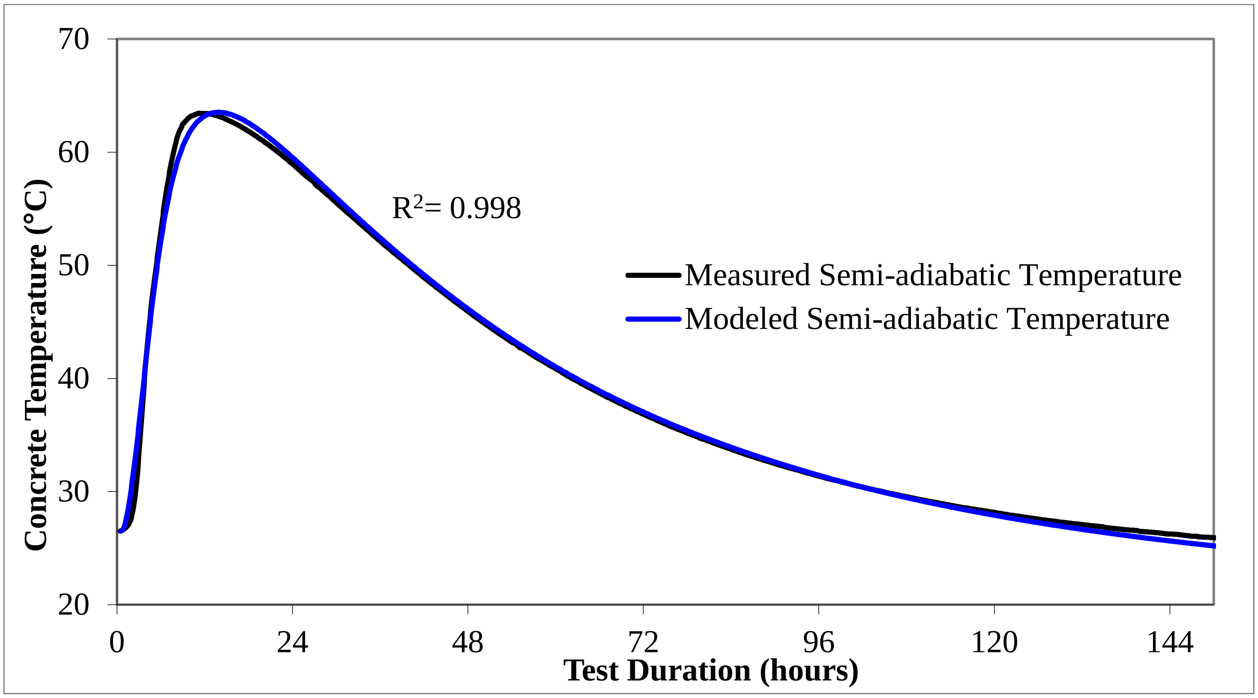

Figure 7-24: Measured vs. modeled semi-adiabatic temperature for SW-CA mix

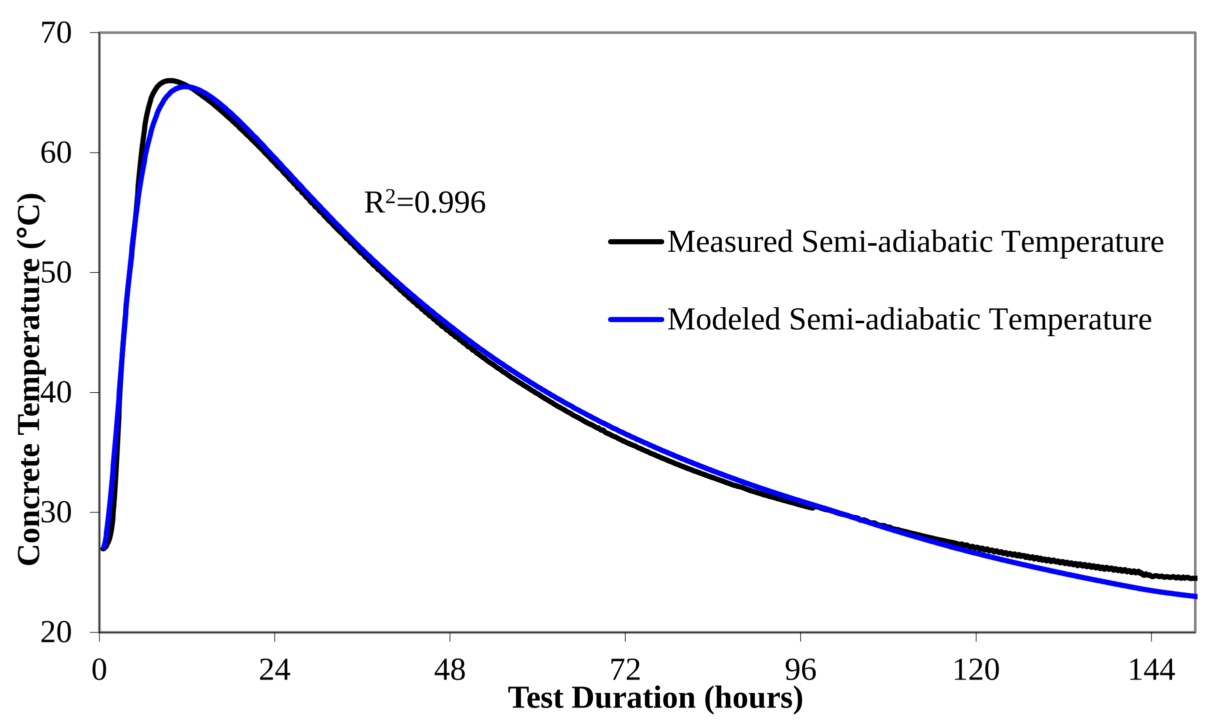

Figure 7-25: Measured vs. modeled semi-adiabatic temperature for SW-CDA mix

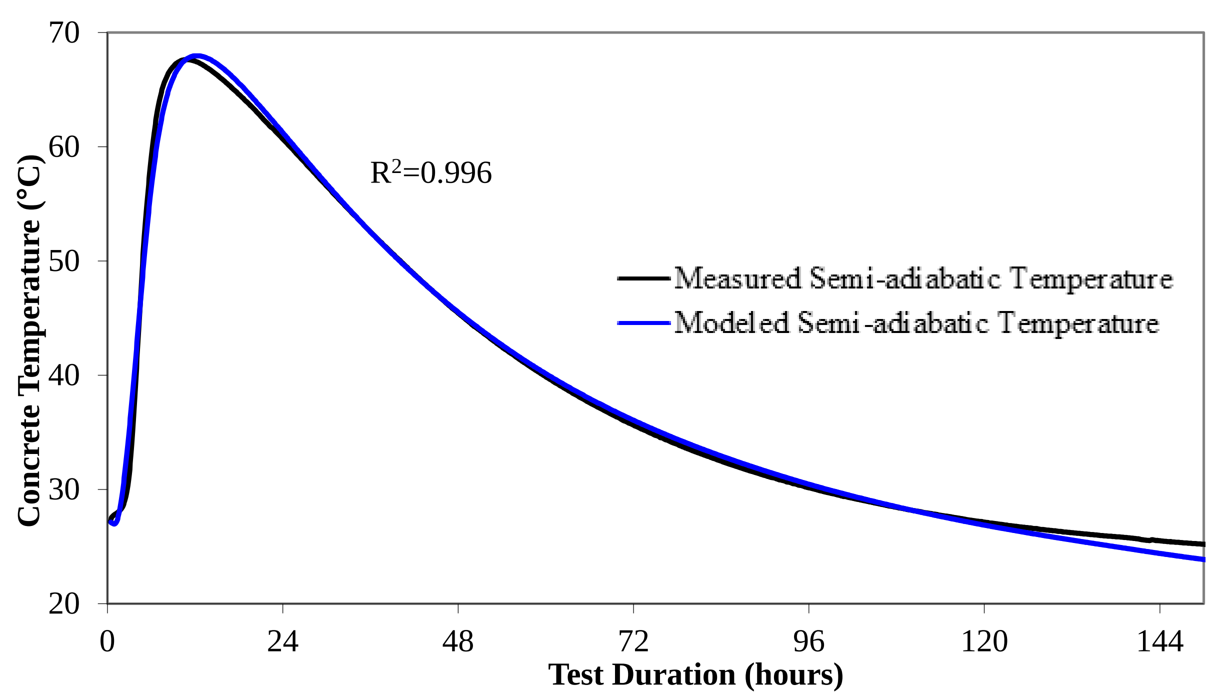

Figure 7-26: Measured vs. modeled semi-adiabatic temperature for JAX-CA mix

The true adiabatic temperature "T_{adia}", modeled using the best-fit hydration parameters defined previously and the false adiabatic temperature (T_{adia}*) are plotted for each mixture in Figures 7-27 through 7-32. The "true" adiabatic temperature is higher than the "false" adiabatic temperature since the former takes into account the effect of temperature on the rate of hydration.

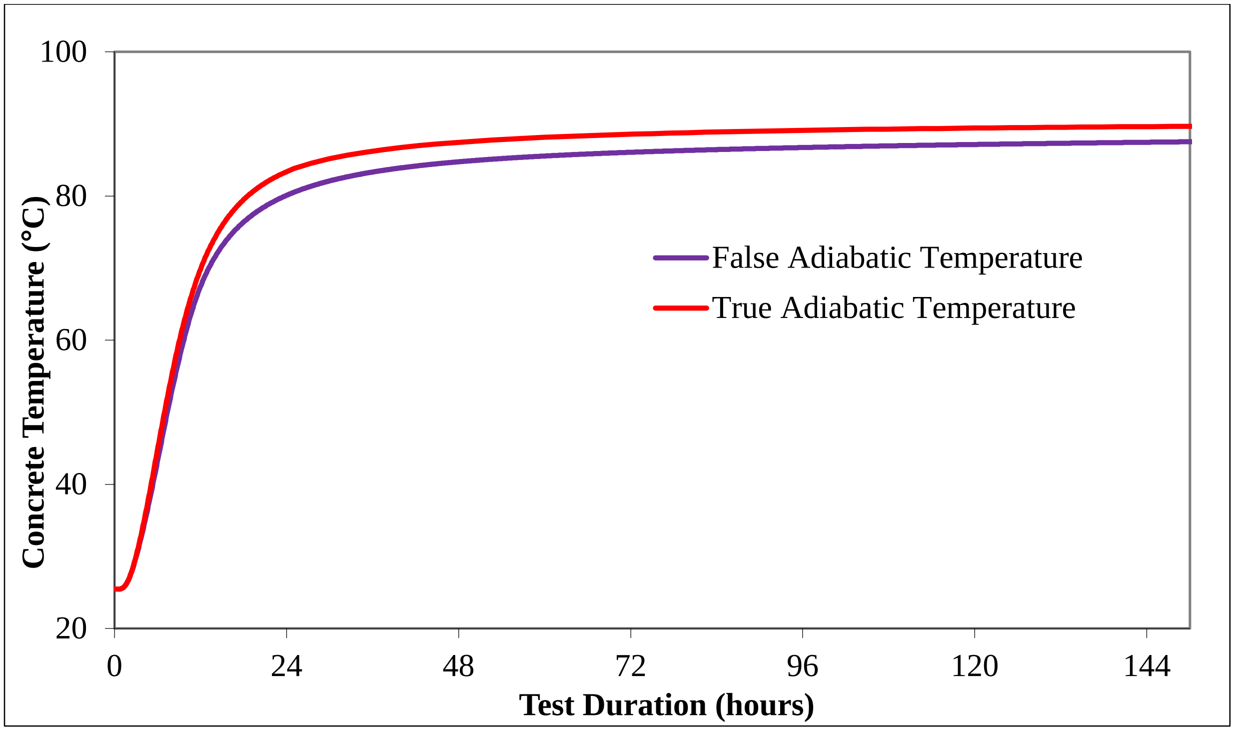

Figure 7-27: True vs. false adiabatic temperature for SW-C mix

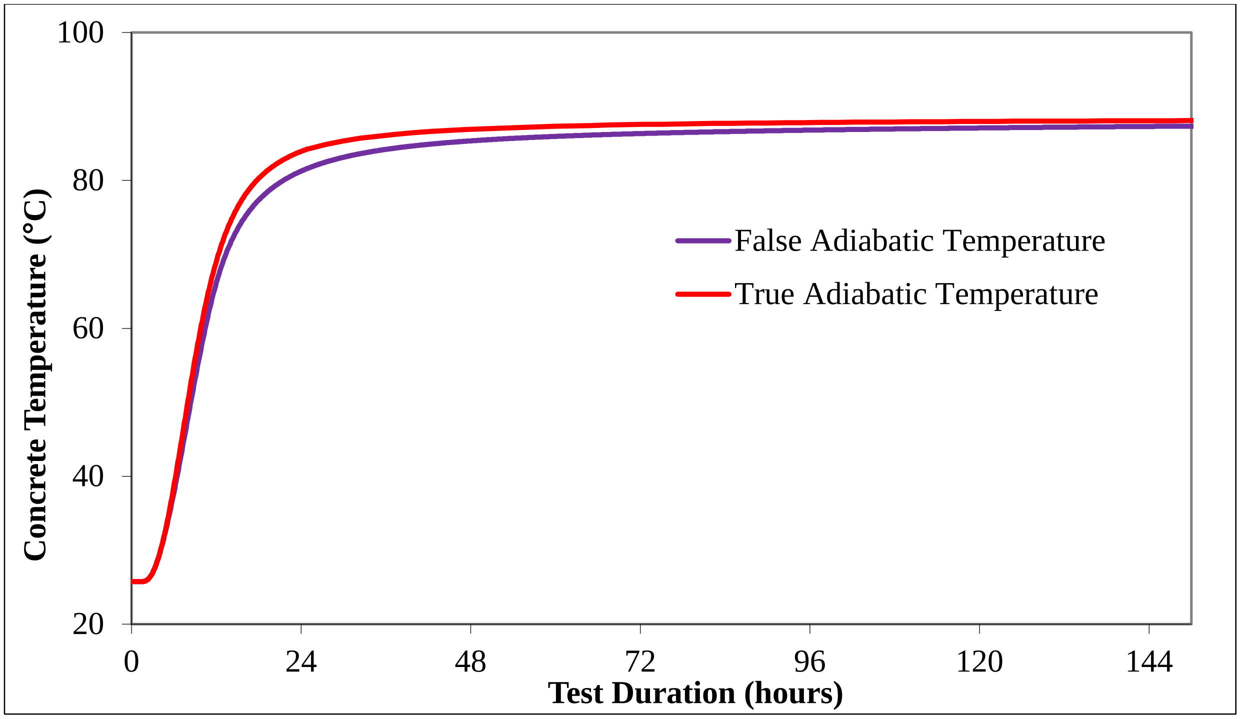

Figure 7-28: True vs. false adiabatic temperature for SW-CNA mix

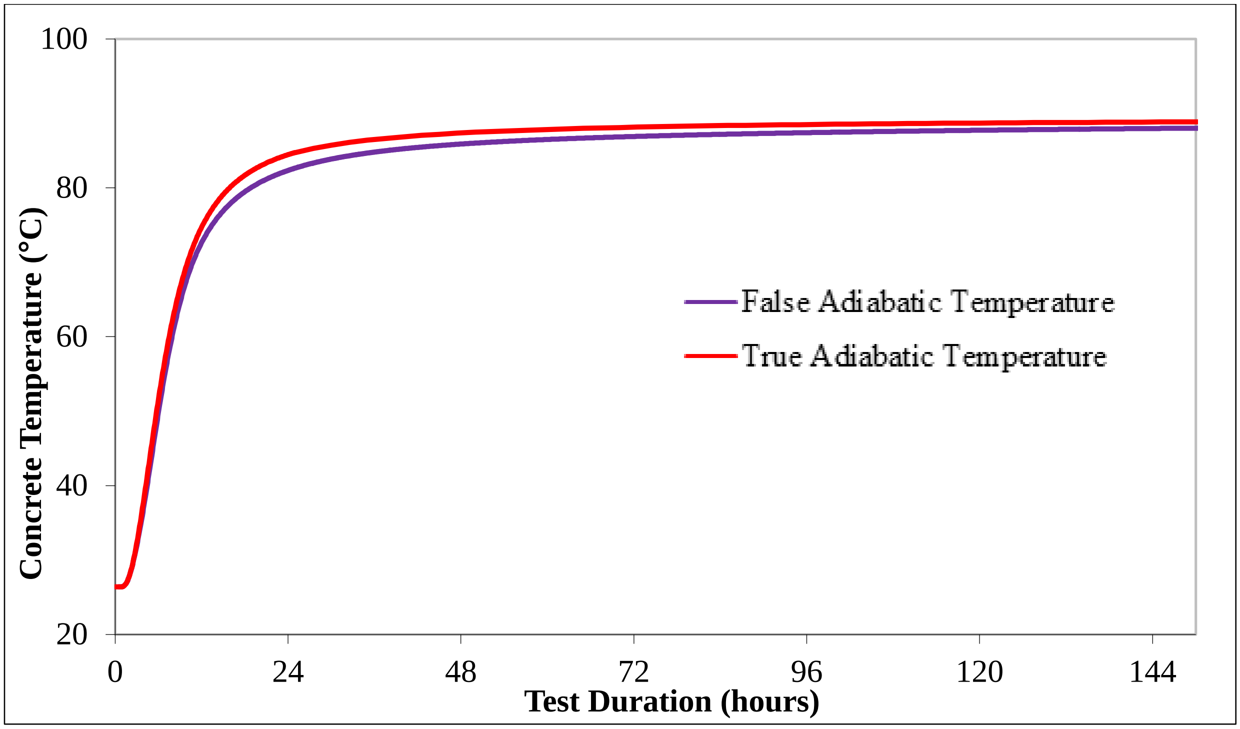

Figure 7-29: True vs. false adiabatic temperature for SW-CHA mix

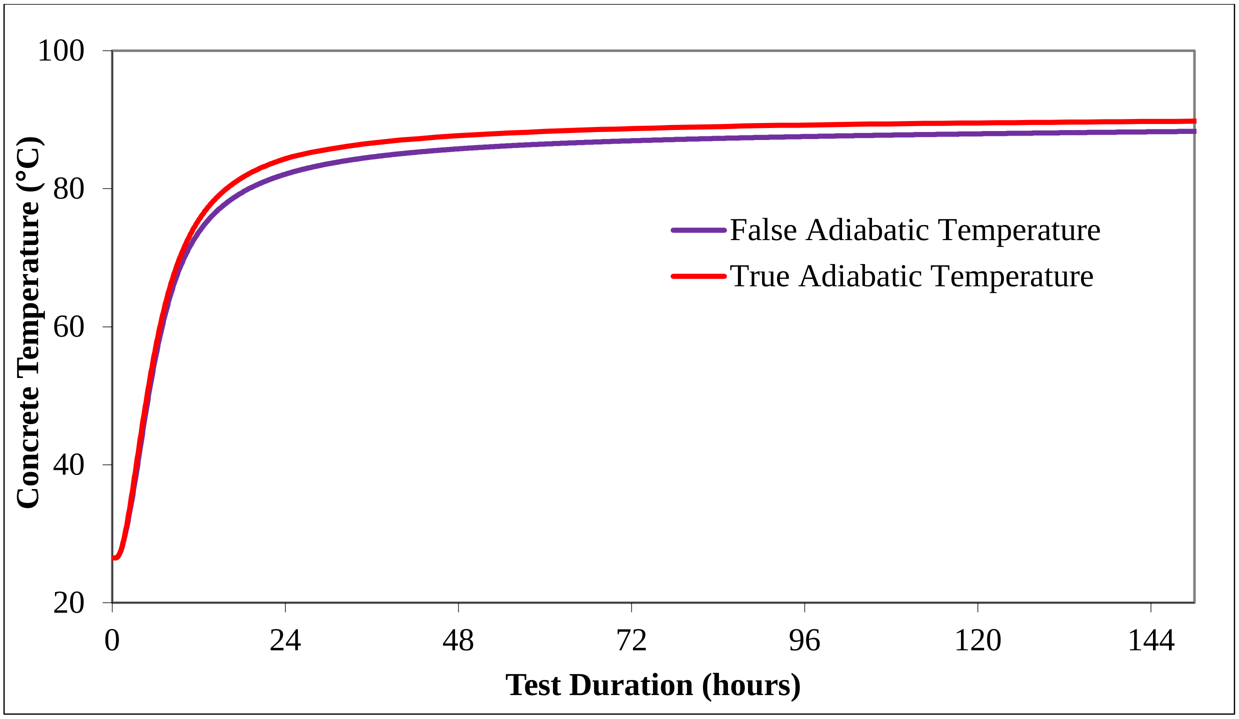

Figure 7-30: True vs. false adiabatic temperature for SW-CA mix

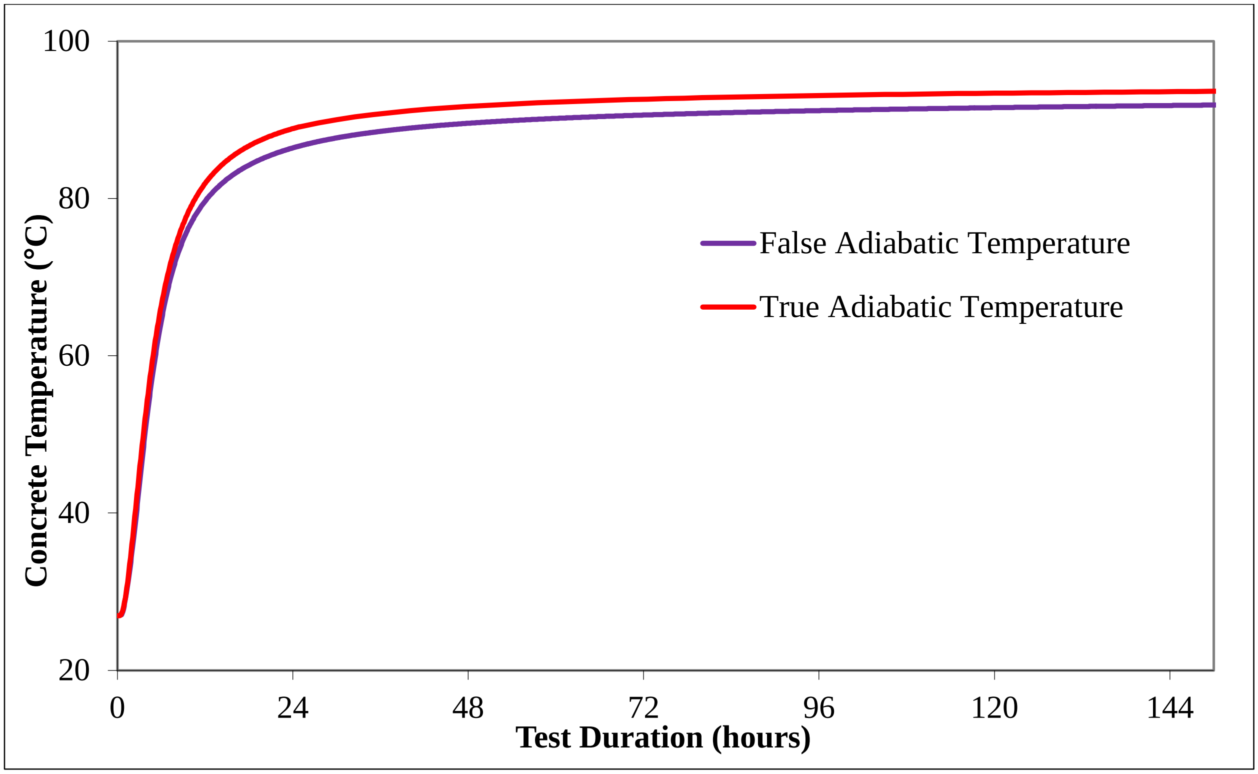

Figure 7-31: True vs. false adiabatic temperature for SW-CDA mix

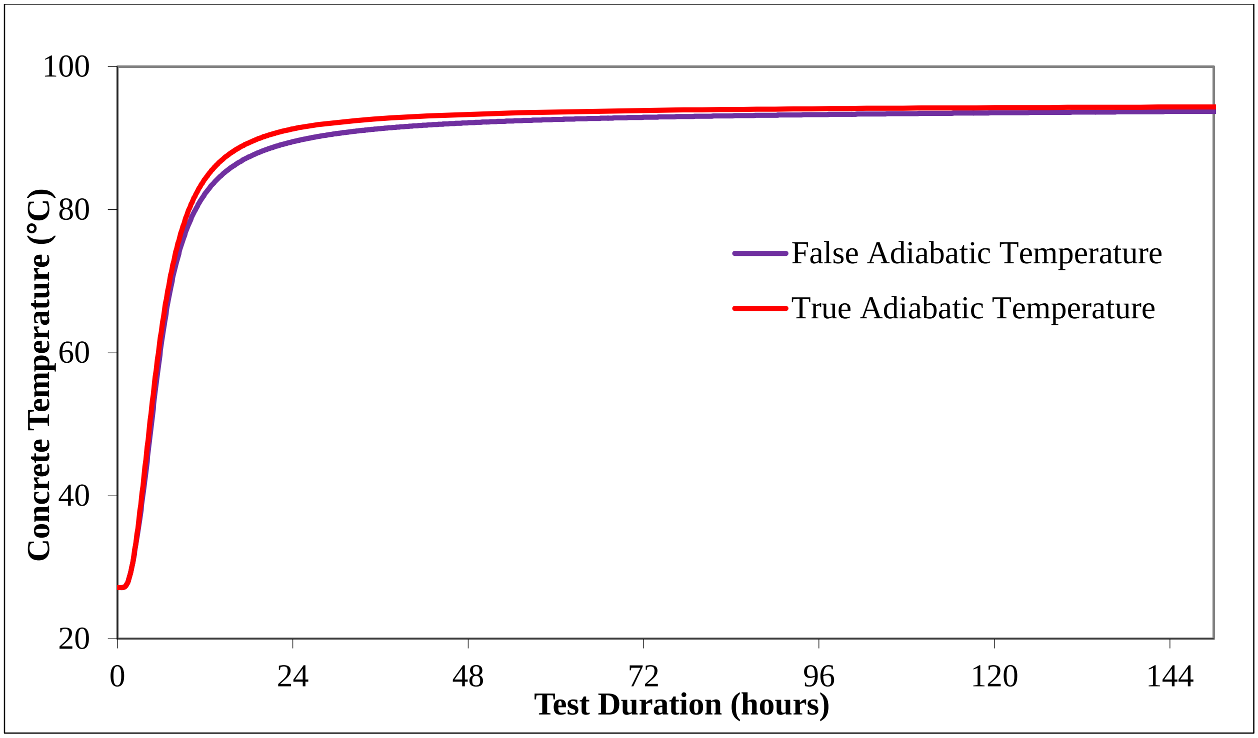

Figure 7-32: True vs. false adiabatic temperature for JAX-CA mix

The adiabatic temperature and the adiabatic temperature rise are presented in Table 7-5 and Figure 7-33 for the concrete mixtures studied here. For the SW mixes, the data clearly indicate that as the accelerator dose was increased, there was a corresponding increase in adiabatic temperature rise. This was expected since the increase in the accelerator dosage increased the rate of hydration, which consequently increased the heat generated. The range of adiabatic temperature rise, from 62.9 to 69.8°C, although not reflecting complete hydration, coincides with the lower range of findings from Freiesleben, Hansen, and Pedersen. They stated that after a long period of hydration, a typical concrete mixture will experience a temperature rise of about 60-80°C when it is left to harden without heat loss to its surroundings (Freiesleben Hansen and Pedersen 1985).

Table 7-5: Adiabatic temperature rise

Average Adiabatic Temperature	**Mix**					
	SW-C	**SW-CNA**	**SW-CHA**	**SW-CA**	**SW-CDA**	**JAX-CA**
Adiabatic Temp (°C) =	91.9	88.6	92.2	94.0	96.8	94.7
Adiabatic Temp Rise (°C)=	66.6	62.9	65.9	67.6	69.8	67.7

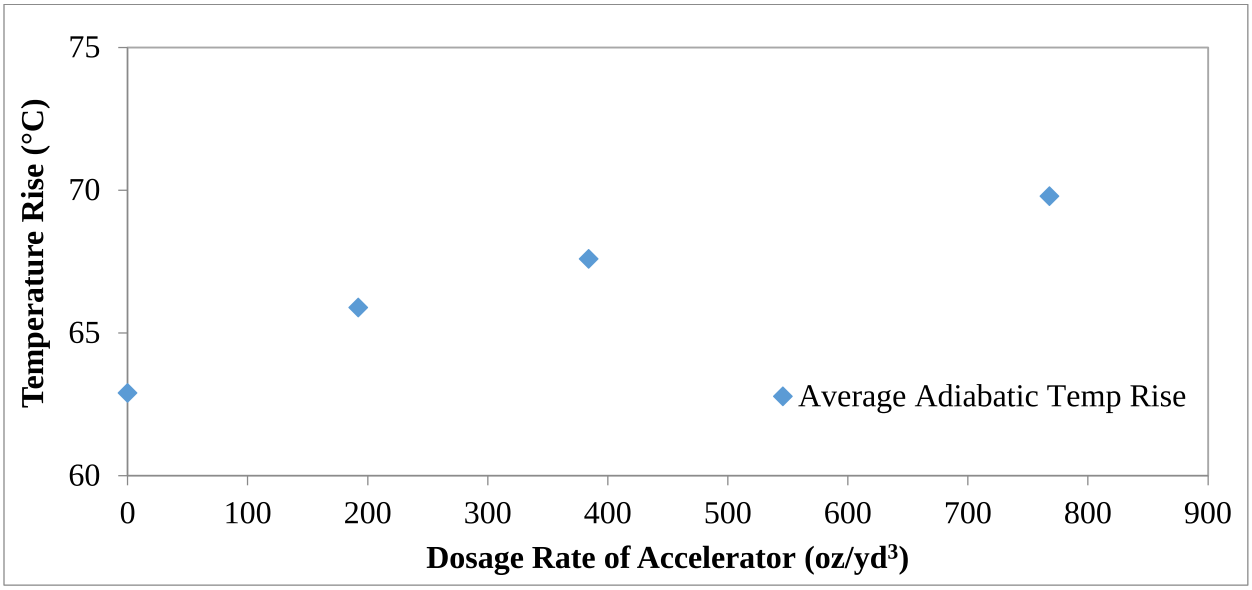

Figure 7-33: Effect of accelerator dosage on adiabatic temperature rise

Although the accelerator dosage for JAX-CA is higher than SW-CA, they both have a similar adiabatic temperature rise. The JAX-CA adiabatic temperature rise is 67.7 °C, while the average SW-CA adiabatic temperature rise is 67.6 °C. Figure 7-34 shows the two mixtures converging at a longer hydration time. It also shows that the JAX-CA mixture has a steeper slope and occurs before the SW-CA mixture acceleration phase of hydration, most likely because of the higher accelerator dosage.

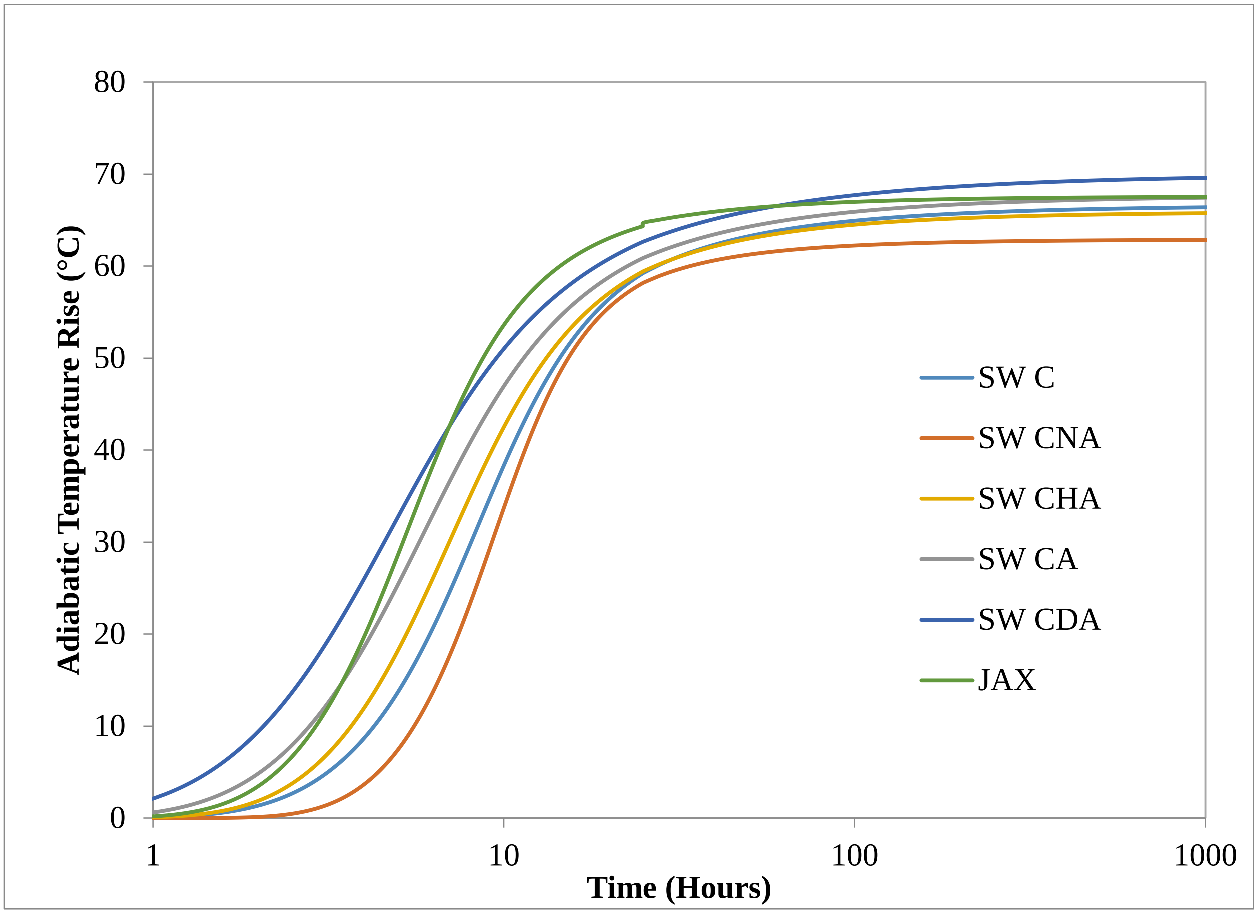

Figure 7-34: Adiabatic temperature rise for each mixture

7.4 Summary of Semi-Adiabatic Testing

The semi-adiabatic calorimeter was able to produce repeatable results through three replicate tests as seen in the measured data. This supports the validity of the testing procedure as a means to compare the change in temperature due to different dosages of accelerator. The model used to predict the semi-adiabatic temperature was shown to be valid when compared to the measured semi-adiabatic temperatures of each concrete mixture. This is important since the adiabatic temperature rise is based solely off this model. The effects of a varying dosage of accelerator on hydration can be ascertained from the hydration parameters which are determined through the analysis of the semi-adiabatic calorimetry tests. The analysis of the tests showed an increase in dosage of accelerator resulted in:

- An increase in the total amount of heat released, as also indicated by a larger α_u parameter, and

- A decrease in set time as also indicated by a shift to the left in the τ parameter.

7.5 References

ASTM C138 / C138M-13, Standard Test Method for Density (Unit Weight), Yield, and Air Content (Gravimetric) of Concrete, ASTM International, West Conshohocken, PA, 2013.

ASTM C173 / C173M-10, Standard Test Method for Air Content of Freshly Mixed Concrete by the Volumetric Method, ASTM International, West Conshohocken, PA, 2010.

ASTM C231-09a, Standard Test Method for Air Content of Freshly Mixed Concrete by the Pressure Method, ASTM International, West Conshohocken, PA, 2009.

ASTM C1074-04, Standard Practice for Estimating Concrete Strength by the Maturity Method, ASTM International, West Conshohocken, PA, 2004.

Concrete Durability Center. (2007). "ConcreteWorks (Version 3.1.0) [Software]." <Available from www.texasconcreteworks.com>.

Freiesleben Hansen, P., and Pedersen, E. J. (1985). "Curing of Concrete Structures." *Draft CEB Guide to Durable Concrete Structures*, CEB-General Task Group 20, ed., Comité Euro-International du Béton (CEB), Lausanne, Switzerland, 1–42.

Juenger, M. C. G., Hema, J., and Solt, S. (2007). "The Effects of Liquid Nitrogen on Concrete Properties." *Center for Transportation Research The University of Texas at Austin*.

Pane, I., and Hansen, W. (2002). "Concrete Hydration and Mechanical Properties under Nonisothermal Conditions." *ACI Materials Journal*, (99-M54), 534–542.

Poole, J. L. (2007). "Modeling temperature sensitivity and heat evolution of concrete." University of Texas at Austin.

Poole, J. L., and Riding, K. A. (2009). "Early Age Cracking : A Case Study in How Materials Modeling Can Improve Concrete Quality." *ACI*, SP 266-5, 57–72.

Poole, J., Riding, K., Folliard, K., Juenger, M. C. G., and Schindler, A. K. (2007). "Hydration study of cementitious materials using semi-adiabatic calorimetry." *ACI Special Publication SP-241-5*, 59–76.

Riding, K., Poole, J., Folliard, K. J., Juenger, M. C. G., and Schindler, A. K. (2012). "Modeling Hydration of Cementitious Systems." *ACI Materials Journal*, 109(2), 225–234.

Schindler, A. K., and Folliard, K. K. J. (2005). "Heat of hydration models for cementitious materials." *ACI Materials Journal*, 102(1), 24–33.

Springenschmid, R., and Morabito, P. (1998). "RILEM TCE1 : Adiabatic and semi-adiabatic calorimetry to determine the temperature increase in concrete due to hydration heat of the cement." *Materials and Structures,* 30(October 1997), 451–464.

The Transtec Group. (2009). “HIPERPAV III (Version 3.20.0006) [Software].” <Available from www.hiperpav.com>.

CHAPTER 8 Assessment of the Accuracy of Concrete Temperature Rise Prediction

8.1 Introduction

The continuous early-age temperature of mixtures used for concrete pavement slabs were predicted using ConcreteWorks (Concrete Durability Center 2007). This pavement stress analysis software was used instead of HIPERPAV (The Transtec Group 2009) because HIPERPAV does not output the predicted temperatures. ConcreteWorks was used to model the continuous early-age concrete temperature of different mixtures by analyzing the mixture proportions, environmental factors, geometric shape, construction practices, and hydration properties of each mixture. This was done because the algorithms used to simulate the pavement temperature, while not exactly the same, are similar to those used in HIPERPAV. This helped provide confidence in the ability to predict concrete temperatures, and understand the effects of materials, construction procedures, and environmental conditions on concrete replacement temperature profiles.

ConcreteWorks was designed at the Concrete Durability Center at the University of Texas to be a user-friendly software package that would enable contractors to optimize the concrete mixture proportioning, perform concrete temperature and thermal analyses on mass concrete elements, perform concrete pavement temperature simulations, and calculate the service-life based on chloride diffusion in mass concrete and bridge deck members (Riding 2007). ConcreteWorks, with its built-in material behavior models, allows engineers and contractors to model early-age temperature development while reducing the amount of laboratory testing needed (Poole and Riding 2009).

This report is focused on the predicted temperature module within ConcreteWorks for concrete pavement slabs. Unlike HIPERPAV, ConcreteWorks shows the predicted temperature as an output. The software uses the same concepts as HIPERPAV in modeling and predicting concrete temperature. The temperature profiles obtained from ConcreteWorks were compared to results for a field slab from the FDOT State Materials Office (SMO) for validation. Concrete pavement temperatures were then simulated for concrete mixtures containing a series of accelerator dosages. The predicted temperature profiles were used to show the effects of varying the accelerator dosage on the temperature profiles of the concrete. ConcreteWorks was also used to simulate the temperature development for concrete replacement slabs based on a mix design that was used on an FDOT project in Miami that had a problem with replacement slab cracking. Simulations were done using inputs from the FDOT mix design and historical Miami environmental conditions for the placement dates of slabs that had high cracking rates.

8.2 Concrete Mixtures

Slab temperatures were simulated for six different concrete mixtures using ConcreteWorks. Five of the mixtures used the same cement, SW, and were adjusted from one base mixture design, FDOT Slab Mixture 1, by adjusting the accelerator dosage. Table 8-1 shows the FDOT original mix design for the slab poured at the FDOT State Materials Office, which is the mix design upon which the lab mixes are based (Table 8-2).

Table 8-1: FDOT slab mixtures materials

Material	**FDOT Slab Mixture**	**Specification**
Type II Cement	900 lb	AASHTO M 85
Coarse Aggregate #57	1680 lb	Lime rock (Oolite)
Fine Aggregate	831 lb	Silica sand
AEA Admixture – air entrainer	3.0 oz	AASHTO M 154-AEA
Type D Admixture – water reducer/retarder	45.0 oz	AASHTO M 194-Type D
Type E Admixture - accelerator	384.0 oz	AASHTO M 194-Type E
Water for concrete	324.8 lb	
Water-to-Cement Ratio	0.384	

The five SW mixtures, shown in Figure 8-2, were used to evaluate the effects of variable dosages of accelerator on the concrete temperature profile. Each SW mixture contained a calcium chloride-based accelerator that complied with ASTM C494/AASHTO M 194 Type E, a water reducing and retarding admixture that complied with ASTM C494/AASHTO M 194 Type D, and an air-entraining admixture that complied with ASTM C260/AASHTO M 154. The amount of water by weight was adjusted for each mix to compensate for the water in the accelerator, so that the same water-cement ratio (w/c) was maintained throughout all of the SW mixtures. The mixture used at the State Materials Office (SMO) had an unintended overdose of accelerator without a corresponding water adjustment, resulting in a higher w/c ratio. Table 8-2 shows the w/c of each mixture, as well as the concrete mixture additions per cubic yard.

Table 8-2: Mixture designs

	Mix Weight per 1 yd^3					
Mixture Name	**SW-C**	**SW-CNA**	**SW-CHA**	**SW-CA**	**SW-CDA**	**SMO**
Materials	Wt. (lb)	Wt. (lb)	Wt. (lb)	Wt. (lb)	Wt. (lb)	Wt. (lb)
Cement	900	900	900	900	900	900
Coarse Agg (SSD)	1680	1680	1680	1680	1680	1680
Fine Agg (SSD)	828	828	828	828	828	828
AEA	–	0.195	0.195	0.195	0.195	0.195
Type A and D	–	3.367	3.367	3.367	3.367	3.367
Type E	–	–	16.801	33.602	67.203	48.00
Type A and F	–	–	–	–	–	–
Mix Water	348	348	338	328	307	328
w/c	0.384	0.384	0.384	0.384	0.384	0.397

8.3 Input Parameters

Like HIPERPAV, ConcreteWorks uses inputs that can be measured from laboratory tests and field reports. Since the scope of this work was to determine the concrete temperature at early ages, strength-based test results were not required, although they can be used to show the maturity and compressive strength in ConcreteWorks. The general inputs used for both mixtures are presented in Table 8-3, while the hydration parameters obtained from isothermal and semi-adiabatic calorimetry are shown in Table 8-4. The Miami temperature prediction analysis used the same inputs as the SMO construction inputs and materials since the data were not available for the Miami site.

Table 8-3: ConcreteWorks general inputs

Parameter	**SW**	**SMO**	**MIA**
Pavement Thickness (in)	11	11	11
Subbase Thickness (in)	default	default	default
Subbase Type	default	default	default
Batch Proportions			
Cement (lbs/yd^3)	900	900	900
Water (lbs/yd^3)	325	325	325
Coarse Aggregate (lb/yd^3)	1680	1680	1680
Fine Aggregate (lb/yd^3)	831	831	831
Material Properties			
Cement Type	Type I/II	Type I/II	Type I/II
Blaine Fineness (m^2/kg)	442	442	442
Coarse Aggregate Type	Limestone	Limestone	Limestone
Fine Aggregate Type	Siliceous River Sand	Siliceous River Sand	Siliceous River Sand
Construction Inputs			
Estimated Placement Temperature (°F)	77	77	100
Pavement Curing	Single Coat Compound	Single Coat Compound	Single Coat Compound
Cure Method Color	Light Grey	Light Grey	Light Grey
Curing Application (hr)	1	1	1
Curing Removal (hr)	4	4	4

Table 8-4: ConcreteWorks inputs – hydration parameters

	SW-C	**SW-CNA**	**SW-CHA**	**SW-CA**	**SW-CDA**	**SMO**
Cement Heat of Hydration (J/kg)	481,800	481,800	481,800	481,800	481,800	481,800
HoH-based E_A(J/mol)	33,004	30,784	24,148	25,420	25,574	35,348
β	0.836	1.072	0.944	0.825	0.743	0.743
τ (hr)	11.596	11.931	8.759	7.938	6.783	6.783
α_u	0.741	0.687	0.725	0.746	0.772	0.772

The environmental conditions for both the SMO field site and the Miami site are shown in Table 8-5. All environmental data were obtained from www.weatherspark.com on 10/24/13 at 9 AM for SMO and 4/9/11 at 11 AM for Miami.

Table 8-5: ConcreteWorks environmental inputs

	Day	**Max Temp**	**Min Temp**	**Max Wind**	**% Cloud Cover**	**Max Hum.**	**Min Hum.**
SMO	1	73	52	8.1	0	97	42
	2	78	47	12.8	6.3	96	42
	3	76	45	9.2	61.5	93	41
	4	78	43	8.1	25	93	41
MIA	1	89	72	13.9	25	87	44
	2	87	73	11.4	25	84	47
	3	87	73	11.4	50	85	49
	4	84	73	8.1	50	85	49

8.4 Results

ConcreteWorks was validated by comparing the measured data from the top, middle, and bottom thermocouples to the simulated temperature outputs at the same reported depths for the SMO pavement slab. Figures 8-1 through 8-3 show this comparison along with the R^2 values that show the fit of each predicted temperature.

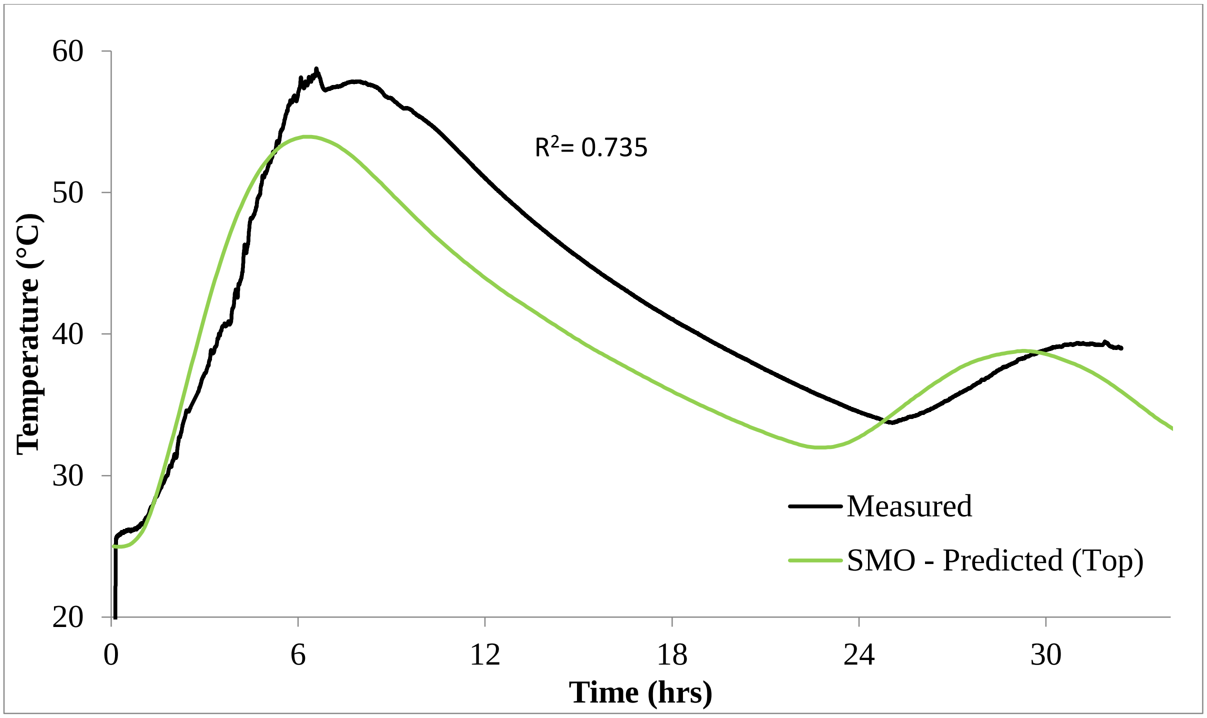

Figure 8-1: SMO – ConcreteWorks predicted temperature vs. measured (top thermocouple)

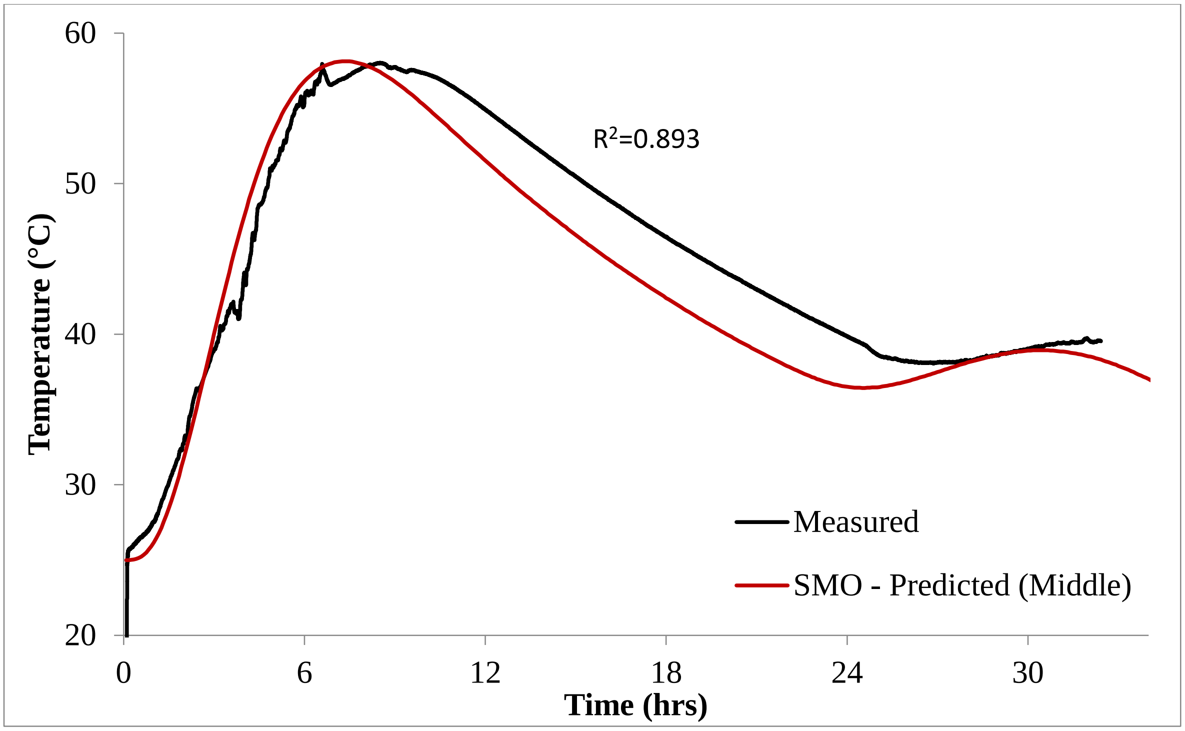

Figure 8-2: SMO – ConcreteWorks predicted temperature vs. measured (middle thermocouple)

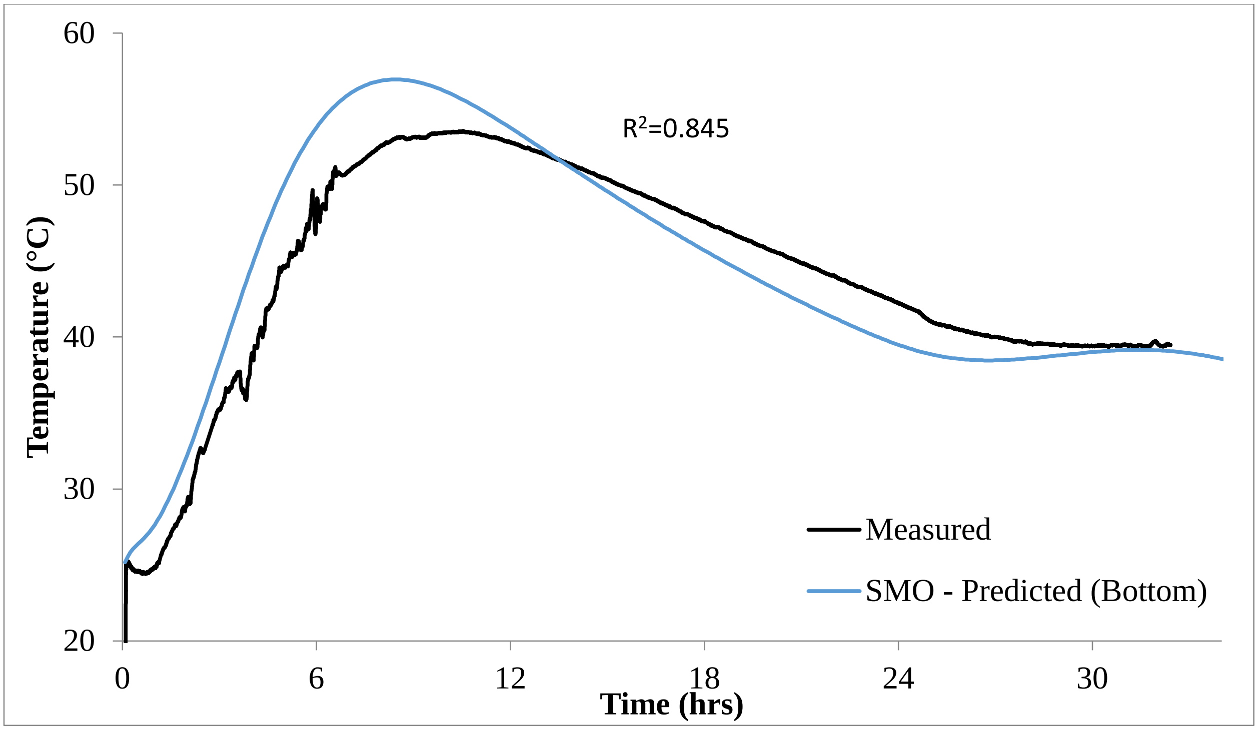

Figure 8-3: SMO – ConcreteWorks predicted temperature vs. measured (bottom thermocouple)

It should be noted that the accuracy of the temperature simulations versus measured values are dependent on the accuracy of the reported depth of the temperature sensors from the field. For example, if the measured values were actually two inches below their reported values, the fit of the simulated values would improve greatly as seen by the R^2 values in Table 8-6.

Table 8-6: Importance of accuracy of depth location for thermocouples

Thermocouple	**R^2 from Reported Depth**	**R^2 if Depth was Taken at 2 Inches Lower**
Top	0.735	0.959
Middle	0.893	0.979
Bottom	0.845	0.951

After validation, ConcreteWorks was used to predict the temperature profile of each mixture. It was also used to simulate the temperature development that occurred in Miami for concrete pavement slabs that were known to have high incidences of cracking. The predicted temperature profiles for the SW mixtures were plotted versus the measured field data for SMO (middle thermocouple) as shown in Figure 8-4.

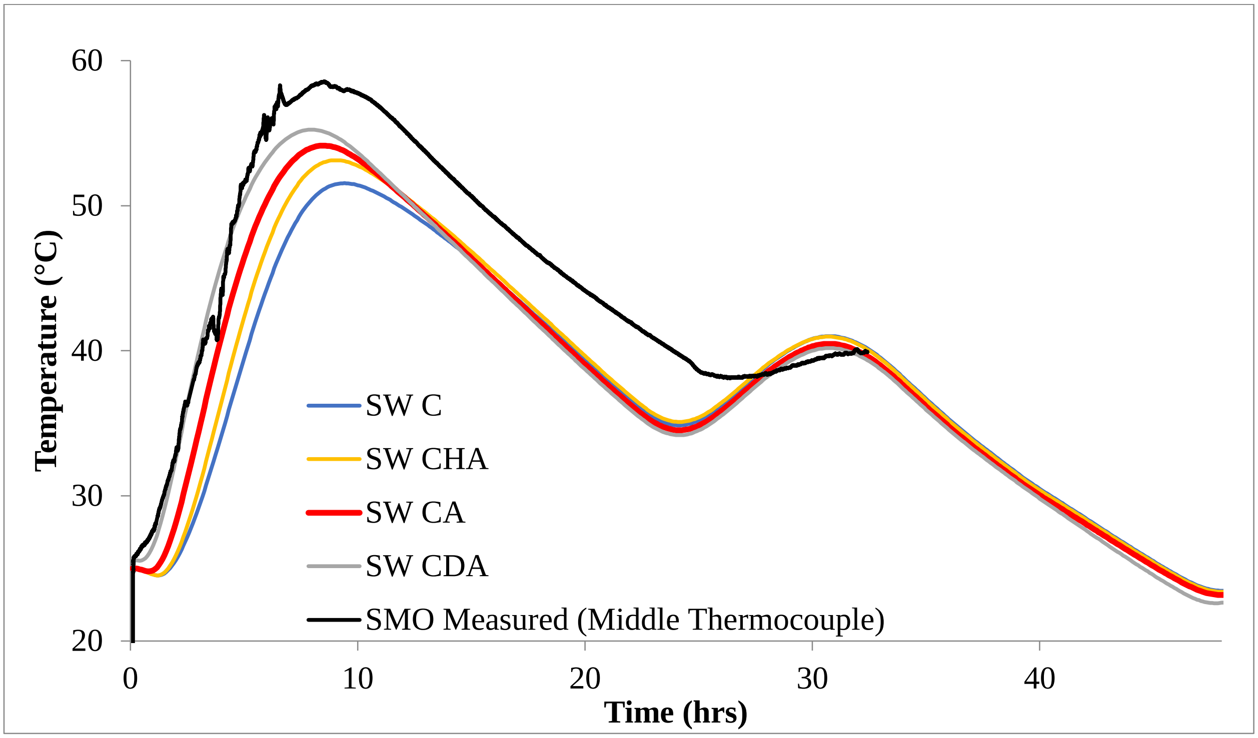

Figure 8-4: Predicted SW temperature profiles vs. measured SMO

The results show that the maximum temperature increased and shifted to shorter times as the dosage of accelerator for the SW concrete mixtures was increased. This trend was expected as the accelerator increased the rate of hydration.

After it was established that ConcreteWorks was capable of reasonably simulating the concrete pavement temperature profile, ConcreteWorks was used to simulate the temperature development of a rapid concrete repair mixture placed in Miami using similar placement temperature and environmental conditions to those found during concrete placements that produced high incidences of cracking in 2011. The maximum temperature profiles simulated for the SW CA mixture at both the Miami and SMO locations were compared. Since the inputs for both locations were the same except for the initial temperature and the environmental conditions, the location with the higher initial and ambient temperature was expected to generate a higher concrete temperature. This trend can be seen in Figure 8-5 since the Miami location had a higher initial temperature and higher ambient temperature.

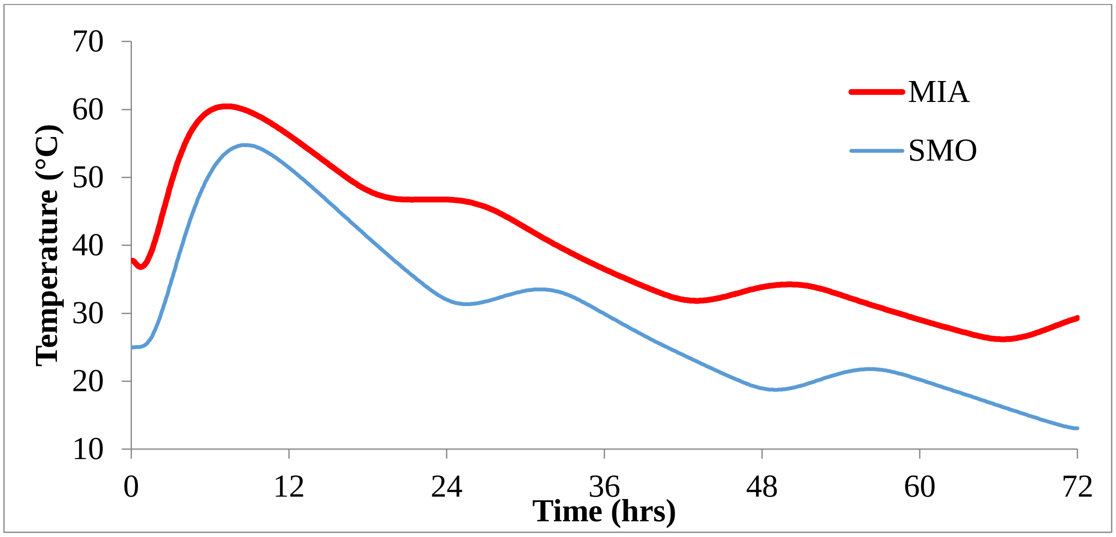

Figure 8-5: SW CA mixture at MIA vs. SMO locations

ConcreteWorks can also be used to determine the temperature at different depths of the slab. Figure 8-6 shows the temperature at the top, middle, and bottom of the SW CA mixture using the same conditions as for the SMO slab. The oscillating change in temperature between the top and bottom of the slab is due to the effect of the ambient temperature rising and falling throughout the day and night.

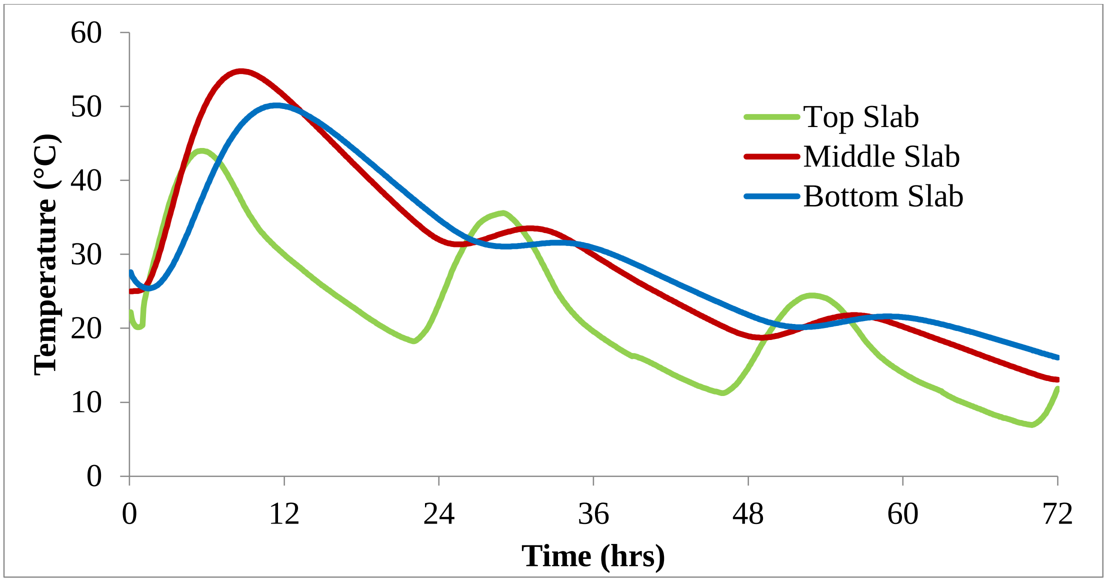

Figure 8-6: SW CA temperature at different depths

ConcreteWorks has a temperature animation in its analysis which helps to show this change in temperature throughout the depth of the slab. Figure 8-7 and 8-8 show still images of the temperature animation, which show temperature versus depth of slab for the SW CA mixture at different times after concrete placement. This animation was used to observe the change in temperature between the top and bottom of the slab. The still times of the animation were chosen to show the peak temperature in Figure 8-7 and a large temperature gradient in Figure 8-8.

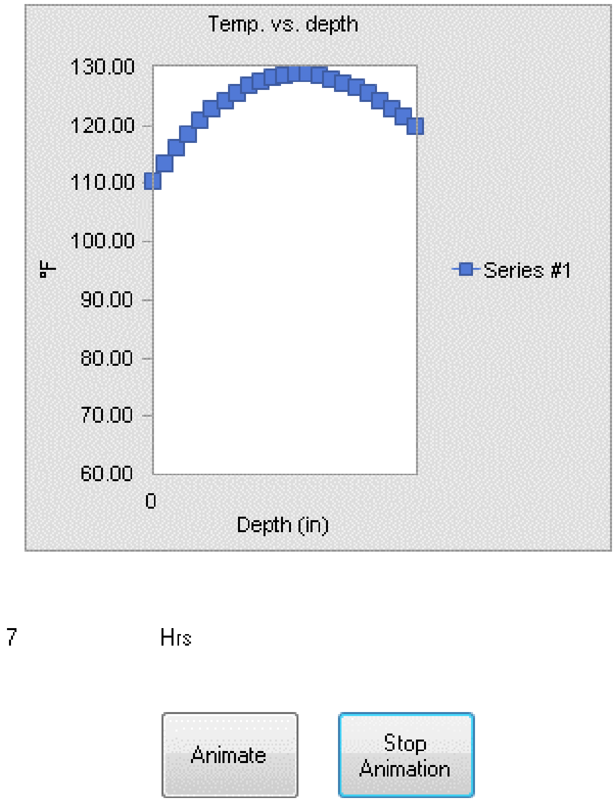

Figure 8-7: Temperature animation at 7 hr

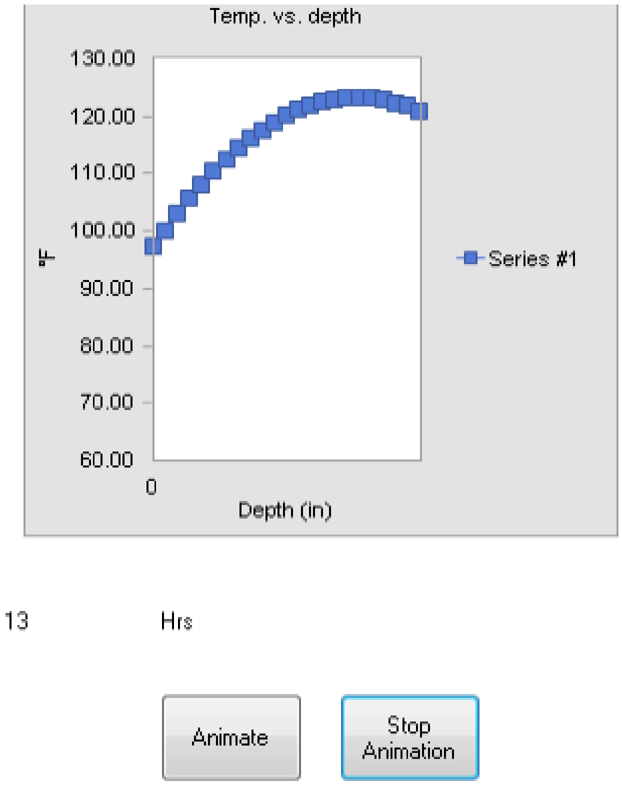

Figure 8-8: Temperature animation at 13 hr

8.5 Conclusions

The concrete temperature prediction of ConcreteWorks was validated by comparing the predicted temperature profile to recorded data from a field slab. This validation shows ConcreteWorks to be a valuable tool in predicting the concrete temperature of a pavement slab. From the analysis of ConcreteWorks, it can be expected that an increase in dosage of accelerator will increase the change in temperature of a concrete pavement slab. This agrees with the findings of the semi-adiabatic testing.

8.6 References

AASHTO M85-06“Standard Specification for Portland Cement” American Association of State Highways and Transportation Officials. Washington, D.C, 2006.

AASHTO M154M/M154-12 “Standard Specification for Air- Entraining Admixtures for Concrete” American Association of State Highways and Transportation Officials. Washington, D.C, 2012.

AASHTO M194M/M194-13 “Standard Specification for Chemical Admixtures for Concrete” American Association of State Highways and Transportation Officials. Washington, D.C, 2013.

ASTM C260 / C260M-10a, Standard Specification for Air-Entraining Admixtures for Concrete, ASTM International, West Conshohocken, PA, 2010.

ASTM C494 / C494M-13, Standard Specification for Chemical Admixtures for Concrete, ASTM International, West Conshohocken, PA, 2013.

Poole, J. L., and Riding, K. A. (2009). “Early Age Cracking : A Case Study in How Materials Modeling Can Improve Concrete Quality.” *ACI*, SP 266-5, 57–72.

Riding, K. (2007). “Early age concrete thermal stress measurement and modeling.” University of Texas at Austin.

CHAPTER 9 Concrete Mechanical Properties and Equivalent Age/Maturity Relationships

9.1 Introduction

An objective of this project was to use field data for modeling of cracking potential of cements contained in high-early-strength (HES) concrete mix designs using HIPERPAV software. Initially, it was intended that data would be collected from several active concrete pavement slab replacement job sites over a period of 9 months; however, only one viable construction project was identified during this period and it was in Jacksonville.

Maturity curves were used together with heat of hydration data to model thermal stresses and temperature rise in concrete elements in order to identify significant factors that contribute to the cracking potential of concrete pavement slabs. Models that predict thermal stresses and temperature rise in concrete elements rely on the determination of concrete mixture temperature sensitivity through heat of hydration measurements and strength data. As concrete temperature sensitivity is dependent on mix design, and in order to perform accurate modeling, it is imperative to determine this property for each specific mixture used. Temperature rise and subsequent cooling can contribute significantly to early-age pavement stresses and their accompanying cracking.

Concrete strength prediction is a concept that is useful in determining the time of formwork removal, or appropriateness of load exposure, such as opening pavements to traffic. Typically, maturity curves or strength and equivalent age data are used in determining concrete strength in field projects. To generate accurate maturity curves, the datum temperature or the activation energy has to be first determined for a specific concrete mix in accordance with ASTM C1074. The objective of Task 9 was to determine the strength-based activation energies and maturity curves/equivalent ages for the mixes adopted in this research project. For the Miami field project, 5 mixes were prepared; namely, C (plain concrete), CNA (water reducer/retarder and air-entrainer), CHA (air-entrainer, water reducer/retarder, and chloride-based accelerator at half field dosage), CA (air entrainer, water reducer/retarder, chloride-based accelerator at field dosage) and CDA (air-entrainer, water-reducer/retarder, chloride-based accelerator at double field dosage). For the Jacksonville field project, due to the limited supply of cement, only one mix design was used; that is, JAX-CA (identical to field mix design). Mix proportions for concrete and mortar mixes are presented in Table 9-1 and 9-2, respectively. Mixture proportions for the mortar mixtures are given for batch sizes required to make 9 cubes.

Table 9-1: Mix proportions for concrete (kg/m^3)

	Mixture Proportions (kg/m^3)						
Name	Cement	Coarse Aggregate	Fine Aggregate	AEA Admixture	Type D Admixture	Water	Type E Admixture
SW-C	534.4	996.7	493.5	0.00	0.00	205.2	0.00
SW-CNA	534.4	996.7	493.5	0.12	2.00	205.2	0.00
SW-CHA	534.4	996.7	493.5	0.12	2.00	199.1	9.98
SW-CA	534.4	996.7	493.5	0.12	2.00	193.1	19.95
SW-CDA	534.4	996.7	493.5	0.12	2.00	180.9	39.91

Table 9-2: Mix proportions for mortar mixes (9-cubes mix)

Materials	SW-C (g)	SW-CNA (g)	SW-CHA (g)	SW-CA (g)	SW-CDA (g)	JAX-CA (g)
Cement	926.9	926.9	926.9	926.9	926.9	882.8
Sand (SSD)	1730.2	1730.2	1730.2	1730.2	1730.2	1683.4
AEA Air Entrainer	0.00	0.20	0.20	0.20	0.20	0.51
Type E Chloride Accelerator	0.00	0.00	17.30	34.60	69.21	61.41
Type D Water Reducer and Retarder	0.00	3.47	3.47	3.47	3.47	1.37
Type F High Range Water Reducer	N/A	N/A	N/A	N/A	N/A	2.16
Mix water	361.1	361.1	350.5	340.0	318.9	248.3
w/c	0.39	0.39	0.39	0.39	0.39	0.32

Procedures outlined in ASTM C1074-11 were adopted here in determining the maturity curves for concrete mixes expressed in terms of equivalent age at 23°C. The maturity function used here is shown in Equation 2-6 (Freiesleben Hansen and Pedersen 1977).

The literature indicates that activation energy varies with cement type, supplementary cementitious material (SCM) use, and admixture type and dosage (Carino and Tank 1992). In order to determine the equivalent age using Equation 2-6, the activation energy for each mix was determined from the mortar compressive strength of cubes cured at three different temperatures. Following ASTM C1074 specifications, mortar mixtures had a fine aggregate-to-cement ratio (by mass) that was the same as the coarse aggregate–to-cement ratio of the concrete mix. The paste constituents had the same water-cement ratio and the same proportions of chemical admixtures used in concrete. Two-inch mortar cubes were cured isothermally at 23ºC, 38ºC and 53ºC. Compressive strength (ASTM C109) was measured as early as possible once setting occurred. Setting time was measured for all mixes to aid in identifying the earliest testing age possible. Testing ages were 6, 12, 24, 72, 168, and 672 hours. Some mixtures were tested at additional ages of 1.5, 3 and 48 hours depending on the setting time. The mortar compressive strength versus age was plotted and fit using regression analysis to exponential and hyperbolic functions shown in Equations 2-8 and 2-9. Using Equation 2-9, the k-values were determined for each strength-age data set at each specific temperature and the best-fit values of S_u, t_o, and k calculated. The activation energy was then determined from the slope of the natural logarithm of the determined k-values versus the absolute temperature of the water-curing bath using the best-fit straight line. The negative of the slope of the line multiplied by the gas constant is the activation energy of the mix, which was used to determine accurately the equivalent age according to Equation 2-7. A similar analysis was done for determining the activation energy using the exponential function, Equation 2-8. The solver function of Microsoft Excel was used to determine the best-fit parameters for S_u, τ, and β. In this case, the value of $1/\tau$ was used to define the reaction rate (similar to "k" in the hyperbolic function). Carino (2004) indicated that both functions fit strength-age data and give similar fits up to 28 days of curing.

In order to develop the maturity curves, 4 x 8 in concrete cylinders were prepared for the five SW mixes used in this study. The same coarse and fine aggregates used in the field project were used in concrete batching. The aggregates were washed, dried and graded to ensure consistent mixes. For each mix, 28 cylinders were prepared. Thermocouples were embedded in 2 cylinders for temperature collection up to 28 days. The compressive strength, tensile splitting strength, elastic modulus, and Poisson's ratio were measured using an MTS hydraulic-driven testing machine operated at a loading rate in compliance with ASTM C 39 requirements for concrete testing. The strength-maturity relationship was established using regression analysis to determine the best-fit equation for strength-equivalent age data on concrete cylinders. The same hyperbolic and exponential functions (Equations 2-8 and 2-9) were used to express the relationship between compressive strength and equivalent age (Carino 2004) noting that "t" is the calculated "t_e" of Equation 2-6 in hours.

9.2 Results and Discussion

9.2.1 Mortar Strength Data and Activation Energy

Mortar cube strengths at the three isothermal temperatures are depicted in Figures 9-1 through 9-6 for SW and JAX mixes. Increasing the temperature increased the compressive strength at an early age but resulted in a decrease in the later strength for the SW-C mix (Figure 9-1). The 53°C SW-C mix had the highest strength up to 1 day, the 38°C mix had the highest strength from 1 to 7 days, and the 23°C mix had the highest strength from 7 to 28 days.

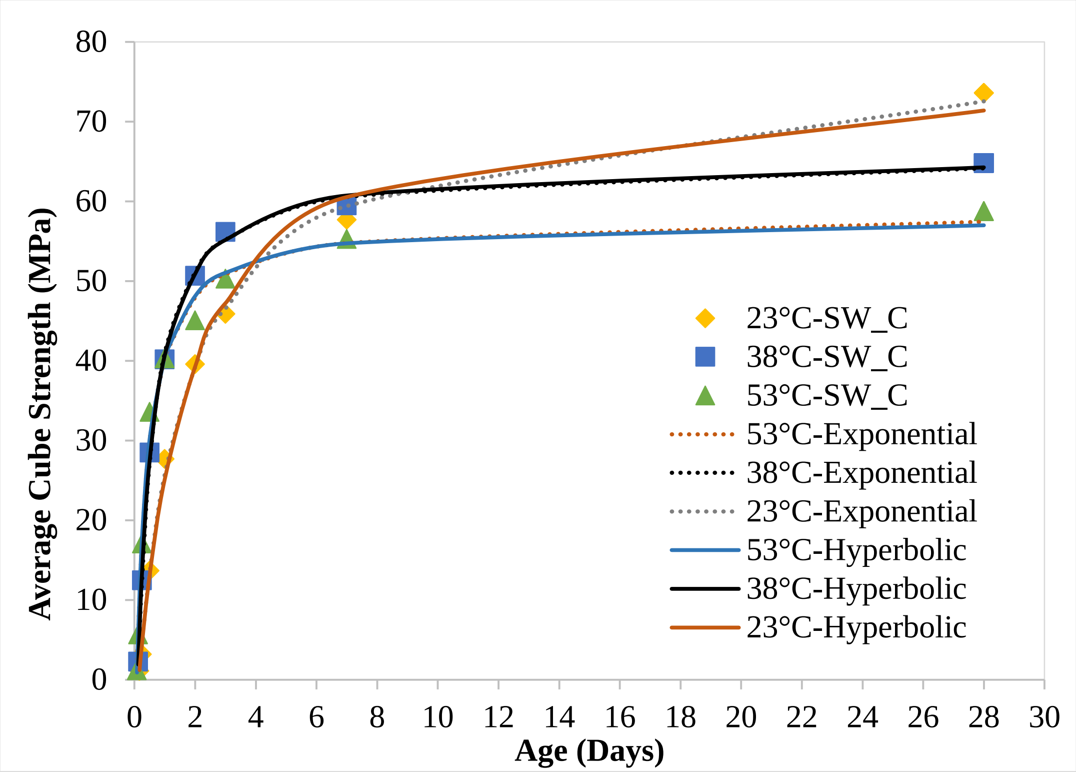

Figure 9-1: Mix SW-C (w/c = 0.39 and no admixtures) mortar cube compressive strength

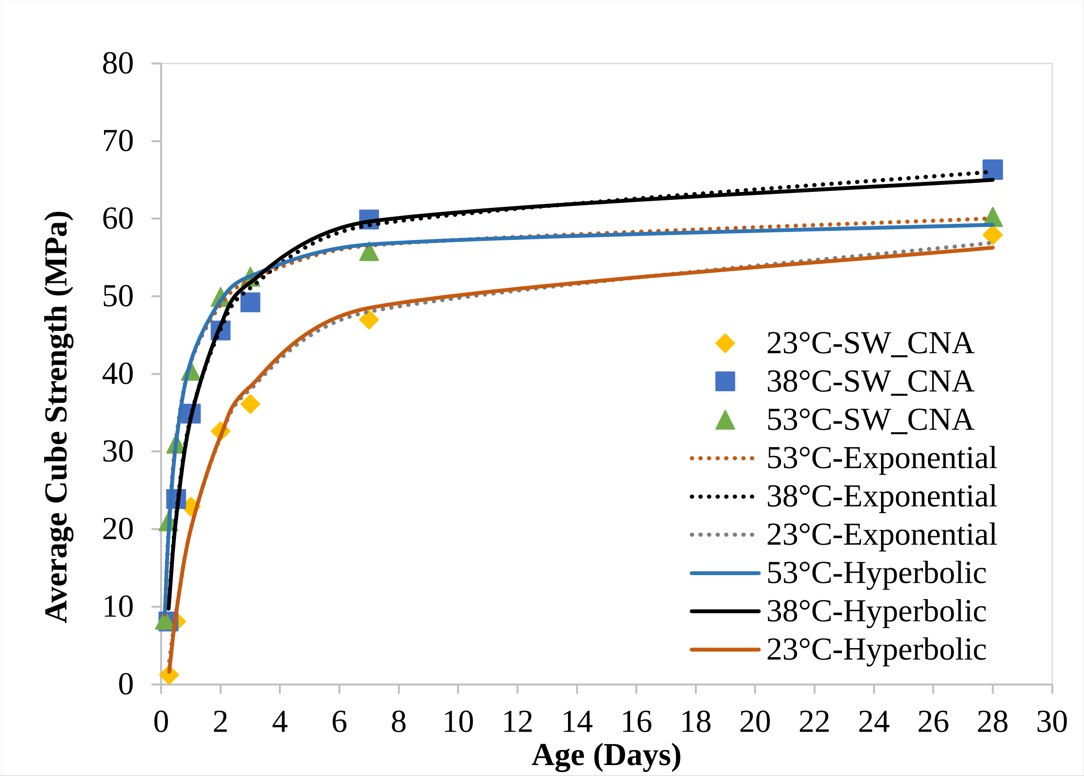

Figure 9-2: Mix SW-CNA (air-entrainer and water reducer/retarder) mortar cube compressive strength

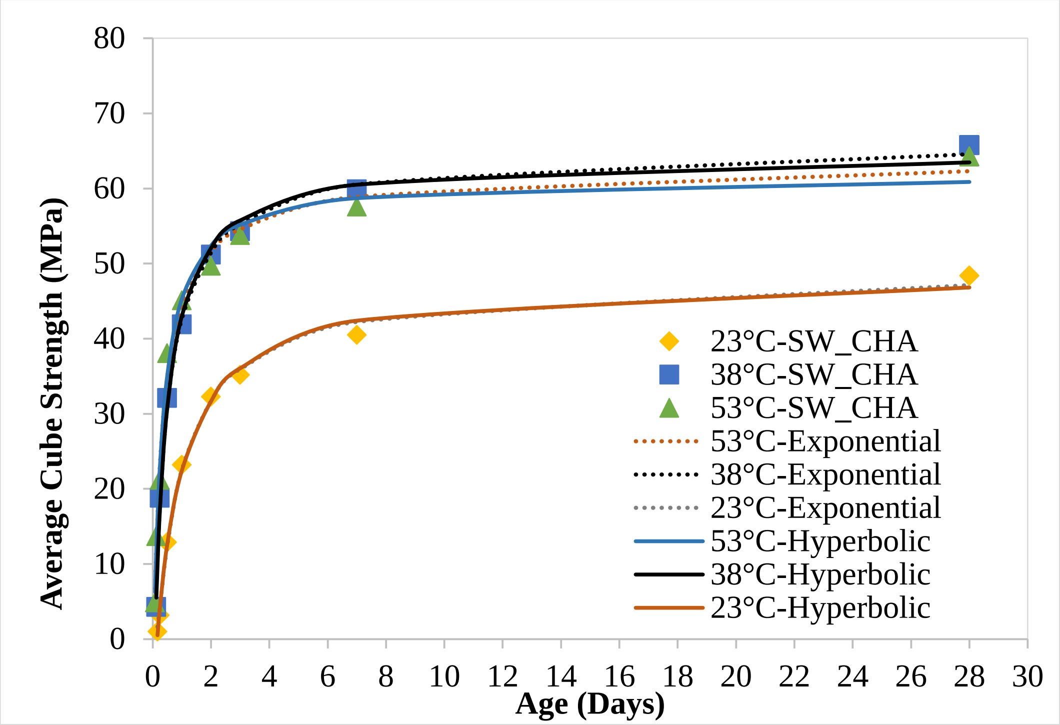

Figure 9-3: Mix SW-CHA (0.5x accelerator) mortar cube compressive strength

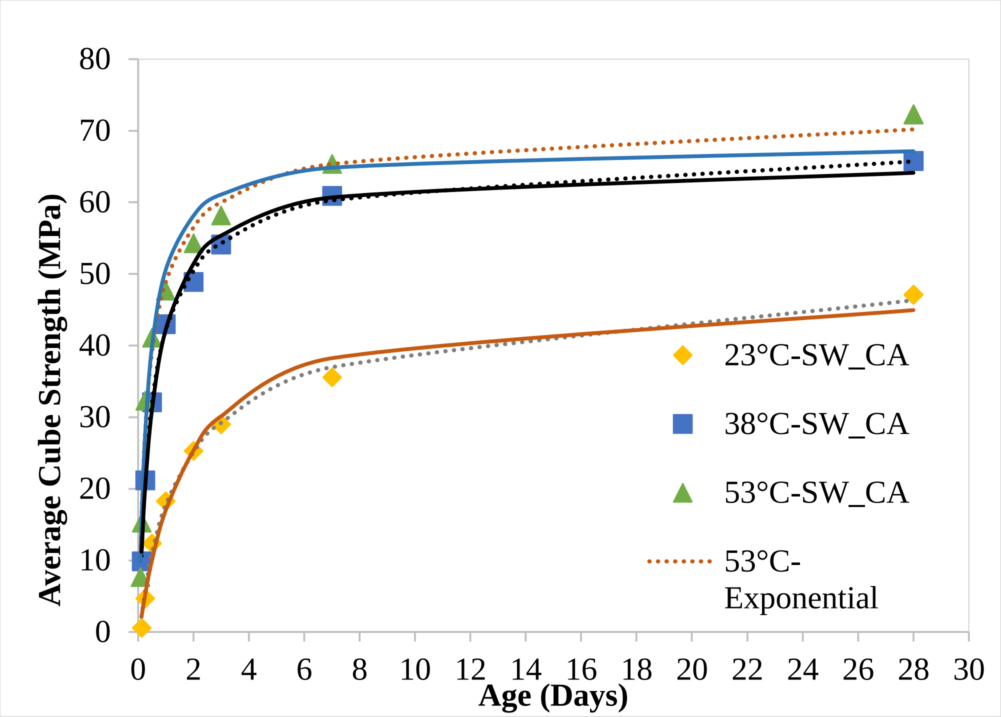

Figure 9-4: Mix SW-CA (accelerator) mortar cube compressive strength

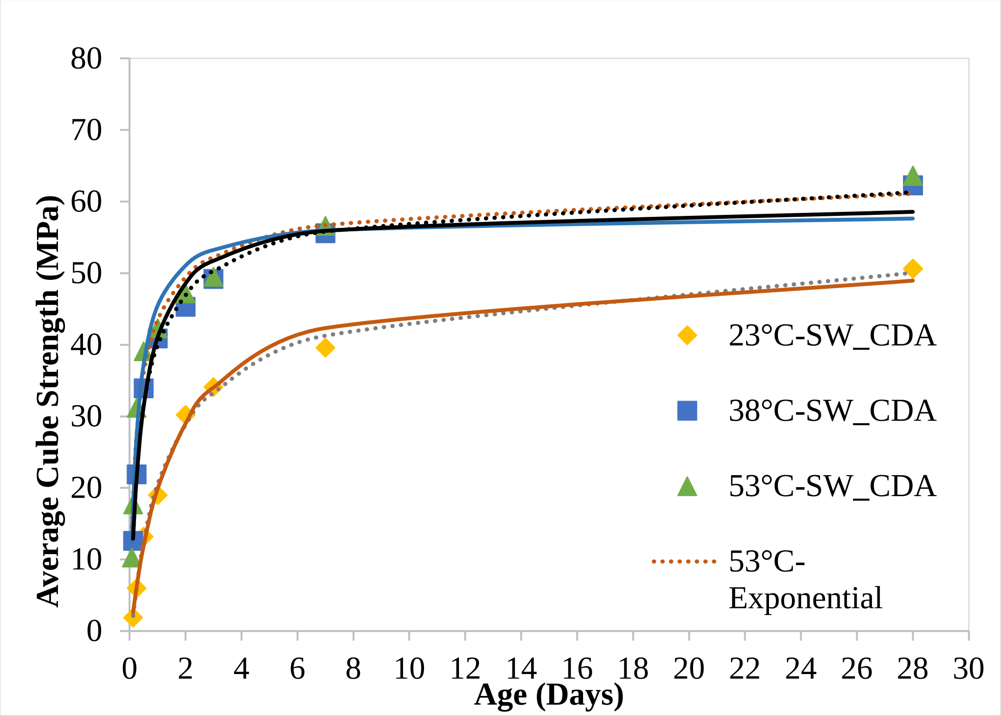

Figure 9-5: Mix SW-CDA (2x accelerator) mortar cube compressive strength

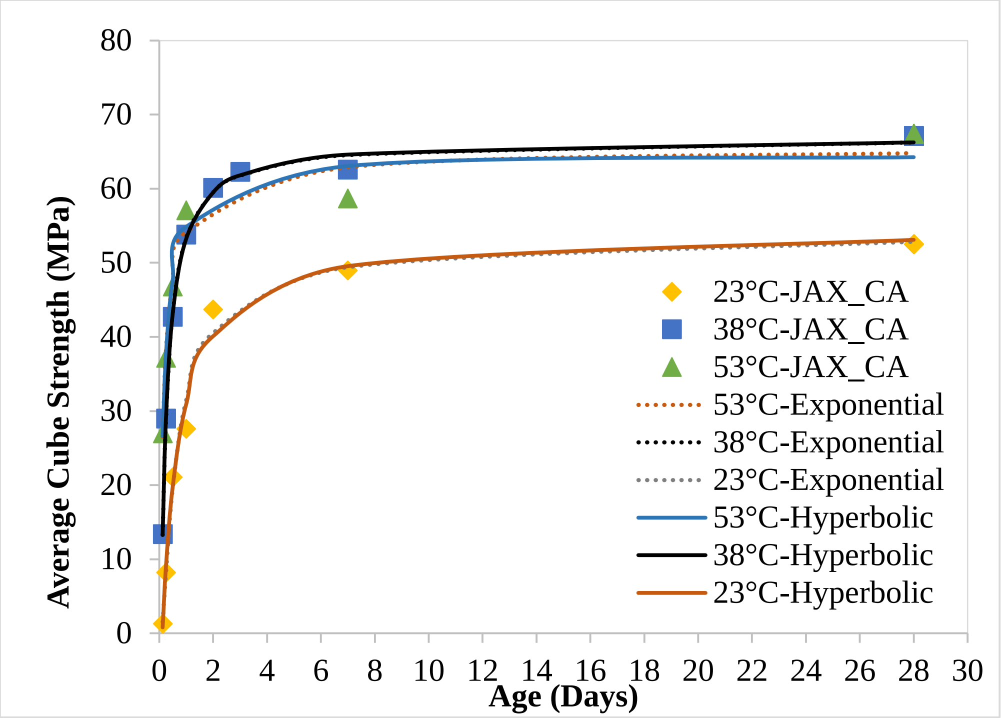

Figure 9-6: Mix JAX-CA (w/c=0.32) mortar cube compressive strength

Similar to SW-C, SW-CNA (Figure 9-2) at 53°C had the highest strength up to 2 days beyond which 38°C mix had the highest strength. At 23°C, the strength gain from 7 to 28 days was highest among the 3 curing temperatures. Comparing SW-CNA to SW-C, it appears that addition of a water reducer delayed the cross-over effect observed at the highest curing temperature to a later age; that is, from 1 day to 2 days. Additionally, the strength at 28 days for 23º C and 53º C was higher for SW-C than SW-CNA indicating the effect of water reducer/retarder extends to an age of 28 days.

For SW-CHA (Figure 9-3), the early strength was highest for 53°C. A cross-over effect was observed at 3 days when 38°C curing generated higher strength than 53°C. Comparing SW-CNA (Figure 9-2) to SW-CHA, the effect of adding a chloride-based accelerator appears to increase the early strength for 38°C and 53°C but not of significance at 28 days. For 23°C, addition of an accelerator did increase the early strength but decreased the strength at 3, 7 and 28 days. It appears that the mode of action of the chloride-based accelerator is temperature sensitive. It has a negative effect on the longer-term compressive strength for mixes cured at room temperature even at this low dose. For the SW-CA mix (Figure 9-4), at twice the accelerator dose for SW-CHA, increasing the curing temperature increased strength at all ages. For SW-CDA (Figure 9-5) at twice the accelerator dose in SW-CA and 4 times the dose in SW-CHA, increasing the temperature increased the strength up to 7 days.

As to the effect of calcium chloride accelerator additions on strength gain, (comparing SW-CNA to SW-CHA, SW-CA, and SW-CDA) at 23°C, additions of an accelerator, for any of the dosages studied here, decreased strength beyond an age of 1 day (Appendix D). This effect was not observed at the higher temperatures studied here. At 38ºC and 53ºC accelerator additions increased strength up to 1 day. Beyond 1 day, the trends appeared to be dose dependent. At 3 days, SW-CDA showed similar strength to SW-CNA but at 7 and 28 days, the SW-CDA mixes had lower strength than SW-CNA. It appears that at this high dose, compressive strength regresses with curing age for all temperatures studied here. For the lower accelerator doses, SW-CHA and SW-CA, the strength at 7 and 28 days appeared to be similar to SW-CNA at 38ºC and 53°C. At 23°C, SW-CHA and SW-CA had lower strength than SW-CNA beyond 24 and 12 hours, respectively. It is also noted that at similar accelerator dosage, JAX-CA and SW-CDA had similar strength gain behavior in spite of differences in cement mineralogy. In conclusion, an optimum accelerator dosage for strength appears to be temperature and age sensitive.

Activation energy values determined from mortar cube testing are presented in Table 9-3 where it can be seen that incorporation of water reducer/retarder reduced the activation energy while additions of a chloride-based accelerator increased the activation energy at high dosage. Using activation energy and equivalent age formula, the maturity curves for concrete mixes were determined, Figures 9-7 through 9-13. It is noted that at a later equivalent age, compressive strength curves for all the mixtures containing accelerator and the SW-CNA mix converge, while the compressive strength of SW-C without any admixtures remains higher. While a decrease in the ultimate compressive strength with addition of accelerators has been previously reported, water-reducing admixtures have been reported to increase the 28-day strength of concrete even at a fixed w/c ratio. The lower ultimate compressive strength of SW-CNA compared to the SW-C mix can be possibly explained by the addition of an air-entraining agent.

Table 9-3: Activation energy summary

Mix ID	**Hyperbolic Function (ASTM C1074-11)**		**Exponential Function (ASTM C1074-11)**	
	Activation Energy E_a (J/mol)	Arrhenius plot R^2	Activation Energy E_a (J/mol)	Arrhenius plot R^2
SW-C	40,467	0.927	38,221	0.927
SW-CNA	34,052	0.993	36,694	0.995
SW-CHA	28,049	0.949	29,109	0.971
SW-CA	44,244	0.958	47,884	0.908
SW-CDA	45,787	0.953	47,078	0.931
JAX-CA	35,707	0.919	41,202	0.995

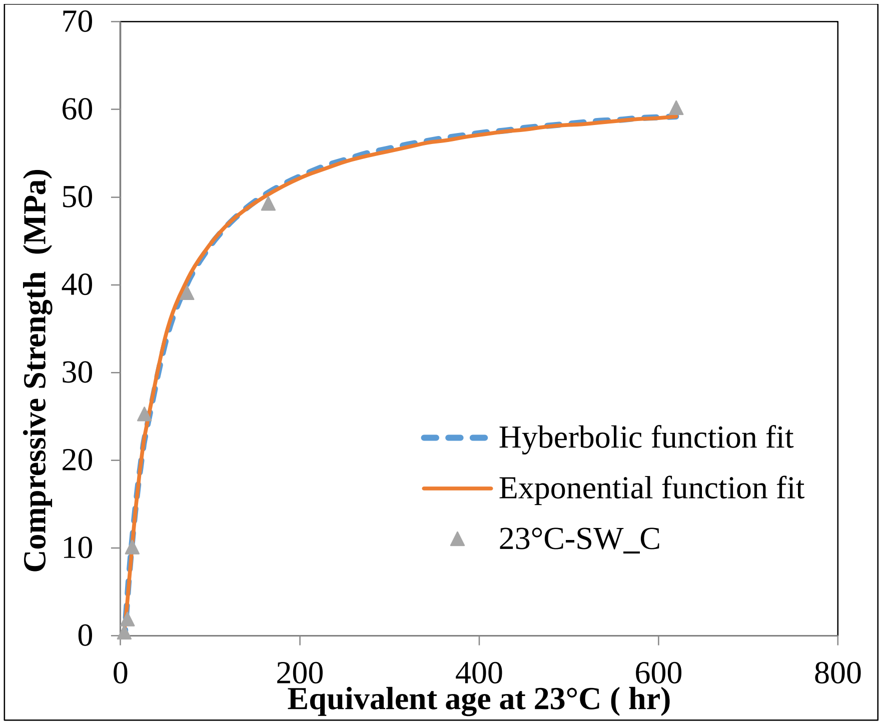

Figure 9-7: Maturity curve for SW-C

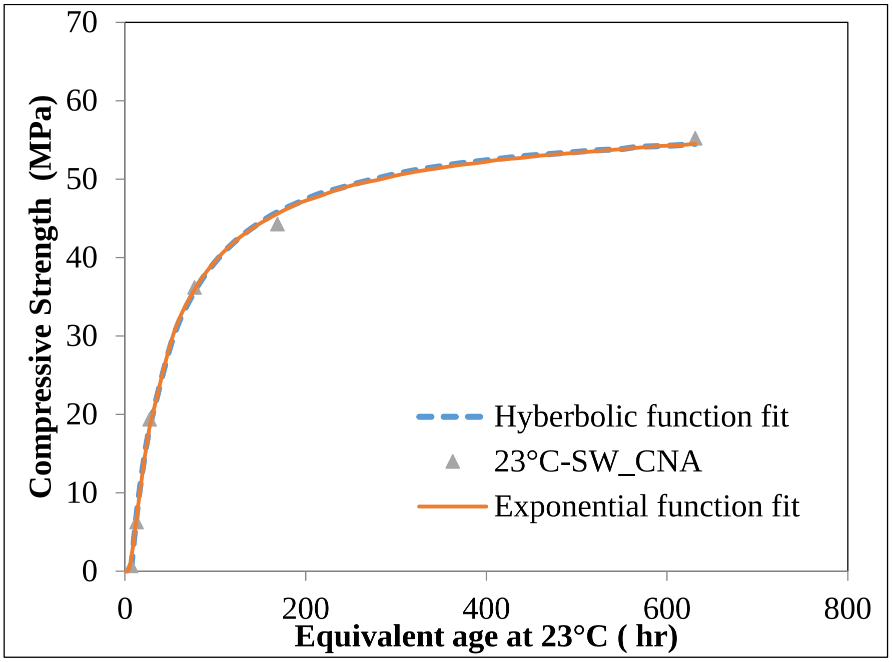

Figure 9-8: Maturity curve for SW-CNA

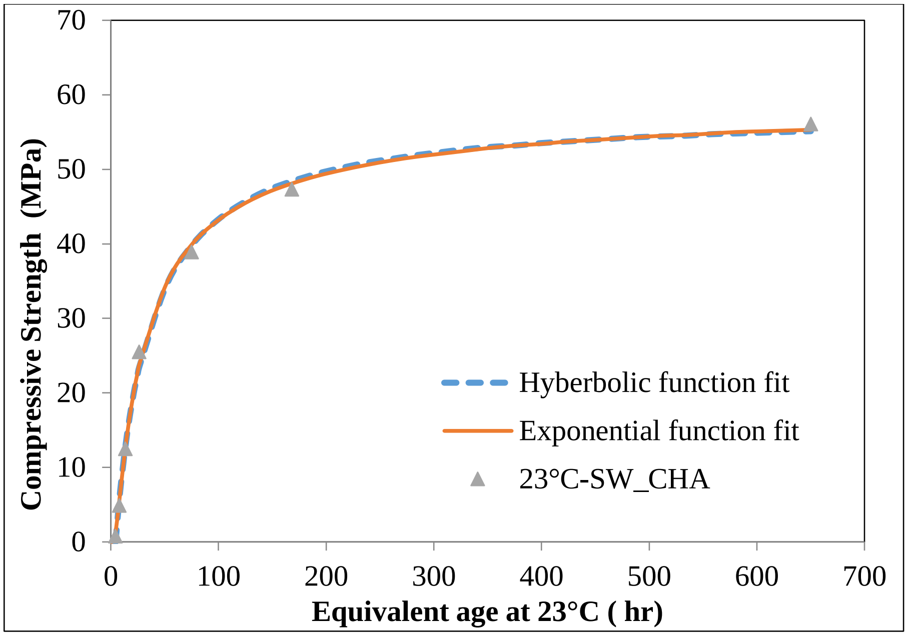

Figure 9-9: Maturity curve for SW-CHA

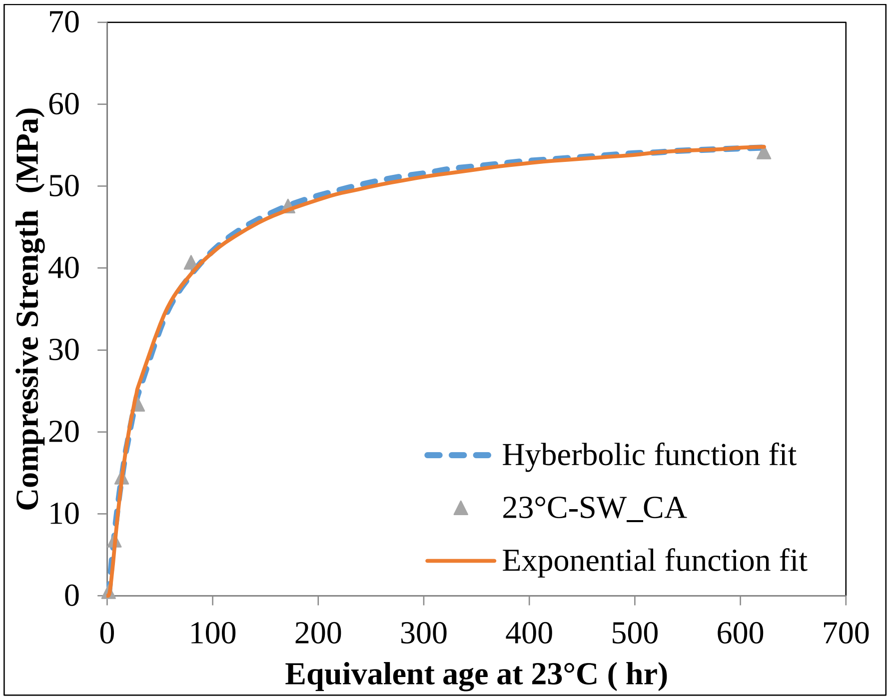

Figure 9-10: Maturity curve for SW-CA

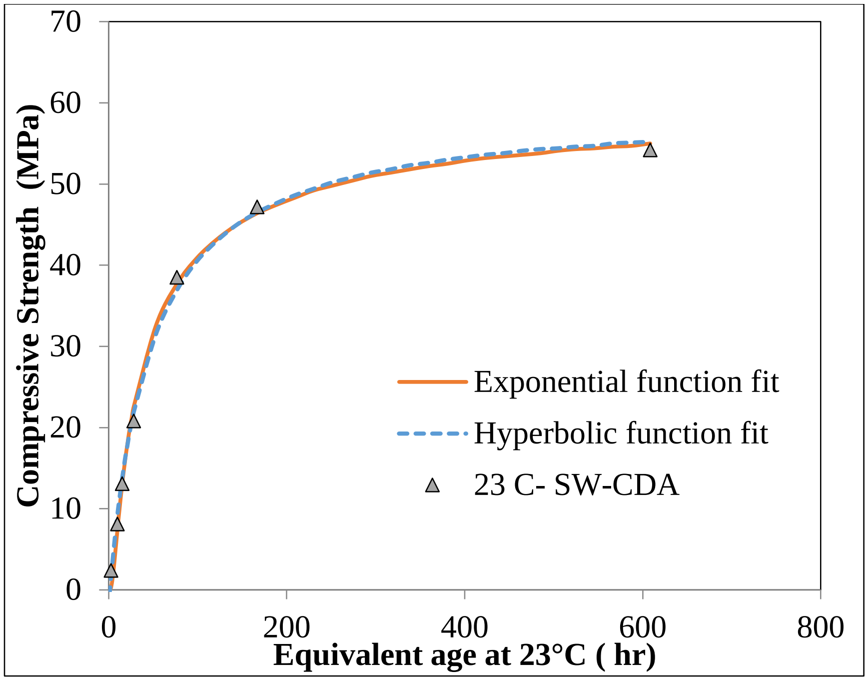

Figure 9-11: Maturity curve for SW-CDA

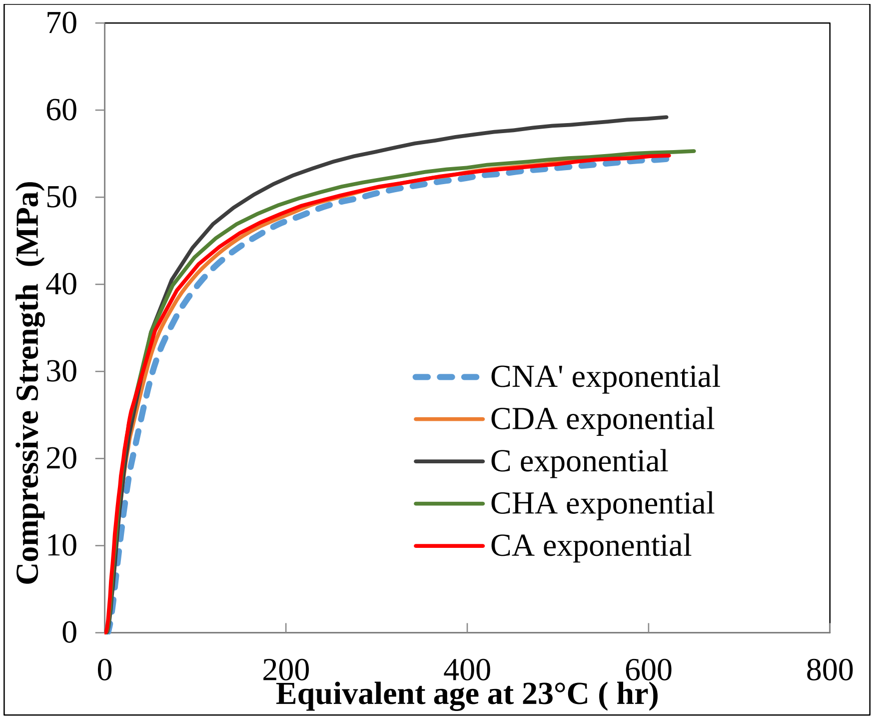

Figure 9-12: Maturity curves for SW Mixes

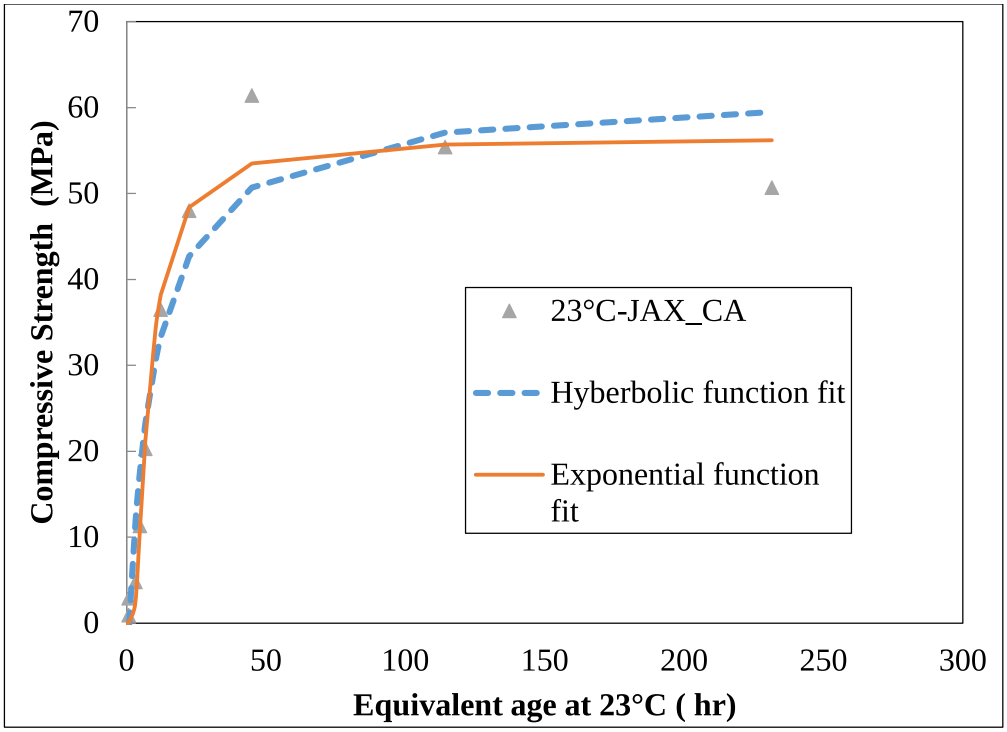

Figure 9-13: Maturity curve for JAX-CA

9.3 References

ASTM C39 / C39M-12a, Standard Test Method for Compressive Strength of Cylindrical Concrete Specimens, ASTM International, West Conshohocken, PA, 2012.

ASTM C109 / C109M-12, Standard Test Method for Compressive Strength of Hydraulic Cement Mortars (Using 2-in. or [50-mm] Cube Specimens), ASTM International, West Conshohocken, PA, 2012.

ASTM C1074-04, Standard Practice for Estimating Concrete Strength by the Maturity Method, ASTM International, West Conshohocken, PA, 2004.

Carino, N. J. (2004). "The Maturity Method." *Handbook on Nondestructive Testing of Concrete*, V. M. Malhotra and N. J. Carino, eds., CRC Press, Boca Raton, FL.

Carino, N. J., and Tank, R. C. (1992). "Maturity Functions for Concretes Made with Various Cements and Admixtures." *ACI Materials Journal*, 89(2), 188–196.

Freiesleben Hansen, P., and Pedersen, J. (1977). "Maturity computer for controlled curing and hardening of concrete." *Nordisk Betong*, 1, 19–34.

CHAPTER 10 Cracking Potential Prediction using HIPERPAV

10.1 Introduction

Due to the high costs incurred and traffic implications associated with repairing slabs, it is important to be able to control induced tensile stresses to reduce the cracking risk of early-age concrete which would subsequently minimize repair work. From the published literature, there are certain mixture design considerations and construction practices which can help reduce these induced tensile stresses in repair slabs. However, due to contractors trying to meet the high-early-strength requirements, some of these recommendations are overlooked, and early-age cracking is still a problem in the field.

Early-age cracking in concrete pavement repair slabs is a recurring problem which can have damaging effects on the long-term durability and serviceability of the concrete. One of the most common causes of early-age cracking in concrete is a change in volume resulting from any one or combination of the following: plastic shrinkage, autogenous shrinkage, drying shrinkage, and thermal contraction. Due to the concrete pavement repair slab being restrained by the existing pavement slabs and by the friction between the slab and the subbase, a reduction in volume induces tensile stresses. As these induced tensile stresses increase and become equal to or greater than the tensile strength of the early-age concrete, which is relatively low compared to the concrete's ultimate tensile strength, the risk of cracking increases.

10.2 Modeling Stress-Strength Relationship of Concrete Pavement Slabs

To simulate early-age induced tensile stress development, any model used should take into account the changing thermal and moisture gradients in the pavement, the changing concrete elastic modulus as the concrete ages, restraint by the subbase, and the high levels of stress relaxation at early ages. Several software packages have been developed to assess the cracking risk associated with changing specific parameters that affect the first 72 hours of a concrete mixture's performance. In this research, the Federal Highway Administration (FHWA)-sponsored software package HIPERPAV (The Transtec Group 2009) was used to predict the cracking risks associated with different mixtures.

In 1996, The Transtec Group, Inc., supported by FHWA, developed a concrete pavement software package, HIgh PERformance PAVing (HIPERPAV), to model the effects of different combinations of design, construction, and environmental factors on the early-age behavior (first 72 hours) of concrete pavements (Rasmussen et al. 1999). A more recent version of the HIPERPAV software with modeling enhancements and strategy comparisons, HIPERPAV III, was used to predict the stress-strength relationship during the early ages of six concrete mixtures used for pavement slabs.

The HIPERPAV III software is comprised of multiple individual modules, which are used together to predict the evolution of several properties such as temperature, modulus, restraint, stress, and strength of concrete mixtures. The parameters modeled, interdependence of these models, and how they are used to calculate the early-age cracking risk of the concrete pavement slabs are shown in Figure 10-1 (Lee et al. 2003; McCullough and Rasmussen 1998; J Mauricio Ruiz et al. 2005).

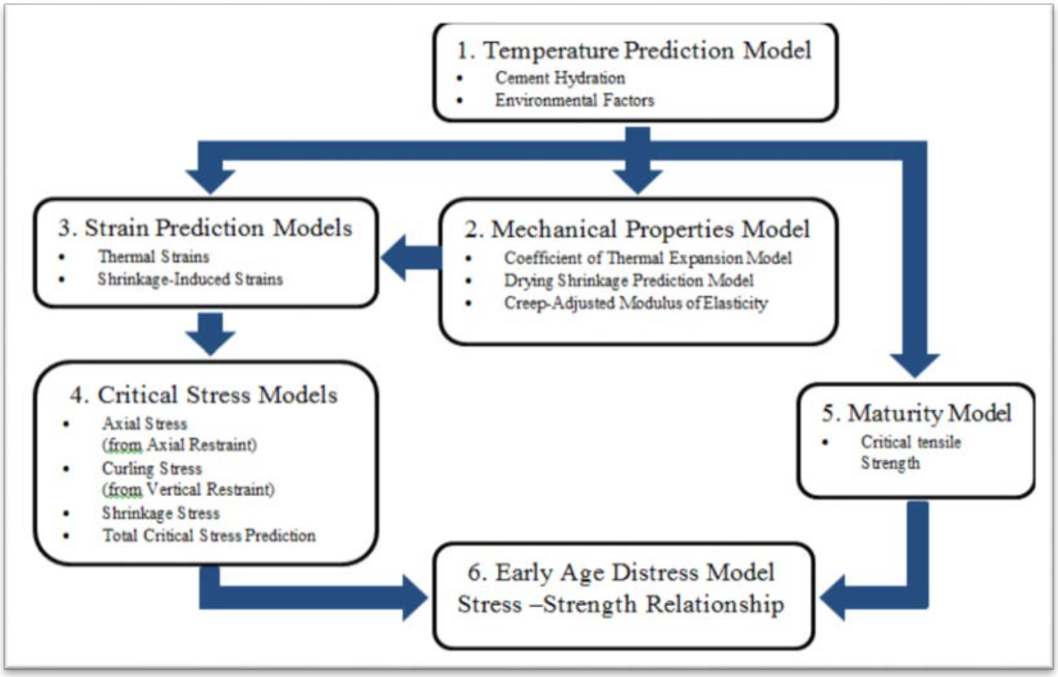

Figure 10-1: Flow chart of HIPEPRAV models used to predict cracking potential

The steps outlined in the flow chart which are used to predict the stress-strength relationship are described in more detail as follows (Lee et al. 2003; McCullough and Rasmussen 1998; Rasmussen et al. 1999; Ruiz et al. 2005):

10.2.1 HIPERPAV Temperature Prediction

HIPERPAV III first uses the experimentally determined hydration data and the environmental factors of each location to predict the concrete temperature profile for each mixture. The equation used to determine the total heat of hydration of cement, H_u, is shown in Equation 2-13 (McCullough and Rasmussen 1998).

The boundary conditions affecting heat transfer associated with the concrete pavement slab are different for the top and bottom of the slab. The top of the slab is subjected to the daily environmental conditions; therefore, convection, irradiation, and solar absorption must be taken into account. The bottom surface of the slab is affected by heat conduction due to the relative temperature difference between the slab and the subbase. The temperature on the top surface of the slab is represented by Equation 10-1; while the temperature on the bottom surface is shown in Equation 10-2 (McCullough and Rasmussen 1998):

$$-k\nabla T \cdot \tilde{n} + q_c + q_r - q_s = 0 \qquad \text{Equation 10-1}$$

$$-k\nabla T \cdot \tilde{n} = 0 \qquad \text{Equation 10-2}$$

where

k = thermal conductivity (W/m·°C),
∇T = temperature gradient (°C/mm),
q_c = heat flux due to convection (W/m^3),
q_r = heat flux due to irradiation (W/m^3),
q_s = solar radiation absorption (W/m^3), and
ñ = direction of heat flow by vector notation

After taking into account the heat of hydration and environmental factors, the temperature of the concrete can be calculated using the general model of heat transfer in two dimensions according to Equation 10-3 (Reynolds and Perkins 1977).

$$\frac{\partial}{\partial x}\left(k\frac{\partial T}{\partial x}\right) + \frac{\partial}{\partial y}\left(k\frac{\partial T}{\partial y}\right) + Q_h = \rho C_p \frac{\partial T}{\partial t} \qquad \text{Equation 10-3}$$

10.2.2 HIPERPAV Mechanical Properties Prediction

HIPERPAV III uses the predicted temperature model to predict the mechanical properties of the concrete such as tensile strength, age-dependent coefficient of thermal expansion (CTE), modulus of elasticity, and drying shrinkage.

10.2.2.1 Tensile Strength

The maturity method outlined in ASTM 1074 is used to calculate the equivalent age of each mixture to determine the tensile strength of the concrete as it evolves with age. The equivalent age of the concrete and degree of hydration equations are presented in Equations 2-6 and 2-10. The compressive or tensile strength can be calculated using the degree of hydration parameters. For HIPERPAV III, the tensile strength will be calculated since it is needed for comparison to the induced tensile stresses. The tensile strength equation is shown in Equation 10-4 (McCullough and Rasmussen 1998):

$$S_{tensile} = S_{28,tensile}\left(\frac{\alpha_t - \alpha_{crit}}{\alpha_{28} - \alpha_{crit}}\right) \qquad \text{Equation 10-4}$$

where

$S_{tensile}$= tensile strength of concrete at age t (lbf/in^2),
$S_{28,\ tensile}$= 28-day tensile strength of concrete from laboratory testing,
α_t=degree of hydration at specific time,
α_{crit}=degree of hydration at final set, and
α_{28}=degree of hydration 28 days

10.2.2.2 Age-Dependent Coefficient of Expansion

The CTE is essential in simulating the thermally-induced deformations of the concrete slab. The CTE of the concrete mixture is calculated using the CTE of both the paste, which drastically decreases with age, and the aggregate as expressed in Equation 10-5 (McCullough and Rasmussen 1998):

$$\psi_{conc} = C_m\left[\sum_{i=1}^{\#\,of\,agg}\left(\psi_{agg,i}\frac{V_{agg,i}}{V_{conc}}\right)+\left(\psi_{paste}\frac{V_{paste}}{V_{conc}}\right)\right] \qquad \text{Equation 10-5}$$

where

ψ_{conc}= age-dependent CTE of concrete mixture (με/°C),
C_m= moisture correction factor,
$\psi_{agg,i}$= age-dependent CTE of i^{th} aggregate (με/°C),
ψ_{paste}= age-dependent CTE of paste,
$V_{agg,i}$= volume of i^{th} aggregate in mixture (m^3),
V_{paste}= volume of paste in mixture (m^3), and
V_{conc}=total volume of concrete mixture (m^3)

10.2.2.3 Age-Dependent Modulus of Elasticity

Concrete is a visco-elastic material with an elastic modulus that increases as the concrete hardens (Mindess et al. 2003). Because of this, the modulus of elasticity must be calculated at each age of the concrete after hardening. Through laboratory testing, the modulus of elasticity can be determined at specific test ages. To calculate the elastic modulus at the ages between the tests, the maturity method outlined in ASTM 1074, combined with an empirically-derived elastic modulus-degree-of-hydration fit function, which is usually used to determine strength values, but was modified for modulus and used. Following the Arrhenius relationship, Equation 2-7, which relates temperature with the rate of reaction, the equivalent age is calculated to determine the degree of hydration at each age. The degree of hydration can then be used to calculate the modulus of elasticity as presented in Equations 10-6 and 10-7. Equation 10-6 is very similar to Equation 10-4 used to calculate the tensile strength (ASTM C1074, McCullough and Rasmussen 1998; Poole et al. 2010) :

$$E_t = E_{28}\left(\frac{\alpha_t - \alpha_{crit}}{\alpha_{28} - \alpha_{crit}}\right)^{2/3}$$ Equation 10-6

$$\alpha_{crit} = 0.43 \times w/cm$$ Equation 10-7

where

E_t = modulus of elasticity of concrete at age t,

E_{28} = 28-day modulus of elasticity of concrete from laboratory testing, and

w/cm = water to cementitious materials ratio.

10.2.2.4 Drying Shrinkage

To determine the ultimate drying shrinkage, the strength and elastic modulus at 28 days must be known from laboratory testing. The equations used to calculate the ultimate drying shrinkage ($\varepsilon_{sh\infty}$) are shown in Equations 10-8 through 10-11 (Bazant and Baweja 2000):

$$\varepsilon_{sh\infty} = \varepsilon_{s\infty}\frac{E(607)}{E(t_0 + \tau_{sh})}$$ Equation 10-8

$$E(t) = E(28)\left(\frac{t}{4 + 0.85t}\right)^{1/2}$$ Equation 10-9

$$\varepsilon_{s\infty} = C_1C_2[26w^{2.1}(f'c)^{-0.28} + 270]$$ Equation 10-10

$$\tau_{sh} = 190.8\, t_0{}^{-0.08} f'c^{-0.25}(k_sD)^2$$ Equation 10-11

where

$\varepsilon_{sh\infty}$ = ultimate (final) shrinkage strain,

$\varepsilon_{s\infty}$ = constant strain value determined by Equation 10-9,

E(t) = elastic modulus (lbf/in^2) of the concrete at age t (days) using Equation 10-8,

t = concrete age (days),

t_0 = age of concrete when drying starts (days),

C_1 = 085 for Type II cement,

C_2 = 1.2 for specimens sealed during curing,

w = water content of concrete (lb/ft^3),

f'_c = 28 day strength of concrete (lbf/in^2),

k_s = cross section shape factor, approx. 1 for slabs,

D = thickness of slab (in), and

τ_{sh} = shrinkage half-time (days)

10.2.3 HIPERPAV Strain Prediction

The outputs from the temperature development, modulus, and drying shrinkage models are used to predict the thermal and shrinkage-induced strains. The strains are calculated as “free strains” as if the concrete slab was unrestrained (the restraint is accounted for later in the software).

10.2.3.1 HIPERPAV Thermal Strain Prediction

The thermal strain is determined by Equation 10-11 (McCullough and Rasmussen 1998):

$$\nabla\varepsilon_T = \nabla T \cdot \psi_{conc} \qquad \text{Equation 10-12}$$

where

$\nabla\varepsilon_T$ = thermal strain gradient (με/mm),

∇T = temperature gradient (°C/mm), and

ψ_{conc} = CTE of concrete mixture.

The thermal strain can be broken up into two models, the curling strain model and the axial thermal strain model. The curling model is presented in Equation 10-13 (Bradbury 1938):

$$\varepsilon_{curl} = \frac{C\psi\Delta T}{2} \qquad \text{Equation 10-13}$$

where

ε_{curl} = curling strain,

C = coefficient dependent on slab length and relative stiffness,

ψ = coefficient of thermal expansion of concrete, and

ΔT = temperature differential (°F)

Equations 10-14 and 10-15 show the axial thermal strain model (McCullough and Rasmussen 1998):

$$\Delta T_z = \frac{\sum_{z=0}^{h}\left[\left(T_{z,current} - T_{z,final\,set}\right)\Delta z\right]}{h} \qquad \text{Equation 10-14}$$

$$\varepsilon_z = \Delta T_z \psi \qquad \text{Equation 10-15}$$

where

ΔT_z = temperature differential used by axial strain model (°C),

h = total slab thickness (mm),

T_z = slab temperature at depth z (°C),

Δz = change in depth (mm),

ε_z = unrestrained axial strain, and

ψ = coefficient of thermal expansion of concrete

10.2.3.2 HIPERPAV Shrinkage Strain Prediction

The total strain due to shrinkage(ε_{cs}) is broken down into autogenous shrinkage strain (ε_{cs0}) and drying shrinkage strain(ε_{csd}). Autogenous shrinkage strain is calculated for concrete mixtures with w/cm ratio below 0.45 by using Equation 10-16 (Ruiz et al. 2005):

$$\varepsilon_{cs0}(t) = \varepsilon_{s0\infty}\beta_{s0}(t) \qquad \text{Equation 10-16}$$

where

$$\beta_{s0}(t) = exp\left[-\left(\frac{t_{s0}}{t - t_{start}}\right)^{0.3}\right] \qquad \text{Equation 10-17}$$

$$\varepsilon_{s0\infty} = \left(-0.65 + \frac{1.3w}{B}\right) \cdot 10^{-3} \qquad \text{Equation 10-18}$$

where

$\beta_{s0}(t)$ = time distribution of autogenous shrinkage,

$\varepsilon_{s0\infty}$ = final value of autogenous shrinkage strain,

t_{s0} = 5 days,

t_{start} = 1 day,

w = water content (kg/m^3), and

B = cement content + silica fume content (kg/m^3)

Drying shrinkage strain is calculated using Equations 10-19 through 10-22 (Ruiz et al. 2005a):

$$\varepsilon_{csd}(t) = \alpha_{sd}\varepsilon_{sd,tot}\beta_{sd}(t)\beta_{sd,RH}$$ Equation 10-19

where:

$$\alpha_{sd} = \frac{u \cdot l_{sd}}{A_c} \leq 1$$ Equation 10-20

$$l_{sd} = \frac{l_{sd,ref}}{0.5 - \frac{w}{B}}$$ Equation 10-21

$$\beta_{sd}(t) = \left(\frac{t - t_s}{t_{sd} + t - t_s}\right)^{0.5}$$ Equation 10-22

where

$\varepsilon_{csd}(t)$ = additional strain due to drying/wetting of concrete,

α_{sd} = cross section affected by surface drying,

$\varepsilon_{sd,tot}$ = final drying shrinkage,

$\beta_{sd,RH}$ = coefficient of drying shrinkage,

$\beta_{sd}(t)$ = time development of drying shrinkage,

u = perimeter of cross section subject to environmental humidity,

A_c = cross section perpendicular to water flow,

l_{sd} = length of surface for water exchange,

$l_{sd,ref}$ = 0.0045 m,

$t - t_s$ = time after start of drying and wetting (days),

t_s = age of concrete at start of drying and wetting (>1 day), and

t_{sd} = 200 days, typical rate of humidity exchange

10.2.3.3 Creep-Adjusted Modulus of Elasticity Prediction

Concrete stress relaxation occurs in concrete at especially high rates at early ages. This results in early-age concrete stresses significantly different than what calculated elastic stresses would indicate. In HIPERPAV, these effects are calculated using a creep-adjusted modulus (Mccullough and Rasmussen 1999). The stresses are calculated using the base restraint, strain, and creep adjusted modulus. Equations 10-23 through 10-25 are used in HIPERPAV to determine the modulus after this stress relaxation is accounted for (McCullough and Rasmussen 1998):

$$E_{eff} = \frac{E_0}{|1 + J_t E_0|}$$ Equation 10-23

where

$$J_t = J'_t \delta_t \xi_t \Phi_t$$ Equation 10-24

$$J'_t = [28.74(1 - e^{-0.801t}) + 8.13(1 - e^{-45.38t}) + 4.468t] \times 10^{-6}$$ Equation 10-25

where

E_0 = Elastic modulus at time of load application (final set),

J_t = adjusted creep factor (mm^2/N),

J'_t = creep factor (mm^2/N),

δ_t = stress correction factor = $0.017\sigma + .701$,

ξ_t = loading time correction factor = $-1.107\ln(\tau) + 1.538$,

Φ_t = temperature correction factor = $0.0257T + 0.487$,

T = age of concrete (days),

σ = average concrete stress (N/mm^2),

τ = time from start of loading (days), and

T = average concrete temperature(°C)

10.2.4 HIPERPAV Critical Stress Prediction

The critical stress models include the previously calculated axial restraint and axial stresses, vertical restraint and curling stresses, and shrinkage stresses. The maximum tensile stress resulting from these strains is then used to determine the critical stress for the early age concrete pavement slab as shown in Equation 10-26 (Mccullough and Rasmussen 1999):

$$\sigma_{critical} = MAX_{TENSILE}\begin{Bmatrix}(\varepsilon_{axial,top}+\varepsilon_{cs})\times R_F\times E_{eff}+\sigma_{curl,top}\\ \varepsilon_{axial,mid}\times R_F\times E_{eff}\\ \varepsilon_{axial,bottom}\times R_F\times E_{eff}+\sigma_{curl,bottom}\\ 0\end{Bmatrix} \qquad \text{Equation 10-26}$$

where

$MAX_{TENSILE}$ = maximum tensile stress,

$\varepsilon_{axial,\ top}$ = axial strain at top of slab,

R_F= Restraint factor, function of base type, joint spacing, thickness, modulus,

$\sigma_{curl,\ top}$ = curling stress at top of slab,

$\varepsilon_{axial,\ mid}$ = axial strain at mid-depth of slab,

$\varepsilon_{axial,\ bottom}$ = axial strain at bottom of slab, and

$\sigma_{curl,\ bottom}$ = curling stress at bottom of slab

After predicting the concrete temperature, CTE, shrinkage, creep-adjusted modulus of elasticity, free strains, and resulting stresses from restraint, the total critical stresses of the concrete pavement slab at each age can be compared to the concrete's predicted strength at the same age. From this comparison, the cracking risk for the first 72 hours of the concrete pavement slab can be assessed. As shown in Figure 10-2, HIPERPAV III displays the results in an analysis tab which shows the critical stresses at the bottom of the slab in blue, critical stresses at the top of the slab in yellow, the maximum critical stress as a solid red line, and the tensile strength of the concrete slab as a solid blue line. If the stress exceeds the strength as shown in this sample figure, HIPERPAV III displays a warning at that respective age. However, since cracking can initiate if the tensile stresses in the concrete pavement are about 70 percent of the ultimate tensile strength of concrete (Hsu et al. 1963), steps should be taken to not only keep the induced tensile stresses below the tensile strengths, but also to ensure that these stresses are minimized as much as possible.

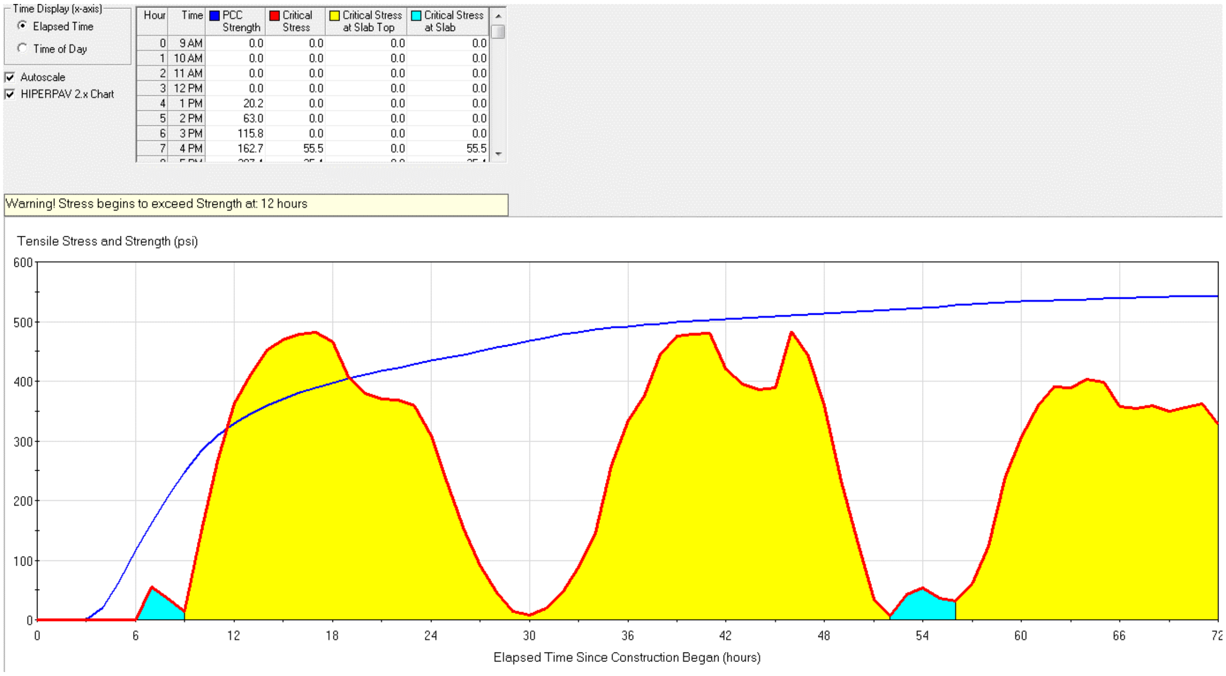

Hour	Time	🟦 PCC Strength	🟥 Critical Stress	🟨 Critical Stress at Slab Top	🟦 Critical Stress at Slab
0	9 AM	0.0	0.0	0.0	0.0
1	10 AM	0.0	0.0	0.0	0.0
2	11 AM	0.0	0.0	0.0	0.0
3	12 PM	0.0	0.0	0.0	0.0
4	1 PM	20.2	0.0	0.0	0.0
5	2 PM	63.0	0.0	0.0	0.0
6	3 PM	115.8	0.0	0.0	0.0
7	4 PM	162.7	55.5	0.0	55.5

Warning! Stress begins to exceed Strength at: 12 hours

Figure 10-2: HIPERPAV III sample analysis output

10.3 Findings

The concrete mixture designs and construction practices chosen for two specific locations were input into the HIPERPAV III software. The mixture design at one location was used with a varying accelerator dosage to observe the effects on cracking potential. HIPERPAV III was used to analyze and compare the effects of these concrete mixture designs and construction practices used on actual slabs in the field to determine the cracking risk of the concrete pavement repair slab.

Six mixtures were analyzed using HIPERPAV III software. Five of the mixtures used the same cement, SW, and were based on one mixture design, Florida Department of Transportation (FDOT) Gainesville slab mixture, while the sixth mixture used JAX cement and was based on FDOT Jacksonville slab mixture. The concrete mixture proportions used in the analysis are shown in Table 10-1.

Table 10-1: Mixture designs

Mixture Weight per 1 yd^3						
	SW-C	**SW-CNA**	**SW-CHA**	**SW-CA**	**SW-CDA**	**JAX-CA**
Materials	Wt. (lb)	Wt. (lb)	Wt. (lb)	Wt. (lb)	Wt. (lb)	Wt. (lb)
Cement	900	900	900	900	900	845
Coarse Agg (SSD)	1680	1680	1680	1680	1680	1611
Fine Agg (SSD)	828	828	828	828	828	1079
AEA	-	0.195	0.195	0.195	0.195	0.488
Type A and D	-	3.367	3.367	3.367	3.367	2.063
Type E	-	-	16.801	33.602	67.203	58.798
Type A and F	-	-	-	-	-	1.309
Mixture Water	348	348	338	328	307	239
w/c	0.384	0.384	0.384	0.384	0.384	0.325

A field slab replicating the SW-CA concrete mixture, a mixture with a known history of cracking problems when used in Miami, FL was prepared at the State Materials Office (SMO) in Gainesville, FL. All inputs used for the modeling of the SW mixtures used the SMO field data. These parameters included geometry, soil properties, and construction practices. However, the field data sheet for the SMO field study reports an unintended overdose of accelerator which is between SW-CA and SW-CDA. The SW-CA mixture was also analyzed using the Miami (MIA) environmental conditions for the time and dates in which concrete placement and cracking was observed; however, the geometry, soil properties, and construction practices from the SMO slab were still used for the MIA analysis since this information was not available for the MIA location. The JAX-CA mixture was compared to a field slab in Jacksonville, FL. All properties from the field slab – geometry, soil properties, and construction practices – were used for the analysis of the JAX mixture.

10.4 HIPERPAV Inputs

To analyze the cracking potential of the concrete mixes using HIPERPAV III, both mechanical and material properties of the concrete mixtures were needed. These properties were determined by performing laboratory testing on each mixture. The construction inputs used for each analysis are shown in Table 10-2.

Table 10-2: HIPERPAV mixture inputs

Mixture	**SW**	**JAX**
General		
Reliability Level (%)	90	90
Slab Thickness (in)	11	9
Slab width (ft)	12	12
Transverse Joint Spacing (ft)	13	6
Dowels	N/A	N/A
Slab Support		
Base Material	Unbound Agg Subbase	Unbound Agg Subbase
Use Subgrade Modulus (psi)	40,000	35,346
Subbase Thickness (in)	8	8
User-Defined Modulus (psi)	87,404	87,404
Axial Restraint	Est. from Material Type	Est. from Material Type
Cement		
ASTM Cement Type	Type I	Type I
Blaine Fineness (m^2/kg)	442	427
PCC Properties		
CTE (/°F)	Default for Limestone Coarse Aggregate	Default for Limestone Coarse Aggregate
Construction Operations		
Construction Day and Time	10/24/13 9:00 AM	10/10/13 1:00 AM
Fresh Concrete Temperature (F)	77	100.4
Initial Subbase Temperature (F)	52	70
Base state	Moist	Moist
Curing Method	Curing Compound	Plastic sheeting
Age Curing Applied (hr)	2	0.6
Age Curing Removed (hr)	5	3.15
Saw cutting Time(hr)	Saw at Optimum Time	3.15

Although saw cutting was not reported for the SMO field study, HIPERPAV strongly recommends not skipping this input as the software calculates stresses based on the assumption that the joint spacing is infinite until saw cutting is considered (McCullough and Rasmussen 1998).

For this reason, an optimal time was chosen for the SMO slab. It must be noted that the optimal time is not the same for each mixture.

The concrete mixture property inputs for HIPERPAV III are shown in Table 10-3. These inputs were obtained from the laboratory testing explained previously along with field data reports. The concrete strength data used to develop the maturity-splitting tensile strength relationship for the concrete mixtures is shown in Figure 10-3.

Table 10-3: HIPERPAV inputs – PCC properties

HIPERPAV	**SW-C**	**SW-CNA**	**SW-CHA**	**SW-CA**	**SW-CDA**	**JAX-CA**
Strength Type	Tensile	Tensile	Tensile	Tensile	Tensile	Tensile
28 Day Strength(psi)	765	685	670	640	615	627
28 Day Modulus(psi)	5325000	4925000	4675000	4675000	4825000	5033333
Heat of Hydration(J/kg)	481800	481800	481800	481800	481800	464960
HoH-based E_A(J/mol)	33004	30784	24148	25420	25574	22978
β =	0.836	1.072	0.944	0.825	0.743	1.072
τ (hrs)=	11.596	11.931	8.759	7.938	6.783	7.000
α_u =	0.741	0.687	0.725	0.746	0.772	0.737
Maturity Data	Tensile	Tensile	Tensile	Tensile	Tensile	Tensile
Strength- based E_A(J/mol)	40467	34052	28049	44244	45787	32416

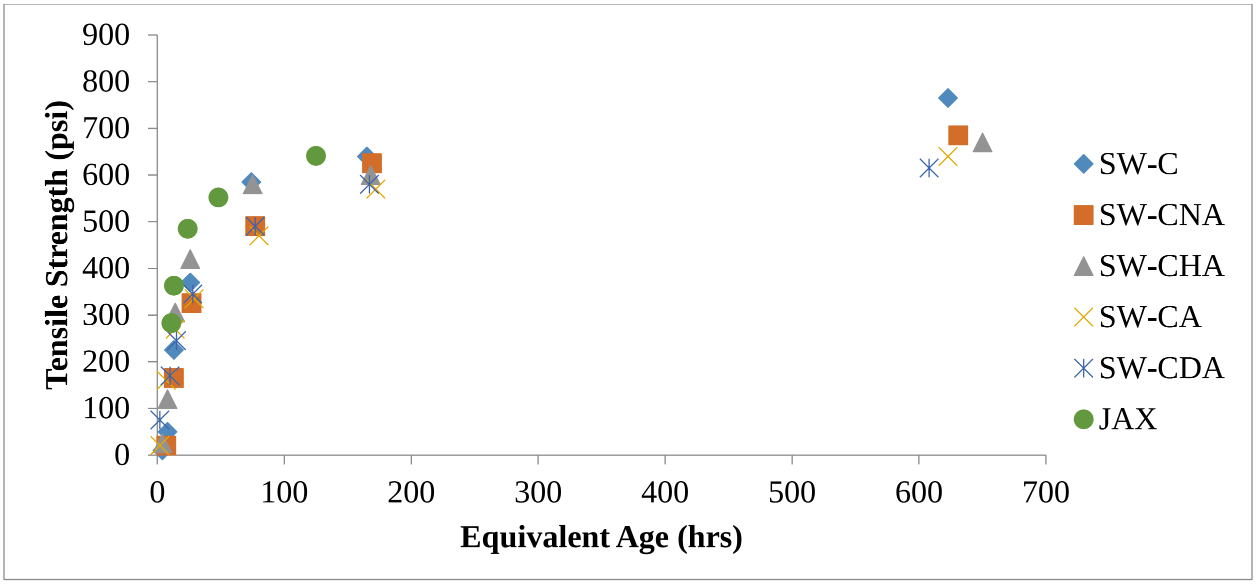

Figure 10-3: Tensile strength – maturity relationship input in HIPERPAV III

Figures 10-4 through 10-11 show the profiles of the environmental factors for the mixtures at the MIA, SMO, and JAX locations, which were used for the analysis in HIPERPAV III. The environmental factors were obtained from www.weatherspark.com for the respective location and date and time of each field mixture.

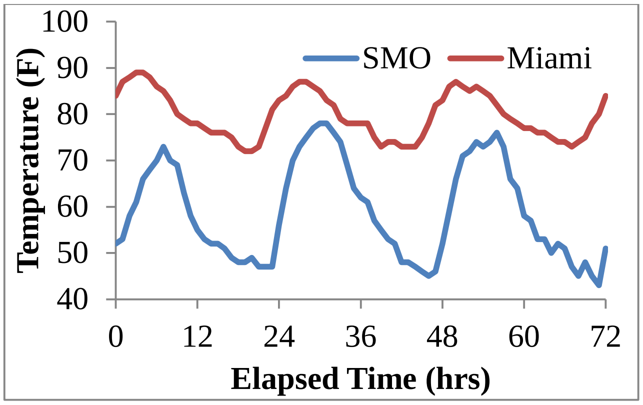

Figure 10-4: SW ambient temperature profiles

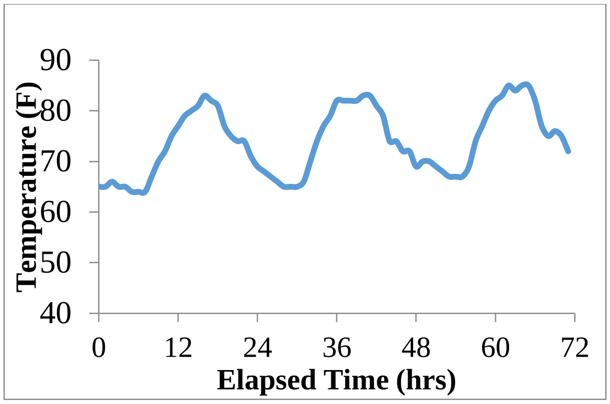

Figure 10-5: JAX temperature profile

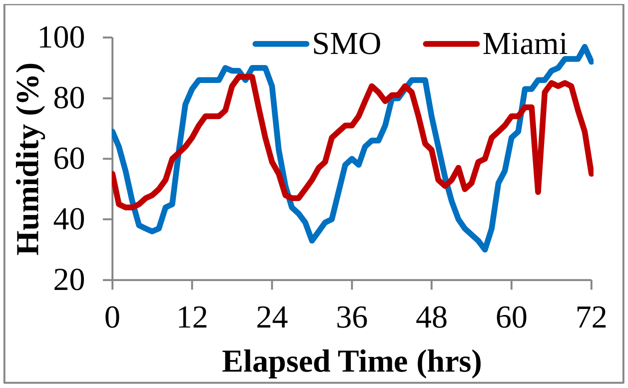

Figure 10-6: SW humidity profiles

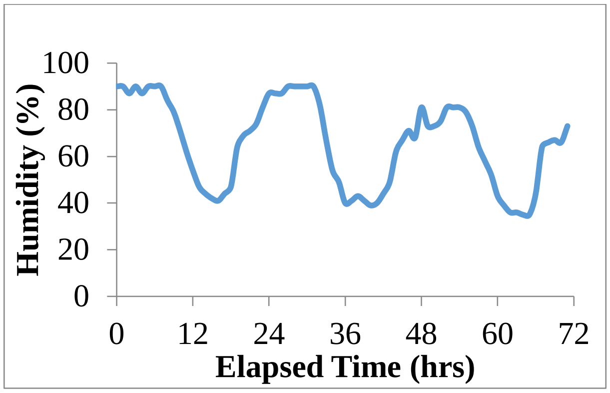

Figure 10-7: JAX humidity profile

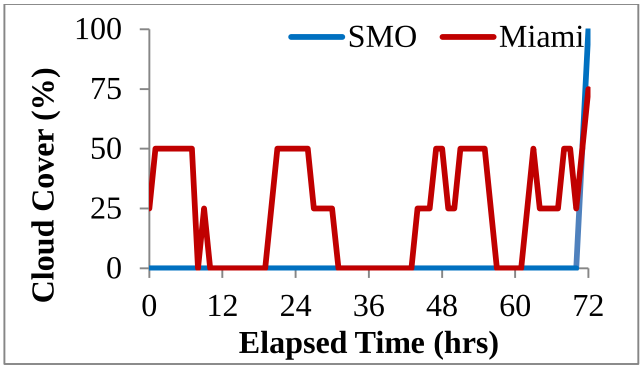

Figure 10-8: SW cloud cover profiles

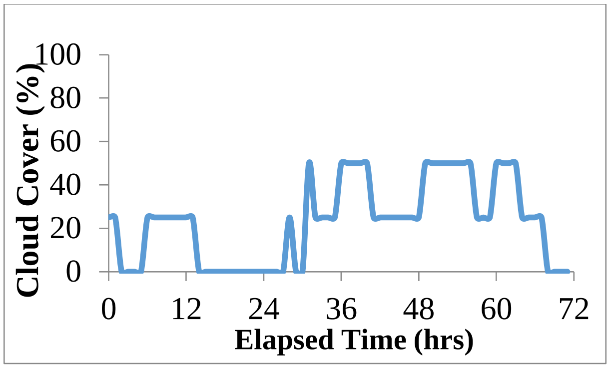

Figure 10-9: JAX cloud cover profile

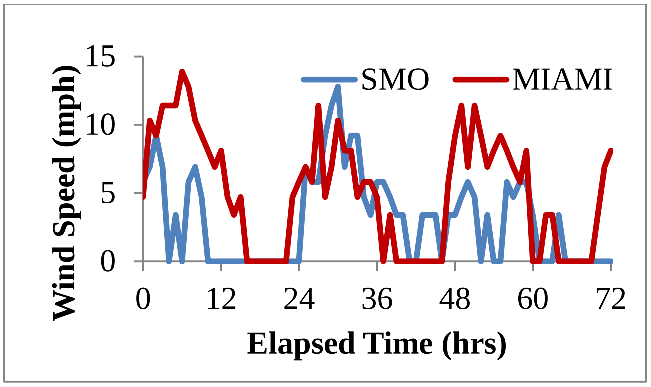

Figure 10-10: SW wind speed profiles

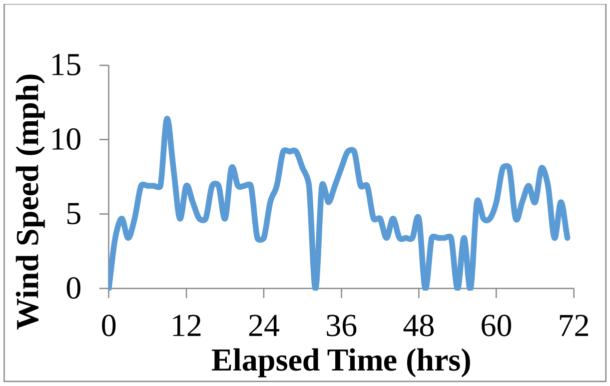

Figure 10-11: JAX wind speed profile

10.5 Analysis

10.5.1 Effect of Accelerator Dosage

As seen in Figure 10-12, at 12 hours, the SW-C and SW-CHA mixtures are the last mixtures to have their stress exceed their strength. The stress of SW-CA exceeds its strength at 5 hours, while for SW-CDA it is at 4 hours. SW-CNA did not follow the same trends since without the addition of an accelerator, the retarding agent controlled the mixture.

Table 10-4: Initial time stress exceeds strength

Initial Time Stress Exceeds Strength (hr)	
SW-C	No Cracking
SW-CHA	6
SW-CA	5
SW-CDA	4

The stress-to-strength ratios of the SW mixtures under SMO conditions are shown in Figure 10-12. “For concretes with calcium chloride added, strength increases due to the accelerator are proportionately greater at early ages” (Klieger 1958). The results show this increase in early strength; however, there is also an increase in the stresses as the dosage of accelerator is increased, mainly a result of the more rapid increase in elastic modulus and higher temperature change. Since the stresses are exceeding the strengths, the results show that as there is an increase in dosage of accelerator, there is an increase in the cracking potential of the SW concrete pavement slab during the early ages. These results agree with the findings of Hope and Manning who observed significant increases in creep strain when a calcium chloride accelerator was added to a plain concrete mix (Hope and Manning 1971). As the creep strains increase, the induced tensile stresses would also increase which would consequently increase the cracking potential for that mixture.

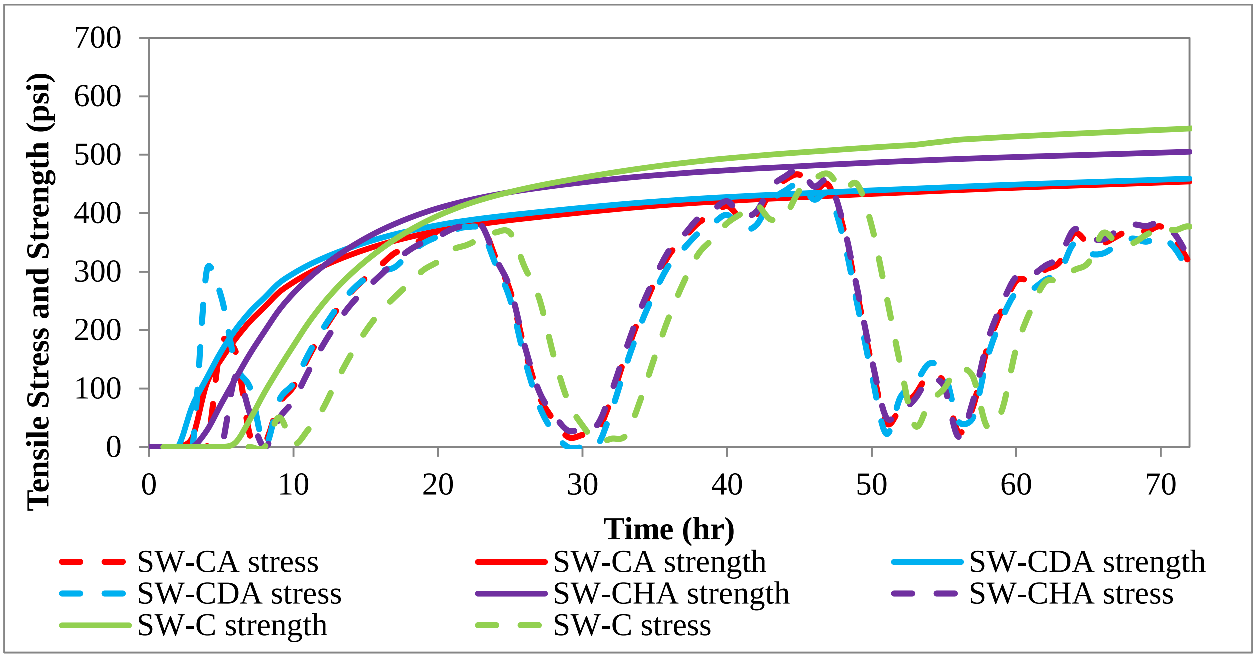

Figure 10-12: Tensile stress and strength of each mixture

10.5.2 Effect of Construction Time of Day

The construction time of a slab will have a direct effect on the ambient temperature, humidity, and solar radiation profile that the concrete is subject to at early ages. These environmental factors can increase the thermal stresses in concrete and cause early-age cracking which can reduce the service life of the concrete mixture (Poole and Riding 2009). To reduce the cracking potential in a concrete mixture the construction time should be chosen carefully.

The field slab for the SW-CA mixture was cast at 9am at the SMO site and between 9 am and 3 pm at the Miami site. The field slab for the JAX mixture was cast in the middle of the night at 1 am. Figure 10-13 shows the stress-to-strength ratio for the SW mixtures if the initial mix time at the SMO was changed in two hour increments. The results show a lower maximum three-day cracking potential for SW construction times between 5 pm and 1 am. These results agree with the findings of Riding et al., where it was observed that tensile stresses at two days for a morning mixture (10:00 am) were 46% higher than for the same concrete mixture cast during the night (10:00 pm) (Riding et al. 2010). In another study, a heightened risk of cracking potential was found in concrete mixtures that were cast between 7am and 5pm (Ruiz et al. 2005b). The findings with this investigation indicate that although the SW-CDA mixture has a consistently higher cracking risk than the other mixtures at each initial start time, the effect of the SW-CDA vs SW-CA on cracking potential is greatly increased during the late morning and early evening hours.

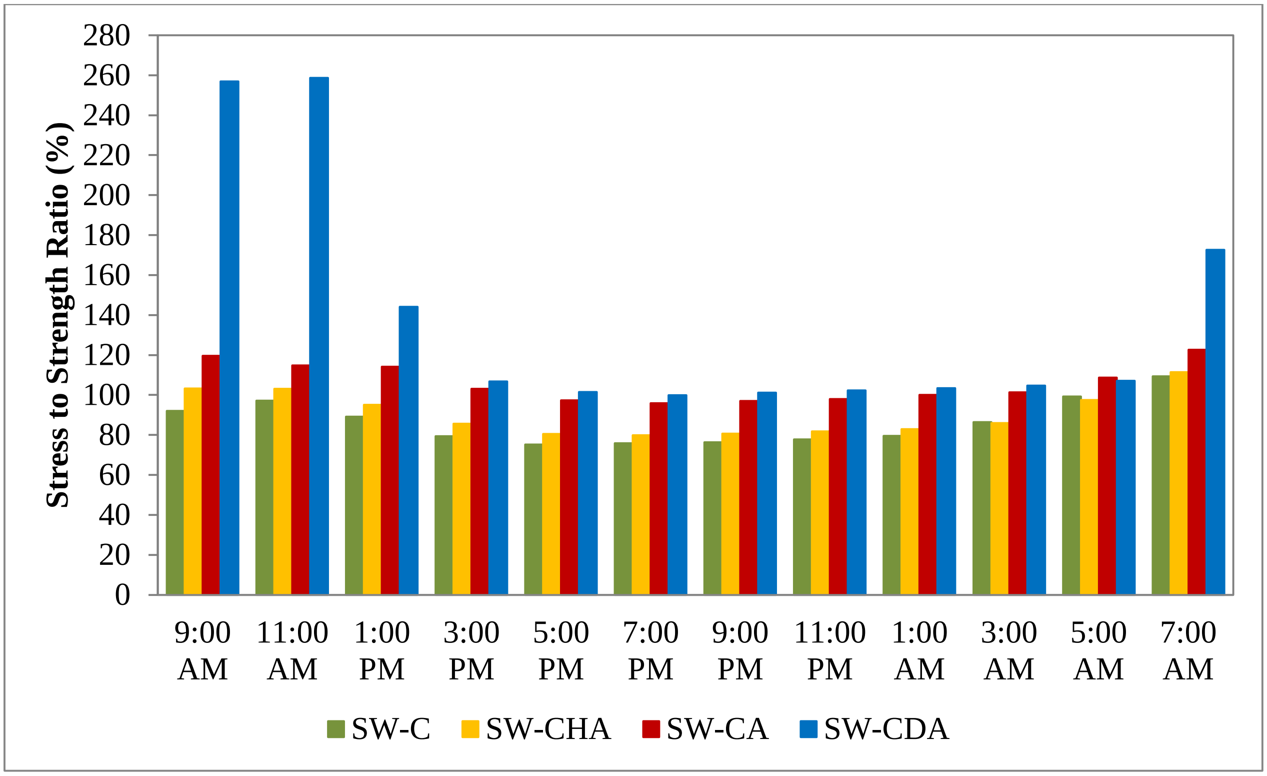

Figure 10-13: Effect of construction time on SW (SMO) cracking potential

The SW-CA mixture at the Miami site has a reported placement time between 9am and 3pm. Figure 10-14 shows that this time range is not the best time to place to decrease the cracking potential. A 3pm placement time is much better than a 9am placement, with a 68 percent stress-to-strength ratio compared to 84 percent, respectively. These results indicate that the best time to start placing the concrete would be around 11 PM.

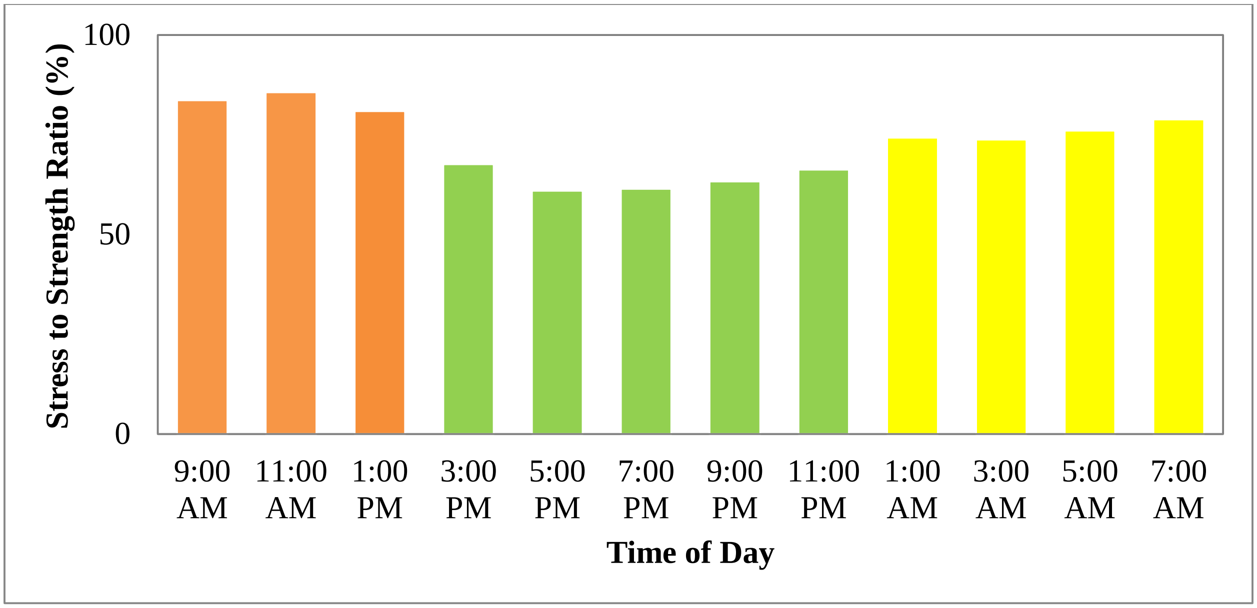

Figure 10-14: Effect of construction time on SW (Miami) cracking potential

Figure 10-15 shows the effect of different construction times on the stress-to-strength ratio for the JAX mixture. These results agree with the SW placement times that the late night hours are better times to place than the morning. All three analyses show that 11pm would be the optimal construction time for these mixtures.

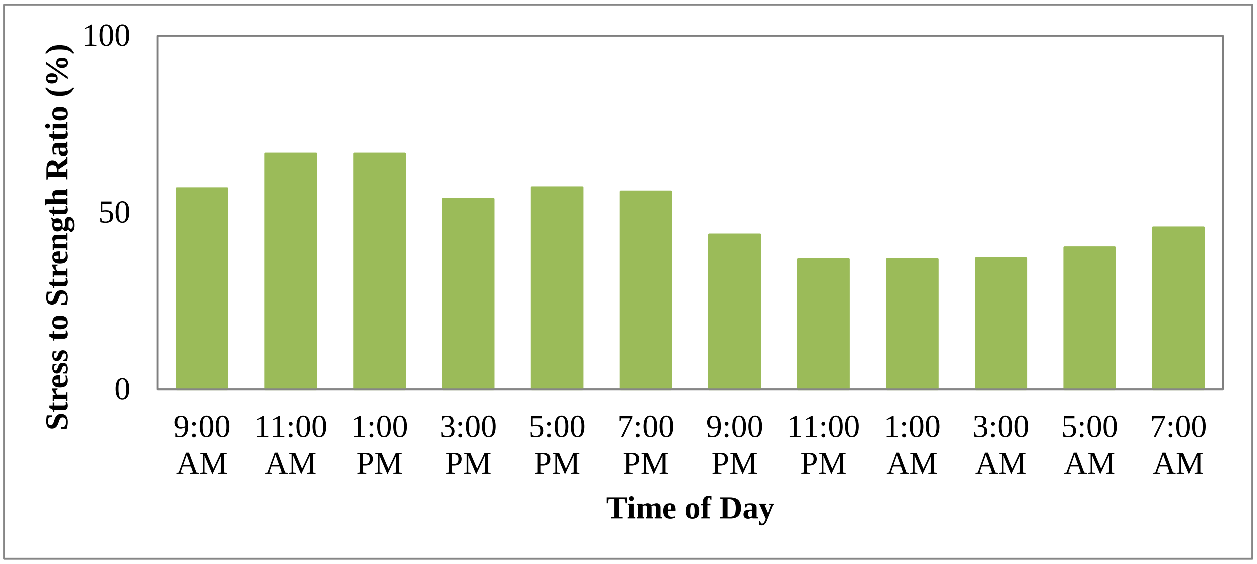

Figure 10-15: Effect of construction time on JAX cracking potential

10.5.3 Effect of Initial Concrete Placement Temperature

Both SW and JAX mixtures are typically placed hot in the field, that is, they both had an initial mixture temperature of 100.4°F (38°C) to increase the strength gain rate. The SMO field slab; however, had an initial portland cement concrete (PCC) temperature of around 77°F (25°C). HIPERPAV was used to make a comparison between placements at different initial temperatures to show the effect that a lower initial temperature would have on the cracking potential of the concrete. Figure 10-16 shows the results of a comparison of initial temperature of the SW-CA mixture if it was placed at the previously determined optimal time of 11 PM. An increase in stress-to-strength ratio can be seen as the initial temperature is changed from 50°F to 110°F. Comparison of the results from the JAX mixture, shown in Figure 10-17, and those for the SW-CA mixture show that an increase in initial temperature will increase the cracking potential of the concrete. At 12 hours, the stress-to-strength values for the JAX mixture at 50°F and 70°F were higher than the hotter mixes, although they were still below a 40% stress-to-strength ratio and not at risk of cracking. The HIPERPAV III analysis shows higher stresses in the bottom of the slab for this mixture at the lower temperatures at 12 hours as shown in Figure 10-18. These higher stresses near the bottom of the slab are most likely a result of early-age curling.

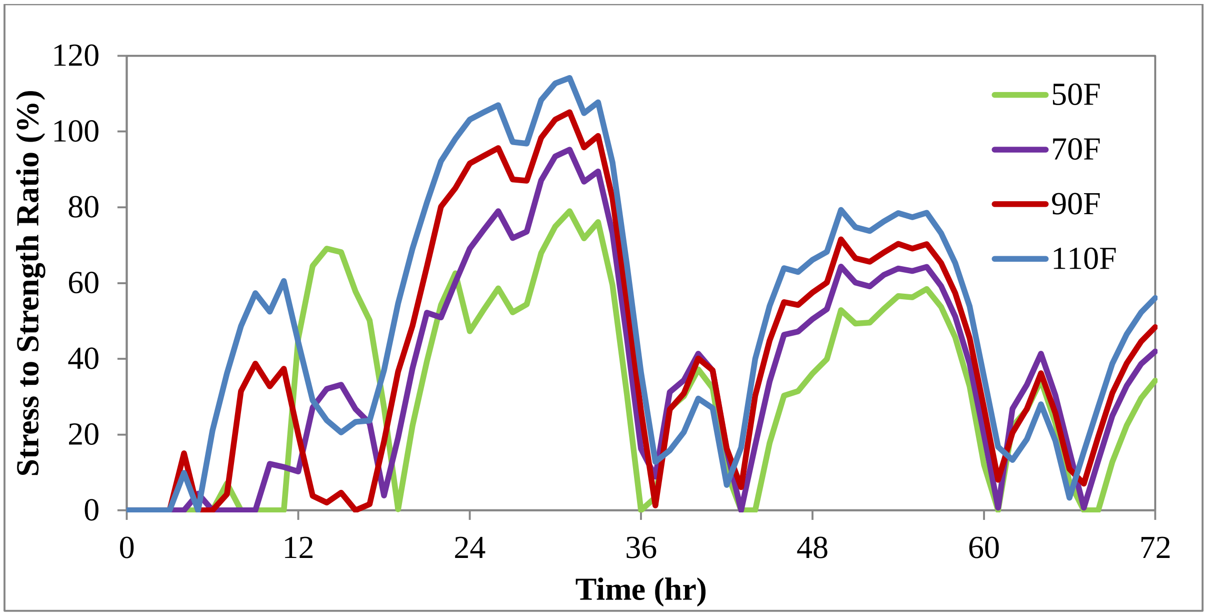

Figure 10-16: SW effect of initial temperature

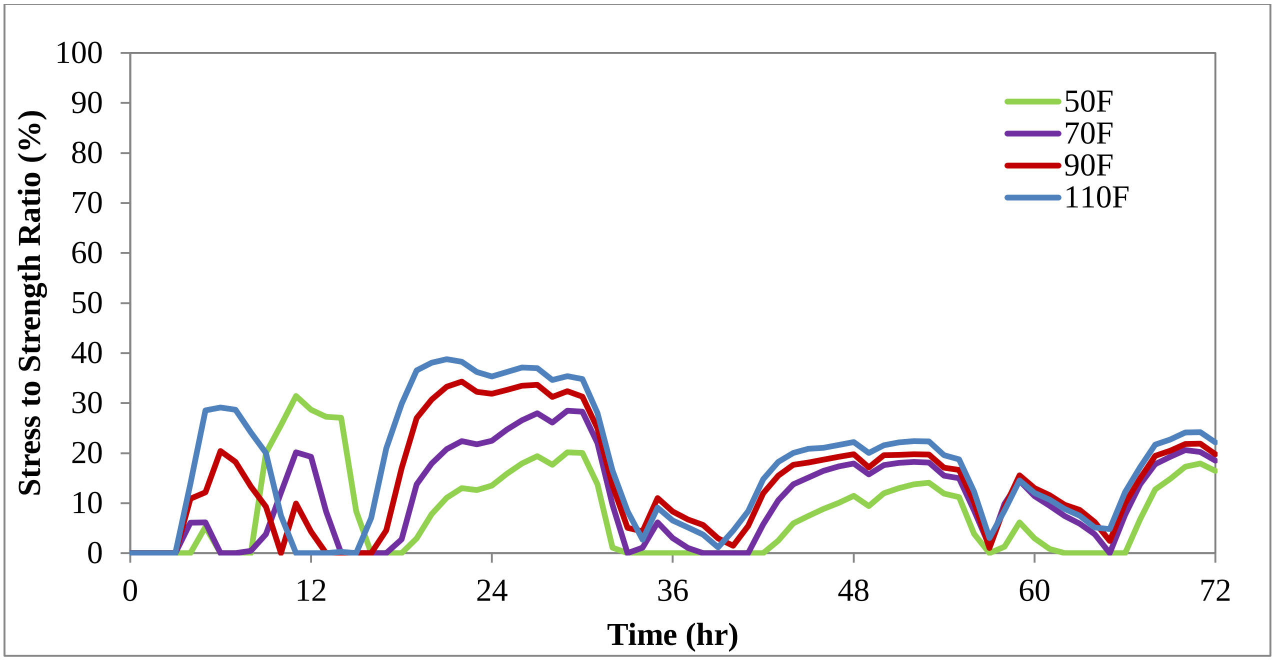

Figure 10-17: JAX effect of initial temperature

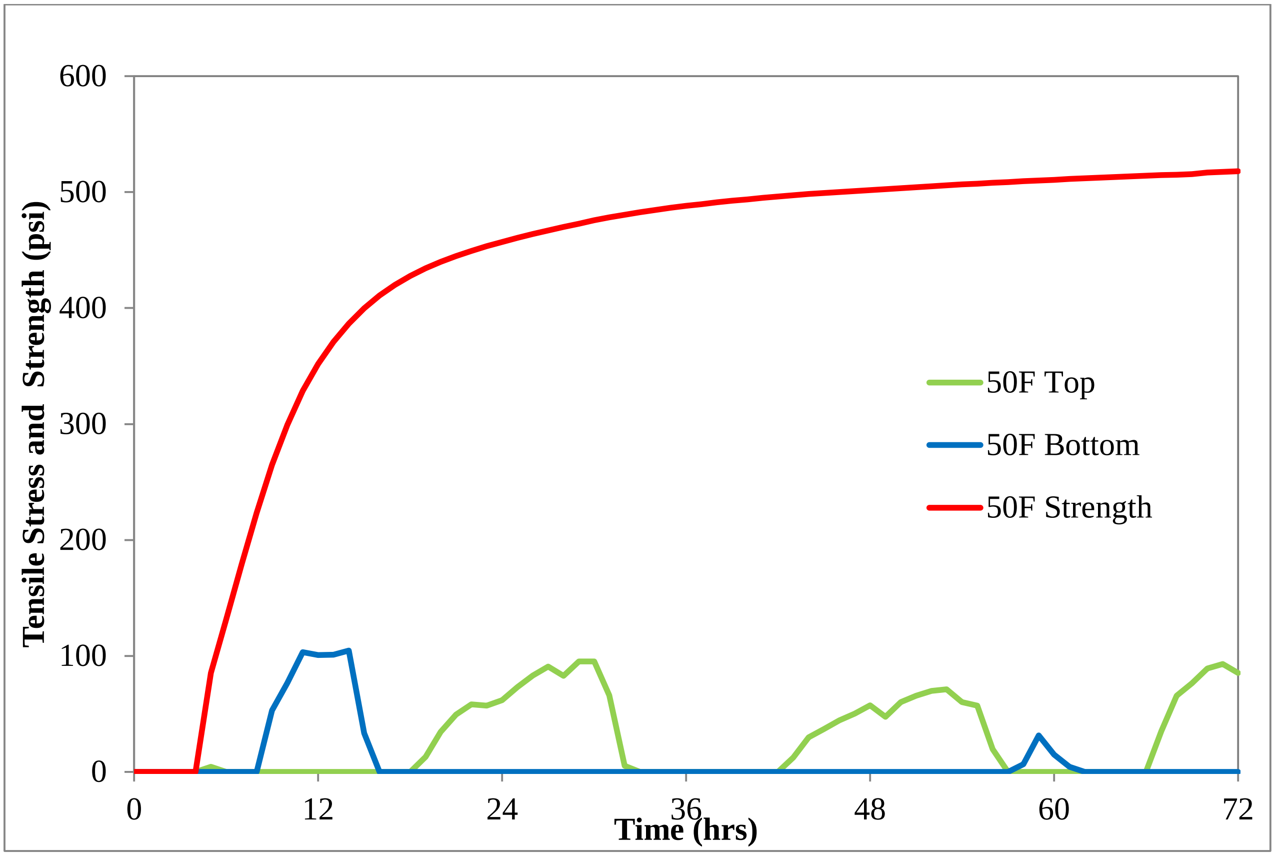

Figure 10-18: JAX mixture strength and stress in the pavement bottom and top for 50°F placement temperature

10.6 Discussion and Conclusions

The results from HIPERPAV III show that an increase in dosage of accelerator does increase the stress-to- strength ratio of the mixture. The results also show that to lower the stress-to- strength ratio, placement should occur typically between 9pm and 1am, and the initial mixture temperature should be as low as possible while still maintaining specific compressive strength requirements.

Since the SW mixtures were analyzed at a 9am placement time, their stresses all surpassed their strengths. This was due to the peak of the heat of hydration curve matching up with the peak of the ambient temperature profile as seen in Figure 10-19. If the SW mixtures were placed at a different time, such as the time used for the JAX mixture (1am), the stresses would have been below their respective strengths. The JAX mixture ambient temperature profile peaks ten hours after the peak of the JAX hydration curve. This delayed peak in ambient temperature allows the concrete temperature to start to cool before the ambient temperature rise can affect it.

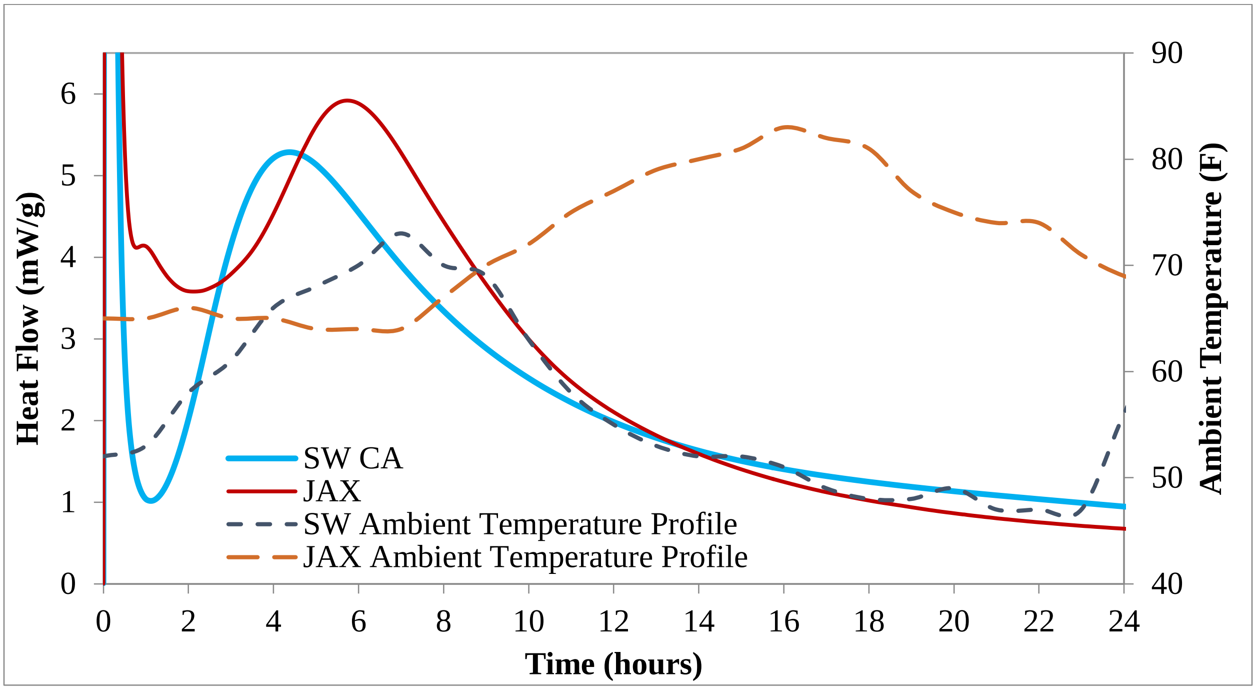

Figure 10-19: Temperature profiles

From the analysis by HIPERPAV III, it can be expected that an increase in dosage of chloride-based accelerator will increase the stress-to- strength ratio of a concrete pavement slab.

Since the dosage of accelerator has been shown to significantly increase thermal strains at early ages from the rapid hydration, this could be one factor that causes an increase in the stress-to-strength ratio.

From observing comparisons in HIPERPAV III, it is important to monitor the placement temperature, as an increase in placement temperature would increase the cracking potential. Therefore, if a concrete mixture is to be placed at a higher initial temperature, such as the case for a “hot mix,” it is necessary to mix during cooler ambient temperatures to reduce the early-age cracking potential.

The construction time of a mixture is an important parameter that can be easily controlled. By mixing during the night time hours, the heat of hydration from the concrete will most likely not be occurring at the same time as the peak daily temperature. By having an ambient temperature peak after the temperature increase from the heat of hydration peak has started to cool, the overall concrete temperature can remain lower than if both temperature peaks occurred at the same time. Additionally, traffic is lower at night, reducing possible conflicts between construction and the traveling public.

10.7 References

ASTM C1074-04, Standard Practice for Estimating Concrete Strength by the Maturity Method, ASTM International, West Conshohocken, PA, 2004.

Bazant, Z., and Baweja, S. (2000). “Creep and Shrinkage Prediction Model for Analysis and Design of Concrete Structures: Model B3.” *ACI Special Publication 194*, 1–83.

Bradbury, R. D. (1938). *Reinforced Concrete Pavements*. Wire Reinforcement Institute, Washington, D.C., 34–49.

Hope, B. B. B., and Manning, D. G. (1971). “Creep of Concrete Influenced by Accelerators.” *ACI Materials Journal*, 68-36.

Hsu, T. T. C., Slate, F., Sturman, G. M., and Winter, G. (1963). “Microcracking of Plain Concrete and the Shape of the Stress-Strain Curve.” *ACI*, 60(14), 209–224.

Klieger. (1958). “Effect of Mixing and Curing Temperature on Concrete Strength.” *ACI*, (54-62), 1063–1081.

Lee, E. B., Lamour, V., Pae, J. H., and Harvey, J. (2003). *Analysis of Sensitivity of Plain Jointed Concrete Pavement in California to Early-age Cracking using HIPERPAV*. University of California.

McCullough, B. F., and Rasmussen, R. O. (1998). *Fast Track Paving: Concrete Temperature Control and Traffic Opening Criteria for Bonded Concrete Overlays Volume I -Final Report*. Transtec, Inc., Austin, TX.

Mindess, S., Young, J. F., and Darwin, D. (2003). *Concrete*. Pearson Education.

Poole, J. L., and Riding, K. A. (2009). “Early Age Cracking : A Case Study in How Materials Modeling Can Improve Concrete Quality.” *ACI*, SP 266-5, 57–72.

Poole, J. L., Riding, K. A., Juenger, M. C. G., Folliard, K. J., and Schindler, A. K. (2010). “Effects of Supplementary Cementitious Materials on Apparent Activation Energy.” *Journal of ASTM International*, 7(9), 1–16.

Rasmussen, R. O., Mccullough, B. F., Ruiz, J. M., and Kim, P. J. (1999). *Fast Track Paving: Concrete Temperature Control and Traffic Opening Criteria for Bonded Concrete Overlays Volume III -HIPERPAV User’s Manual*. Transtec, Inc., Austin, TX.

Reynolds, W. C., and Perkins, H. C. (1977). *Engineering Thermodynamics*. McGraw-Hill, New York.

Riding, K. A., Poole, J. L., Schindler, A. K., Juenger, M. C. G., and Folliard, K. J. (2010). “Effects of Construction Time and Coarse Aggregate on Bridge Deck Cracking.” *ACI Materials Journal*, 106-M50.

Ruiz, J. M., Rasmussen, R. O., Chang, G., Dick, J., Nelson, P., Schindler, A. K., Turner, D., and Wilde, W. (2005a). *Computer-Based Guidelines For Concrete Pavements Volume III-Technical Appendices*. The Transtec Group, Inc., Austin, TX.

Ruiz, J. M., Rasmussen, R. O., Chang, G., Dick, J., and Nelson, P. (2005b). *Computer-Based Guidelines For Concrete Pavements Volume II—Design and Construction Guidelines and HIPERPAV II User’s Manual*. Federal Highway Administration, McLean, VA.

The Transtec Group. (2009). “HIPERPAV III (Version 3.20.0006) [Software].” <Available from www.hiperpav.com>.

Zdenek, B., and Baweja, S. (1995). “Creep and Shrinkage Prediction Model for Analysis and Design of Concrete Structures : Model B3.” *ACI Materials Journal*, SP-194.

CHAPTER 11 Conclusions and Recommendations

11.1 Conclusions

The following conclusions are based on the findings from this study:

- ConcreteWorks did an excellent job of simulating the temperature development of the concrete pavement slab. The temperature development of high-early strength concrete mixtures followed the same fundamental physics that normal strength concrete mixtures follow.
- The cracking potential of concrete is substantially affected by the temperature of the concrete at the start of slab placement, and the ambient conditions during placement. They affect the rate of temperature and strength gain of high-early-strength concrete and, consequently, its tendency to crack.
- The cracking probability of concrete used for pavement slab replacement is not only increased by higher placement temperature, and placement during the hotter portions of the day, but also by increasing the dosage of accelerator.
- The pavement replacement slab placed at the State Materials Office in Gainesville, FL exhibited cracking that was hidden by the curing compound until traffic loads removed the curing compound. Cracking was likely the result of thermal and drying effects. It is probable that cracking occurs more frequently than currently recognized but is not observable until after traffic wears away the curing compound.

11.2 Recommendations

Based on the findings from this study, the following recommendations were made:

- Do not specify hot weather mixes for concrete pavement slab replacement. Additionally, specify a maximum concrete placement temperature to reduce concrete peak temperature during curing and consequently reduce the cracking potential.
- Require placement of concrete replacement slabs to be done between the hours of 9 pm and 3 am.

- Collect data from each concrete slab replacement job to develop a replacement slab database. Collected data should include mix design, time and amount of accelerator addition at jobsite, concrete delivery and placement times, concrete delivery and placement temperatures, ambient weather conditions, time of curing compound application, time curing protection added and removed, type of curing protection, type and condition of base material, slab dimensions, time of sawing, time of opening to traffic, and replacement slab cracking data (how many replaced, mix design used for each slab, how many cracked, and time crack observed).

11.3 Suggestions for Future Work

Based on the findings from this study, the following recommendations were made:

- Perform a controlled field study that places high-early strength concrete slabs and monitors the slabs for temperature and cracking. Slabs should be placed at different times, mixing temperatures, and accelerator dosages to validate the modeling performed in this study.
- Develop guidelines for proportioning low-cracking mixtures that could meet FDOT strength requirements for opening to traffic for different weather conditions and time-to-traffic opening criteria. Currently, the research team has identified one concrete mixture design parameter that influences cracking probability: accelerator dosage. A project that could identify many of the additional parameters that affect cracking and strength gain could be used to develop design guidelines. This would give contractors options when developing mixtures that could meet project specific requirements while limiting the probability of cracking.

Appendix A – Activation Energy Fit Curves

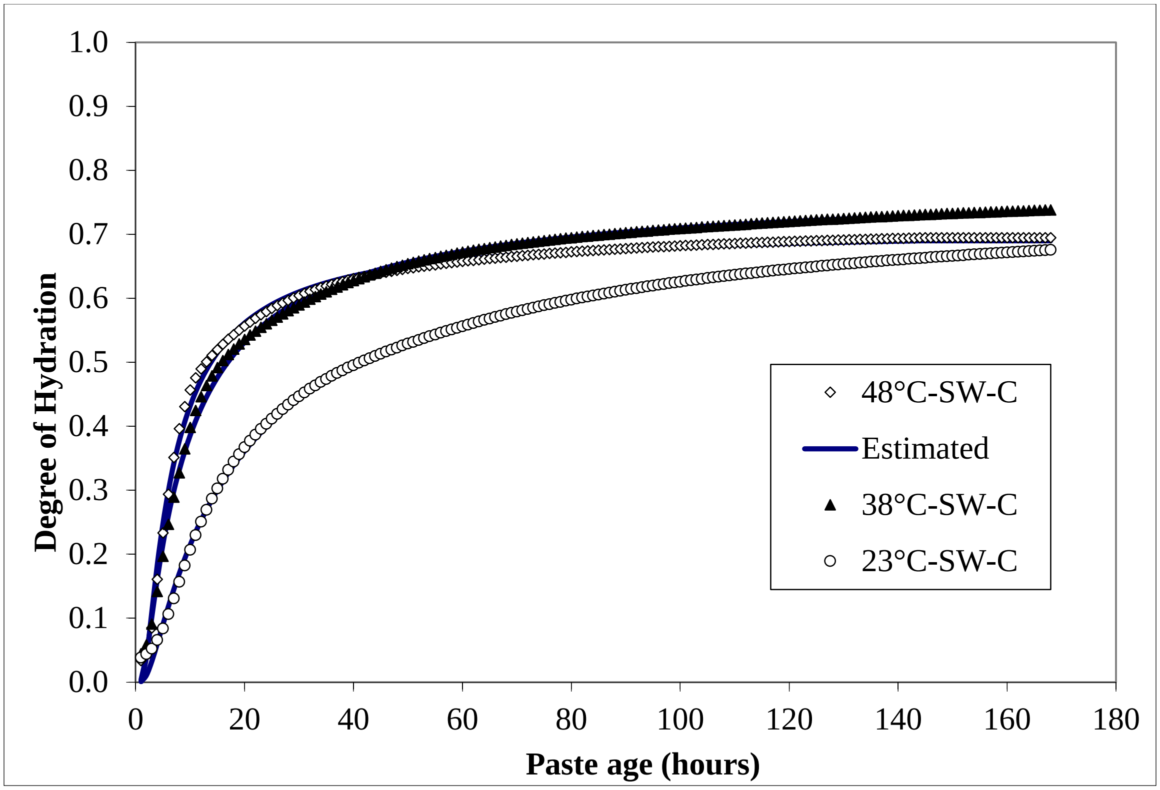

Figure A-1: Degree of hydration as a function of age for mix SW-C

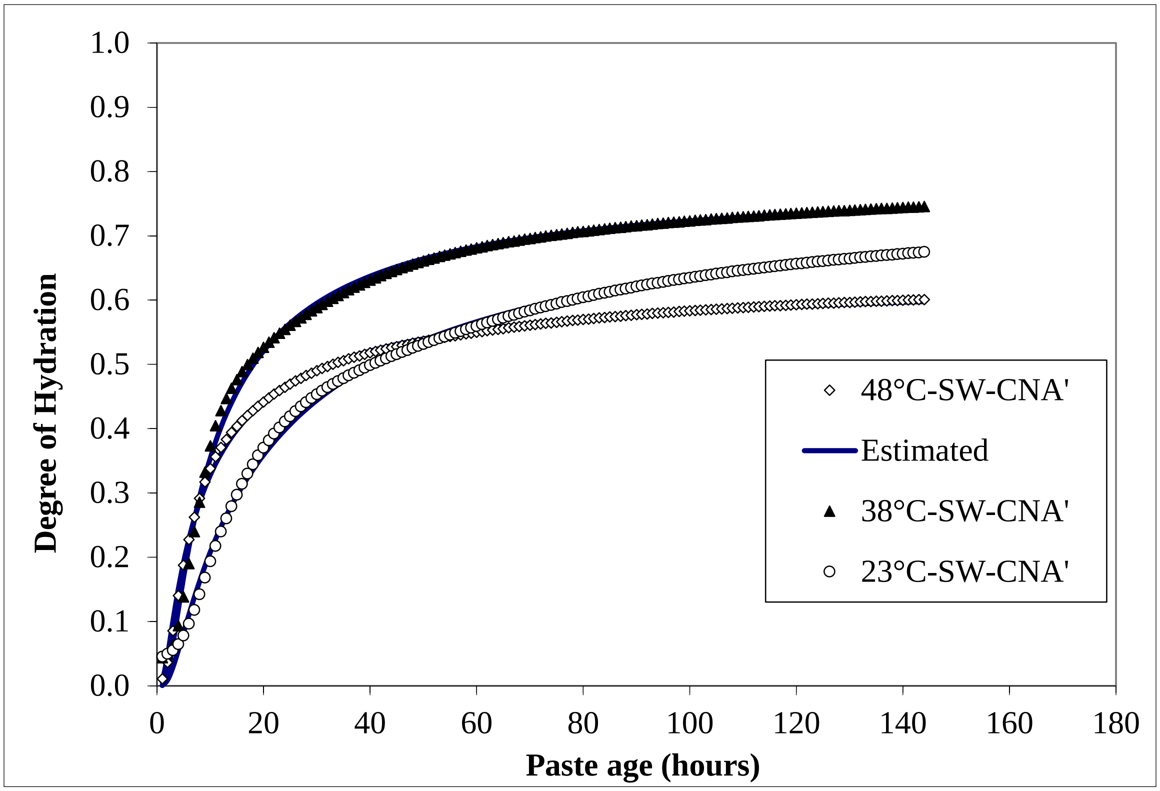

Figure A-2: Degree of hydration as a function of age for mix SW-CNA

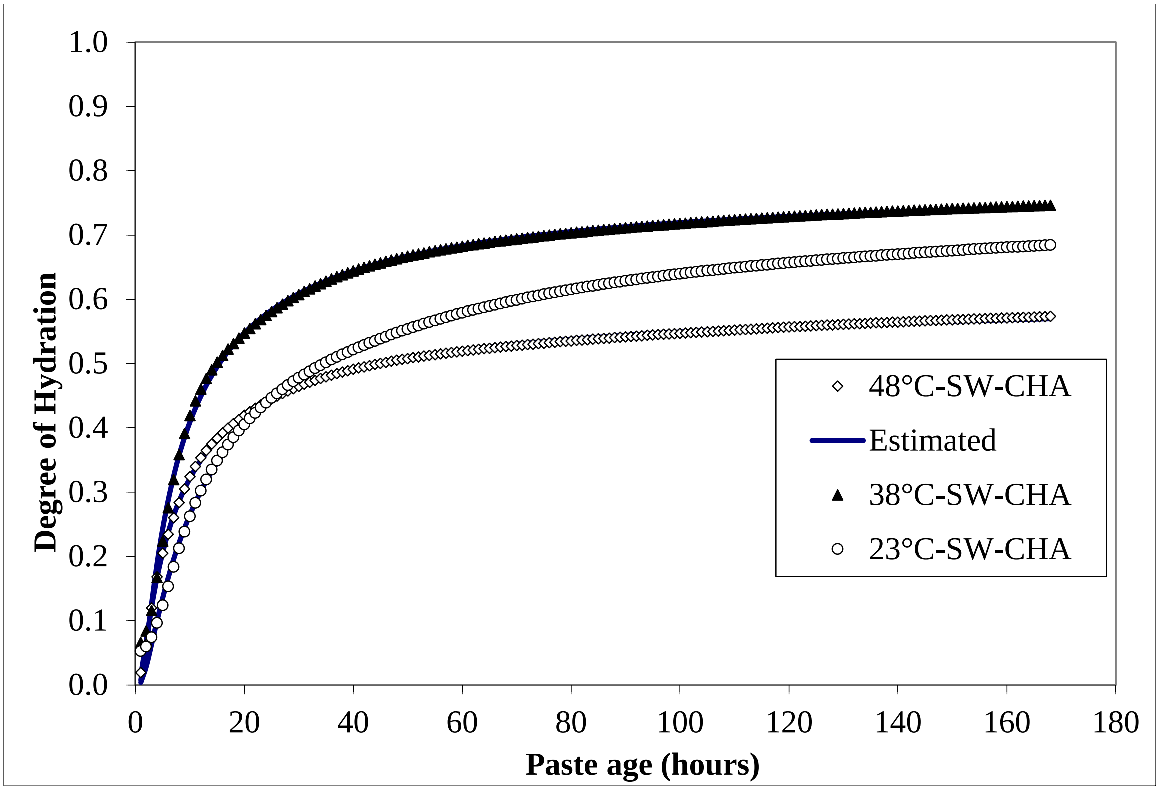

Figure A-3: Degree of hydration as a function of age for mix SW-CHA

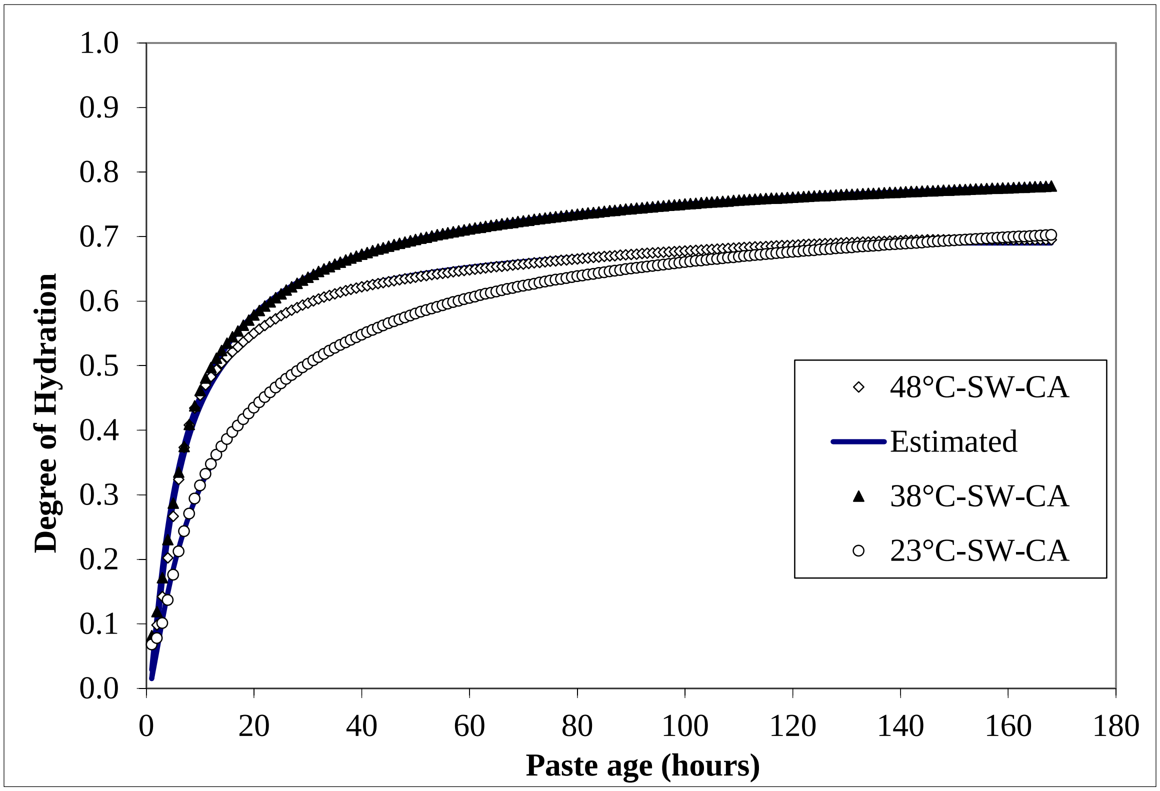

Figure A-4: Degree of hydration as a function of age for mix SW-CA

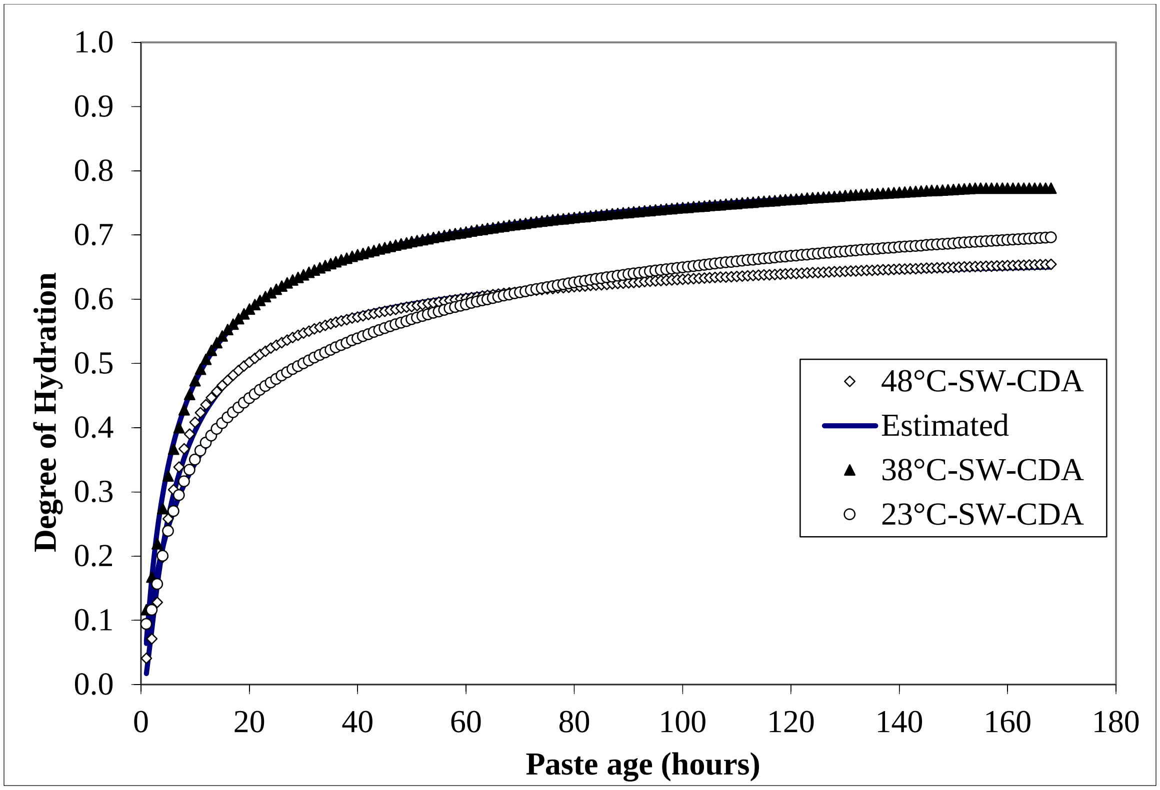

Figure A-5: Degree of hydration as a function of age for mix SW-CDA

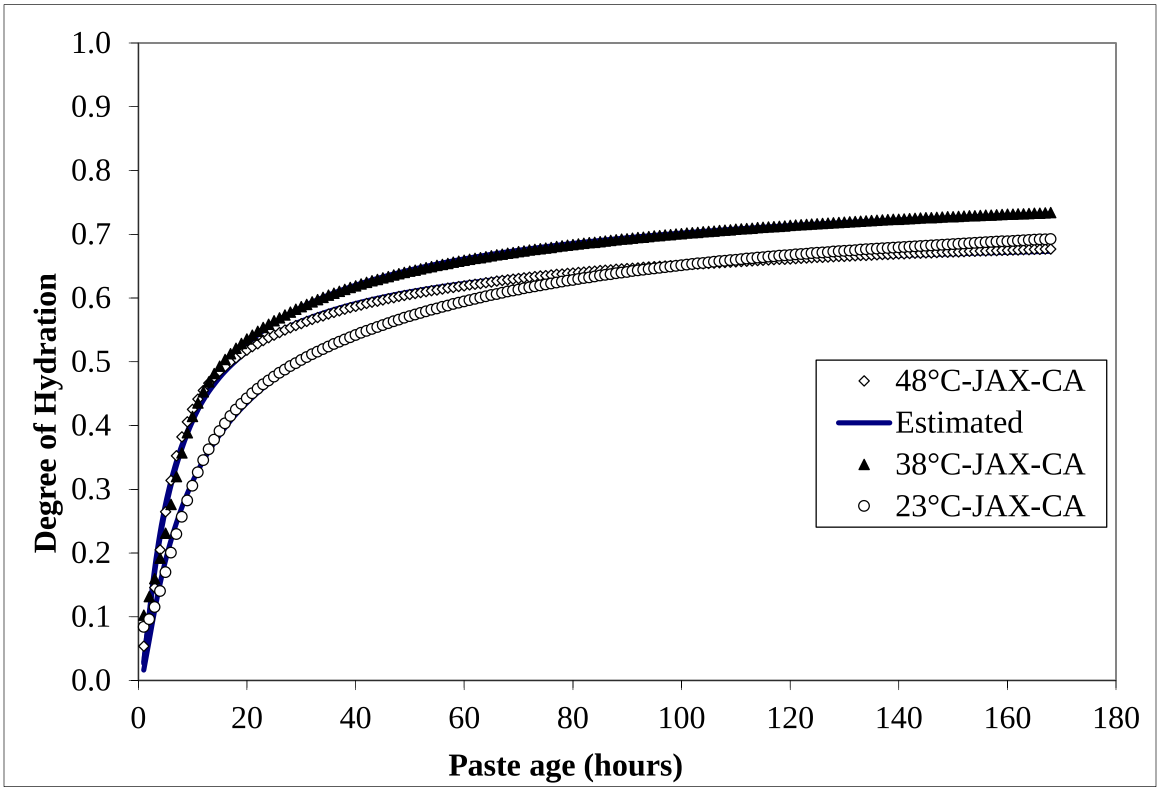

Figure A-6: Degree of hydration as a function of age for mix JAX-CA

Appendix B – Arrhenius Plots

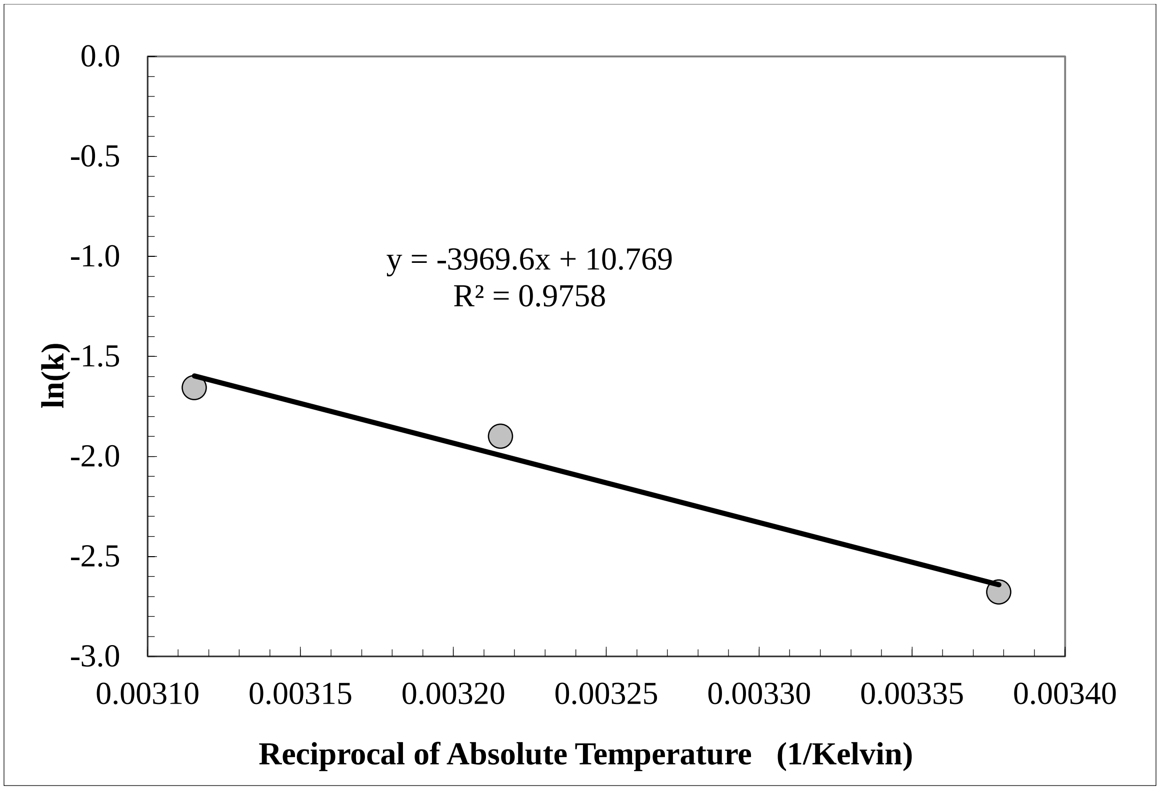

Figure B-1: Arrhenius plot for mix SW-C

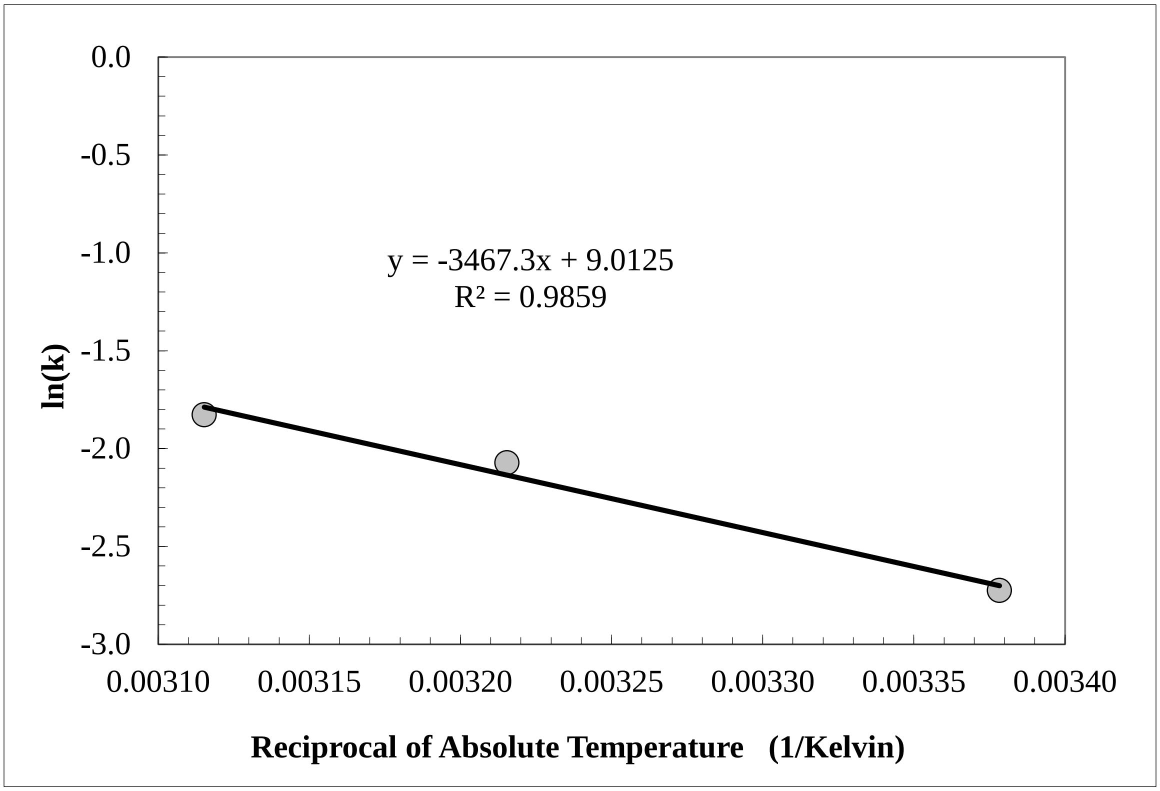

Figure B-2: Arrhenius plot for mix SW-CNA

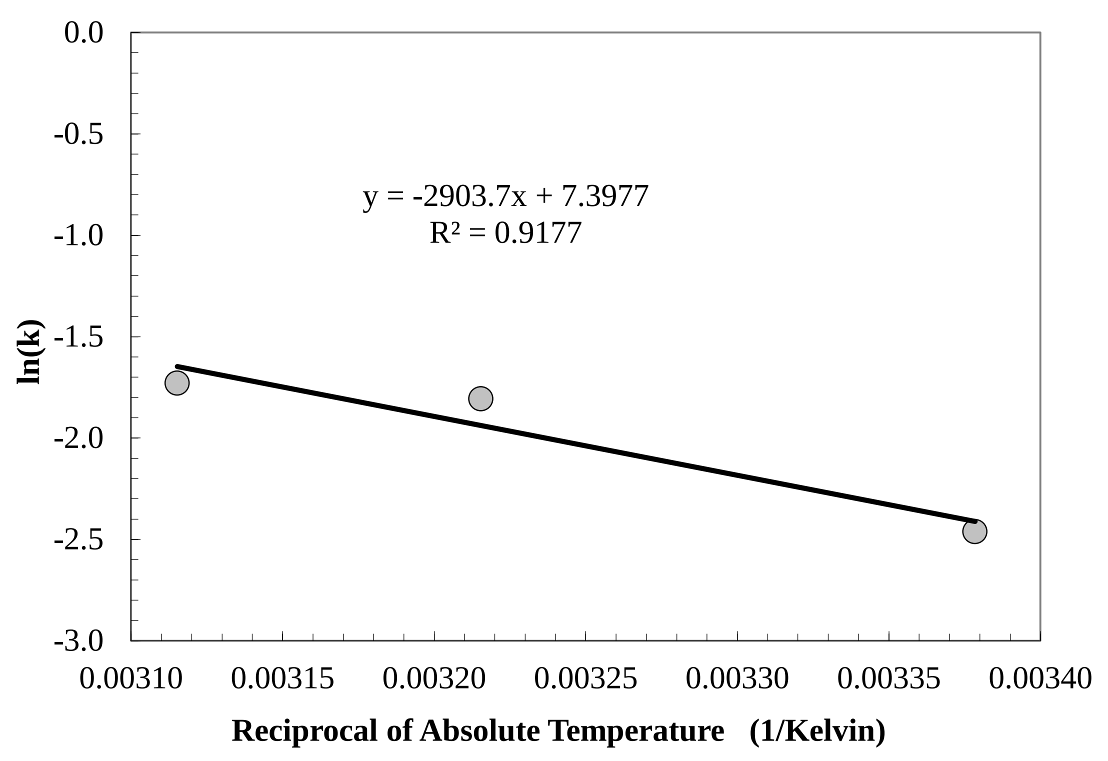

Figure B-3: Arrhenius plot for mix SW-CHA

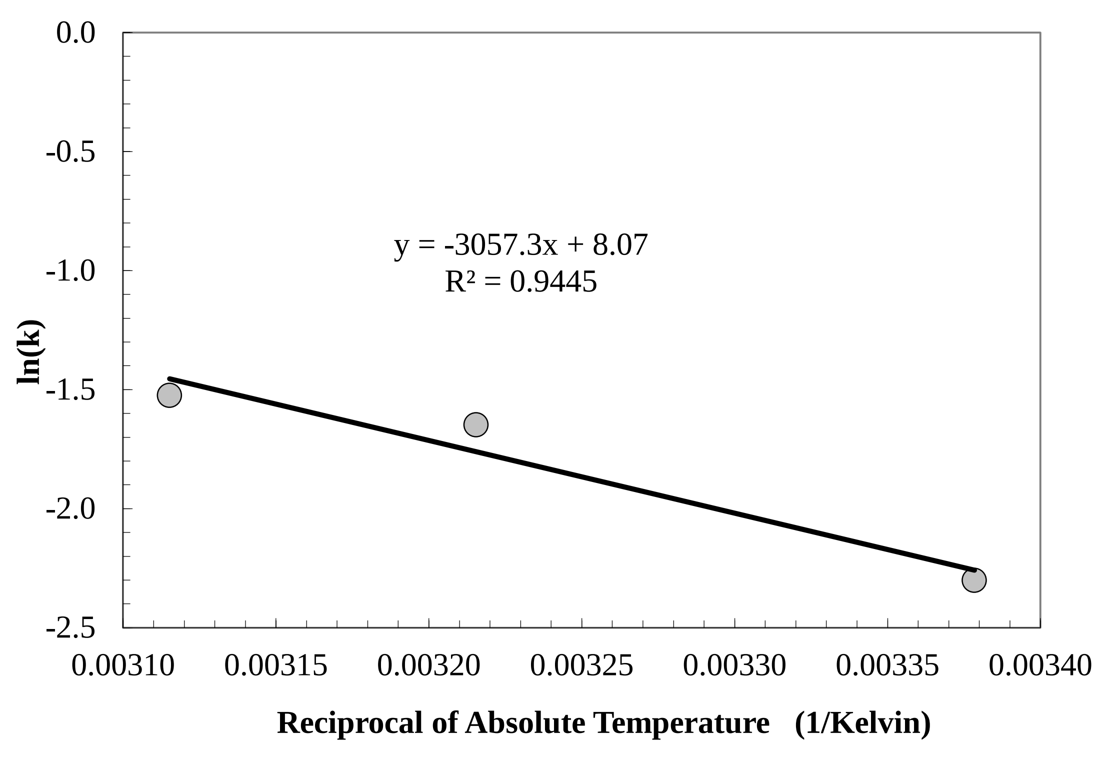

Figure B-4: Arrhenius plot for mix SW-CA

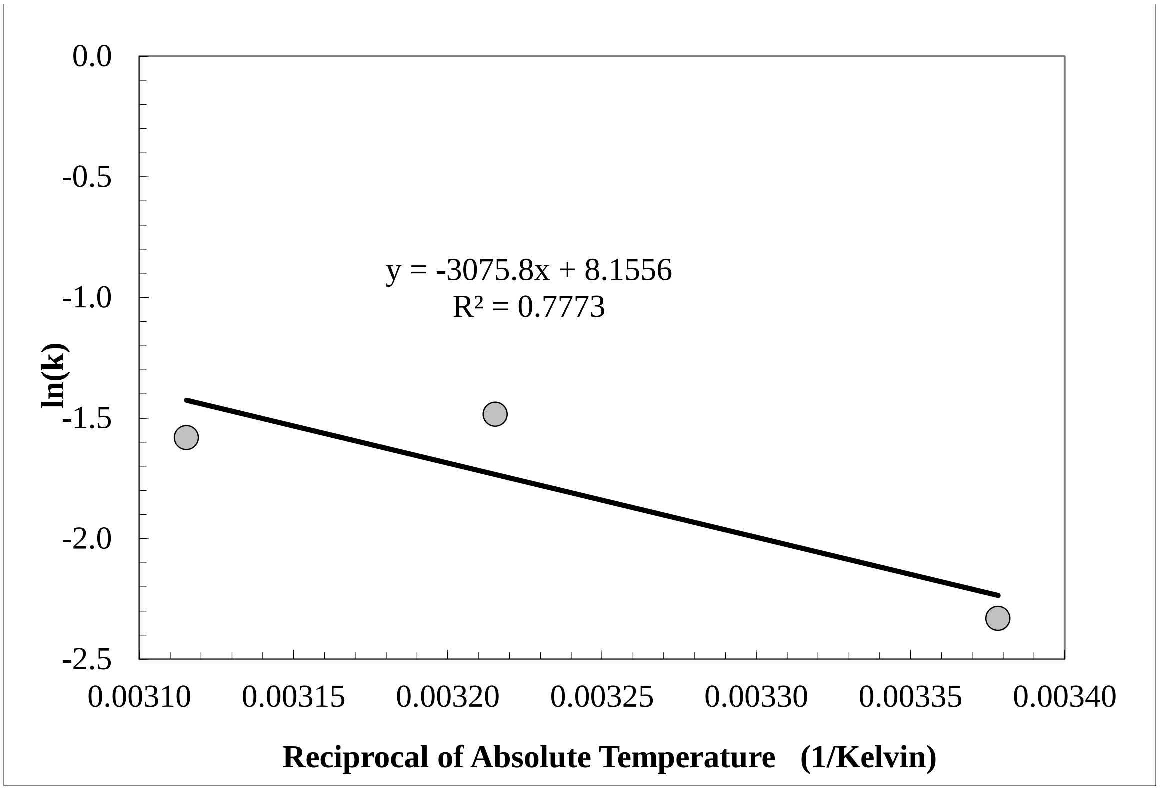

Figure B-5: Arrhenius plot for mix SW-CDA

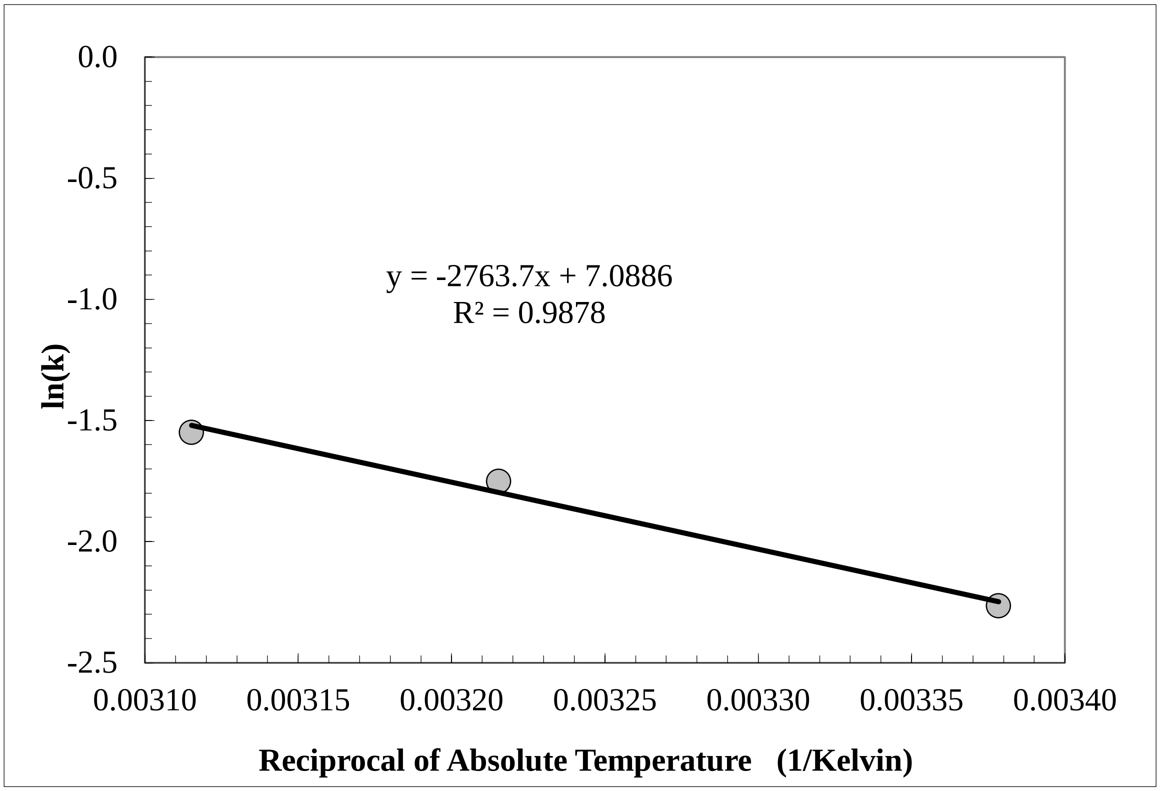

Figure B-6: Arrhenius plot for mix JAX

Appendix C – Construction Steps for Semi-adiabatic Calorimeter

Construction Steps for Semi-adiabatic Calorimeter

1) Install the data logger software (Pico logger, see Mfg. Manual) on the computer/laptop where data will be collected.
2) Construct concrete sample chamber (7 in diameter, 14 in height) out of galvanized steel sheeting

Figure C-1: Steel compartment

3) Measure inner height of the drum , divide it into 3 and mark those dimensions (This is done so that the sample /compartment will be at the centroid of the drum, and enough insulation would be provided on all sides)
4) Drill 1/2 inch hole on the side of the drum (1/3 of the height from the bottom, this is where the long-range wire will be fitted connecting the drum to the station)

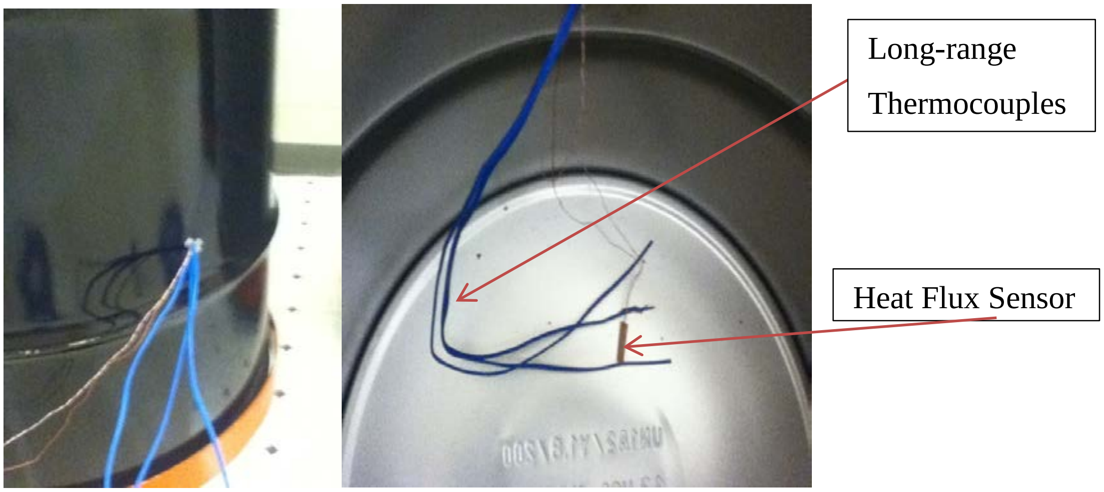

Figure C-2: Perforation along the length of the drum

5) Assemble the Type T thermocouples

Cut PVC wire to desired length [Measured from the drum to the data collection station i.e. long- range]

Use the type T miniature connector to create the following:

- Long-range Female/Male [female end (A) embedded on the side of steel compartment and the male end (B) connects to the Data logger, fit the wire through the ½ hole prior to completing the second end]
- Short- range Male which will be embedded in the Sample and connect to long female connector (Qty 1)
- Long-range Male (L-RM) connectors which connect to data logger and attach on the side of the steel compartment (Qty 2, 1 on the compartment and the other one at 1 inch away)

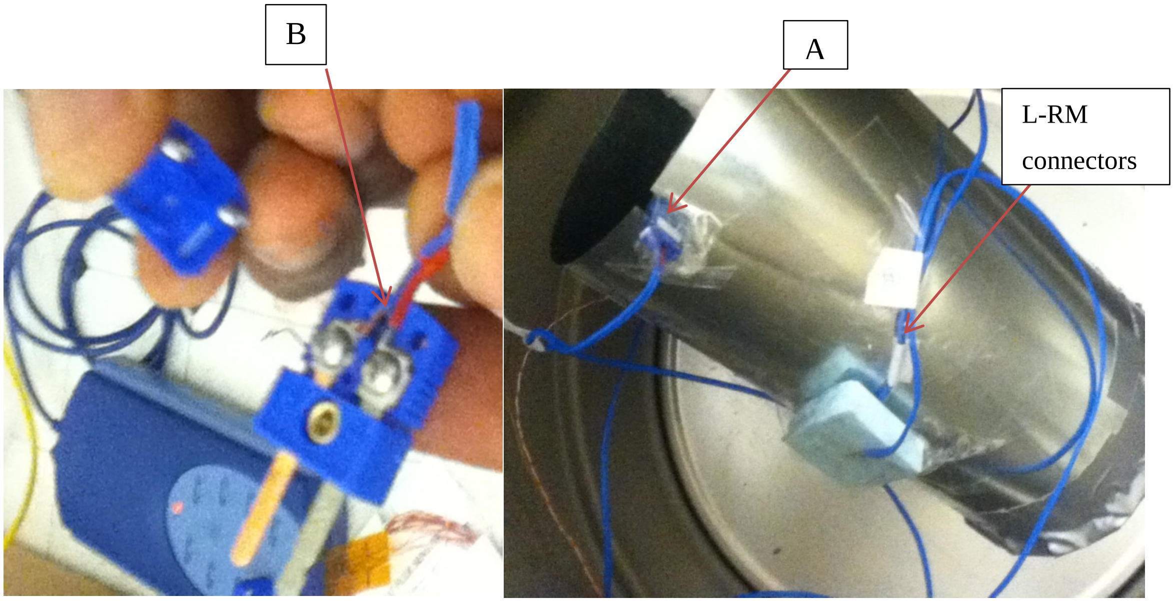

Figure C-3: Male/female connectors attached to the steel compartment

<u>Note</u>: To form the thermocouple on the side of the steel frame, rip off the insulator of the PVC wire (about 1-1/2 inch in length), and twist the wires together.

6) Test the thermocouples

Using body heat (fingers), check the temperature readings for the thermocouples.

7) Tape the thermocouples and heat sensor to the sides of the compartment

- Thermocouples preferable at the midpoints (7 inch)

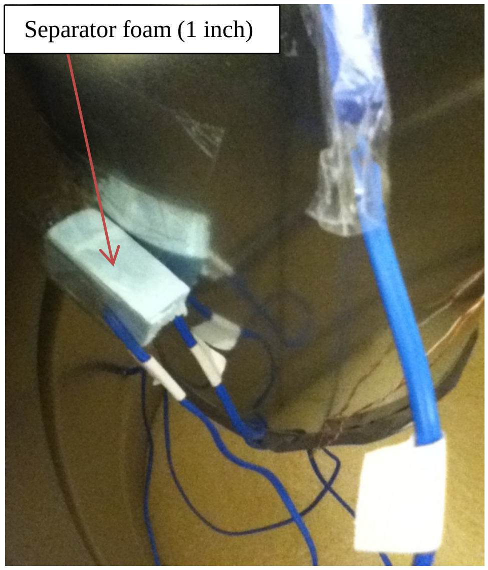

Figure C-4: Placement of thermocouples on the outside of the sample chamber

8) Re-test the Heat sensor and Thermocouples

9) Mix and place the insulation foam

Follow the manufacturer’s guide; mix the insulation foam in small amounts.

a) Fill the bottom third of the drum while holding the steel compartment in place (centered) [wait for foam to cool off between pourings, 10-15 minutes]

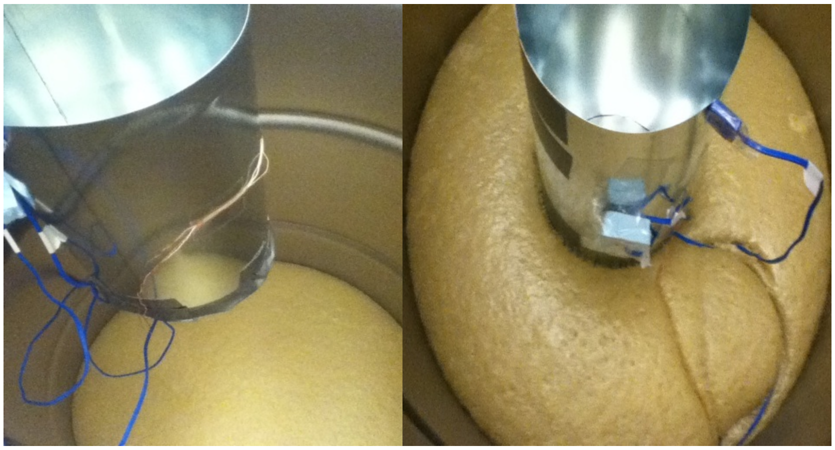

Figure C-5: Foam pouring and placement of compartment

b) Fill the remaining portion of the drum, so that the foam lines up with the top of the steel compartment as seen below

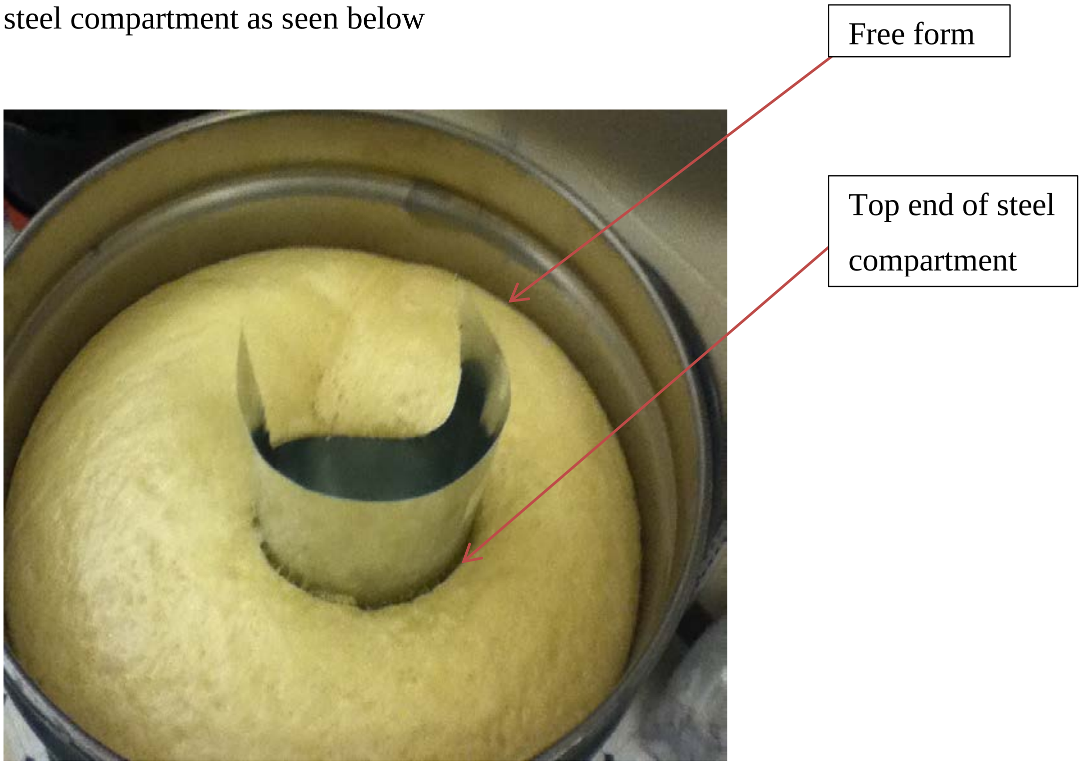

Figure C-6: Line-up of insulator foam with compartment

c) Monitor the heat sensor and the thermocouples, and let the foam cure overnight (8-10 hours)
d) Finish the top surface of the foam

Figure C-7: Top surface finishing

e) Cut acrylic sheet to make the smooth top cover, use the “great stuff” insulation foam sealant or a small amount of the Aeromarine foam to glue it down or fill up any holes. Use the high temperature silicone to finish the edges.

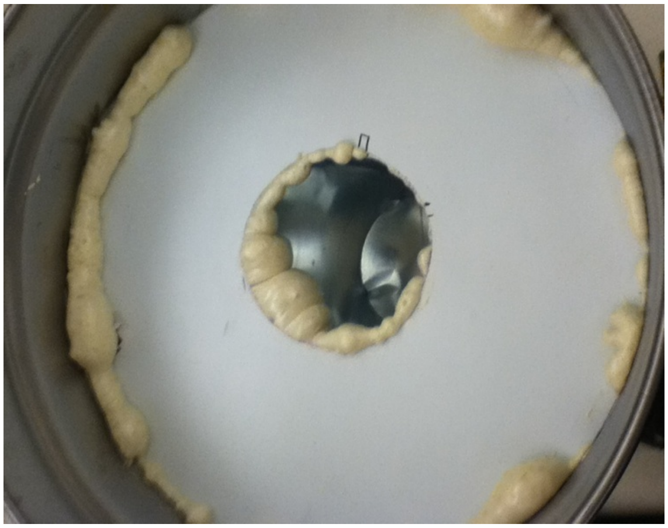

Figure C-8: Installed smooth acrylic finish

10) Fabrication of the top cover

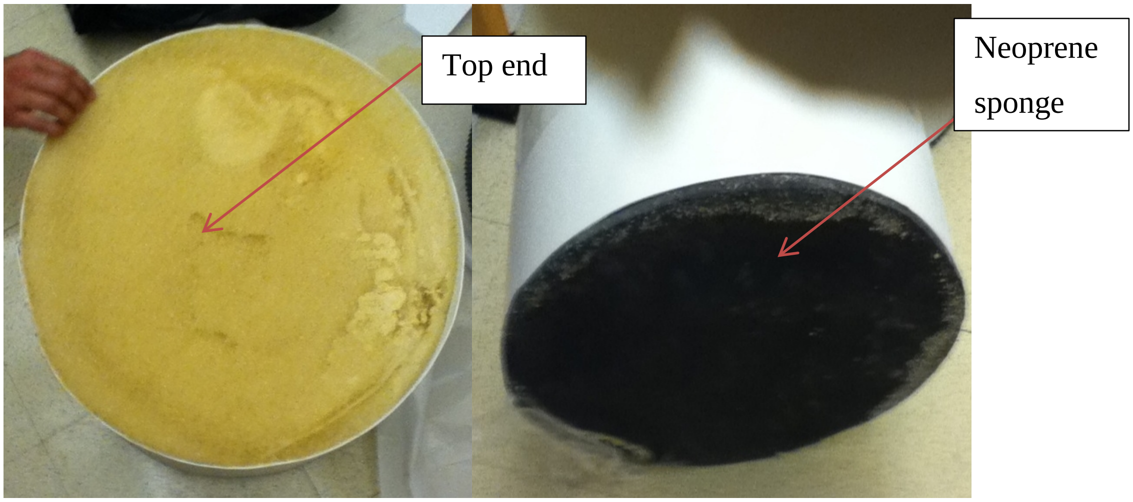

Figure C-9: Fabrication of top cover

a) Measure the top portion of the drum to include its original cover (7-8 inch in total height) at multiple locations and cut the acrylic sheet in length and height to provide a circular form. Cut an additional inner piece from the acrylic which will constitute the actual top over. Use the hinge screws to keep the inner form together.

   Note: Measure the dimensions such that the drum closes completely with minimal heat loss.

b) Cut a circular piece of the neoprene sponge to create a smooth contact area between the bottom and top cover of the drum, which will reduce heat loss by providing air-tight fitting and cover any imperfection between the two surfaces. Use duct tape to attach it from the interior of the top cover.

c) With the outer form in place, place a small piece of acrylic over the compartment hole followed by the inner piece with the neoprene sponge. Then mix and pour the Aeromarine foam.

d) Let the foam cure and mark the fit positioning of the top cover/drum prior to removal. This is done to keep the best position of the top cover/drum intact to minimize heat losses due to misalignment.

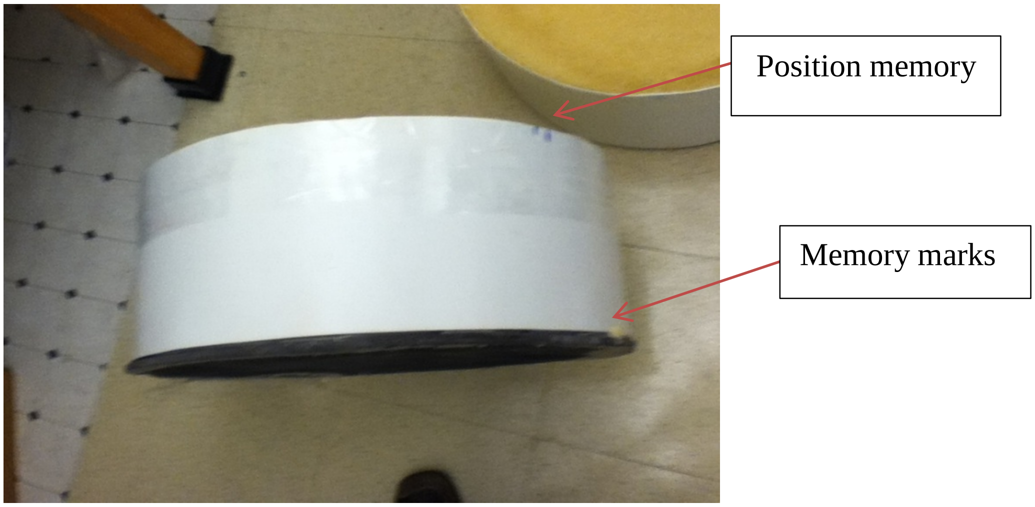

Figure C-10: Marking of best fit position

11) Finish the top surface, then use the great stuff or a small amount of the Aeromarine foam to attach the top of the steel drum.

Figure C-11: Finished product